

AD-A175 172

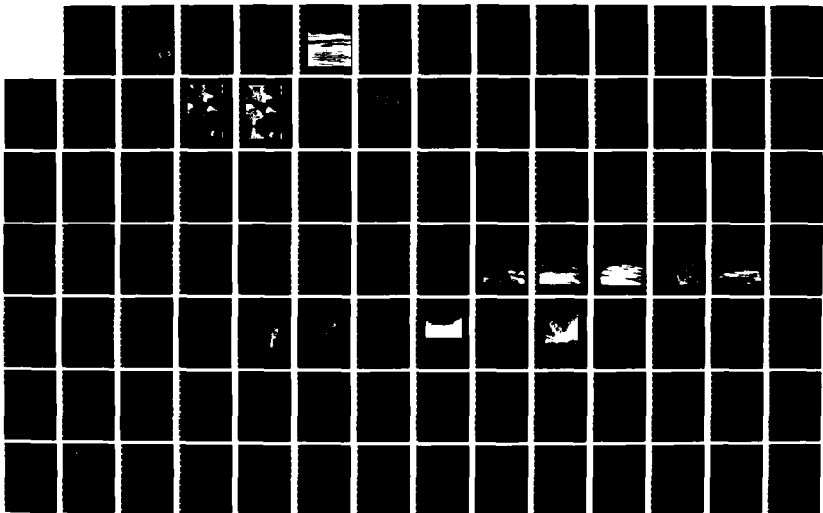
ONRL WORKSHOP PROCEEDINGS - ROLE OF SURFACTANT FILMS ON
THE INTERFACIAL P (U) OFFICE OF NAVAL RESEARCH LONDON
(ENGLAND) F L HERR ET AL 21 NOV 86 ONRL-C-11-86

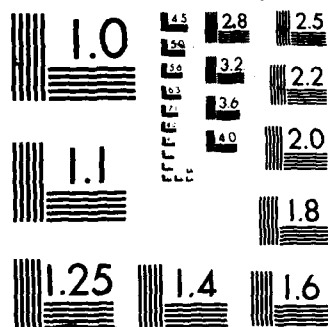
173

UNCLASSIFIED

F/G 8/10

NL





XEROCOPY RESOLUTION TEST CHART

12



ONRL Report C-11-86

AD-A175 172

ONRL Workshop Proceedings--Role of Surfactant Films
on the Interfacial Properties of the Sea Surface

Frank L. Herr and Jerome Williams, Eds.

November 21, 1986

DTIC FILE COPY

DTIC
ELECTE
DEC 18 1986
S E D

Approved for public release; distribution unlimited

U.S. Office of Naval Research, London

UNCLASSIFIED

SECURITY CLASSIFICATION OF THIS PAGE

REPORT DOCUMENTATION PAGE

1a REPORT SECURITY CLASSIFICATION UNCLASSIFIED			1b RESTRICTIVE MARKINGS		
2a SECURITY CLASSIFICATION AUTHORITY			3 DISTRIBUTION/AVAILABILITY OF REPORT		
2b DECLASSIFICATION/DOWNGRADING SCHEDULE					
4 PERFORMING ORGANIZATION REPORT NUMBER(S) C-11-86			5 MONITORING ORGANIZATION REPORT NUMBER(S)		
6a NAME OF PERFORMING ORGANIZATION US Office of Naval Research Branch Office, London		6b OFFICE SYMBOL (If applicable) ONRL	7a NAME OF MONITORING ORGANIZATION		
6c ADDRESS (City, State, and ZIP Code) Box 39 FPO, NY 09510			7b ADDRESS (City, State, and ZIP Code)		
8a NAME OF FUNDING/SPONSORING ORGANIZATION		8b OFFICE SYMBOL (If applicable)	9. PROCUREMENT INSTRUMENT IDENTIFICATION NUMBER		
8c ADDRESS (City, State, and ZIP Code)			10. SOURCE OF FUNDING NUMBERS		
PROGRAM ELEMENT NO.		PROJECT NO.	TASK NO.	WORK UNIT ACCESSION NO.	
11 TITLE (Include Security Classification) ONRL Workshop Proceedings--Role of Surfactant Films on the Interfacial Properties of the Sea Surface					
12 PERSONAL AUTHOR(S) Frank L. Herr and Jerome Williams, Eds.					
13a TYPE OF REPORT Conference	13b TIME COVERED FROM TO	14. DATE OF REPORT (Year, Month, Day) 21 November 1986	15 PAGE COUNT 283		
16 SUPPLEMENTARY NOTATION					
17 COSATI CODES			18 SUBJECT TERMS (Continue on reverse if necessary and identify by block number)		
FIELD	GROUP	SUB-GROUP	~Surface films; Organic films; Marine microlayer, <i>✓</i> ~Remote sensing; Capillary waves; Monomolecular films. <i>✓</i>		
02	03, 10				
17	09				
19 ABSTRACT (Continue on reverse if necessary and identify by block number) <i>✓</i> <i>Proceedings of a workshop held in London, UK, to address the effects of the marine microlayer on the microwave signature of the sea surface. A total of 12 papers present biological, chemical, and physical aspects of the problem, ranging from attempts to describe the nature of the layer to its effect on electromagnetic energy. Three working group reports (surface film chemistry, microlayer dynamics, and remote sensing) complete this document. Reports:</i>					
20 DISTRIBUTION AVAILABILITY OF ABSTRACT <input checked="" type="checkbox"/> UNCLASSIFIED/UNLIMITED <input type="checkbox"/> SAME AS RPT <input type="checkbox"/> DTIC USERS			21 ABSTRACT SECURITY CLASSIFICATION UNCLASSIFIED		
22a NAME OF RESPONSIBLE INDIVIDUAL C. L. Fox			22b TELEPHONE (Include Area Code) (44-1) 409-4340	22c OFFICE SYMBOL 11	

DD FORM 1473, 84 MAR

83 APR edition may be used until exhausted
All other editions are obsolete

SECURITY CLASSIFICATION OF THIS PAGE

UNCLASSIFIED
GSA Government Printing Office: 1985-507-047

UNCLASSIFIED

Block 18 (Cont'd)

Slicks

Marine chemistry

Synthetic aperture radar

SAR targets

Young ice

Accession For	
NTIS GRA&I	<input checked="checked" type="checkbox"/>
DTIC TAB	<input type="checkbox"/>
Unannounced	<input type="checkbox"/>
Justification	
By	
Distribution/	
Availability Codes	
Dist	Avail and/or Special
A-1	



UNCLASSIFIED

ROLE OF SURFACTANT FILMS ON THE INTERFACIAL PROPERTIES OF THE SEA SURFACE

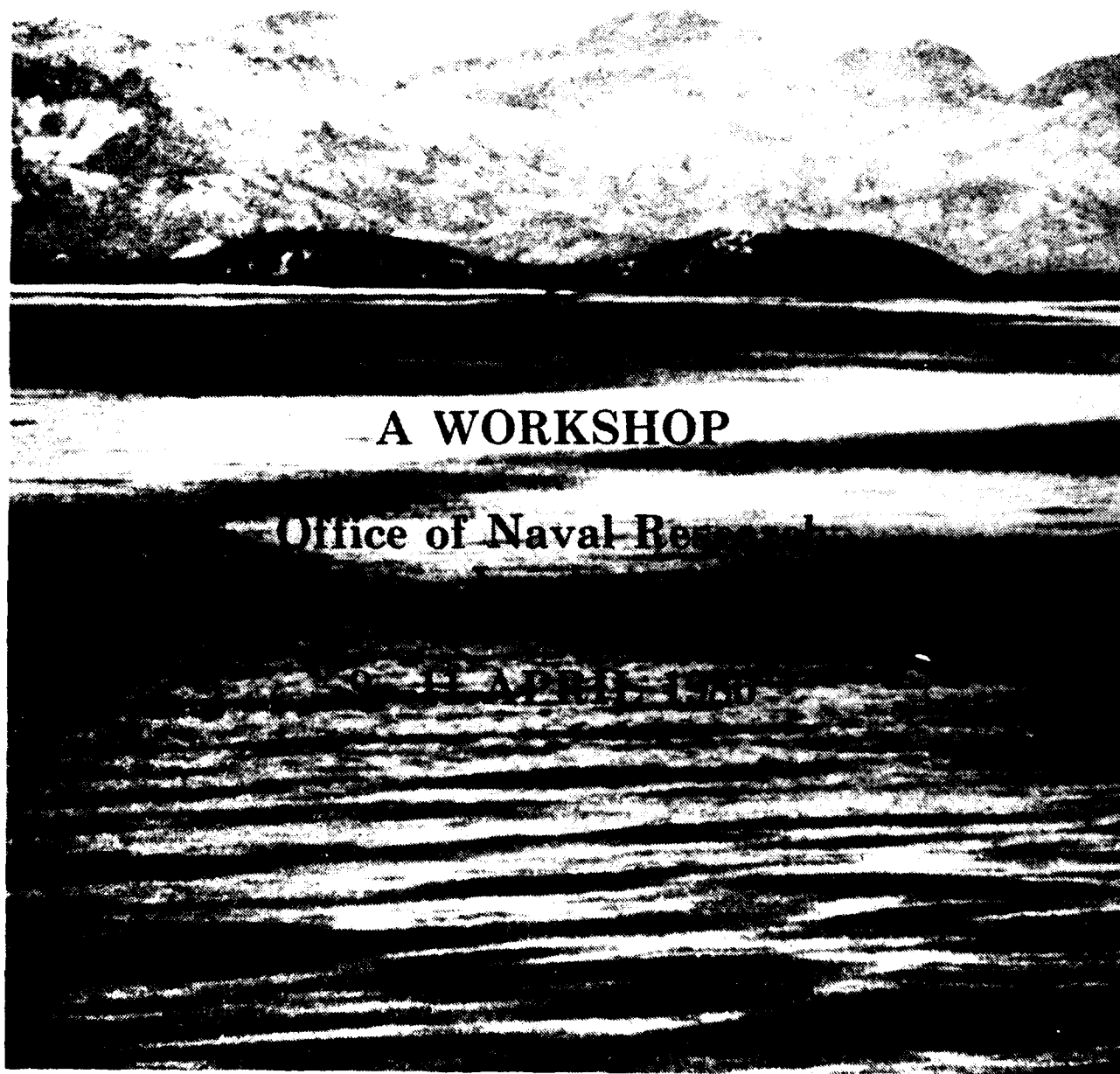


TABLE OF CONTENTS

Introduction	Frank L. Herr and Jerome Williams	vii
Physicochemical Effects of Organic Films at the Sea Surface and Their Role in the Interpretation of Remotely Sensed Imagery	William Garrett	1
Surface Films in Oceanography	John C. Scott	19
The Physical Appearance of Biogenic Slicks	John C. Scott	41
A Note on the Grease Ice "Microlayer" Effect on Remote Sensing	Ola M. Johannessen	49
On Phenomena Affecting Sea-Surface Remote Sensing and Interface Microlayer	Jin Wu	61
The Chemical Composition of the Sea-Surface Microlayer and Its Relation to the Occurrence and Formation of Natural Sea-Surface Film	P.M. Williams	79
The Chemistry of Near-Surface Seawater	Peter S. Liss	111
The Molecular Structure of the System Wake/ Monomolecular Surface Film and Its Influence on Water Waves	Heinrich Hühnerfuss and Werner Alpers	121
Maximum of Damping Ratio in Rippled Water Covered by Monomolecular Films	Pietro Paolo Lombardini	15
Dynamic Properties of Film-Covered Surfaces	E.H. Lucassen-Reynders	175
Damping of Short Waves by Insoluble Surface Films	Kristian Dysthe and Yitzhak Rabin	187
Acoustic and Capillary Wave Sensing of the Moving Microlayer	John F. Vesecky and Richard G. Johnson	215
On the Surface Response Properties of the Microlayer	J. Adin Mann, Jr.	245
Working Group Reports		
Surface Film Chemistry		271
Microlayer Dynamics		275
Remote Sensing		277
Attendees List		281

INTRODUCTION

Over the past two years the Office of Naval Research has been preparing for an initiative focused on processes indigenous to the air-sea interface of the ocean, specifically the role of surfactant molecules. A series of workshops have been held emphasizing topics necessary for defining scientific issues and technical approach. The chemistry and biology of the sea interface was addressed at an initial workshop held October, 1984 (1). While processes were investigated as they affected remote sensing techniques, the workshop did not highlight the physical processes which relate surfactants to imaged features. These dynamical processes, especially wave dampening, required an additional workshop to be given the prominence they deserve in any program of ocean interfacial effects.

With the advent of high resolution methods for remote sensing of the oceans, the extent to which biogenic surfactant films modify signatures in the IR, visible, and microwave regions of the electromagnetic spectrum has become increasingly appreciated. Infrared imagery, synthetic aperture radar imagery, and most recently, visible photography of ocean sun glitter have shown dramatically the wide extent of surfactant film effects covering numerous areas of the World Ocean. These examples of molecular phenomena (since biogenic surfactant films are monomolecular in contrast to thicker petroleum films) appearing prominently from space have exposed our limited understanding of this area of environmental science. Further, as we begin to develop the science it is immediately apparent that the instruments required for quantifying the fundamental parameters controlling short wavelength windwaves, e.g. surface tension, surface elastic modulus, surface surfactant concentration, are inadequate. The development of new ones will need a considerable infusion of techniques from other disciplines.

Even a quick look at the literature of surfactant effects shows the strong participation of European scientists. Many U.S. groups have superbly developed chemical and biological processes and have advanced our understanding of the flux of constituents across the air-sea interface. In contrast, a select group of collaborating European scientists have concentrated on the theory and practice of surfactant effects on wave dynamics and the subsequent influences on radar backscatter.

The ideal location to juxtapose European expertise with American interest is the Office of Naval Research, Branch Office in London, England. This workshop has been jointly sponsored by ONR/London and the Oceanic Chemistry Program at ONR, Washington, D.C. Three days were devoted to scientific deliberation beginning with a day and a half of lectures and discussion by participants followed by a review of the technical issues during the second afternoon. On the final day,

the participants broke into three smaller groups to consider chemical oceanographic processes, surfactant effects on dynamics, and remote sensing relationships. Each group submitted a report including consensus suggestions for future research directions. These reports follow this introduction.

As the following papers abundantly illustrate, the study of surfactant films on the ocean's surface requires a strongly interdisciplinary group. The processes are optical, biological, chemical, and physical oceanographic. Fluid mechanics, acoustics, as well as, electrical and chemical engineering offer promising new insights and techniques. Furthermore, the scales over which the phenomena operate are quite large. The papers are arranged to draw the reader into this diverse assemblage. William Garrett, John Scott and Ola Johannessen review the problem of surfactant modification of remotely sensed parameters. Jin Wu follows with a view of the placement of surface films within a fluid mechanical framework of the ocean surface boundary layer. Peter Williams and Peter Liss provide the current status of the chemical characterization of natural oceanic surfactants.

At this point, the discussion moves toward classical chemical and chemical engineering viewpoints of surfactant effects on hydrodynamics. First, Heinrich Huehnerfuss and Werner Alpers describe how the structure of surfactant molecules affects wave dampening. Then, Pietro Lombardini shows how experimental surface films affect the dampening ratio, and suggests relationships to radar backscatter. The theoretical framework for surfactant effects on capillary-gravity waves is next developed by Emmie Lucassen-Reynders and Yitzak Rabin. Finally, John Vesecky and Jay Mann explore innovative approaches to the development of instrumentation.

The mechanical and physicochemical characteristics of natural surfactants within the dynamical context of the ocean's surface is virtually unknown. This volume presents the problem, shows the best, relevant science being done today, and hints at the novel work forthcoming.

Frank L. Herr
Jerome Williams
November, 1986

(1) Hartwig, E.O., and F.L. Herr, Chemistry and Biology of the Sea-Surface Interface: Relationship to Remote Sensing, ONR Workshop, Sanibel, FL, October 1984.

PHYSICOCHEMICAL EFFECTS OF ORGANIC FILMS AT THE SEA
SURFACE AND THEIR ROLE IN THE INTERPRETATION OF
REMOTELY SENSED IMAGERY

William D. Garrett
Naval Research Laboratory
Washington, DC 20375

SCOPE

This paper reviews the physical effects of biogenic and pollutant organic films on air-sea interfacial properties and exchange processes, as well as the mechanisms by which these parameters are altered. The implications of these film-induced modifications of sea-surface reflectivity, emissivity and absorbance on remotely sensed visible, thermal, and microwave imagery will be assessed. Consideration will be given to the oceanic processes responsible for the formation of films and those which act to disperse the organic slicks. Present knowledge of the frequency and distribution of natural sea-surface films on a spatial and temporal basis will be presented. The chemical constitution of these films and the specific biological sources of the surface-active, organic, film-forming substances will be discussed elsewhere. While some references are found in the text, most literature citations are in Table 1, a state-of-knowledge review on the effects of various types of organic films on physical properties and processes at the air-sea interface.

BACKGROUND

Polar, organic molecules adsorb at important aquatic phase boundaries in the marine environment; at air-bubble and particle surfaces and at the atmosphere-ocean interface. When the surface concentration of the organic, surface-active material attains a critical level where the molecules of the surface film come into contact (about 1 mg per meter), the film becomes relatively incompressible, a thin layer of water at the air-sea interface is immobilized, and the sea surface can no longer be considered to be "free". During horizontal surface compression the organic film changes from a gas-like phase to a more condensed state at low film pressures of 1 to 2 mN per meter, and it is at this point that the film modifies a number of small-scale hydrodynamic and capillary-sensitive processes at the air-sea interface. In general, the small-scale dynamics of the air-sea interface are influenced by the film compressibility and by film flow across a surface tension gradient (Marangoni effect). Surface tension is inherent in both of these rheological parameters, and is itself an indicator of the existence of a coherent organic film capable of modifying interfacial processes.

FORMATION AND DISPERSION OF ORGANIC SEA SURFACE FILMS

Sensible sea surface films (slicks) occur when the surface concentration of film-forming molecules is increased to the

previously mentioned critical level by (1) vertical transport into the sea surface from below by forced or convective upwelling, rising air bubbles, or buoyant detritus, (2) compression of existent surface-active molecules in the sea surface by horizontal convergent processes due to internal waves, Langmuir cells, etc., or (3) direct input of man-made surface-active material to the sea surface from municipal dumping, petroleum production activities, ship effluents, and the like. It should be noted that film-forming molecules of biogenic origin exist at all times in the sea surface. While the surface concentration of such molecules varies temporally and spatially, there is a potential for the formation of natural organic films throughout the global sea surface.

Film pressures (surface tension reduction) have been measured by a number of investigators for a wide variety of natural slicks. The film pressures are usually less than the collapse pressures of the organic films, indicating that they are monomolecular. Consequently, there are a number of chemical, physical, and biological processes which act to disperse the adsorbed film-forming molecules and destroy these relatively fragile films. Figure 1 depicts the previously discussed transport modes by which polar, organic material reaches the sea surface, as well as the numerous processes acting on an existing film to remove its constituent molecules from the air-sea interface.

The most influential factors limiting the existence of sea-surface films are the dynamic air-sea interfacial processes, such as breaking waves, bursting bubbles, sea spray, and wave processes which disperse the films by entrainment into the underlying water. In addition, constituents of a surface film are selectively removed by dissolution, evaporation, biological degradation, and photocatalytic oxidation. Once horizontal convergence in the sea surface relaxes, the film has an intrinsic spreading pressure which transports its constituents into the surrounding nonslicked sea surface in order to maximize entropy. Once the surface concentration of the film-forming molecules falls below the critical value, processes such as capillary waves are no longer modulated, and the monomolecular film is no longer evident as a visible slick.

INFLUENCE OF ORGANIC SURFACE FILMS ON THE INTERPRETATION OF REMOTELY SENSED SIGNALS

Knowledge of the chemical nature and physical properties of the sea surface is essential to provide "sea truth" (the oceanic equivalent of "ground truth") for the proper interpretation of data from remote sensing systems. Since it has been shown that organic surface films modify the properties of the air-sea interface and its associated boundary layers, such films may also influence both passive and active remotely sensed signals. The magnitude of the physical effects of the surface film is a function of its chemical nature, its thickness, and the surface concentration of interfacially active molecules at the air-sea interface. Many of the surface effects produced by films can be produced by a layer of

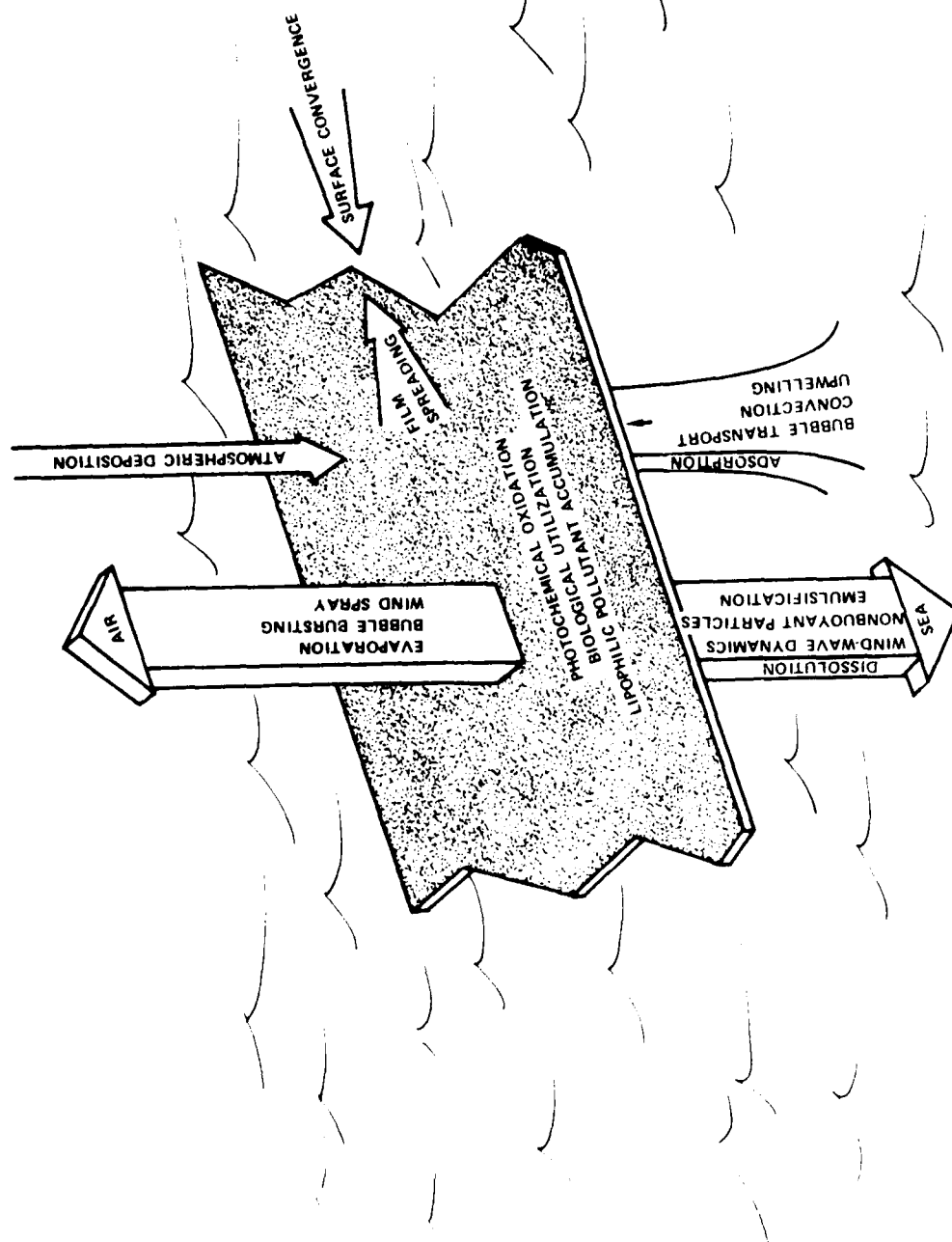


Figure 1: Physical, chemical, and biological processes involved in the life history of an organic sea surface film.

adsorbed organic material only one molecule in thickness (approximately 3 nanometers). Films of this kind, e.g. natural sea slicks, require as little as one milligram of organic material per square meter of ocean surface for their formation. Organic films attenuate and resist the formation of capillary waves, modify breaking waves and the resulting distribution of entrained bubbled, influence bubble bursting phenomena and surface bubble lifetimes, and produce temperature anomalies by various mechanisms.

These effects are reviewed in Table 1 (Impact of Natural and Man-Made Surface Films on the Properties of the Air-Sea Interface) for natural sea slicks, petroleum films, and experimental monomolecular films added to the sea surface for research purposes. In addition, literature dealing with film effects on sea surface reflectivity, absorbance, and emissivity in the visible, thermal, and microwave is included. The table estimates the level of knowledge, field and/or laboratory, for a particular effect caused by these three organic-film types. In the limited space available in this report it is not possible to discuss the specific data and the mechanisms postulated for the various film-induced process modifications. However, Table 1 provides this author's assessment of the level of understanding concerning these organic-film effects.

This assessment is carried on to Table 2 (Effects of Natural Organic Seasurface Films on the Properties of the Air-Sea Interface), in which a particular film-modified process is related to its effect on remotely sensed signals for various active and/or passive spectral regions.

Since natural slicks attenuate and resist the formation of capillary waves, affected sea surface areas have different reflectance characteristics from those of surrounding nonslicked waters. When passive reflectance is sensed, the relative intensity of the signal is dependent upon the look angle, the relative position of the sensor with respect to the sun, meteorological conditions and other factors. With active sensors such as microwave radar, the power of the backscattered radiation is sharply reduced by the ripple-damped sea surface under the influence of the organic film.

In general, natural slicks appear slightly cooler than adjacent water surfaces when sensed by thermal infrared. Although the emissivity of a water surface is not altered by the presence of a monomolecular layer of organic material, the cool-surface effect is produced by an immobilizing of the near surface water by the "rigid" surface film, which inhibits convectional overturn of the surface water cooled by evaporation. Natural slicks are not expected to retard evaporation to a significant extent. Consequently, warm signatures of sea slick have not been observed, but the organic films appear cooler than the surrounding nonslicked water surface when measured by thermal radiometry.

TABLE 1. IMPACT OF NATURAL AND MAN-MADE SURFACE FILMS ON THE PROPERTIES OF THE AIR-SEA INTERFACE

SURFACE EFFECT OR PROCESS MODIFICATION	TYPE OF ORGANIC SURFACE FILM**		
	NATURAL	PETROLEUM	EXPERIMENTAL*
Capillary Wave Attenuation	++(10,13,14,38)	++(17)	++(2,27,28)
Gravity Waves	-(10)	?	++(2,27,28)
Breaking Wave Inhibition	?	?	++(2)
Gas Transport Reduction	-(17)	+(11,17,23, 24,33,37)	+(6,17,22,31)
Foam Stability	+(17)	+(17)	+(15)
Air Bubble Bursting	+(5,16)	+(17)	+(16,36)
Surface Temperature	++(9)	++(12,34)	++(21,30,31)
EM Reflection	++(4,7,32,39-41)	++(3,8,34,41)	++(2,16,26,29)
Light Transmission	?	++(20)	?
EM Emission	?	++(19,25)	++(1)

- Significant influence of surface film unlikely

+ Demonstrated in laboratory; field studies if any were inconclusive

++ Effect demonstrated by laboratory and field research

? Potential influence, but not proved by experiment

* A continuous, monomolecular film added to sea surface for research purposes

** Numbers in brackets correspond to entries in the bibliography.

TABLE 2. EFFECTS OF NATURAL ORGANIC SEASURFACE FILMS ON REMOTELY SENSED SIGNALS

<u>SEASURFACE EFFECT</u>	<u>SENSOR APPROACH - SPECTRAL REGION</u>	<u>INFLUENCE ON SIGNAL</u>
Capillary wave damping	Active reflectance - microwave radar	Reduced backscatter power
	Passive reflectance - UV, visible, near IR	Modified light reflectance
Inhibition of convective overturn at surface	Passive emission - thermal IR	Slicks appear cooler
Inhibition of wave breaking-Modified sea foam stability	Passive emission - microwave	Affects microwave brightness temperature
Reduced sea surface roughness	Passive emission - microwave	Reduced brightness temperature

Passive microwave sensors can detect sea foam and white water through a resulting increase of seasurface emissivity. Air bubbles and foam at the air-water interface are responsible for the passive microwave signals, while entrained air bubbles beneath the surface do not participate in the effect. Surface-active material modifies sea foam through several mechanisms. Organic films may resist wave breaking and also act to destabilize foams and bubbles once they reach the water surface. Water-soluble, surface-active materials, on the other hand, are foam stabilizers. The net effect of these opposing processes has not been determined experimentally at sea.

When petroleum spills or municipal effluents are present, thicker films are implicated in the production and modification of remotely sensible signals. In general the influences of petroleum films are similar to those of natural slicks, except for thermal IR sensors, to which a petroleum surface film may appear either cooler or warmer than adjacent clean water. The sensed IR signal may be due the modification of a number of possible physical effects, including emissivity, reflectivity, heat exchange, and inhibition of convectional overturn at the sea surface.

Petroleum spills may be sensed across a broad spectral range by numerous sensor systems. Because oil spills vary greatly in thickness and in their physical and chemical characteristics, the portion of the spill sensed varies according to the sensing system used for observation. For example, microwave radar senses the entire area affected by the oil in which the capillary wave

structure is diminished, whereas dual-frequency, passive microwave radiometry senses only the thicker layers of the spill and can be used to determine spill volume and locate significant quantities of oil to guide spill-removal operations. Table 3 reviews the types of false signals encountered when various sensors are used to detect petroleum slicks on the sea. Both natural surface films and other pollutants may be incorrectly identified as petroleum by many remote sensing systems. The use of multi-spectral sensing is sometimes required to avoid ambiguities.

TABLE 3. OIL SPILL DETECTION BY REMOTE SENSING*

<u>SENSOR APPROACH</u>	<u>SPECTRAL REGION</u>	<u>FALSE ALARMS</u>
Active reflectance	Microwave radar, 1-5cm	Natural organic slicks Wind slicks, ship wakes Pollutant organic slicks (detergents, sewage sludge) Kelp/debris Dense cloud cells Unrippled water under calm conditions
	UV, <0.4 μ m	Natural organic slicks Suspended solids
	Visible, 0.4-0.65 μ m	Natural organic slicks Pollutant organic slicks Suspended solids Shallow water Broken cloud deck
	Near IR, >0.65 μ m	Natural organic slicks Other pollutant slicks
Passive emission	Thermal IR, 3-14 μ m	Natural organic slicks Pollutant organic slicks Ship wakes Thermal discharges and effluents Upwelling
	Microwave, 0.2-1cm	Foam patches Kelp/debris Dense cloud cells

* Adapted from Maurer and Edgerton, 1975

In most instances sea truth must be determined if remotely sensed data are to be correctly interpreted. For example, negative seasurface return of side-looking microwave radar signals may be due to the following sea truth situations in which capillary waves are either diminished or absent: (1) zones of calm where no organic film is necessarily involved; (2) hydrodynamic damping in a ship's wake; (3) wind slicks; (4) natural sea slicks caused by organic films which attenuate and resist the formation of capillary waves; and (5) thicker layers of wave-damping petroleum oils or other organic film-forming pollutants.

FREQUENCY AND DISTRIBUTION OF BIOGENIC SEA SURFACE FILMS

To understand the importance and significance of biogenic films to both basic and applied scientific problems, it is essential to know the extent of the sea surface under their influence; i.e. their frequency and distribution, both spatially and temporally. The lifetime and fate of natural and petroleum slicks in the marine environment have been related to a number of dispersive processes (Garrett, 1972; NAS, 1985). Because of the great influence of wind and waves, the probability of encountering slicks or persistent oil films in the open ocean may be related to average wind conditions such as those depicted in Figure 2 (January) and Figure 3 (July). These figures are based on data from the U.S. Navy Marine Climatic Atlas of the World. The numbers on the figures represent the percentage of time that winds are 7 knots (3.6 m sec^{-1}) or less, a condition under which natural surface films are stable enough to be visible through their capillary wave damping effects and their resistance to wind-generated ripples and surface turbulence. The shaded areas are zones of the world ocean where winds are 10 knots (5.1 m sec^{-1}) or less 50% of the time. The shaded area represents a rough measure of the potential for slick development and persistence when the surface concentration of film-forming material is sufficiently high.

For example, in January (Figure 2) meteorological conditions in the North Atlantic and Pacific Oceans would normally preclude the persistence of coherent organic films while a broad band from the equator to approximately 40 degrees south latitude is relatively calm and has the potential for slick formation and endurance. In the Northern Hemisphere in summer (Figure 3), relatively low-wind conditions exist in regions of the northern seas, the Mediterranean, and in certain zones along the Tropic of Capricorn.

It is emphasized that these figures represent wind velocity regimes and are not actual sea-slick data. While charts of this kind do not guarantee the existence of sensible surface films, they are a device to predict the probability of their occurrence. Furthermore, these wind-probability diagrams can be useful in predicting the longevity of petroleum spills and the lifetimes of surface pollutants from rivers and municipal dump sites, as the



Figure 2: Wind velocity regime - January. Cross-hatched areas have winds of 10 knots (5.1 m sec^{-1}) or less 50% of the time. Numbers are percentage of time that winds are 7 knots (3.6 m sec^{-1}) or less.



Figure 3: Wind velocity regime - July. Cross-hatched areas have winds of 10 knots (3.1 m sec⁻¹) or less, 50% of the time. Numbers are percentage of time that winds are 7 knots (2.5 m sec⁻¹) or less.

same processes which disperse natural slicks operate to transport pollutants from the water surface into the atmosphere and into the underlying water column.

Primary Productivity

The existence of natural slicks is also related to the biological productivity of a particular area, since they are formed from surface-active, organic substances of biogenic origin. Natural slicks may form anywhere in the unfrozen ocean if winds are sufficiently calm.

The primary biological producers in the sea are algae and some bacteria, organisms which are capable of synthesizing high-energy organic materials from inorganic compounds. The energy required for this biological synthesis is primarily photic, no energy being derived from organic compounds by the primary producers. Thus, although primary production is not an exact measure of the organic content of seawater, high productivity corresponds to fertile oceanic areas where the levels of organic substances available for natural slick formation are also high. Other biological producers, secondary (herbivorous) and tertiary (carnivorous), are involved in organic chemical production. Of these, secondary production by herbivorous zooplankton is the more important, but is usually small in comparison with primary production. Because of these factors, the distribution of primary production in the world ocean, Figure 4, will be used as a measure of the potential for slick formation for a particular marine region. Figure 4 in conjunction with figures 2 and 3 (average wind conditions) can be used to estimate the likelihood of natural organic films at a particular location.

It should be noted that Figure 4 represents primary production in mg C/m²/day averaged on a yearly basis and does not indicate seasonal variations. Primary production by photosynthesis is influenced by (1) the quantity of light energy available to the organisms, and (2) the availability of inorganic nutrients. Seasonal effects are most pronounced at higher latitudes, especially in polar regions, due to large differences in photic levels between winter and summer. In polar regions ice cover attenuates light penetration and may further reduce production even during the short vegetative period.

In other regions of the oceans primary production is determined largely by nutrient levels, and it may or may not be seasonally variable. In general, the nutrition factor favors productivity on continental shelves, slopes, and in upwelling regions due to enhanced vertical transport and mixing and to nutrient inputs from continental sources. Highly productive upwelling areas in the Pacific Ocean include the near coastal waters of Central and South America, Japan, Canada, and the Kamchatka Peninsula. In the Atlantic Ocean productive upwelling regions exist off West Africa, northeast Brazil and the southeast coast of South America. Other areas of high productivity include the Bering Sea, portions of the Indian Ocean affected by monsoon

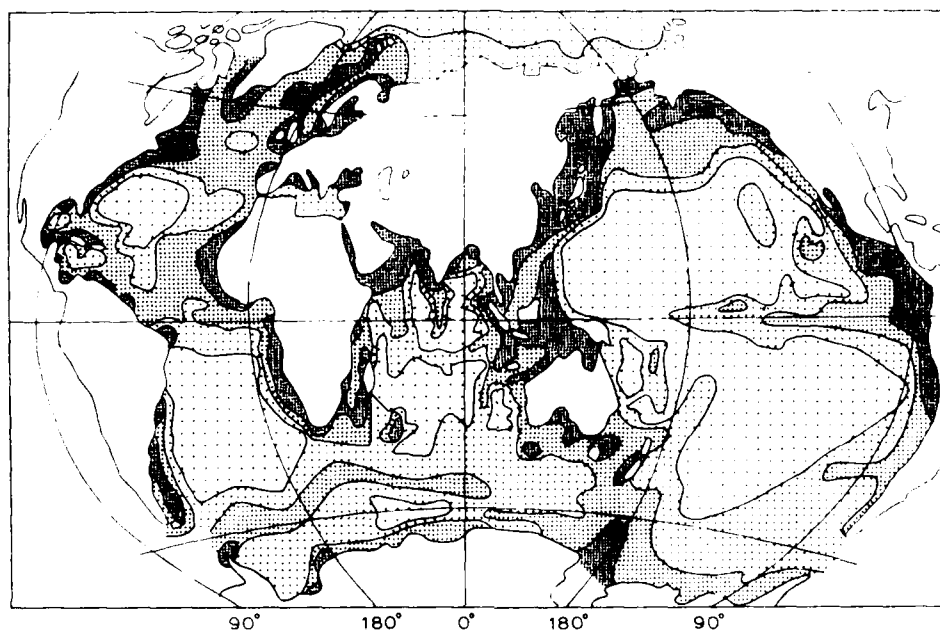


Figure 4: Distribution of primary production in the world ocean.
From Parsons et al. (1977); reproduced with the permission
of the author.

winds, and the coastal areas of seas, gulfs, and bays. In open-ocean waters away from continental sources of nutrients, upwelling is essential for the stimulation of primary productivity. Examples of such regional processes leading to upwelling include the Equatorial and Antarctic divergences, polar fronts, and zones of winter convectional mixing.

In general, the potential for slick formation based on biological productivity is greatest in coastal areas and outside the region bounded by the north and south 40-degree parallels. For certain ocean areas productivity and air-sea dynamics sometimes operate in opposition to one another for the prediction of slick probability. For such cases, the dispersive effects of wind and waves will predominate in the determination of slick-forming potential.

In most instances, the true condition of the sea surface must be known if remotely sensed data are to be correctly interpreted. For example, the backscatter of microwave radar signals may be affected by any of the following events at the sea surface which diminish capillary waves: (a) zones of calm where no surface film is necessarily involved; (b) hydrodynamic damping in the wake of a ship; (c) wind slicks; (d) natural sea slicks caused by organic films which attenuate capillary waves and resist their formation; and (e) thicker layers of wave-damping petroleum oils or other organic film-forming pollutants. Other active and passive sensors used for the detection of oil on water also are subject to a number of possible false signal sources (Table 3). Conversely, sensor response to organic films on the sea, both natural and man-made, may be confused with other information being sought by remote sensing systems. Thus, it is essential to identify the ocean regions where organic films are prevalent so that possible interference with the interpretation of signals received by remote sensing systems can be taken into account.

RECENT SPACE-DERIVED IMAGERY OF SEA SURFACE FILMS

In recent years hand-held photographs taken from spacecraft have depicted a number of interesting, and in some cases, unexpected sea surface features. These include sub-mesoscale spiral eddies with diameters of 25 kilometers and less, ship tracks, and petroleum oil films from ships, oil-well blowouts or natural seeps. Such features are more evident in sun-glint photography where they are highlighted by slick-like sea surface effects which produce light reflectance anomalies. Space Shuttle mission 41-G was dedicated in part to a photographic survey of oceanographic phenomena. The mission produced numerous photographs of these glint-illuminated phenomena indicating that they were not merely an occasional event, but were of broad extent over several portions of the world ocean.

The highly structured sea surface patterns enhance the visibility of the spiral eddies, ship tracks, and other surface/subsurface events. Consequently, the physical and/or

chemical mechanisms responsible for the sea surface reflectance patterns are of great interest and importance. These surface patterns appear not only in optical, but also in synthetic aperture radar imagery from the Shuttle Orbiter (Kaltenbach et al., 1984). Negative (reduced) backscatter of light or radar signals may be attributed to sea surface areas where the capillary or short-gravity wave fields have been attenuated by natural or pollutant organic films, while areas of higher backscatter represent a free-surface or ambient sea condition. Although physical processes such as wind or current may produce local modulations of the small-wave field, the appearance, distribution and texture of the slick-like patterns are more suggestive of organic films, scums or oily layers, all of which are well known to attenuate and resist the formation of capillary and short gravity waves.

Determination of the organic surface film involvement in the surface reflectance patterns will eventually require coordinated sea truth experiments in conjunction with aircraft and space sensing. The organic films may be (1) monomolecular layers of biogenic surface-active material, (2) a highly compressed multilayer of films, scums and foam, or (3) a thicker layer of anthropogenically mobilized petroleum oil. It is possible to distinguish between these various forms of organic films by surface measurements and observations, with supporting information supplied from airborne thermal infrared and microwave radiometric and radar sensing systems.

BIBLIOGRAPHY

1. Alpers, W., H. J. Blume, W. D. Garrett, and H. Huhnerfuss, 1982. The effect of monomolecular surface films on the microwave brightness temperature of the sea surface. Int. J. remote Sensing, 3: 457-474.
2. Barger, W. R., W. D. Garrett, E. L. Mollo-Christensen and K. W. Ruggles, 1970. Effects of an artificial sea slick upon the atmosphere and the ocean. Journal of Applied Meteorology, 9: 396-400.
3. Beard, J. T. and J. A. Wiebelt, 1966. Reflectance of film covered water surfaces as related to evaporation suppression. Journal of Geophysical Research, 71: 3835-3841.
4. Beard, J. T. and J. L. Gainer, 1970. Influence of solar radiation reflectance on water evaporation. Journal of Geophysical Research, 75: 5155-5163.
5. Blanchard, D. C., 1978. Control of jet-drop dynamics by organic material in seawater. Journal of Geophysical Research, 83: 6187-6191.

6. Blank, M., 1962. The permeability of monolayers to several gases. In: Retardation of Evaporation by Monolayers: Transport Processes (ed. by V. K. La Mer), Academic Press, pp. 75-95.
7. Brown, W. E., C. Elachi and T. W. Thompson, 1976. Radar imaging of ocean surface patterns. Journal of Geophysical Research, 81: 2657-2667.
8. Catoe, C. E. and F. L. Orthlieb, 1971. Remote sensing of oil spills. Proceedings of the Joint Conference on Prevention and Control of Oil Spills, American Petroleum Institute, Washington, D.C., pp. 71-84.
9. Clark, H. L., 1967. Some problems associated with airborne radiometry of the sea. Applied Optics, 6: 2151-2157.
10. Davies, J. T. and E. K. Rideal, 1963. Interfacial Phenomena, Academic Press, pp. 266-274.
11. Downing, A. L. and G. A. Truesdale, 1955. Some factors affecting the rate of solution of oxygen in water. Journal of Applied Chemistry, 5: 570-581.
12. Estes, J. E. and B. Golomb, 1970. Oil spills, method for measuring their extent on the sea surface. Science, 169: 676-678.
13. Ewing, G., 1950. Slicks, surface films and internal waves. Journal of Marine Research, 9: 161-187.
14. Garrett, W. D., 1967. Damping of capillary waves at the air-sea interface by oceanic surface-active materials. Journal of Marine Research, 25: 279-291.
15. Garrett, W. D., 1967. Stabilization of air bubbles at the air-sea interface by surface-active material. Deep-Sea Research, 14: 661-672.
16. Garrett, W. D., 1968. The influence of monomolecular surface films on the production of condensation nuclei from bubbled seawater. Journal of Geophysical Research, 73: 5145-5150.
17. Garrett, W. D., 1972. Impact of natural and man-made surface films on the properties of the air-sea interface. In: The Changing Chemistry of the Oceans (ed. by D. Dyrssen and D. Jagner), pp. 75-91.
18. Garrett, W. D. and W. R. Barger, 1980. Experimental sea slicks in the MARSEN (Maritime Remote Sensing) exercise, Naval Research Laboratory Report #8454, 18 pp.

19. Garrett, W. D. and P. M. Smith, 1984. Physical and chemical factors affecting the thermal IR imagery of ship wakes. Naval Research Laboratory Memorandum Report 5376, 24 pp.
20. GESAMP, 1977. IMCO/FAO/UNESCO/WNO/WHO/IAEA/UN Joint Group of Experts on the Scientific Aspects of Marine Pollution (GESAMP). Impact of Oil on the Marine Environment. Reports and Studies GESAMP No. 6, 250 pp.
21. Grossman, R. L., B. R. Bean and W. E. Marlatt, 1969. Airborne infrared radiometer investigation of water surface temperature with and without an evaporation-retarding monomolecular layer. Journal of Geophysical Research, 74: 2471-2476.
22. Hawke, J. G. and A. E. Alexander, 1962. The influence of surface-active compounds upon the diffusion of gases across the air-water interface. In: Retardation of Evaporation by Monolayers: Transport processes, (ed. by V. K. La Mer), Academic Press, pp. 67-73.
23. Heymann, E. and A. Yaffe, 1942. The stability of multimolecular films of hydrocarbon oils, containing spreaders, on water surfaces. Transactions of the Faraday Society, 38: 408-417.
24. Heymann, E. and A. Yaffe, 1948. The equilibrium spreading coefficient of amphipathic organic liquids on water. The Journal of Physical Chemistry, 49: 239-245.
25. Hollinger, J. P. and R. A. Menella, 1973. Measurement of the distribution and volume of sea surface oils using multi-frequency radiometry. Science, 168: 245-246.
26. Hühnerfuss, H., Alpers, W., Cross, A., Garrett, W. D., Keller, W. C., Lange, P. A., Plant, W. J., Schlude, F., and Schuler, D. L., 1983. The modification of X- and L-band radar signals by monomolecular sea slicks. Journal of Geophysical Research, 88: 9817-9822.
27. Hühnerfuss, H., Alpers, W., Garrett, W. D., Lange, P. A., and Stolte, S., 1983. Attenuation of capillary and gravity waves at sea by monomolecular organic surface films. Journal of Geophysical Research, 88: 9809-9816.
28. Hühnerfuss, H., Alpers, W., Jones, W. L., Lange, P. A., and Richter, K., 1981. The damping of ocean surface waves by a monomolecular film measured by wave staffs and microwave radars. Journal of Geophysical Research, 86: 429-438.
29. Hühnerfuss, H., and Garrett, W. D., 1981. Experimental sea slicks: their practical applications and utilization for basic studies of air-sea interactions. Journal of Geophysical Research, 86: 439-447.

30. Jarvis, N. L., 1962. The effect of monomolecular films on surface temperature and convective motion of the water/air interface. Journal of Colloid Sciences, 17: 512-522.
31. Jarvis, N. L., C. O. Timmons and W. A. Zisman, 1962. The effect of monomolecular films on the surface temperature of water. In: Retardation of Evaporation by Monolayers: Transport Processes (ed. by Academic Press), pp. 41-56.
32. Kaltenbach, J. L., M. R. Helfert, and G. L. Wells, 1984. The view from the Shuttle Orbiter - observing the oceans from manned space flights, Proc. SPIE 489, ocean Optics VII., pp. 203-207.
33. Liss, P. S. and F. N. Martinelli, 1978. The effect of oil films on the transfer of oxygen and water vapor across an air-water interface. Thalassia Jugoslavica, 14:215-220.
34. Maurer, A. and A. T. Edgerton, 1975. Flight evaluation of U.S. Coast Guard airborne oil surveillance system. Proceedings of Conference on Prevention and Control of Oil Pollution, American Petroleum Institute, Washington, D.C., pp. 129-141.
35. NAS, 1985. Oil in the Sea: Inputs, Fates, and Effects, National Academy Press, Washington, D.C., 601 pp.
36. Patterson, M. P. and K. T. Spillane, 1969. Surface films and the production of sea-salt aerosol. Quarterly Journal of the Royal Meteorological Society, 95: 526-534.
37. Powell, R. W., 1943. The influence of surface films of oil on the evaporation of water. Transactions of the Faraday Society, 39: 311-318.
38. Scott, J. C., 1972. The influence of surface-active contamination on the initiation of wind waves. Journal of Fluid Mechanics, 56: 591-606.
39. Scully-Power, P., J. Hughes and W. T. Aldinger, 1985. Navy Oceanographer Shuttle Observations, STS 41-G, Quicklook Report, Navy Underwater Systems Center Technical Document 7379.
40. Soules, S. D., 1970. Sun glitter viewed from space. Deep-Sea Res. 17: 191-195.
41. Vesecky, J. F. and R. H. Stewart, 1982. The observation of ocean phenomena using imagery from the SEASAT synthetic aperture radar: an assessment. Journal of Geophysical Research, 87: 3397-3430.
42. Parsons, T. R., M. Takahashi, and E. Hargrave, 1977. Biological Oceanographic Processes. Pergamon Press, Oxford.

Surface Films in Oceanography

John C. Scott

Ocean Sciences Division
Admiralty Research Establishment
Southwell
Portland
Dorset DT5 2JS

Abstract

This paper considers a wide range of interpretation problems concerning the mechanical properties of surface films in the oceanographic context: wave damping and wind-wave suppression; remote sensing effects, infra-red, microwave and visible; film distribution mechanisms; the use of films as surface markers; and the oceanographic relevance of film pattern observations. Some results are reported from recent observational trials, in which surface films were used as ocean markers.

1. Introduction

For centuries it has been appreciated that a surface film, spread on a water surface, can damp out water waves [1]. The two earliest effects reported were the reduction of wave breaking [2], and the improvement of the light-transmitting properties of a wind-blown surface [3].

The first effect is almost certainly due to the reduction of the aerodynamic roughness of the waves by the surface film, which stabilizes the wind-blown surface against the formation of the ripple and longer wave roughness.

The case for this is argued in [4], although it is there pointed out that no definitive experiment at sea has yet been done to verify the hypothesis. The principal direct evidence, as opposed to indirect inference from laboratory work, is the repeated testimony of mariners, who went on record in the eighteenth and nineteenth centuries to credit their own lives to this effect, having been saved at sea [1,4]. Regrettably, this evidence is open to the charge of bias, since mariners who found that oil did not prevent the breaking of dangerous waves were rather less likely to make a subsequent dissenting contribution to the argument.

Although the case seems nevertheless quite sound, it should be realised that the modern explanation barely differs from that usually attributed to Aristotle [2], and is quite close to that given by Benjamin Franklin, in 1774 [5].

The optical effect of a film, by which shallow water divers are supposed to improve the illumination of the sea bed by spreading oil

on the surface above them [5], is almost certainly to do with the steadying influence of the oil on the surface, the human eye being distracted by the moving, flickering light patterns focussed by surface ripples. Any significant effect on the average level of illumination is probably negligible.

Ancient though they are, these two examples are significantly related to the physics of the two most important of the topics of interest today: effects of films on the air/sea interaction, and on the visibility (or imageability) of sub-surface oceanic motions.

This paper will review briefly the physical mechanisms associated with surface film effects, and will attempt to draw together several recent oceanographic observations, including some recent work of the author involving man-made surface films.

2. The Physical Properties of Surface Films

The first important thing about surface films is the obvious one, that they reduce the surface tension of the water surface, becoming adsorbed [6]. Until the surface becomes saturated with added surface film material, the surface tension will decrease steadily as the surface concentration of material is increased.

It is well known that surface tension acts, along with gravity, to determine the propagation speed of water waves, and that its relative effect increases as the wavelength decreases. The gravitational effect and the surface tension effect become equal for a wavelength around 17mm, and waves of shorter wavelength are often called capillary waves, following the now obsolete term for surface tension, capillarity.

Reducing the surface tension would thus be expected simply to reduce the phase speed of waves, and indeed it does. However, when we turn to theoretical estimates of the damping of free progressive waves on liquids, we find that the surface tension itself has only a small effect, hardly significant in the oceanographic context.

What proves to be important in surface film effects is rarely the mean surface tension of the surface. What is far more important is that the surface tension varies as the surface is compressed and extended mechanically. Propagating waves regularly extend and compress the surface, and this variation in surface tension is seen as an elasticity - a dilatational elasticity - tending to oppose the wave motion.

This elasticity, being a direct consequence of the fact that surface tension decreases as a film is compressed, is present in all films. Lucassen-Reynders and Lucassen [7] have provided a thorough introduction to the theory of ripple propagation including dilatational elasticity effects, and Lucassen [8] has extended this treatment to longer wavelength waves. The foundations of the theory

were laid by Lamb in 1895 [9], although the significance of its results was not fully appreciated until the middle of this century.

Dilatational elasticity, being universal to surface films, is arguably the most important film parameter. Other influences do exist, however, and some have been found to be important.

If the film material is soluble, then the surface forms a continuously adjusting dynamic equilibrium with the underlying bulk solution, and the effects of extension and compression are modified by material exchange [10,11,12]. Such an effect appears as a dilatational viscosity, tending to reduce the surface elastic effect at low wave frequencies. If the adsorbed molecules require some finite time to adjust to their final surface configuration, this can increase the elastic effect at high wave frequencies, again contributing to the dilatational viscosity. Another way of looking at this dilatational viscosity is as the imaginary component of a single complex dilatational elastic modulus.

There is also a shear counterpart to the dilatational modulus, related to in-plane shearing motion of the film. In at least some surface-active materials, this has been indicated to make a significant contribution to wave damping, since the wave-induced compression and extension also involves some shear. Huhnerfuss and his co-workers [13] have demonstrated the importance of shear viscosity in some of the organic materials which act most strongly as wave damping agents. Huhnerfuss has also developed a relatively simple method of measuring a form of surface viscosity parameter [14] which indicates the presence of significant differences between these materials.

Ting et al. [15] have provided data on the relative magnitudes of dilatational and shear parameters in the case of octanoic acid.

Analytically speaking, these two complex moduli are sufficient for the full description of linear surface dynamics. Any additional mechanisms, involving more complex molecular interactions at the surface [16], should in all cases be resolvable into shear and dilatational components.

3. Wave Damping and Wind Waves

So far, this discussion has looked only at freely propagating water waves. For these, it is now firmly established that the existence of a surface dilatational elasticity significantly modifies the wave motion. The resistance of the elastic surface to compression and extension by the propagating wave completely changes the free surface boundary condition for the classical hydrodynamic equations [7,9], and leads to energy dissipation in a viscous boundary layer, akin to that found adjacent to a rigid wall, or (more appropriately) that adjacent to an inextensible (but flexible) membrane.

One of the more interesting results of the hydrodynamic analysis is that it predicts the existence of a second propagating wave mode, one which can occur only when the dilatational elasticity is non-zero. This second mode is often called the Marangoni wave, after the distinguished nineteenth-century Italian Carlo Marangoni, who played a major part in laying the foundations for our modern knowledge of surface elastic effects. It is essentially an in-plane (longitudinal) wave motion, similar to that obtained when a thin elastic membrane is tugged at one edge.

A second feature of classical hydrodynamic theory is that, as the dilatational elasticity is increased from zero (clean surface) up to inextensibility, the wave damping passes through a maximum value, about twice that predicted for an inextensible film [7,17]. This theoretical result has been amply verified experimentally [7]. The maximum value is found to occur at a particular value of dilatational elasticity; a value for which the longitudinal (Marangoni) wave propagates at the same phase speed as the transverse wave.

Both longitudinal and transverse (normal) surface waves freely propagate away from their place of generation, unless acted on further by external forces.

A more relevant wave situation in the oceanographic context is that of the generation of wind waves. A shear flow is present in the adjacent air, and the water boundary is unstable to wave-like perturbations. If we begin, as before, looking simply at the effect of surface tension itself, we find that reducing the surface tension is actually likely to destabilize the surface [see, for example, 19,20]. The dilatational elasticity, however, positively stabilizes the surface [21,22], and this therefore significantly reduces wind-wave growth. This is evidently the mechanism which explains the stilling effect of surface films on exposed, wind-blown surfaces, and the effect is a major one, as may easily be verified with a small quantity of cooking oil or detergent on any exposed water surface.

It should be pointed out here that wind-wave tank experiments reported by Arkharov et al. [23] found that surface-active materials actually enhanced the wave generation process at a wind speed of 12m/s. There is no easy way of reconciling this result with the rest of the reported observational data, and it may be wise to treat this as an anomalous result, until it may be supported independently.

When a wind begins to blow across a still, clean water surface, the first waves generated are ripples, of wavelength around 20mm. As these ripples propagate downwind they grow, in both amplitude and wavelength, taking energy from the wind in the process. A surface-active film stabilizes the surface, so that a higher wind speed is needed to generate waves. For some wind speeds, no waves at all may be generated [24].

On a film-free ocean surface, the waves develop steadily, increasing in amplitude and wavelength, and eventually we observe fresh ripples being generated on the backs of the longer waves.

In a fully developed sea, well away from land, when the wind has been blowing for some considerable time, the wave field includes a long wavelength swell. As soon as these swell waves become reasonably large, the wind begins the generation process again, on the exposed areas of the swell waves, and the wave field becomes an essentially random mixture of swell, shorter waves and ripples, with aerodynamic roughness covering a wide range of length scales.

If the wind is constant, the swell propagation direction is aligned with the wind. However, it is a matter of common experience that the shorter waves, particularly the ripples, are only approximately aligned relative to the swell waves. This appears to be associated with the 'short-crested' nature of these shorter waves, and also with spatial variability in the essentially turbulent lower atmosphere.

Swell waves moving into a film covered region are apparently almost unaffected in amplitude, but are made smoother, both aerodynamically and electromagnetically, by the suppression of fresh wind-ripples and the longer waves into which they develop. On moving out of the film region once more, the swell waves once more develop a covering of growing ripples.

4. Breaking Waves

The short waves generated on the backs of the longer waves determine the energy transferred from the wind to these waves [25]. A wave of given wavelength in deep water is restricted in the height it may reach, and if energy is being added at a greater rate than can be accommodated by viscous damping and wave growth, then the wave will break, the excess energy being lost in the turbulent motion of a spilling crest or forward-falling jet.

Thus, it is possible that even a spilling breaker of great height may be reduced to safe behaviour if the energy input can be 'turned off' by suppressing the ripples and shorter waves, and thereby reducing its aerodynamic roughness. A clear indication of this is given in the observations of Toba and Kunishi [26] for smaller breaking waves. It is expected that this is the essential mechanism involved in the reduction of dangerous seas by oil-pouring [1,4]. A review of surface film effects relevant to breaking waves is given in [27].

5. Wind Speed Effects on Surface Films

Surface films are physically moved along the surface by the wind stress, and by mass transport associated with second-order wave stresses [28- 30]. This effect, combined with the extension and compression of the film associated with the wind wave motion, is

likely to cause breakdown of the integrity of the film, and small-scale mixing of the surface film with the underlying water. Even insoluble organic materials may be completely dispersed in the water bulk by this means.

Surface film effects are certain to be limited to the lower wind speeds by this effect, and this is, indeed, common experience. It is even possible that at high sustained wind speeds, the sea surface is surface chemically cleaner than any other water surface, outside the laboratory.

Estimates of the upper wind speed limit for surface film effects are difficult to provide, and indeed they are certain to depend on both the chemical composition of the film and the temperature of the surface microlayer. Some laboratory measurements have indicated that films are unlikely to survive for long at wind speeds (close to the surface) greater than about 6m/s (about 12 knots) [31]. This figure seems reasonably well supported by other experiential evidence. It is possible, however, that film effects may persist for longer, at higher wind speeds, in regions where film materials are being concentrated by some form of oceanic convergence. Numerical estimates of film endurance are not possible at present.

Film forming materials will be mixed deep within the upper ocean boundary layer by plunging breakers, turbulence, and organized wind-driven convection systems such as Langmuir circulations. When the wind ceases, the dispersed material will slowly re-appear at the surface, carried thence by rising bubbles, storm-generated turbulence in the surface layers, and by molecular diffusion. Thorpe [32,33] has reviewed such oceanic processes.

6. Remote Sensing Effects of Surface Films

6.1 Effects on Surface Emissions

Films may have significant effects on both passive and active techniques of oceanographic remote sensing. They are found to affect the electromagnetic emissions of a surface at microwave frequencies, and possibly also at infra-red. Alpers et al. [34,35] report microwave radiometer measurements at 1.43 and 2.65GHz which indicate that an oleyl alcohol film may have an effect on the molecular structure of the surface microlayer below the chemical film. Other molecular effects of a surface skin could include modification - perhaps as a barrier - of the evaporation characteristics of the surface, and this would also be expected to change the radiometrically sensed surface temperature [36]. Effects on radiation due to other effects, such as swell, ripples, and foam are reviewed by Shutko [37].

Other possibilities arise from the wave damping properties of the film. Changes induced in the structure of the near-surface boundary layer by a reduction in aerodynamic roughness may affect evaporation.

6.2 Reflection (Sunglint) Images

An imaging system that is sensitive to visible radiation will detect the direct solar radiation reflected by the ocean, in the absence of cloud. If the ocean were flat, then only a single specular image of the sun would be recorded, as a brilliant, sharply defined mirror image. The sea is never so smooth, and the reflection observed covers a large (roughly circular) area. Facets of the surface both within and outside the mirror image region will be able to contribute to the sunglint image, or not, depending on their surface slope and orientation relative to the sun and the observer.

The NOAA satellite images include, in their visible wavelength channel, a wide swath of sunglint. Observations relating the images observed in this way with infra-red emission images, and with other oceanographic data, are reported by La Violette et al. [38]. The mechanisms involved in sunglint were established in 1954, by Cox and Munk [39-41], including some observations on the visibility of oil slicks.

These satellite images have a horizontal resolution about 1km. More detailed images have more recently been made available, as a result of manned spacecraft. The photographs made by Scully-Power in 1984, from the Space Shuttle 'Challenger' [42], have shown that the observational power of sunglint imagery increases dramatically with finer resolution. The detail shown on many of the images obtained by Scully-Power shows widespread evidence of sub-mesoscale surface features, and the only reasonable explanation for their visibility is through the effect of surface films on the surface roughness.

Cox and Munk clearly demonstrated that a reduced-amplitude wind-wave spectrum would have the observed effects on the sun's reflected image, and there is no reasonable alternative explanation for the patterns which is tenable for all the images obtained [43]. Wind distribution effects, such as those observable in some SEASAT radar images, typically involve longer horizontal scales than are seen in the sunglint images.

Apart from space shuttle observations, there are very few opportunities for good-quality high resolution images of the ocean surface. Sheres et al. [44] have recently reported one interesting case, in which photographs taken from a high-flying aeroplane were able to resolve refraction in swell waves off the coast of California. In these observations, a slick area was observed in the region of greatest horizontal shear, an observation of considerable relevance for the interpretation of recent shuttle images.

The surface slopes associated with wind-generated ripples are generally greater than those found with longer (gravity-dominated) waves, angles greater than 30 degrees being commonplace, even in gentle winds. Thus the well-understood dependence of sunglint on surface slope allows the imaging technique to be sensitive to a wide range of sea-surface conditions.

6.3 Imaging Radar Systems

Microwave pulses are scattered by the sea surface, which has roughness in the same order of length scales as the microwave wavelength. If the backscatter, as a function of position on the surface, is used to form an image, then spatial variations of the roughness will be imaged. This is the principle of the sideways-looking airborne radar (SLAR) or real-aperture radar, which has been able to detect oceanic features such as internal waves.

Only surface roughness variations are detected in SLAR, in contrast to the imaging mechanisms of SAR (Synthetic Aperture Radar), which also involve the motion of the scatterers relative to the radar. The considerable advantage of SAR over SLAR is that it allows a horizontal resolution of the order of 10m with antennae of practicable size. The L-band system carried by SEASAT showed the enormous potential of SAR for imaging oceanographic features. Even though the imaging mechanisms are presently little understood, several spaceborne SARs are planned for the near future.

Scatterometry is another active radar technique which responds to variations in surface roughness, although it does not produce images of the surface. The scattered returns are processed to give roughness data which is found to correlate extremely well with wind speed.

Surface-active films act directly to reduce the amplitude of surface waves in a wavelength region highly relevant to microwave scattering. Their immediate effect on wind-wave generation is principally in the surface wavelength range 20mm to 50mm, a range directly relevant to X-band radar (wavelength 24 to 37.5mm). However, as was indicated above, it is these ripples which develop quickly into longer surface waves, of wavelength better matched to the scattering of the longer wavelength radars, such as C-band (37.5 to 75mm) and L-band (230mm). A considerable amount of work has been done on the effects of surface films - both surface-active chemical films and mineral oil films - on radar backscatter [45-49].

It is important to realise that surface film effects are not the only mechanisms capable of modulating the surface wave spectrum in a radar imageable way. Surface currents can also affect the spectrum seen by the radar, both through modulating (straining) the spatial periodicity of existing waves and also through wave-wave interactions. The efficiency of wind-wave generation may additionally be modified, if the currents are with or against the wind direction. Surface modulation mechanisms are reviewed from the point of view of SAR by Rufenach et al [50].

Another hydrodynamic effect capable of affecting wave spectra is turbulence. It is commonly observed that turbulence at the surface, due to ship waves or to upwelling of water from deeper regions produces a smooth patch in otherwise wave-covered water. The turbulence appears to prevent the organised wave motion from persisting or developing in these regions. It should be remembered,

though, that any such turbulence, from whatever cause, may aid the transport of surface-active material from the bulk water to the surface, where it may become adsorbed.

It would perhaps be expected that surface film effects on imaging radars would be more dependent on radar wavelength than surface current and surface straining mechanisms. Films would be expected to have an immediate effect on wind-waves in the X-band region, say, but a smaller, relatively delayed effect on waves in the L-band region.

The mechanisms by which the wavy water surface is imaged by radar are by no means clear, particularly in the case of synthetic aperture radar. Although several likely mechanisms have been proposed, it has not been possible to test them adequately, because there are presently no means of measuring the necessary parameters of the surface wave field. Reliably accurate wave measurements for wavelengths less than 0.5m are presently impossible in the open sea, except close to fixed platforms such as towers, and these may interfere aerodynamically with the wind-wave generation process.

At best, time series data is measured, and this is of doubtful value for relating to radar images, which are more concerned with instantaneous spatial distributions than temporal distributions. Techniques such as stereo photography are more appropriate, if less convenient, and there is a present trend towards developing such techniques.

The lack of adequate experimental verification is a serious obstacle to progress in radar imaging, made more difficult by the expense presently involved in deploying imaging radars, and then processing their data.

Another potential factor in SAR imaging which is difficult to quantify is that of foam from breaking waves. At wind speeds as low as 8 m/s, in the open ocean, quantities of white foam can be observed being dragged, bubbling, away from the crests of swell waves, and moving down the forward wave slope considerably faster than the wave speed, by as much as 0.5 m/s. Such moving scattering entities may have their own contribution to SAR image contrast. Since foam stability is strongly influenced by surface-active materials, there is a potential surface film influence through this mechanism. Wave breaking itself, even without foam, also leads to redistribution of the energy of the wave field towards the shorter wavelength region.

7. Film Distribution on the Ocean Surface

7.1 Surface and Above-Surface Mechanisms

So far, this paper has considered only the effects of films on the wave properties of the surface, and the consequences of these effects for the various techniques that are capable of imaging the

wave properties. Another major area of difficulty in our understanding of oceanic surface film effects concerns the way in which the films come to be arranged in the uneven distributions which are imaged.

In the absence of any external influence (such as wind and currents), surface-active material will spread until the surface tension is constant, everywhere over the surface. In practice, the horizontal stresses associated with water currents, and wind and wave stresses on the surface are sufficiently large compared with the horizontal spreading stresses that this uniform distribution arises only when winds are very light, and the seas calm. Perhaps the phrase 'glassy calm' was coined for such conditions.

Several mechanisms have been identified which could result in the uneven distribution of films on the open sea. With perhaps a single exception, that of internal waves, these mechanisms are poorly understood.

Film material, otherwise uniformly spread, will accumulate wherever there is a convergent surface flow. This may be in the adjacent air, an updraught having a convergent flow at the surface. Stommel [51] reported surface streaks, parallel with the wind, which adjusted to changing wind conditions faster than would be expected if water motion were involved. Such patterns are likely to correspond to circulations in the air. Gerling [52] reports SAR and scatterometer data from SEASAT which indicate the presence of atmospheric roll vortices which influence the wave patterns on the sea surface.

Barger et al. [53], and Kuznetsov and Panin [54] describe measurements of the wind structure over waves, and indicate differences associated with the presence of surface slicks.

On the surface itself, the surface waves have horizontal radiation stresses associated with them [55], and, as noted above, the stress exerted on the surface by the wind is strongly dependent on the surface roughness.

If any one of these three factors: wind distribution, wave stress, or surface roughness, is non-uniform over the surface, then zones of divergence and convergence can arise on the surface, without any prime cause in the underlying water. If surface-active (wave damping) material is present, then any small initial non-uniformity might result in a rapid growth of that non-uniformity, the film concentrations reinforcing the action of the initial cause.

Such a situation would be sufficiently complex without the three potential initiating factors being themselves implicitly related. The wave field, through its aerodynamic roughness, influences the wind boundary layer, affecting the energy transfer from wind to waves, and thus affecting the wave field.

Possible film distribution mechanisms along the lines indicated above have been discussed by Kraus [56,57], in considering the field observations reported by Van Straaten [58]. These observations indicated that slicks could be aligned either parallel or perpendicular to the wind (and wave) direction, a situation difficult to explain using a single film concentrating mechanism. Kraus' suggestions have, unfortunately, not been evaluated in the field, and they are rather too highly speculative for comfort.

8. Below-Surface Mechanisms

Apart from these essentially surface-based causes of non-uniform film distributions, it is also possible that observed surface patterns are manifestations of sub-surface motions. Internal waves and Langmuir circulations are perhaps the best known of these.

8.1 Internal Waves

Internal waves are gravity waves, supported by vertical density gradients in the stratified ocean. They travel relatively slowly compared with surface waves, and whilst their effect on the surface elevation is negligible, they do cause significant surface currents. A given area of surface moves backwards and forwards, as the wave passes below it, in the direction of wave propagation.

The oscillating spatial distribution of the propagating surface current variation gives rise to regions of convergence and divergence, which will modulate the surface concentration of any film material present. Both currents and convergence regions thus exist together, although not in phase, and this is likely to aggravate the problems found in interpreting SAR images in film-covered regions. This is particularly so for radar wavelengths close to the ripple wavelengths most susceptible to damping effects, such as X-band (24 to 37.5mm) and C-band (37.5 to 75mm).

The first published observations relating surface slicks to internal waves are due to Ewing [59,60], who observed internal-wave-induced temperature variations in the water, simultaneous with the occurrence of slick bands. LaFond and LaFond [61] reported surface tension variations associated with internal wave propagation.

Yermakov et al. [62-64] showed, from laboratory experiments, that the surface film mechanism of producing slick regions above internal waves is potentially very sensitive. They pointed out that when the surface concentration of film material is in a particular range, dependent on the material, only very small degrees of compression and expansion are needed to give large changes in wave damping behaviour. On the basis of wave damping relationships, they deduced a criterion for slick effects that the surface dilatational elasticity should be greater than about 3.5 mN/m, and indicated that the greatest contrast between slick and non-slick areas was found in the 2 to 3cm wavelength region. It appears that this value of elasticity is consistent with what observations there have been but

these are extremely inadequate, in the absence of a simple routine method of measuring surface tension on the sea surface.

8.2 Langmuir Circulations

Langmuir circulations [65] are helical vortex circulations in the upper layer of the open sea, driven by the wind. They are always aligned with the wind, and are observed as a result of the slicks which form at the convergence zones. Their formation mechanism is not yet fully understood. Whilst it is unlikely that the films play any major part in their formation [66], it is nevertheless true that the films formed by surface-active material carried into the convergence regions are a major cause of their being observed. Sutcliffe et al. [67] discuss the origin and fate of the organic material found in Langmuir circulations.

8.3 The Scully-Power Shuttle Observations

Many fascinating internal wave patterns were observed and photographed from the Shuttle CHALLENGER by Scully-Power, in 1984 [42]. Those observed propagating into the Mediterranean from the Strait of Gibraltar, generated by tidal flows of the density stratified ocean over the sills in the Strait, are proving very interesting from the point of view of the ocean dynamics in this area.

8.4 'Spiral Eddies'

A significant fraction of the patterns seen in the Scully-Power images have so far not found an adequate oceanographic explanation. These are the 'spiral eddies', observed in several geographical regions, but most strikingly near the Gulf Stream, and in the Eastern Mediterranean. These eddies appear, literally, as surface spirals, delineated by thin, sharply defined surface slicks, which appear to follow streamlines, converging on the centre of the spiral.

It is probable that the flow beneath one of these spirals is that of an upper ocean eddy, a rotating, approximately circular body of water. It would be expected that surface markers above an eddy would follow spiral streamlines, as there would be a net flow towards the centre, at the surface.

Atmospheric effects may be ruled out, as the patterns observed show no particular alignment relative to the wind, and are unlikely to have such organised structures on the time and space scales found.

Similar spirals have been reported in the visible light imagery from LANDSAT, from the Baltic, made imageable by the presence of blue-green algae [68].

One interesting feature of the spiral patterns is that a given pattern usually comprises either left-handed or right-handed spirals, presumably depending on which hemisphere they are in.

9. How is the film material formed into lines?

Some possible surface convergence mechanisms were outlined above: internal waves, Langmuir circulations, and atmospheric effects. These mechanisms will all give accumulations of whatever surface active material is present on the surface. However, these mechanisms alone cannot explain all of the observations, the case of the 'spiral' eddies being notable in this respect.

One possible clue is given by the observations of Sheres et al. [44]. In the sunglint image obtained in this work, a slick region coincides exactly with a region of strong horizontal shear, made evident by refraction of the swell waves that are seen clearly to either side of the slick region. These observations have recently been supported by similar results (although from real-aperture imaging radar rather than sunglint) reported by McLeish and Ross [69], who also found a slick region associated with a shear zone, at the Gulf Stream front off Cape Hatteras. In both cases, the slick width was about 1 km, and surface velocity changes of 1 to 1.5 m/s were found, although the overall deduced horizontal shear was much smaller in the McLeish and Ross case.

McLeish and Ross suggest that the slick is associated with a surface convergence along the frontal boundary, although they give no supporting evidence of this. Sheres et al. suggest an alternative explanation, that the slick region they observed may have been due to wave stresses in the shear zone, which acts as a low pass filter for waves, and a barrier for the higher wave frequencies. This latter seems unlikely for the Sheres observations, which used sunglint, and would therefore be imaging distributions of wind ripples, rather than swell waves. It would be a more likely explanation for the McLeish and Ross radar observations, which involved longer surface wavelengths in the imaging process. Sheres et al. do acknowledge other reported observations of slicks in their area, some of which actually had floating debris in them.

It is not at all clear in either case how the shear zone acts as a collecting region for surface film material. However, it is reasonably well established by these cases that slicks and horizontal shear zones can be coincident.

If such is the case, then the observations of spiral slicks overlying eddies could be taken as consistent with this evidence, since there will be shear associated with the spiralling surface flow. The results of Yermakov et al. [62-64], considered above, show that the relative surface concentration of film material, by whatever sub-surface cause, need not be particularly large to result in a large variation of wind-wave damping.

Some support for the association of shear and slick regions was gained in the SIR-B experiment of October 1984, using an L-band synthetic aperture radar in the shuttle CHALLENGER. ARE were making detailed thermal structure measurements in a deep water site off the

Bay of Biscay, coincident with one of the very few effective imaging passes of the Shuttle in the Deep Water Site.

Fortunately, in the imaged pass, a surface chemical slick had been laid deliberately on the sea surface. Oleyl alcohol was spread from the observing ship MV PROFILER, using an adaptation of the chemical spreading technique described by Huhnerfuss and Garrett [70], in which frozen chunks of the material were thrown about 25m from the sides of the ship.

A slick approximately 100m wide was formed this way, and this was imaged quite clearly by the radar. As can be seen in the image, however, the straight-line slick had been severely disturbed in the interval between the time of laying the slick and the time of the image, about 45 minutes later. The slick is broken into two parts, relatively displaced. Throughout the whole period from the chemical deployment up to the imaging time, PROFILER had been travelling in a straight line, at a steady 4 knots, towing a 200m long thermistor chain, which measured the thermal structure of the ocean between about 10m and 180m.

The isotherms deduced from the chain data indicate clearly the presence of a significant eddy disturbance in the region of the SAR image, and the slick position can be seen to be close to the edge of the eddy, the region of greatest shear.

The hydrodynamic processes associated with this eddy are apparently very complex. In the sloping shear region at the edge of the eddy there is evidence of very strong mixing, and some surface convergence is apparent, shown by a large dip in the near-surface isotherms. Unfortunately, the chemical slick narrowly missed being laid directly in this convergence region, which seems to be the region of strongest shear, but it was sheared to a considerable extent. Some further deductions may be made from the radar image which are significant in this context.

A faint pattern of curved dark lines may be seen in the image, not quite suggesting an easily recognisable pattern such as a spiral, but nevertheless indicative of similar shear activity. Such dark lines in a radar scattering image indicate low scattering strength, and would be consistent with the presence of a slick region.

One of the more visible darker lines is indeed seen to pass through the ship's track in the position where the surface convergence region was observed, above the strong shear zone.

Although admittedly rather tenuous, because of the low contrast in the images of these shadowy features, there appears to be a link here between shear boundaries, convergence lines, and radar-imaged slicks.

The mechanism relating convergence and shear is, however, unclear.

A further set of observations was made in 1985, in the region of the Iceland-Faeroes frontal system. Twelve oleyl alcohol slicks were laid in this region, which is known to be one of extremely active shear, being the boundary between counter-flowing water masses of different buoyancy characteristics.

An imaging radar was flown during these experiments - this time a real-aperture X-band radar on board a light aircraft. In addition to the radar images of the surface, sunglint pictures were taken of the surface. In one sequence of three slicks, laid over a track of length 6 n.mi., intense shear activity was observed, one slick being sharply broken, and quickly dispersed by the oceanic flows.

There are several points of interest arising from these observations. At the time they were made, the wind was very light, and this made radar images of very low contrast, so low that the slicks were barely detectable. However, sunglint produced very high contrast in these conditions.

There is thus an interesting complementary quality to the two types of observation, which helps to offset the disadvantage of sunglint that it requires clear skies.

No natural slicks were observed in the region of this shear activity, although we had observed - from deck level - large areas containing many irregular slicks in other parts of the frontal system. Regrettably, the aircraft was not present during these observations.

10. Surface Films as Surface Markers

The experiments described above have indicated that wave-stilling chemical slicks can be very useful for showing the horizontal shear behaviour of the ocean, a property not easily observed by other means, particularly at the lower values of surface current involved.

With the ever-increasing availability of above-surface observation platforms capable of resolving below 100m at the ocean surface, it is expected that the use of deliberately added surface film material could develop into a useful technique which complements in-water measurements. The possibility of high-resolution sunglint imaging systems operating from unmanned space platforms should be considered seriously in this context.

11. Conclusions

In this review of surface film effects on the ocean, several major areas of relative ignorance have been identified, associated with almost all of the stages in the production of surface film patterns. Problems have been identified in the way the film material affects the wave spectrum; the way the spectrum and its spatial variations are imaged by the various techniques; and the way

the ocean can act to produce spatial variations of the film concentration and the wave field, together.

A combined observational/theoretical/experimental approach will undoubtedly be needed to further the understanding of the overall problem. It is apparent, however, that the state of observation is severely hampered at present by the great expense of field work, and the experimental aspects of the work are extremely difficult. Theoretical modelling urgently requires input from these aspects if it is to develop satisfactorily.

References

1. Scott, J.C., 'The historical development of theories of wave-calming using oil', *History of Technology*, 3, 163-186 (1978)
2. Plutarch, 'What is the reason for the clearness and calm produced when the sea is sprinkled with oil', *Moralia: Quaestiones Naturales*: Vol.11, No.12 (e.g. Trans. F.H.Sandbach, Heinemann, 1965)
3. C. Plinius Secundus (Pliny the Elder), *Historia Naturalis*, Book 2, Chapter 103 (completed A.D.77) (e.g. Trans H.Rackham, Loeb Classical Library, Heinemann, 1967)
4. Scott, J.C., 'Oil on Troubled Waters: A bibliography on the effects of surface-wave motions', Multi-Science Publishing Co. 83pp (1979)
5. Franklin, B., 'Of the stilling of waves by means of oil', *Philosophical Transactions*, 64, 445-460 (1774)
6. Gaines, G.L., 'Insoluble Monolayers at Liquid-Gas Interfaces', Interscience (1966)
7. Lucassen-Reynders, E.H. and Lucassen, J., 'Properties of capillary waves', *Advances in Colloid and Interface Science*, 2, 347-395 (1969)
8. Lucassen, J., 'Effect of surface-active material on the damping of gravity waves: A reappraisal', *Journal of Colloid and Interface Science*, 85, 52-58 (1982)
9. Lamb, H., 'The calming effect of oil on water waves', in 'Hydrodynamics', 2nd Edition, Cambridge University Press, Article 304, 552-555 (1895)
10. Davies, J.T. and Vose, R.W., 'On the damping of capillary waves by surface films', *Proceedings of the Royal Society*, 286, 218-234 (1965)
11. Van den Tempel, M. and Van de Riet, R.P., 'Damping of waves by surface-active materials', *Journal of Chemical Physics*, 42, 2769-2777 (1965)
12. Cini, R. and Lombardini, P.P., 'Damping effect of monolayers on surface wave motion in a liquid', *Journal of Colloid and Interface Science*, 65, 387-389 (1978)
13. Huhnerfuss, H., Lange, P. and Walter, W., 'Wave damping by monomolecular surface films and their chemical structure. Part II: Variation of the hydrophilic part of the film molecules including natural substances', *Journal of Marine Research*, 42, 737-759 (1984)

14. Huhnerfuss, H., 'Surface viscosity measurement - a revival of a nearly forgotten surface chemical method', *Journal of Colloid and Interface Science*, 107 84-95 (1985)
15. Ting, L., Wasan, D.T., Miyano, K., and Xu, S-Q, 'Longitudinal surface waves for the study of dynamic properties of surfactant systems. II Air-solution interface', *Journal of Colloid and Interface Science*, 102, 248-259 (1984)
16. Goodrich, F.C., 'On the damping of water waves by monomolecular films', *Journal of Physical Chemistry*, 66, 1858-1863 (1962)
17. Dorrestein, R., 'General linearized theory of the effect of surface films on water ripples', *Proceedings, Koninklijke Nederlandse Akademie van Wetenschappen, Series B*, 53, 350-356 (1951)
18. Lucassen, J., 'Longitudinal capillary waves. Parts I and II', *Transactions of the Faraday Society*, 64, 2221-2235 (1968)
19. Benjamin, T.B., 'Effect of surface contamination on wave formation in falling liquid films', *Archiwum Mechaniki Stosowanej*, 16, 615-626 (1964)
20. Whitaker, S., 'Effect of surface active agents on the stability of falling liquid films', *Industrial and Engineering Chemistry Fundamentals*, 3, 132-142 (1964)
21. Gottifredi, J.C. and Jameson, G.J., 'The suppression of wind-generated waves by a surface film', *Journal of Fluid Mechanics*, 32, 609-618 (1968)
22. Gottifredi, J.C. and Jameson, G.J., 'The interpretation of measurements of the amplitude of capillary waves generated by a wind', *Chemical Engineering Science*, 23, 403-405 (1968)
23. Arkharov, A.V., Petrichenko, S.A., and Pudov, V.D., 'Effect of surfactants on wind-driven waves', *Oceanology*, 22, 137-139 (1982)
24. Hino, M., Kataoka, S. and Kaneko, D., 'Experiment of surface film effect on wind-wave generation', *Coastal Engineering in Japan*, 12, 1-8 (1969)
25. Wu, J., 'Evaporation reduction by monolayers: Another mechanism', *Science*, 174, 283-385 (1971)
26. Toba, Y. and Kunishi, H., 'Breaking of wind waves and the sea surface wind stress', *Journal of the Oceanographical Society of Japan*, 26(2), 71-80 (1970)
27. Scott, J.C., 'The effect of organic films on water surface motions', in: *Oceanic Whitecaps and their Role in Air-Sea Exchange*

Processes, (E.C.Monahan and G.MacNiocaill, eds), pp.159-165, Galway University Press (1986)

28. Reisbig, R.L., Alofs, D.J., Shah, R.C., and Banerjee, S.K., 'Measurement of oil spill drift caused by the coupled parallel effects of wind and waves', *Memoires Societe Royale des Sciences de Liege*, 6 Serie, 6, 67-77 (1973)

29. Lange, P., and Huhnerfuss, H., 'Drift response of monomolecular slicks to wave and wind action', *Journal of Physical Oceanography*, 8, 142-151 (1978)

30. Wu, J., 'Sea-surface drift currents induced by wind and waves', *Journal of Physical Oceanography*, 13 1441-1451 (1983)

31. Scott, J.C., 'The influence of surface-active contamination on the initiation of wind waves', *Journal of Fluid Mechanics*, 56, 591-606 (1972)

32. Thorpe, S.A., 'The effect of Langmuir circulation on the distribution of submerged bubbles caused by breaking wind waves', *Journal of Fluid Mechanics*, 142, 151-170 (1984)

33. Thorpe, S.A., 'Small-scale processes in the upper ocean boundary layer', *Nature*, 318, 519-522 (1985)

34. Alpers, W., Blume, H.J.C., Garrett, W.D., and Huhnerfuss, H., 'The effect of monomolecular films on the microwave brightness temperature of the sea surface', *International Journal of Remote Sensing*, 3, 457-474 (1982)

35. Blume, H.J.C., Huhnerfuss, H., and Alpers, W., 'Variation of the microwave brightness temperature of sea surfaces covered with mineral and monomolecular oil films', *IEEE Transactions on Geoscience and Remote Sensing*, 21, 295-300 (1983)

36. Vines, R.G., 'Evaporation control: a method of treating large water storages', in 'Retardation of Evaporation by Monolayers: Transport Processes', Ed. V.K.La Mer, Academic Press, 137-160 (1962)

37. Shutko, A.M., 'The status of the passive microwave sensing of the waters - lakes, seas, and oceans - under the variation of their state, temperature, and mineralization (salinity): Models, experiments, examples of application', *IEEE Journal of Oceanic Engineering*, 10, 418-437 (1985)

38. La Violette, P.E., Peteherych, S., and Gower, J.F.R., 'Oceanographic implications of features in NOAA satellite visible imagery', *Boundary- Layer Meteorology*, 18, 159-175 (1980)

39. Cox, C., and Munk, W., 'The measurement of the roughness of the sea surface from photographs of the sun's glitter', *Journal of the Optical Society of America*, 44 838-850 (1954)

40. Cox, C., and Munk, W., 'Statistics of the sea surface derived from sun glitter', *Journal of Marine Research*, 13, 198-227 (1954)
41. Cox, C., and Munk, W.H., 'Some problems in optical oceanography', *Journal of Marine Research*, 14, 63-78 (1955)
42. Scully-Power, P., 'Navy Oceanographer Shuttle Observations STS 41-G: Mission Report', NUSC Technical Document 7611, 26 March 1986
43. Hartwig, E.O., and Herr, F.L., 'Chemistry and biology of the sea-surface interface. Relationships to remote sensing', Office of Naval Research Workshop, American Institute of Biological Sciences, 1984
44. Sheres, D., Kenyon, K.E., Bernstein, R.L. and Beardsley, R.C., 'Large Horizontal surface velocity shears in the ocean obtained from images of refracting swell and in situ moored current meter data', *Journal of Geophysical Research* C, 90, 4943-4950 (1985)
45. Huhnerfuss, H., Alpers, W., and Jones, W.L., 'Measurements at 13.9GHz of the radar backscattering cross-section of the North Sea covered with an artificial surface film', *Radio Science*, 13, 979-983 (1978)
46. Huhnerfuss, H., Alpers, W., Jones, W.L., Lange, P.A., and Richter, K., 'The damping of ocean surface waves by a monomolecular film measured by wave staffs and microwave radars', *Journal of Geophysical Research*, 86, 429-438 (1981)
47. Huhnerfuss, H., and Alpers, W., 'The occurrence of sea slicks on the ocean surface and their influence on remote sensing signals', *Proceedings of the 1982 International Geoscience and Remote Sensing Symposium (IGARSS'82)*, Digest Vol.1, 2.1-2.4 (1982)
48. Johnson, J.W., and Croswell, W.F., 'Characteristics of 13.9GHz radar scattering from oil films on the sea surface', *Radio Science*, 17, 611-617 (1982)
49. Huhnerfuss, H., Alpers, W., Cross, A., Garrett, W.D., Keller, W.C., Lange, P.A., Plant, W.J., Schlude, F., and Schuler, D.L., 'The modification of X and L band radar signals by monomolecular sea slicks', *Journal of Geophysical Research*, 88, 9817-9822 (1983)
50. Rufenach, C.L., Fedor, L.S., Apel, J.R., and Gonzalez, F.I., 'Surface and internal ocean wave observations', *Advances in Geophysics*, 27, 141-196 (1985)
51. Stommel, H., 'Streaks on natural water surfaces', *Weather*, 72-74 (1951)
52. Gerling, T.W., 'Remote sensing of the ocean-surface wind field with a scatterometer and a synthetic aperture radar', *Johns Hopkins APL Technical Digest*, 6, 320-329 (1985)

53. Barger, W.R., Garrett, W.D., Mollo-Christensen, E.L., and Ruggles, K.W., 'Effects of an artificial sea slick upon the atmosphere and the ocean', *Journal of Applied Meteorology*, 9, 396-400 (1970)
54. Kuznetsov, O.A. and Panin, G.N., 'On the influence of an oil film on the surface of the sea on turbulence in the lower layers of the atmosphere', *Metrologiya i Gidrologiya*, No.5, 97-99 (1974)
55. Dore, B.D., 'On wave-induced surface drift', *Wave Motion*, 7, 123-164 (1985)
56. Kraus, E.B., 'Organized convection in the ocean surface layer resulting from slicks and wave radiation stress', *Physics of Fluids*, 10, S294-S297 (1967)
57. Kraus, E.B., 'Wind stress along the sea surface', *Advances in Geophysics*, 12, 213-255 (1967)
58. Van Straaten, L.M.J.U., 'Periodic patterns of rippled and smooth areas on water surfaces', *Proceedings, Koninklijke Nederlandse Akademie van Wetenschappen*, 53, 1217-1227 (1950)
59. Ewing, G.C., 'Relation between band slicks at the surface and internal waves in the sea', *Science*, 111, 91-94 (1950)
60. Ewing, G., 'Slicks, surface films, and internal waves', *Journal of Marine Research*, 9, 161-187 (1950)
61. LaFond, E.C., and LaFond, K.G., 'Perspectives of slicks, streaks and internal waves', *Bulletin of the Japanese Society of Fisheries Oceanography, Special Number (Prof. Uda's Commemorative Papers)*, 49-57 (1969)
62. Yermakov, S.A., Pelinovsky, Ye.N., and Talipova, T.G., 'Influence of surface films on changes in wind-wave spectra under the action of internal waves', *Izvestiya, Atmospheric and Oceanic Physics*, 16, 788-794 (1980)
63. Yermakov, S.A., Kozlov, S.I., Pokazeyev, K.V., and Rozenberg, A.D., 'Laboratory study of the effect of internal waves on regular surface waves', *Oceanology*, 22, 145-149 (1982)
64. Ermakov, S.A., and Pelinovsky, E.N., 'Variation of the spectrum of wind ripple on coastal waters under the action of internal waves', *Dynamics of Atmospheres and Oceans*, 8, 95-100 (1984)
65. Langmuir, I., 'Surface motion of water induced by wind', *Science*, 87, 119-123 (1938)
66. Leibovich, S., 'The form and dynamics of Langmuir circulations', *Annual Reviews of Fluid Mechanics*, 15, 391-427 (1983)

67. Sutcliffe, W.H., Baylor, E.R., and Menzel, D.W., 'Sea-surface chemistry and Langmuir circulation', *Deep-Sea Research*, 10, 233-243 (1963)
68. Ulbricht, K.A., 'LANDSAT image of blue green algae in the Baltic Sea', *International Journal of Remote Sensing*, 4, 801-802 (1983)
69. McLeish, W., and Ross, D.B., 'Wave refraction in an ocean front', *Journal of Geophysical Research C*, 90, 11929-11938 (1985)
70. Huhnerfuss, H., and Garrett, W.D. 'Experimental sea slicks: Their practical applications and utilization for basic studies of air-sea interactions', *Journal of Geophysical Research*, 86, 439-447 (1981)

THE PHYSICAL APPEARANCE OF BIOGENIC SLICKS

These photographs were taken about 0750 GMT on June 28, 1986, in the Faeroe Bank Channel, around position 61° 20'N, 7° 40'W, just to the South-West of the Faeroes, near the edge of the Faeroes shelf. The water depth is steeply sloping downwards in this region, along the ship track, which passed from the Faeroes shelf into the Channel. The wind was light, less than 10 knots, and was approximately constant throughout the series of photographic frames, which were all made within 10 minutes. The ship, MV SEA SEARCHER, was making about 10 knots, equivalent to a distance about 3 km over the 10 minute period. The weather has been calm for at least the previous 48 hours. All of the frames were taken from the same position on the ship, at Bridge level (about 6m), and the sky was uniformly overcast.

The photographs illustrate the complex nature of the variation of surface roughness inside and outside slick and non-slick regions. They indicate how little roughness variation can give a strong visual image, and also how clear-cut the boundaries of slicks can be.

The first few frames are from an almost completely slick-covered surface, with darker (rougher) patches showing through the slick.

Frame 5/5 shows the structure of one of these dark patches. The dark appearance clearly comes from small 'pock-marks', made up of groups of short waves (estimated wavelength 50mm) distributed quite thinly over a much smoother, though still wave-covered, surface. There was no obvious orientation to the dark patches observed. Close inspection of photograph shows that the wave-fronts which make up most of the dark patches are rather longer than the patches, and that the observed 'dark' region may simply be place where the local surface slope exceeds a particular value.

Frame 5/6, taken less than minute after the previous frame, shows the same patchiness, but this time we can also see the completely unruffled slick region in the foreground. The boundaries of the darker region appear to be extremely sharp, occupying less than 1m. The position of these boundaries did not appear to change significantly while within sight of the moving ship. These darker regions were observed to be roughly aligned, approximately East-West, the ship crossing them on a South-West track.

Frame 5/8, again within seconds of the previous frame, shows an isolated 'spur' of roughness, less than about 10m in width. This frame is interesting since it shows the ripples which causes the dark region extending (with reduced amplitude) several metres into the foreground slick region.

Frames 5/9 and 5/10, which are almost adjacent (place 10 to the left of 9), were taken 8 or 9 minutes after the previous frames. A completely different condition is apparent here, the slick regions being isolated within larger rough regions, instead of vice versa.

In this condition, the dark region appears quite uniformly rough, and the slick regions contain the same sort of wavelengths as the rough regions (estimated to be 200-300mm). The slicks stand out clearly from the rougher regions, and are aligned East-West, as were the earlier patterns.

The gradual transition from the 'rough-on-slick' condition to the 'slick-on-rough' condition found in these results suggests that the difference is quantitative rather than qualitative, the surface concentration of biogenic material decreasing away from the shallow water region. The ship eventually moved completely out of the slick region.

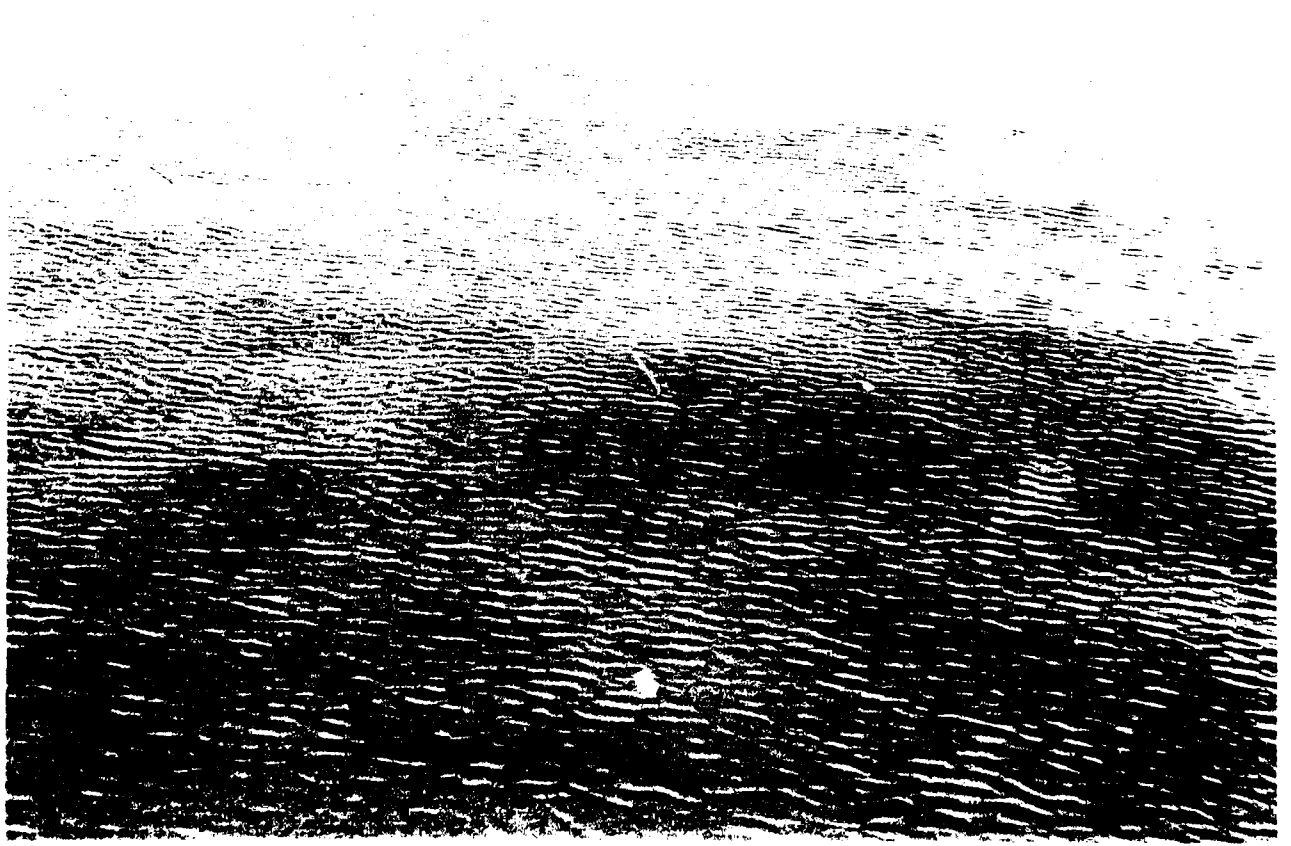
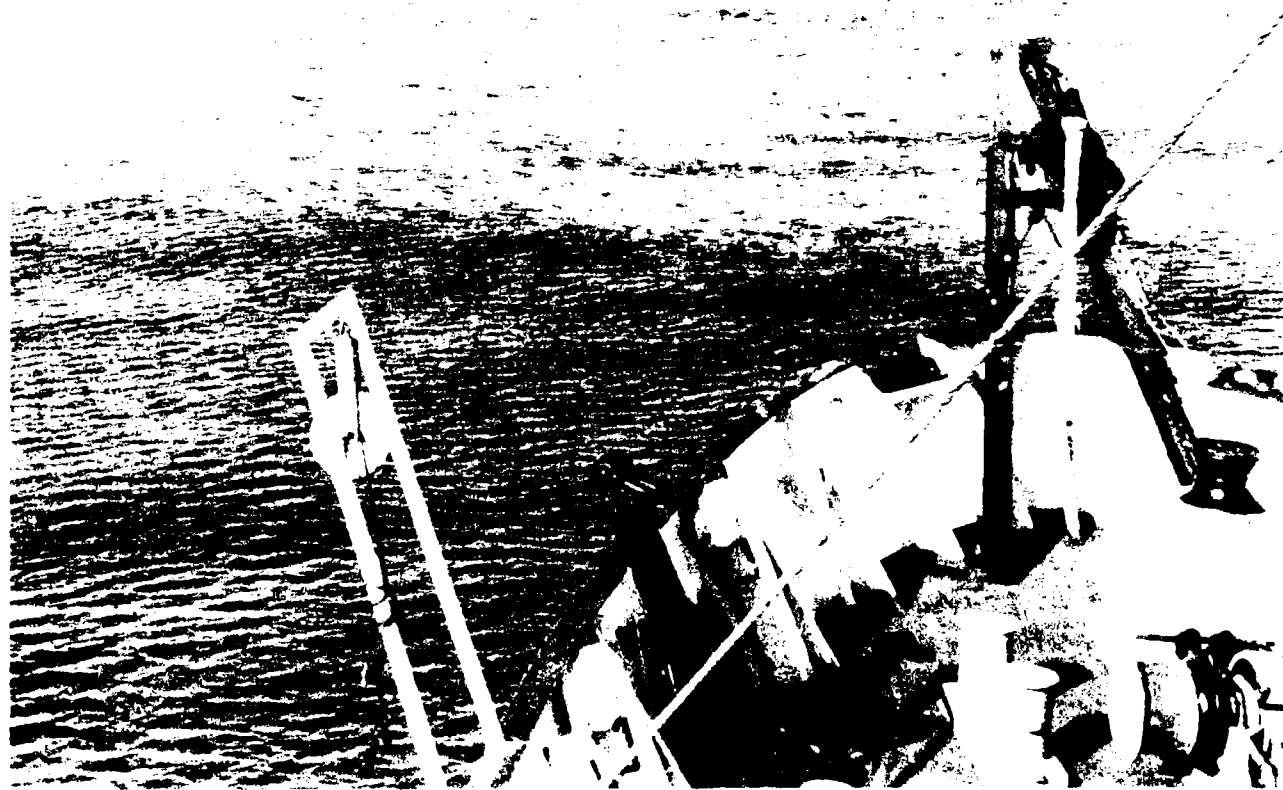






Figure 10





I have under several Arctic winter experiments in the Gulf of St. Lawrence, Fram Strait, Greenland and Barents Sea observed how ice is formed under presence of wind, surface waves and swells. The freezing happens very suddenly resulting first in the formation of grease ice. Grease ice is a "soupy" low viscosity liquid, in the order of a cm or less in thickness, riding on the top of the waves. When it forms it rapidly dampens out capillary waves and short surface waves, with wavelengths in the same order as used on a X-C-L band SAR. This damping has a significant effect on both passive and active microwave sensors in such a way to give suppressed or even no information of wind, waves and swell. Ship detection with SAR would probably also be severely hampered. I should stress that this grease ice formation is not a local event, only occurring near the ice edge. From low-flying aircraft in the Greenland Sea, I have observed the grease ice over several thousand km². In this note I am reporting some observations from the Norwegian Remote Sensing Experiment, NORSEX (1983), Johannessen et al. (1983), where the effect on grease ice on passive and active microwave sensors are quantified.

Observations

The NORSEX Experiment in the marginal ice zone north of Svalbard took place in the fall of 1979 from 17 September to 12 October during freezing conditions. Coordinated passive and active microwave measurements were obtained from ship, airborne and satellite instruments together with in-situ observations. Two remote sensing aircraft from NASA (a C-130 and a CV-990) took part in the experiment. The sensors on the C-130 aircraft included a 14.6 GHz airborne microwave scatterometer (AMS-CAT), a 13.3 GHz scatterometer, a 4.5 to 7.2 GHz stepped frequency microwave radiometer (SFMR), and 18.0, 21.0, and 37.0 GHz multifrequency microwave radiometer (MFMR), a 10.7 GHz passive microwave imaging system (PMIS), a thermal infrared radiometer (PRT-5), and two Zeiss metric cameras. Six flights were conducted over the marginal ice zone.

The NASA CV-990 was instrumented with a Jet Propulsion Laboratory L-band (1.215 GHz) synthetic aperture radar (SAR) with a resolution of 25 m. Two flights were performed, one of which was simultaneous with a C-130 flight on October 1.

A combined passive and active microwave sensor system measured ice and ocean signatures at a height of 6.5 m from the R/V Polarsirkel, an icebreaker. These sensors, from the University of Bern, included five

microwave radiometers at 4.9, 10.4, 21, 36, and 94 GHz, a scatterometer at 10.4 GHz, and an infrared PRT-5. Photographs were taken of every radiometric target.

The L-band SAR image obtained under light wind conditions (4 m/s) figure 1, shows the ice to have a wavelike edge with scale length of 20-40 km. Moreover, eddies are present at the ice edge with dimensions of 5 to 15 km in diameter. The black signature associated with the eddies and the black circular signature 5 km across between the two eddies (fig. 2), was from the ice observer onboard the C-130 identified as grease ice. Six hours before the SAR image was obtained on October 1, R/V Polarsirkel fortunately passed through the 5 km circular black signature along the track S1 to S2 (fig. 2). Ship-based brightness temperature at 4.9 GHz, sea surface temperature and "bucket" salinity were obtained and are shown in fig. 3 as well as the backscatter profile from the SAR image acquired six hours later. The region of low backscatter and high brightness temperature is the grease ice associated with the 5 km region of water colder and less saline than its surroundings (interpreted as an eddy shed from the ice edge) allowing freezing of grease ice to occur. From the SAR profile it is seen that the backscatter is 6 dB lower for the grease ice region compared to its surroundings, while the brightness temperature at 4.9 GHz increases with 20-30°K, thereby masking the "normal" ocean roughness at 4 m/s wind. A photograph from a grease ice region (fig. 4) clearly demonstrates this effect. Most of the area in the photograph is covered with grease ice where the capillary and short gravity waves are damped out. However, in a few places at the crest of the waves, the grease ice is broken up allowing the capillary and short waves to exist.

In the introduction I mentioned that the grease ice formation is not only a local occurrence near the ice edge, but it can take place over thousands of km². This condition was observed when I was onboard a low-flying Norwegian Air Force P3 on a course from northern Norway to the ice edge in the Greenland Sea on 25 April 1985. Furthermore, transient thin ice signatures over large regions both from the Greenland and Barents Sea have been identified in the analysis of the Nimbus 7 SMMR observations.

While wind and waves were masked by the grease ice, its boundary, under light wind conditions (4 m/s) was used to indicate the ocean frontal boundary off the ice edge. A synoptic mapping of the surface temperature and salinity of the frontal zone by R/V Polarsirkel on 1. October (Johannessen, 1983) is shown in figure 5 together with the main structure of the ice edge as derived from the SAR images obtained the same day. At

E1 the boundary of the grease ice appears to follow the same pattern as the frontal structure (-1.50°C , less than 33%), thus suggesting that the boundary of the grease ice in this case can be used as an indicator of the location of the front. During this day, the air temperature was -10°C , allowing grease ice formation on the cold, low salinity side of the front, thus enhancing the boundary.

Discussion and Summary

In polar regions, even when wind, waves and swell are present, freezing of grease ice occur. We have shown from one set of observations during light winds (4 m/s), that grease ice can decrease the L-band SAR backscatter with as much as 6 dB and raise the brightness temperature at 4.9 GHz with 20-30°K compared to its surrounding. The grease ice will therefore mask the normal ocean image mechanisms associated with wind, waves and swells. Under a winter expedition in the Gulf of St. Lawrence in 1970, I also observed that grease ice at higher wind speed is a transient phenomena. At wind speeds of about 8-10 m/s it was still present "riding" the waves. When the wind increased to over 10 m/s, it disappeared, being broken up by the waves. At lower wind speeds it again formed.

It is also shown that the boundary of grease ice in SAR imagery under light winds and freezing conditions can be interpreted as frontal boundary, simply because freezing occurred on the cold and low salinity side of the front.

In cold and low salinity polar regions where grease ice can form, one can speculate on the effect grease ice has on the detection of eddies and internal waves. Horizontal shear and convergence are associated with these two phenomena. Will these physical feature when interacting with the grease ice and surface waves cause an enhance signature when comparing to the surrounding or will it be suppressed? To indicate that enhancement may occur, eddying in a thin melting ice field observed by Landsat in June 1976 to the east of Svalbard is shown in figure 6, Vinje(1985). The eddies stand very clearly out, but will the same effect be seen in a SAR image?

The grease ice is as mentioned a "soupy" low viscosity liquid riding the ocean surface. This may occur up to 8-10 m/s. When present the wave breaking is drastically reduced or not occurring at all. This should prevent air bubbles from being injected in the upper layer, thereby reducing the ambient noise. I do not know of any measurements of this effect, but it could be very significant and could also have operational implications.

In summary we have at present only a beginning understanding on how grease ice affects remote sensing signatures, and furthermore how this "soupy" thin viscous "microlayer" affect the ambient noise. During MIZEX 87 to occur in March 1987 in the Fram Strait, such investigations are planned.

References:

Johannessen O.M., J.A. Johannessen, J. Morison, B.A. Farrelly, and E. Svendsen. Oceanographic Conditions in the Marginal Ice Zone North of Svalbard in Early fall 1979 with an Emphasis on Mesoscale Processes. *Journal of Geophysical Research*, Vol. 88, no C5, March 30., 1983.

NORSEX GROUP: Norwegian Remote Sensing Experiment in a Marginal Ice Zone. *SCIENCE* Vol.220, 20. May 1983.

Vinje T. : Drift, Composition, Morphology and Distribution of the Sea Ice Fields in the Braents Sea. Norsk Polarinstitutt Skrifter Nr. 179c, 1985.

Figure list:

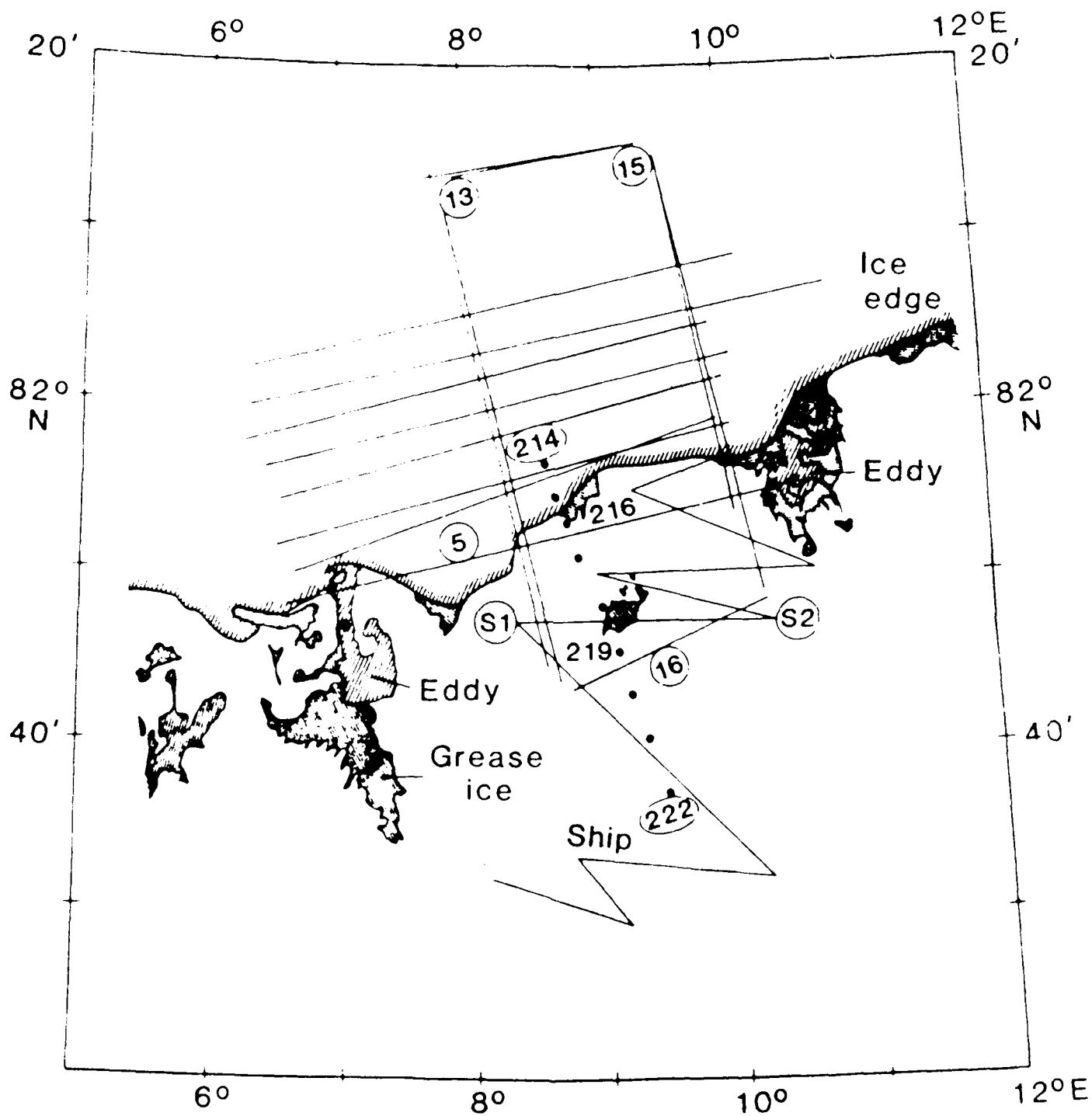
- Figure 1: Jet Propulsion Laboratory synthetic aperture radar, L-band 1.215 GHz image of the marginal ice zone October 1. 1979. (after NORSEX Group, 1983).
- Figure 2: Schematic representation of the SAR image of October 1., showing the ice eddies, and grease ice. Thin lines show the flight tracks of the NASA C-130 and the zigzag ship track on October 1. (after NORSEX 1983).
- Figure 3: Surface temperature and salinity from R/V Polarsirkel, SAR backscatter (relative scale), and ship-based brightness temperature at 4.9 GHz on October 1. along the track from S1 to S2. (after NORSEX 1983).
- Figure 4: Grease ice, the "soupy" viscous liquid riding the waves. At a number of crests the grease ice is broken allowing capillary and short gravity waves to exist. Photo taken by E.A. Svendsen during the NORSEX experiment in the Marginal Ice Zone northwest of Svalbard in fall of 1979.

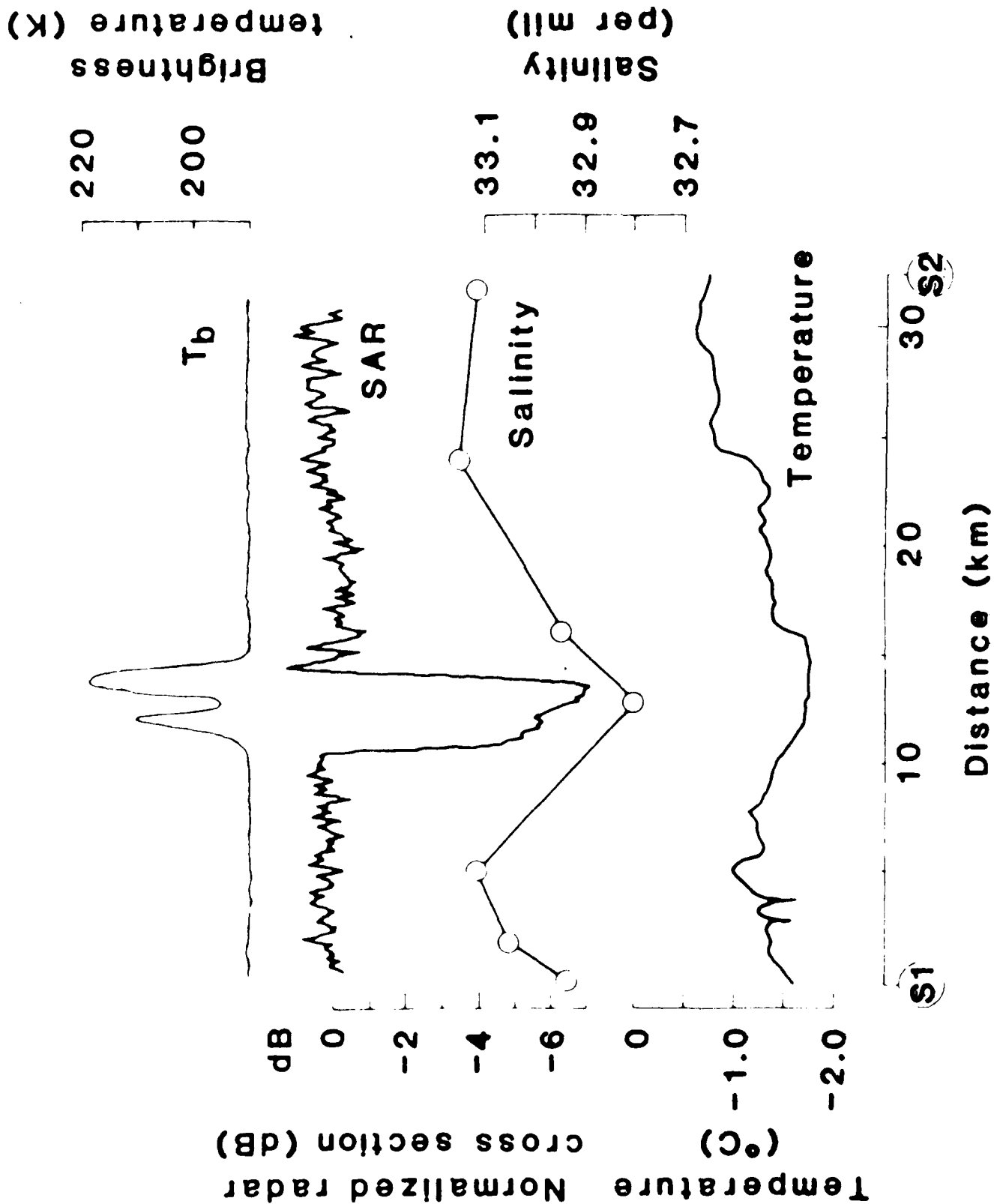
Figure 5: Surface temperature and salinity mapped by R/V Polarsirkel on October 1.. Thin lines indicate ship track, and hatched areas indicate grease ice. Crosses indicate the frontal boundary interpreted from the SAR image the same day (after Johannessen et al, 1983).

Figure 6: Eddying in a thin, melting ice field as observed by LANDSAT 8 June 1976 between Edge øya (right and the southern tip of Spitsbergen (left). Similar features were also observed this area on the two following days before clouds covered the area. High pressure conditions prevailed with calm or very weak northwesterly winds (Photo: NASA) (after Vinje 1985).

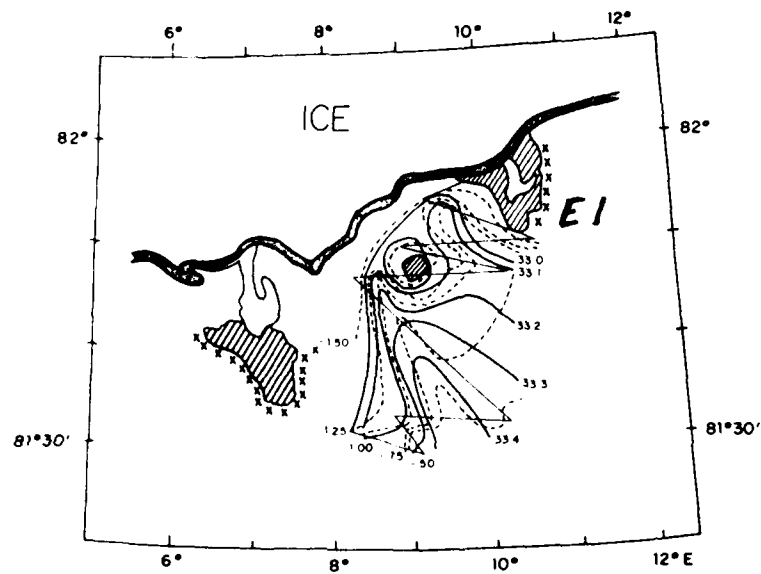
NORSEY JPL 1-BAND SAR
01 OCT 1979 1115-1302 GMT

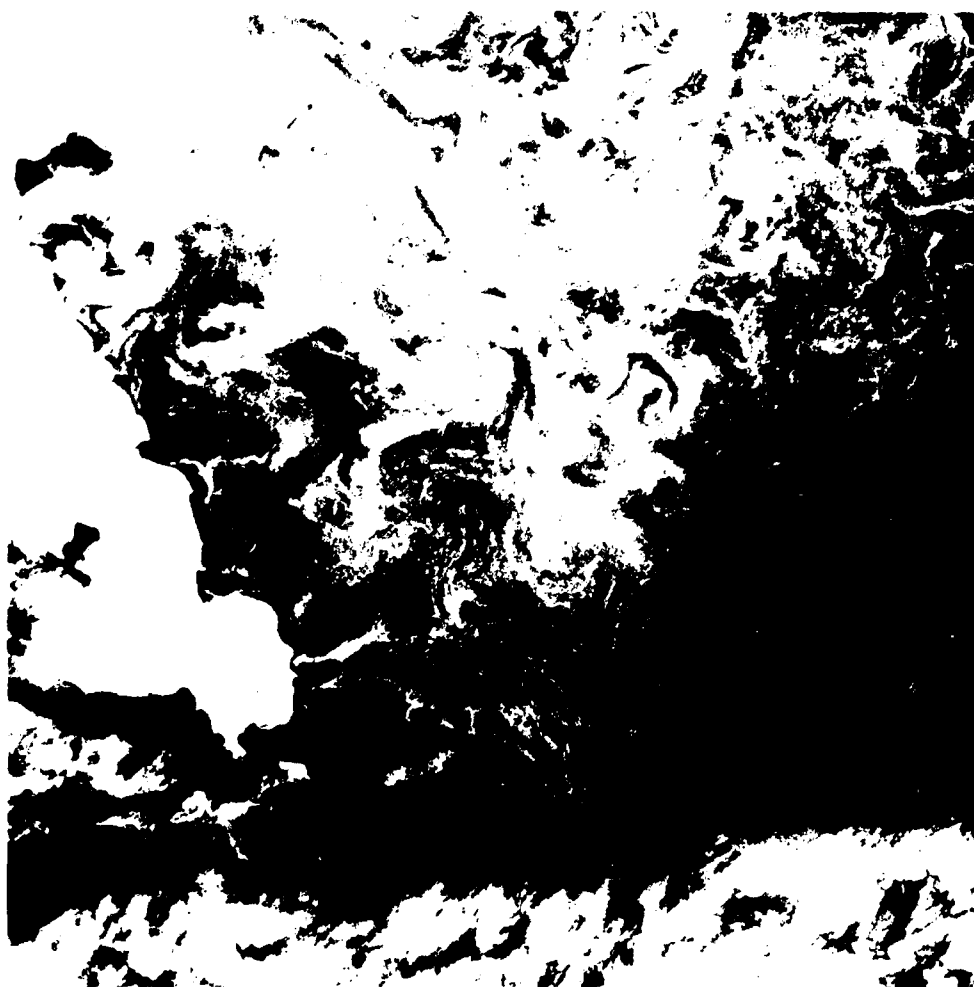












ON PHENOMENA AFFECTING SEA-SURFACE REMOTE SENSING AND INTERFACE MICROLAYER

by

Jin Wu

Air-Sea Interaction Laboratory
College of Marine Studies, University of Delaware
Lewes, Delaware 19958

ABSTRACT

Two groups of phenomena relevant to sea-surface remote sensing and interface microlayer are discussed. Parameters describing fine structures of the sea surface, the mean-square slope and roughness length, are summarized along with effects of the surface film on these quantities. Laboratory and field results are reviewed to show that the viscous sublayer below the air-sea interface is thinner than, and behaves differently from, that over the solid surface.

1. INTRODUCTION

Recent progress in the remote sensing of oceans has pressed for further understanding of the interface between the atmosphere and ocean, as sea-surface sensors have been used in all techniques. Many of the studies have been conducted under high winds, where strong returns from the sea surface are received. The prevailing winds over the oceans, however, are generally light; recent satellite photographs of the sea surface under these wind conditions show a probable substantial coverage by natural films, from which significantly different returns were reported (Hühnerfuss, et al., 1983a; Hühnerfuss, et al., 1983b). Two groups of interface phenomena affecting seasurface remote sensing are discussed.

2. FINE STRUCTURES OF CLEAN AND SLICK SEA SURFACES

Roughness Length of Clean and Slick Surfaces

Clean Surface: Roughness of the sea surface is generally described by the roughness length defined in the following equation,

$$U/z_* = (1/\kappa) \ln(z/z_0) \quad [1]$$

where U is the wind velocity at elevation z above the mean sea surface; u_* is the wind-friction velocity, $u_* = (\tau/\rho_a)^{1/2}$, in which τ is the wind stress and ρ_a the density of air; $\kappa = 0.4$ is the von Karman universal constant; z_0 is the roughness length. The wind-friction velocity can be obtained from the wind-stress coefficient, C_{10} , which was proposed as (Wu, 1980)

$$C_{10} = \tau/\rho_a U_{10}^2 = (u_*/U_{10})^2 = (0.8 + 0.065U_{10}) \times 10^{-3} \quad [2]$$

where U_{10} is the wind velocity measured at 10 m above the mean sea surface and expressed in m s^{-1} . It is generally accepted that the growth of the roughness length follows the Charnock (1955) equation; the latter with the recently determined proportionality constant (Wu, 1980) can be written as

$$z_0/(u_*^2/g) = a, \quad a = 0.0185 \quad [3]$$

in which g is the gravitational acceleration, and a the Charnock constant.

The wind stress actually consists of two portions, the momentum fluxes to aqueous flows and to waves. The former is transmitted by the form drag due to separation of airflows from wavelets (Wu, 1968), while the latter is the momentum flux extracted by long waves due to their growth in the wind direction (Stewart, 1961). The fraction of wind stress associated with the direct momentum flux to long waves was found to be about 0.2 (Hasselmann, et al., 1973; Phillips, 1977). Since the form drag on the roughness elements does not support all the wind stress, the Charnock equation is rewritten as

$$z_r = a(ru_*^2)/g \quad [4]$$

where $r = 0.8$ is the ratio between the momentum flux to aqueous flows and the wind stress, and z_r is used to be distinguishable from z_0 .

It was suggested (Wu, 1969) that the airflow over the wind-disturbed water surface separates from the wavelet with its phase velocity (c) smaller than the wind-friction velocity. This proposal with $c/u_* = 1$ as the criterion for flow separation is consistent with laboratory (Wu, 1968; Banner and Melville, 1976) as well as field (Wu, 1970) data. Consequently, we can obtain the length of wavelets (λ_r) satisfying $c/u_* = 1$ from the dispersion relationship (Lamb, 1932)

$$c = \left[\frac{g\lambda_r}{2\pi} + \frac{2\pi\sigma}{\rho_w\lambda_r} \right]^{1/2} \quad [5]$$

when σ is the surface tension, and ρ_w the density of water. These wavelets are therefore the major contributor of roughness elements; the length of these wavelets is presented in Fig. 1. The length of waves having the minimum phase velocity, $\lambda = 1.73$ cm for $c_{\min} = 23$ cm s⁻¹ is also shown in the figure. The procedure of identifying the critical wavelet is not applicable at low winds where the minimum phase velocity is larger than the wind-friction velocity. Consequently, no airflow separation should occur over wavelets for $U_{10} < 7$ m s⁻¹. This is very interesting, because at this very wind velocity the atmospheric surface layer becomes aerodynamically rough (Wu, 1981).

Slick Surface: Effects of an artificial slick upon the atmospheric surface layer of the sea surface have been studied by Barger et al. (1970), with the spontaneous spreading of film-forming chemical, oleyl alcohol (octadecen-1-ol, the cis isomer). Vertical wind profiles were measured for both clean and slick surfaces and were found to follow the logarithmic distribution shown in Eq. [1]. Values of the roughness length reported by Barger et al. are reproduced in Fig. 2.

As the wind velocity increases from 1 to 4 m s⁻¹, the roughness length of the clean surface is seen in Fig. 2 to increase sharply. This is due to the rapid growth of small waves in this region, accompanying the transition of the atmospheric surface layer from smooth to rough. For the present purpose, it suffices to say that a stem of rapid growth is clearly demonstrated.

During the passage of the slick over the measuring station, the small waves were observed to be damped and the roughness length changed drastically. A stem of rapid growth of the roughness growth is also demonstrated, but shifted to wind velocities between 5 and 7 m s⁻¹. Below this velocity region the surface is aerodynamically smooth; above this velocity region the roughness length of the slick surface is comparable to that of the clean surface. The latter effect was suggested due to the disruption of the surface film by the wind (Wu, 1971).

Mean-Square Slopes and Slope Spectrum

Mean-Square Slopes: The sea surface is covered with ripples; the structure of these ripples is generally described by the mean-square slope, $\overline{s^2}$,

$$\overline{s^2} = \int_0^{\infty} k^2 \psi(k) dk$$

$$\psi(k) = (B/\pi)k^{-4} \quad k_Y < k < k_0 \quad [6]$$

$$\psi(k) = (B'/\pi)k^{-4} \quad k_0 > k < k_Y$$

where $\psi(\vec{k})$ is the directional wave number spectrum, \vec{k} and k are respectively the wave-number vector and scalar, k_0 is the wave number at the spectral maximum, k_Y is the maximum wave number where the effect of surface tension is negligible, and k_Y is the neutrally stable wave number; B and B' are the spectral coefficients for the gravity and capillary ranges, respectively. The two wave numbers k_Y and k_0 can be expressed respectively as $(\rho_w g / \sigma)^{1/2}$ and g / U_{10}^2 .

Cox and Munk (1954) deduced slopes of the sea surface from the sun glitter; their data are reproduced in Fig. 3a. Some of their measurements were conducted in the interior of a dense slick, where waves shorter than about 30 cm were reported to be absent. Consequently, for this portion of the data, Eq. [6] can be written as

$$\overline{s^2} = B \ln[(U_{10}^2 / g) k_s] \quad [7]$$

Fitting the above expression to the data, we have (Wu, 1972)

$$B = 4.6 \times 10^{-3}, \quad \lambda_s = 2\pi / k_s = 38 \text{ cm}$$

where λ_s is the minimum wavelength of the slick surface, and is in rather close agreement with the observed value.

Relative to those obtained in the slick, the data from clean surface at low winds are seen in Fig. 3a to have an almost parallel upward shift. The mean-square slope associated with this shift, about 0.0115, should be the contribution from wave components with their wave number greater than k_s . Consequently, the cutoff wave number k_c at low winds can be obtained from Eqs. [6] and [7], provided that k_c is smaller than k_Y ,

$$0.0046 \ln(k_c / k_s) = 0.0115, \quad k_c = 2.5 \text{ cm}^{-1} \quad [8]$$

The value of k_c is seen indeed smaller than k_Y , which is about 3.6 cm^{-1} . The closeness of these two values indicates that the contribution to the mean-square slope at high winds above the extension of the line fitted through the clear-surface data at low winds must come from wave components in the capillary range,

$$\overline{s_r^2} = \overline{s^2} - B \ln(k_Y U_{10}^2 / g) = B' \ln(k_f / k_Y) \quad [9]$$

in which k_f is used to replace k_Y with k_c approaching k_Y as a limit. Since both terms on the left-hand side of the above expression vary with U_{10} , the term on the right-hand side must vary with U_{10} . Consequently, fitting a line to the data replotted in Fig. 3b allows an independent determination of the spectral coefficient B' .

$$B' = 3.15 \times 10^{-2}$$

Slope Spectra: The directional wave-number spectra were illustrated in the last section to be compatible with the measured mean-square slopes of the sea surface. However, it is generally considered that the elevation spectrum does not have resolution fine enough to describe the structure of ripples. Moreover, large discrepancies exist among various sets of reported measurements of the mean-square slope (Long and Huang, 1976; Tang and Shemdin, 1983). Much of these can be resolved with the slope spectrum.

An optical system for measuring continuous two-dimensional slopes of the wind-disturbed water surface has been developed (Haimbach, 1985). The system consists of a collimated light source (a laser), a high-speed photodiode matrix camera, two digital wave-height probes and an interfaced computer. The laser beam directed vertically upward is refracted by the water surface, and is projected following Snell's law onto a horizontal screen. The displacement of the projected laser beam on the screen from its neutral position is tracked by the computer-interfaced camera; the latter has a 100 x 100 matrix and is operated at 400 frames per second.

Using the above technique, time series of highly resolved two-dimensional water-surface slopes were obtained in the Wind-Wave-Current Research Facility. The data were processed to obtain spectra of both upwind-downwind and crosswind slopes; see Fig. 4. In the figure, each slice is the spectrum at a given wind-friction velocity, and f is the frequency of waves. Substantial contributions are seen from gravity waves; this may provide the explanation for discrepancies in the reported mean-square slope measured in various tanks as well as those between laboratory and field results (Wu, 1977).

As the wind velocity increases ($u_* > 60 \text{ cm s}^{-1}$), the spectrum in the capillary range appears to be not only saturated but also isotropic and has an f^{-1} shape. The saturated region extending to as high as 45 Hz can be described by

$$S(f) = 0.0214 f^{-1} \quad [10]$$

$$S_{ud}(f) = S_c(f) = 0.0107 f^{-1}$$

where the subscripts indicate the upwind-downwind (ud) and crosswind components. At even higher frequencies ($> 45 \text{ Hz}$), there appears to be a cutoff, with the spectrum following an f^{-2} trend.

3. VISCOUS SUBLAYER BELOW THE AIR-SEA INTERFACE

Variation of Viscous-Sublayer Thickness

The aqueous boundary layer of the upper ocean is generally turbulent. Due to the damping of turbulence by the air-sea interface, a viscous region has been considered to exist immediately below the sea surface; this region is very thin and is the so-called viscous sublayer. Its thickness was considered to behave similarly as that over a solid surface (Schlichting, 1968)

$$\delta_v^+ = \delta_v u_{*w} / \nu_w = 8 \quad [11]$$

where δ_v and δ_v^+ are the physical and nondimensional thicknesses of the viscous sublayer, u_{*w} is the friction velocity of aqueous flows, and ν_w is the kinematic viscosity of water; the thickness of the viscous sublayer is considered here to correspond to the depth where the velocity deviates from the linear profile; in other words, the sublayer thickness varies inversely with the friction velocity.

Drift currents immediately below the wind-disturbed water surface were systematically measured in a circulating wind-wave tank (Wu, 1984). The results confirmed the existence of a viscous sublayer at the air-water interface, with the current varying linearly with depth and the shear stress determined from the linear profile comparing very favorably with the wind stress. The thickness of the viscous sublayer below the air-water interface is presented in Fig. 5a; an almost constant thickness, $\delta_v = 0.8$ mm, is seen except at the lowest wind velocity. Consequently, for most wind velocities the nondimensional thickness of the viscous sublayer below the air-sea interface, instead of having a constant value, increases with the friction velocity as illustrated in Fig. 5b and represented by the following expressions,

$$\begin{aligned} \delta_v^+ &= 4 & u_{*w} < 0.2 \text{ cm s}^{-1} \\ \delta_v^+ &= 4 + 6.3(u_{*w} - 0.2)^2 & 0.2 \text{ cm s}^{-1} < u_{*w} < 1.0 \text{ cm s}^{-1} \quad [12] \\ \delta_v^+ &= 8 & u_{*w} > 1.0 \text{ cm s}^{-1} \end{aligned}$$

where u_{*w} is expressed in cm s^{-1} ; these expressions are illustrated in Fig. 5b. In summary, the nondimensional thickness of the viscous sublayer is smaller than that over the solid surface and also varies with currents.

The above results are consistent with the single current profile reported by McLeish and Putland (1975), the temperature profiles measured by Khundzhua et al. (1977) as well as the concepts advanced by Saunders (1973), who suggested that the turbulent process should penetrate closer to the air-sea interface than to the solid boundary.

Further Supports of Proposed Variation

Thermal Sublayer: Within the viscous sublayer, exchanges of momentum and heat are mainly due to molecular process (Khundzhua et al., 1977). Relative efficiency of momentum and heat transfers depends on the molecular Prandtl number (Schlichting, 1968): $P = \nu_w/D_t$, where D_t is the molecular thermal diffusivity. For water with $P = 7$ approximately, the momentum diffusion is more effective than the thermal diffusion. Consequently, we have inside the viscous sublayer a region where the heat transfer is through the molecular process; this region is the co-called thermal sublayer.

The thickness of the thermal sublayer (δ_t) can be related to the net heat flux (Q) across the air-sea interface (through the sublayer) and the difference in temperatures at the sea surface and the lower boundary of the sublayer (ΔT) as (Saunders, 1973)

$$\Delta T = (1 - r)^{1/2} \frac{Q \nu_w}{c_p \rho_w u_{*w}} = \Lambda \frac{Q \nu_w}{c_p \rho_w u_{*w}'} \quad [13]$$

$$\Lambda = (1 - r)^{1/2} u_{*w}'/u_{*w} \text{ and } u_{*w}' = u_* (\rho_a/\rho_w)^{1/2}$$

where c_p is the specific heat and u_{*w}' is the current-friction velocity calculated from the wind stress assuming the stress continuity. Subsequently, field experiments have been conducted to determine the value of Λ .

Oceanic data reported by various investigators (Grassl, 1976; Simpson and Paulson, 1980; Paulson and Simpson, 1981) are compiled in Fig. 6a; different values of the wind-stress coefficient were adopted in their data analysis. For a fair comparison, their results were recalculated by uniformly adopting the wind-stress coefficient shown in Eq. [2]. The recalculated values of Λ shown in Fig. 6a are presented in Fig. 6b, and are seen to be much less scattered.

The results shown in Fig. 6 have a rather clear trend: Λ increasing with U_{10} at low winds and approaching a constant value at high winds. The scattered data do not warrant a detailed curve fitting; two expressions in simplest forms were proposed to approximate the trend (Wu, 1985):

$$\begin{aligned} \Lambda &= 2 + (5/7)U_{10} & U_{10} < 7 \text{ m s}^{-1} \\ \Lambda &= 7 & U_{10} > 7 \text{ m s}^{-1} \end{aligned} \quad [14]$$

where U_{10} is expressed in m s^{-1} . Lines corresponding to the above expressions are drawn in Fig. 6b; the trend illustrated by the lines is consistent with that of Eq. [12].

Diffusion Sublayer: The rate of gas transfer of non-reactive gas across the sea surface is considered to be governed by molecular process within the viscous sublayer immediately below the air-sea interface (Bolin, 1960; Deacon, 1977). The nondimensional resistance of gas transfer (R) across the sublayer can be expressed as

$$R = \delta_v^+ / D_g \quad [15]$$

where D_g is the molecular diffusivity of gas. The transfer velocity of gas (V) is related to the flux as

$$V = \text{Flux} / \Delta C \quad [16]$$

where ΔC is the difference in gas concentrations between boundaries of the sublayer, with its upper boundary at the sea surface. Consequently, the transfer velocity can be found from

$$V = \frac{u_{*w}}{R} = \frac{Du_*}{\delta_v^+} \quad [17]$$

In other words, for a given gas the rate of transfer is proportional to the friction velocity of aqueous flows, and inversely to the nondimensional thickness of the viscous sublayer.

Data on the rate of gas transfer across the air-sea interface were reviewed by Deacon (1981) and by Hasse and Liss (1980). In the former review, the nondimensional thickness of viscous sublayer below the interface was considered to be constant, $\delta_v^+ = 11.6$. On the basis of this value, the calculated rate of gas transfer was found to be only a fraction of the measured quantity at light winds ($< 7 \text{ m s}^{-1}$). The most distinguished feature of the latter review is that the rate of gas transfer was found to vary much more gradually with wind velocity than the above predicted trend.

The friction velocity of aqueous flows at various wind velocities can be estimated from Eqs. [2] and [13] with $r = 0.2$, and the nominal thickness of the viscous sublayer can be calculated from Eq. [12]; the results are presented in Fig. 7a. The sublayer is seen only one half as thick as that over the solid surface at light

winds, and increases toward the solid-surface value at moderate winds.

For a given gas under a certain sea state, the transfer velocity is shown in Eq. [17] to be inversely proportional to the nondimensional thickness of the viscous sublayer. Consequently, the ratio between the transfer velocity (V_w) calculated with Eq. [12] and the earlier estimate (V_d) with $\delta_v^+ = 11.6$ can be expressed as

$$V_w/V_d = 11.6/\delta_v^+ \quad [18]$$

and is shown in Fig. 7b. In other words, the revised theoretical value is greater than the earlier estimate by a factor of V_w/V_d .

The trend of the modification factor shown in Fig. 7b is of interest in explaining discrepancies between field measurements and predicted values. The measured rates of gas transfer were pointed out by Deacon (1981) to exceed the theoretical value by a factor of two to three at light winds, where the revised theoretical value is about twice the earlier prediction. The modification factor decreases as the wind velocity increases; therefore, the revised theoretical value has a much more gradual overall variation with the wind velocity; this is the main feature of field measurements pointed out by Hasse and Liss (1981). In summary, the field measurements of gas transfer appear to support recent results on the aqueous viscous sublayer.

4. DISCUSSION

We first discussed the most representative length of wavelets which constitute the sea-surface roughness. Inasmuch as the roughness is associated prominently with remote sensing of the sea surface, this therefore provides the basis for evaluating effects of the surface film through wave damping. Subsequently, we show that effects of the surface film on roughness length disappear as the wind velocity increases beyond 7 m s^{-1} .

The mean-square slope of both clean and slick sea surfaces measured by Cox and Munk were reanalyzed. Contrary to common thinking, the capillary waves contribute insignificantly at low winds ($< 7 \text{ m s}^{-1}$). The waves damped by the film have lengths falling between 1.73 and 30 cm. Another interesting feature is that the effects of film on the mean-square slope also diminish at wind velocities greater than 7 m s^{-1} .

Finally, all evidence indicates that the aqueous viscous sublayer exists immediately below the air-sea interface; it is

thinner than, and also behaves differently from, that over the solid surface. Further understanding of the structure of the viscous sublayer is essential for investigations of the interface microlayer.

Acknowledgement: I am very grateful for the sponsorship provided by the Fluid Dynamics Program, Office of Naval Research under Contract No. N00014-83K-0316.

REFERENCES

- Banner, M. L. and W. K. Melville, 1976: On the separation of airflow over water waves. *J. Fluid Mech.* 177, 825-842.
- Barger, W. R., W. D. Garrett, E. L. Mollo-Christensen and K. W. Ruggles, 1970: Effects of an artificial sea slick upon the atmosphere and the ocean. *J. Appl. Meteorol.* 9, 396-400.
- Bolin, B., 1960: On the exchange of CO_2 between the atmosphere and the sea. *Tellus* 12, 274-281.
- Charnock, H., 1955: Wind stress on a water surface. *Quart. J. Roy. Meteorol. Soc.* 81, 639-640.
- Cox, C. S. and W. H. Munk, 1954: Statistics of the sea surface derived from sun glitter. *J. Mar. Res.* 13, 198-227.
- Deacon, E. L., 1977: Gas transfer to and across an air-water interface. *Tellus* 29, 363-374.
- Deacon, E. L. 1981: Sea-air gas transfer: The wind-speed dependence. *Boundary-Layer Meteorol.* 21, 31-37.
- Grassl, H., 1976: The dependence of the measured cool skin of the ocean on wind stress and total heat flux. *Boundary-Layer Meteorol.* 10, 465-474.
- Haimbach, S. P., 1985: Development of slope spectra of the wind-disturbed water surface. Ph.D. Dissertation, University of Delaware.
- Hasse, L. and P. S. Liss, 1980: Gas exchange across the air-sea interface. *Tellus*, 32, 470-481.
- Hasselmann, K. et al., 1973: Measurements of wind wave growth and swell decay during the Joint North Sea Wave Project (JONSWAP). Herausgegeben von Deutsch Hydrograph Institute Reihe A12.
- Hühnerfuss, H., W. Alpers, W. D. Garrett, P. A. Lange and S. Stalte, 1983a: Attenuation of capillary and gravity waves at sea by monomolecular organic surface films. *J. Geophys. Res.* 88, 9809-9816.
- Hühnerfuss, H. et al., 1983b: The modification of X and L band radar signals by monomolecular sea slicks. *J. Geophys. Res.* 88, 9817-9822.

- Khundzhua, G. G., A. M. Gusev, Ye. G. Andreyev, V. V. Gurov and N. A. Skorkhovotov, 1977: Structure of the cold surface film of the ocean and heat transfer between the ocean and the atmosphere. *Atmos. Oceanic Phys.* 13, 506-509.
- Lamb, H., 1932: *Hydrodynamics*. 6th edition. Cambridge University Press.
- Long, S. R. and N. E. Huang, 1976: On the variation and growth of wave-slope spectra in the capillary-gravity range with increasing wind. *J. Fluid Mech.* 77, 209-228.
- McLeish, W. and G. E. Putland, 1975: Measurements of wind-driven flow profiles in the top millimeter of water. *J. Phys. Oceanogr.* 5, 516-518.
- Paulson, C. A. and J. J. Simpson, 1981: The temperature difference across the cool skin of the ocean. *J. Geophys. Res.* 86, 11044-11054.
- Phillips, D. M., 1977: *The dynamics of the upper ocean*. 2nd edition. Cambridge University Press.
- Saunders, P. M., 1973: The skin temperature of the ocean, A review. *Mém. Soc. Roy. Sci. Liège 6^e Ser.* 93-98.
- Schlichting, H., 1968: *The boundary-layer theory*. McGraw-Hill.
- Simpson, J. J. and C. A. Paulson, 1980: Small-scale sea surface temperature. *J. Phys. Oceanogr.* 10, 399-410.
- Stewart, R. W., 1961: The wave drag of wind over water. *J. Fluid Mech.* 10, 189-194.
- Tang, S. and O. H. Shemdin, 1983: Measurements of high frequency waves using a wave follower. *J. Geophys. Res.* 88, 9832-9840.
- Wu, Jin, 1968: Laboratory studies of wind-wave interaction. *J. Fluid Mech.* 34, 91-112.
- Wu, Jin, 1969: A criterion for determining airflow separation from wind waves. *Tellus* 21, 707-717.
- Wu, Jin, 1970: Wind-wave interactions. *Phys. Fluids* 13, 1926-1930.
- Wu, Jin, 1971: Evaporation retardation by monolayers: Another mechanism. *Science* 174, 283-285.
- Wu, Jin, 1972: Sea-surface slope and equilibrium wave spectra. *Phys. Fluids* 15, 741-747.
- Wu, Jin, 1977: Direction slope and curvature distributions of wind waves. *J. Fluid Mech.* 79, 463-480.
- Wu, Jin, 1980: Wind-stress coefficient over sea surface near neutral conditions - A revisit. *J. Phys. Oceanogr.* 10, 727-740.
- Wu, Jin, 1981: On critical roughness Reynolds number of the atmospheric surface layer. *J. Geophys. Res.* 86, 6661-6665.
- Wu, Jin, 1984: Viscous sublayer below a wind-disturbed water surface. *J. Phys. Oceanogr.* 14, 138-144.
- Wu, Jin, 1985: On the cool skin of the ocean. *Boundary-Layer Meteorol.* 31, 203-207.

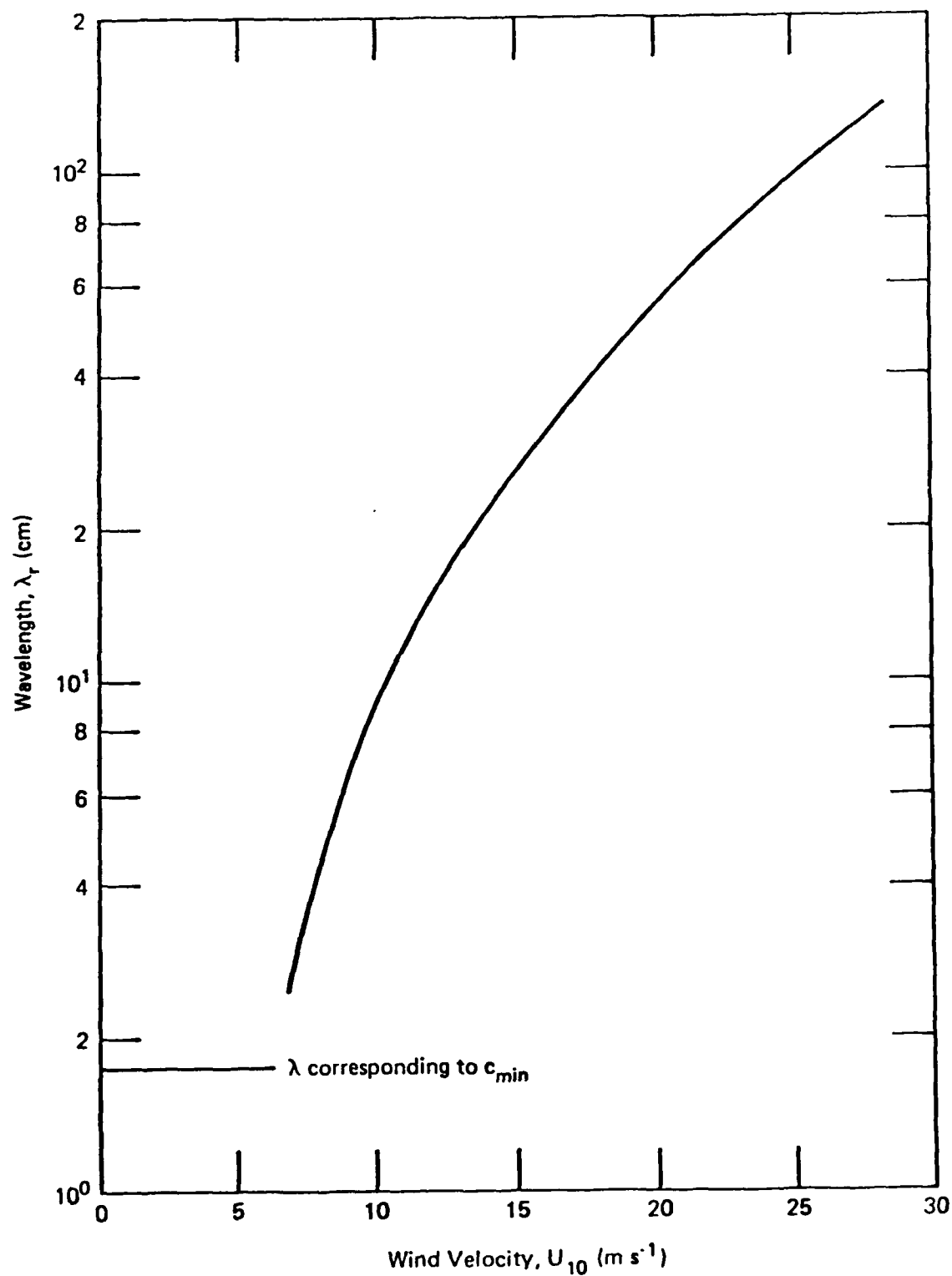


FIGURE 1 — WAVELENGTHS OF RIPPLES ACTING AS ROUGHNESS ELEMENTS AT VARIOUS WIND VELOCITIES.

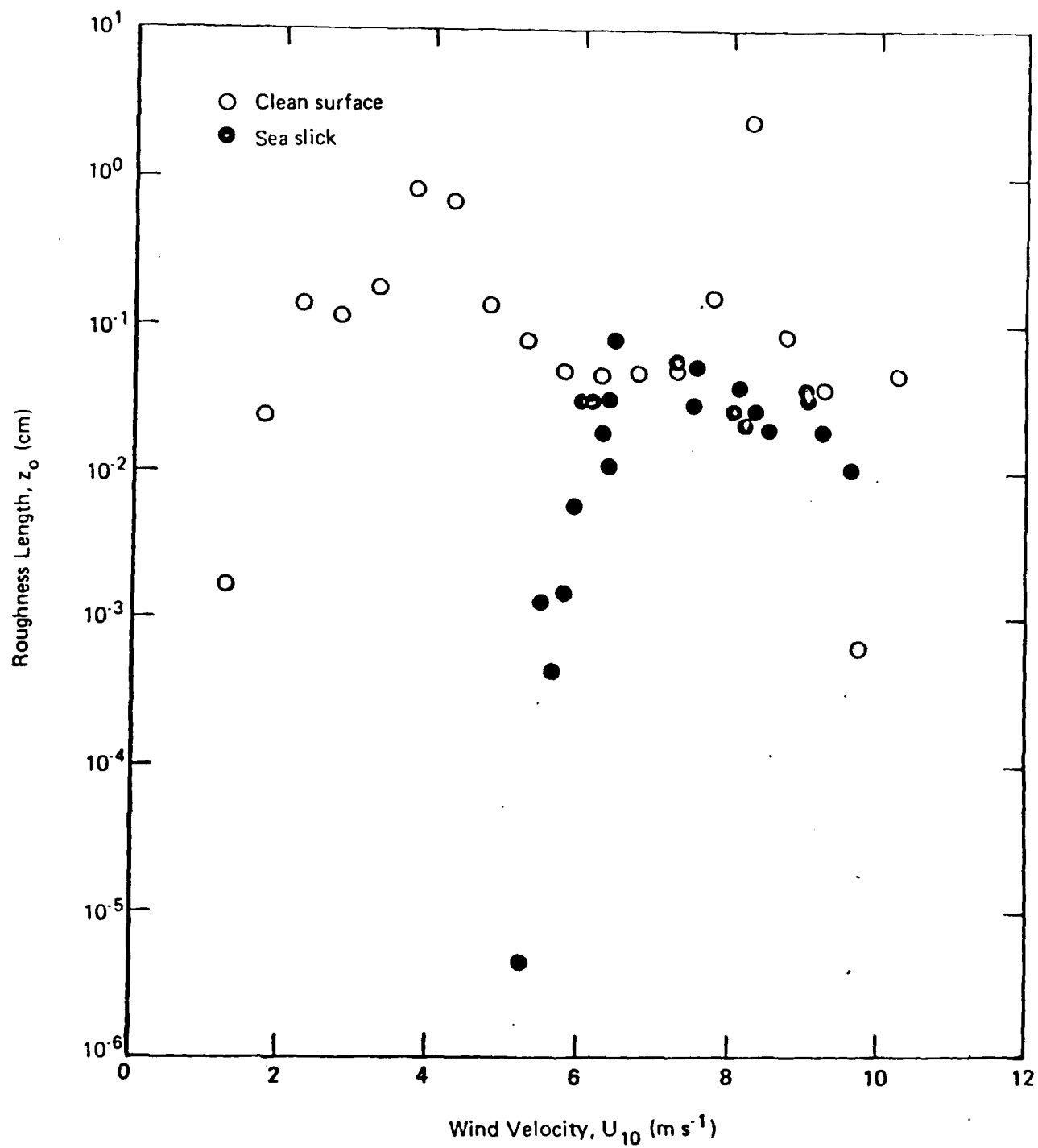


FIGURE 2 — COMPARISON OF SURFACE ROUGHNESS MEASURED OVER SEA SLICK AND OVER CLEAN SURFACE (From Ref. 4).

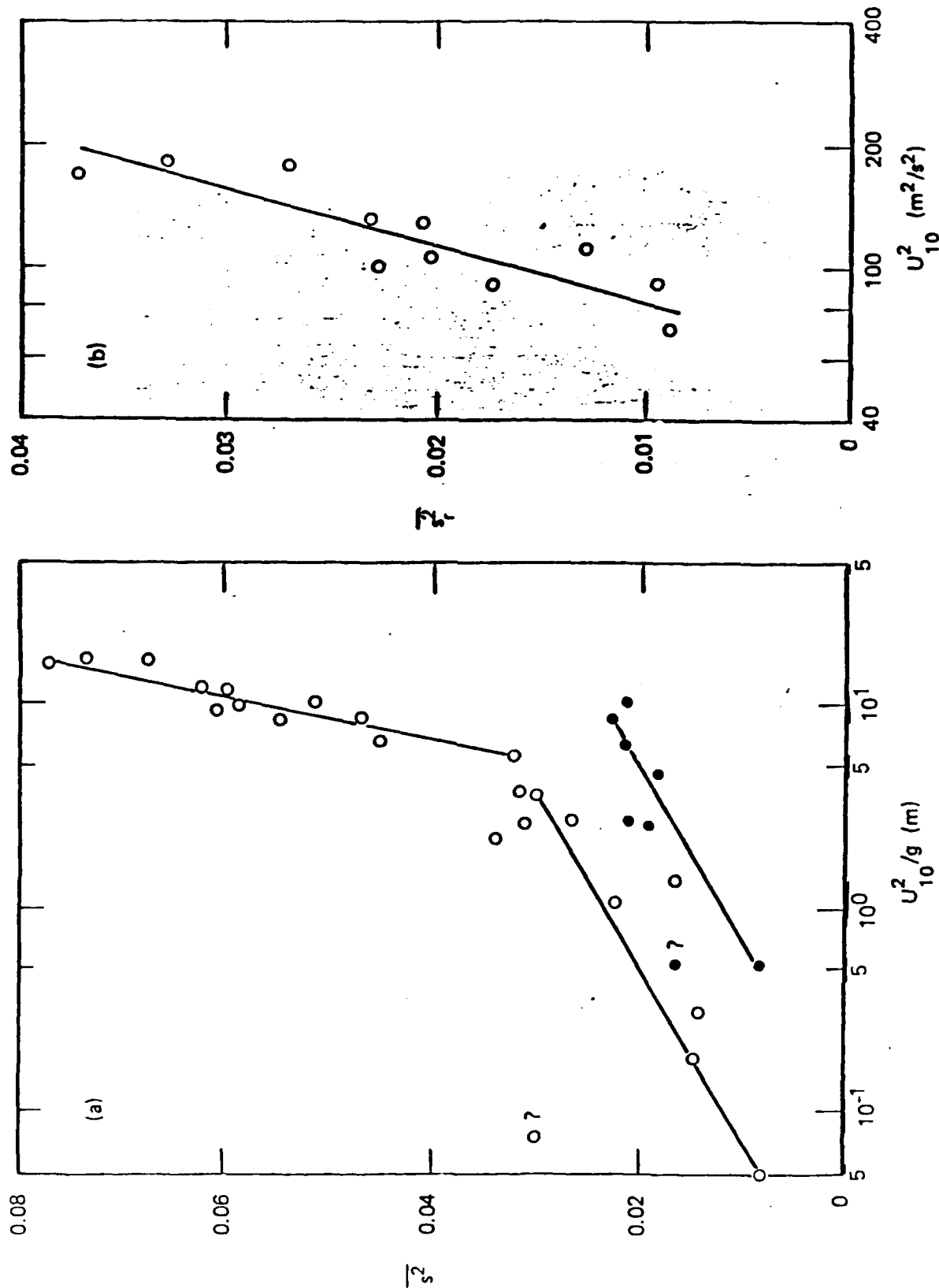


FIGURE 3 - DETERMINATION OF SPECTRAL COEFFICIENTS FROM MEAN-SQUARE SLOPES. The data obtained from the clean surface are shown as open circles, and from the slick surface as solid circles; only data at high wind velocities are shown in (b). The two data points deviating clearly from the main group and marked with question marks were ignored for the curve fitting.

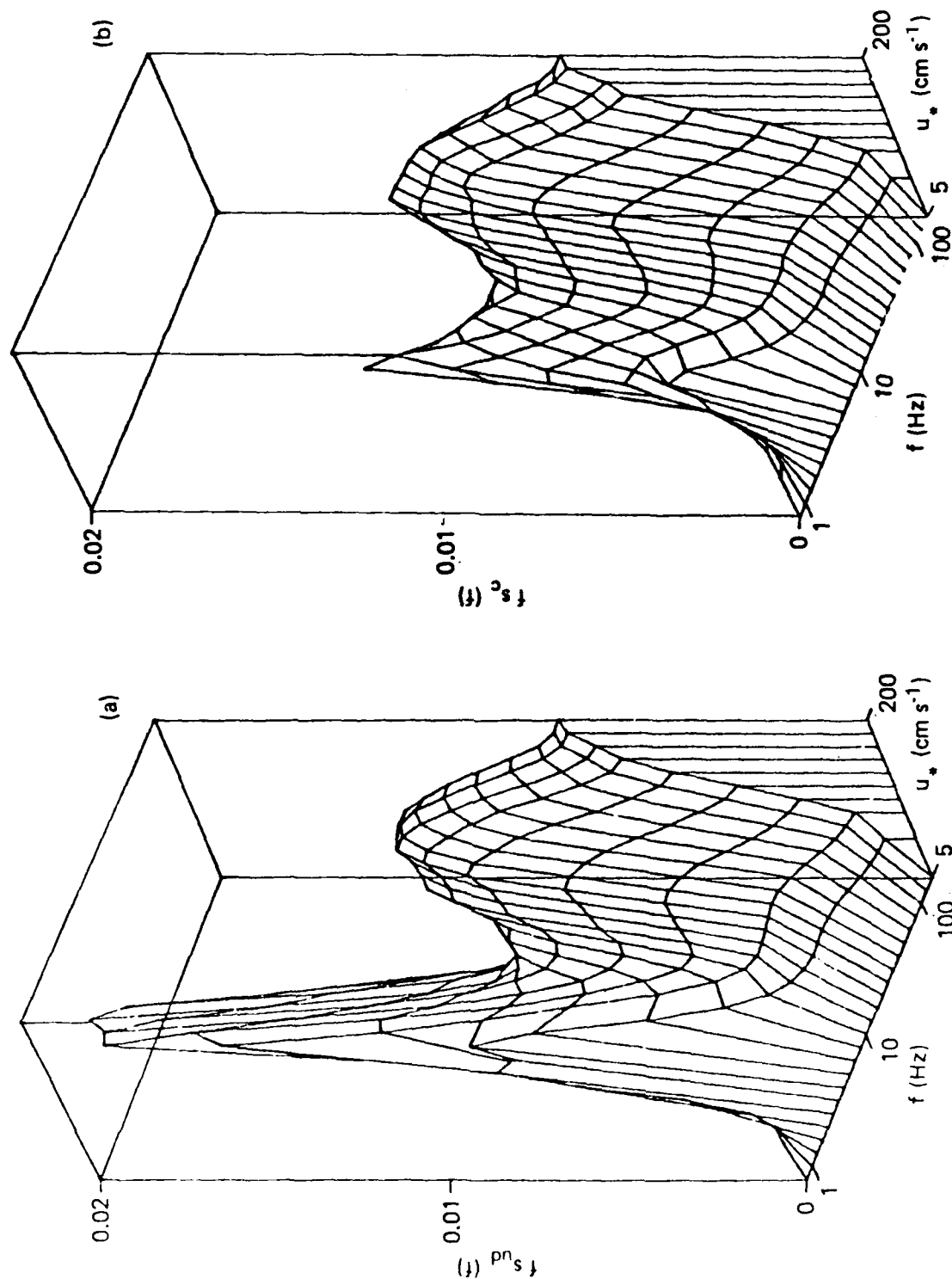


FIGURE 4 - AREA PRESERVING UPWIND-DOWNWIND (a) AND CROSSWIND (b) WATER-SURFACE SLOPE FREQUENCY SPECTRA VS. WIND-FRICTION VELOCITY (u_*).

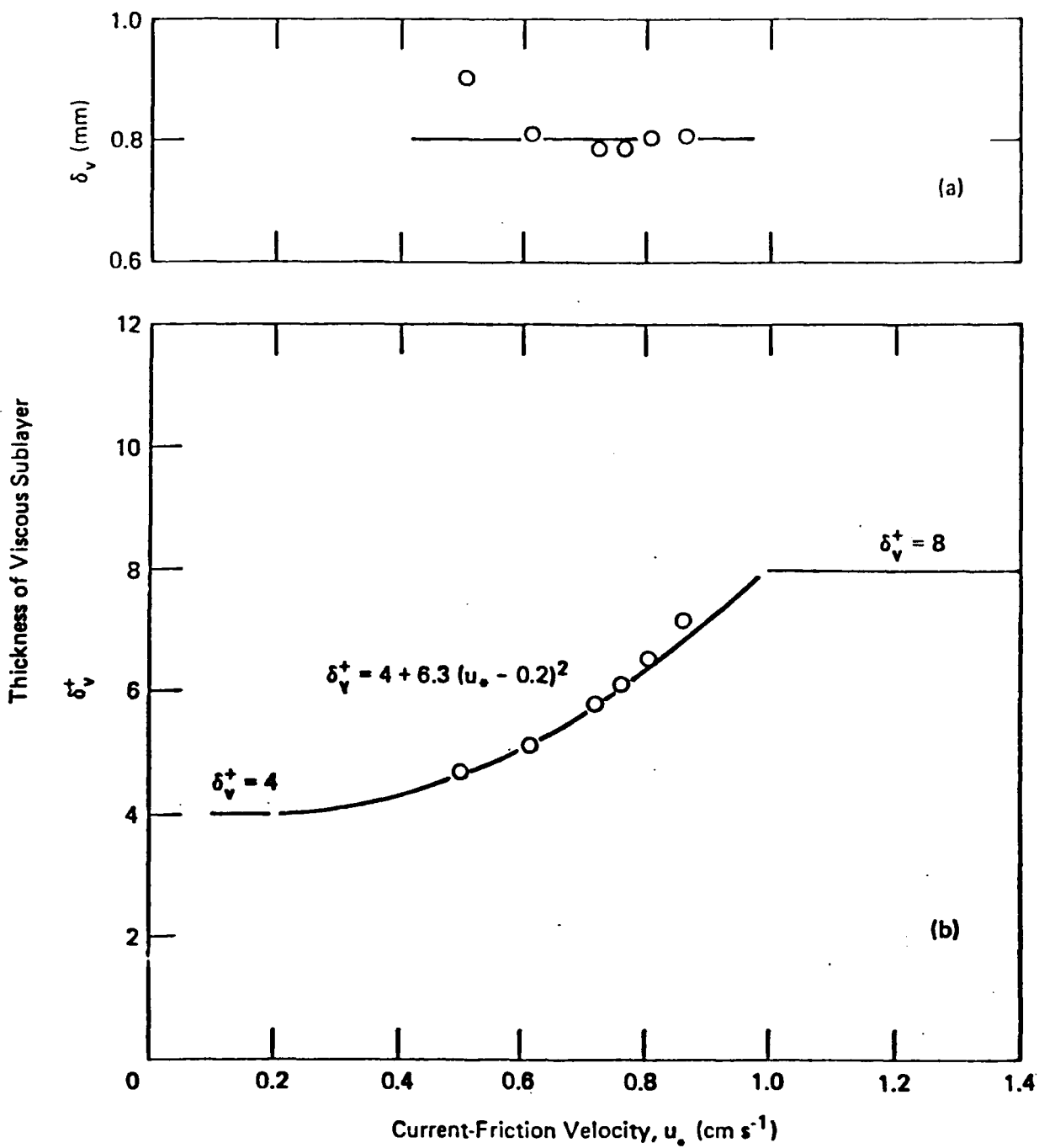


FIGURE 5 – PHYSICAL (a) AND NON-DIMENSIONAL (b) VARIATIONS OF THICKNESSES OF VISCOUS SUBLAYER WITH FRICTION VELOCITY.

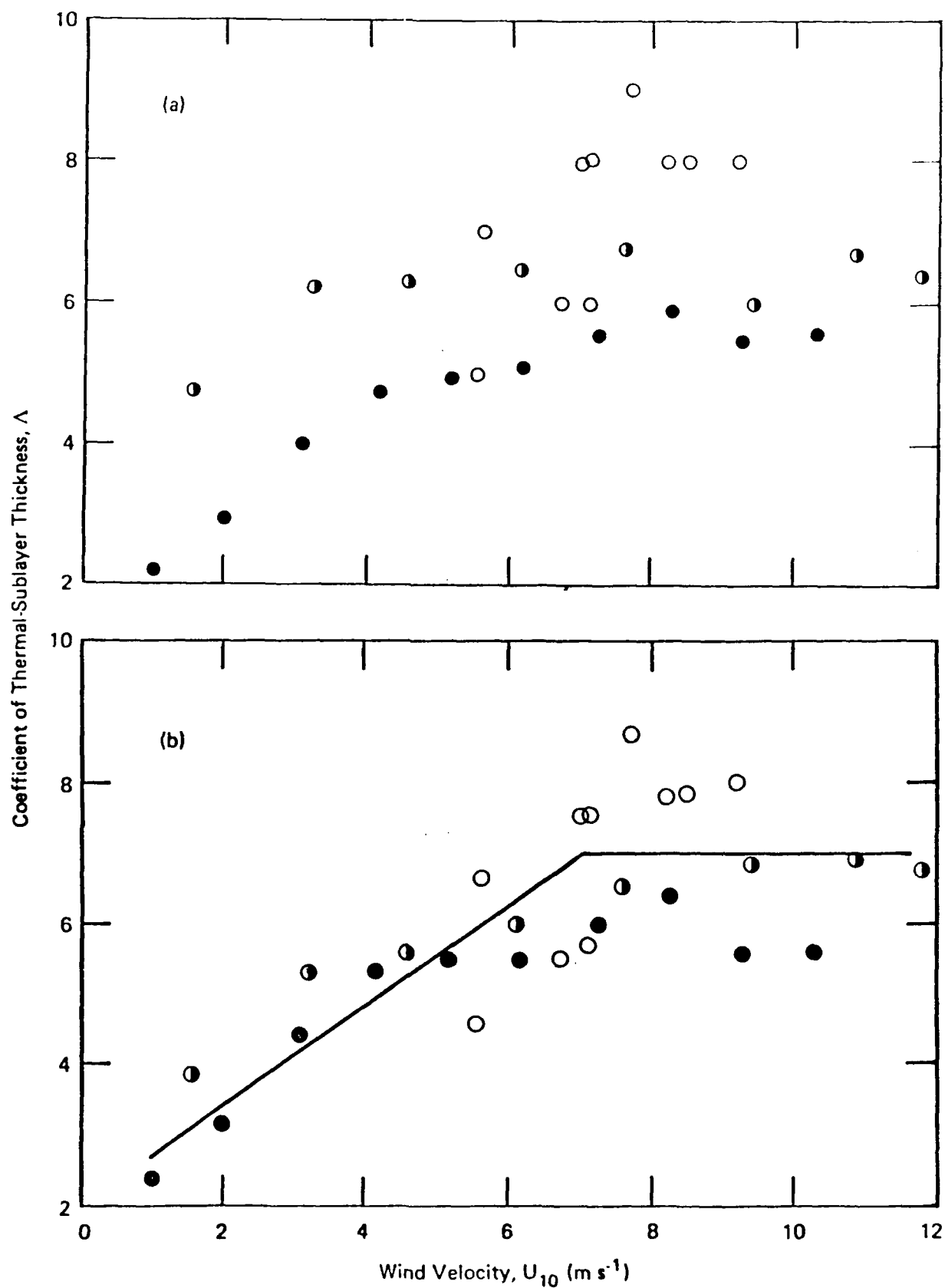


FIGURE 6 — FREQUENTLY CITED OCEANIC RESULTS ON COEFFICIENTS OF THERMAL-SUBLAYER THICKNESS. The data are from Grassl [1976], ●; Simpson and Paulson [1980], ○; and Paulson and Simpson [1981], ◐. The original data are shown in (a), and the values corrected with a common expression of C_{10} in (b).

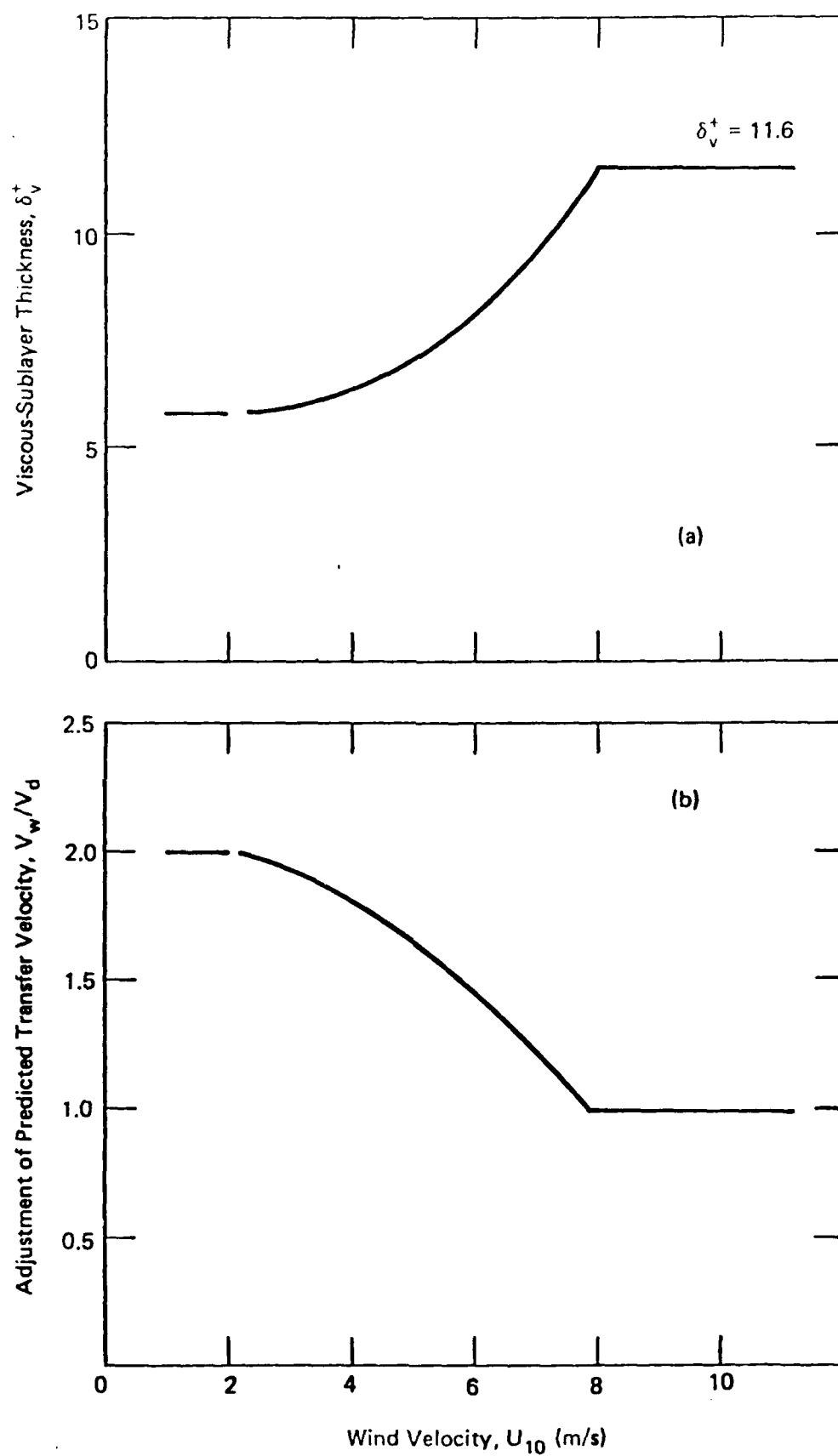


FIGURE 7 - THICKNESS OF AQUEOUS VISCOUS SUBLAYER (a) AND INCREASE OF TRANSFER VELOCITY DUE TO THINNING OF VISCOUS SUBLAYER (b).

THE CHEMICAL COMPOSITION OF THE SEA-SURFACE MICROLAYER AND ITS RELATION TO THE OCCURRENCE AND FORMATION OF NATURAL SEA-SURFACE FILMS

P. M. Williams

Institute of Marine Resources, A-018, Scripps Institution of Oceanography, University of California, San Diego, La Jolla, California 92093

Introduction

One basic question in relating the effects of the sea-surface microlayer to the interpretation of remotely-sensed microwave and optical signatures is the chemical composition of the sea-surface microlayer (surface films) and whether or not this composition is variable in time and space. That is, are these compositional changes of sufficient magnitude to significantly affect the various remote sensing signatures, or can the sea-surface microlayer effects be considered isotropic such that the simple presence or absence of films and not their compositional changes is the important factor -- at least in considering uncontaminated films derived from natural biological sources. Obviously, widespread, episodic blooms and/or mortality of marine organisms leading to the release of large quantities of surface active organics (e.g., Lee and Williams, 1974), significant oil spillage, or widespread atmospheric inputs, such as from forest fires or volcanic emanations could cause transient effects at the sea surface which could appreciably affect remote-sensing signatures.

The question is: What evidence is there for or against major compositional variability in natural sea-surface films? In this report, the composition of the organic fraction of films, principally the "dissolved plus colloidal" phase, is discussed for original films and for films generated *in situ*. Some speculations are also included relevant to the nature of the organic components and to their conformation in the surface microlayer.

The data presented is derived primarily from five "surface-film" cruises (1979-1983) to the Gulf of California, the west coast of Baja California, and in the Southern California Bight (Figure 1). There was a minimum of anthropogenic inputs or disturbances in all these areas during these cruises, and hence the chemistry may be considered representative of the "natural" sea-surface

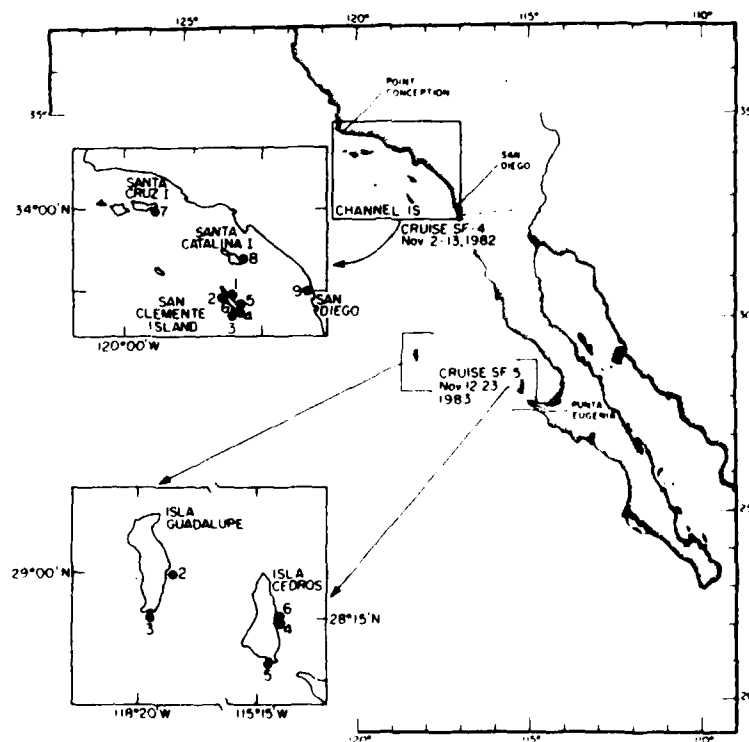
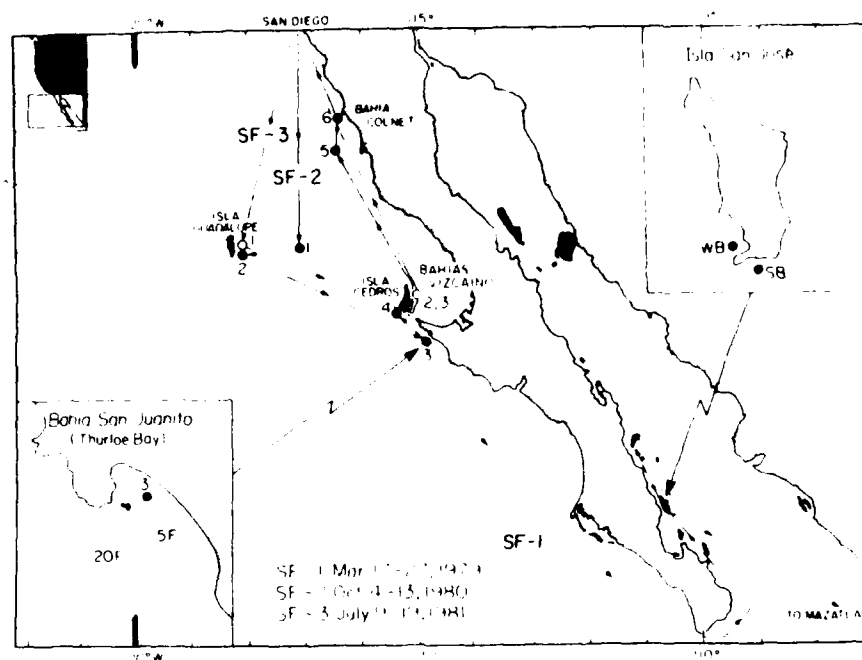


Figure 1. Cruise tracks and sampling stations. Top: Cruises SF-1, -2, -3, taken from Williams *et al.* (1986). Bottom: Cruises SF-4, -5. The Event numbers referred to in the text and Figures are individual sampling sites at the above stations.

microlayer. Coastal and open-ocean regimes with eutrophic and oligotrophic waters were studied as were some diurnal effects and the presence of an El Niño event.

Chemical and biological data from the first three cruises (SF-1, SF-2, and SF-3) has been published or is in press (Williams *et al*, 1980; Horrigan *et al*, 1981; Van Vleet and Williams, 1983; Henrichs and Williams, 1985; Carlucci *et al*, 1985; Carlucci *et al*, 1986; Williams *et al*, 1986). The chemical data from cruises SF-4 and SF-5 has not been published. In addition to the dissolved and particulate organic components, these above-cited papers included measurements of inorganic nutrients, bacterial and planktonic populations, bacterial heterotrophy, phytoplankton primary productivity, chlorophyll-a and phaeopigments, adenosine triphosphate (ATP), UV-adsorption, film pressures, and surface potentials. Some of these parameters are discussed in this paper.

A complete description of the sampling platform, surface potential apparatus, analytical methodology, and descriptive data for Cruises SF-1, -2, and -3 can be found in the references cited above. All film samples were collected with various stainless steel or Nitex screens which nominally sampled the upper 220 to $260 \pm 10 \mu\text{m}$ (stainless steel) and $300 \pm 15 \mu\text{m}$ (Nitex) of the surface microlayer. Subsurface samples were collected in glass bottles at a depth of 5-15 cm. All samples were immediately filtered through $35 \mu\text{m}$ pore size Nitex netting into glass bottles and kept in ice until processing on shipboard.

Chemical Composition

I. Dissolved protein, carbohydrate and lipid

The content of dissolved plus colloidal (passes a $1.0 \mu\text{m}$ pore-size glass fiber filter) protein, (THAA; total hydrolyzable amino acids), total carbohydrate (TCHO; as glucose equivalents), and total lipid (TL; as stearic acid equivalents) in films and subsurface waters (expressed as carbon) is shown in Table 1 and Figures 2 and 3. These are the three major organic components of all organisms, but together constitute, on average, only 26% (range = 14-42%) of the total dissolved organic carbon (DOC), while THAA nitrogen accounts for 23% (range = 7-57%) of the dissolved organic nitrogen (DON) in films. If humic substances (fulvic plus humic acids) are included (Figure 3), then the total "identifiable" carbon is only 43%, on average, of the DOC. This assumes that the two determinations of humic material (15 and $19 \mu\text{moles C l}^{-1}$,

Table 1. Protein, carbohydrate and lipid carbon as percent of total dissolved organic carbon.

Cruise (no. stations)	% Protein ¹	% Carbohydrate ²	% Lipid ³	Total
SF-2 (5)	6	17	4	27
SF-3 (5)	12	21	1	34
SF-4 (4)	3	13	4	20
SF-5 (4)	6	13	3	22 (43) ⁴
Mean	7	16	3	26

¹ Total hydrolyzable amino acid carbon.

² Glucose equivalent carbon.

³ Hexane-soluble stearic acid equivalent carbon.

⁴ Includes humic material, assuming its mean concentration (17 $\mu\text{moles C l}^{-1}$) is applicable to these four stations. See text.

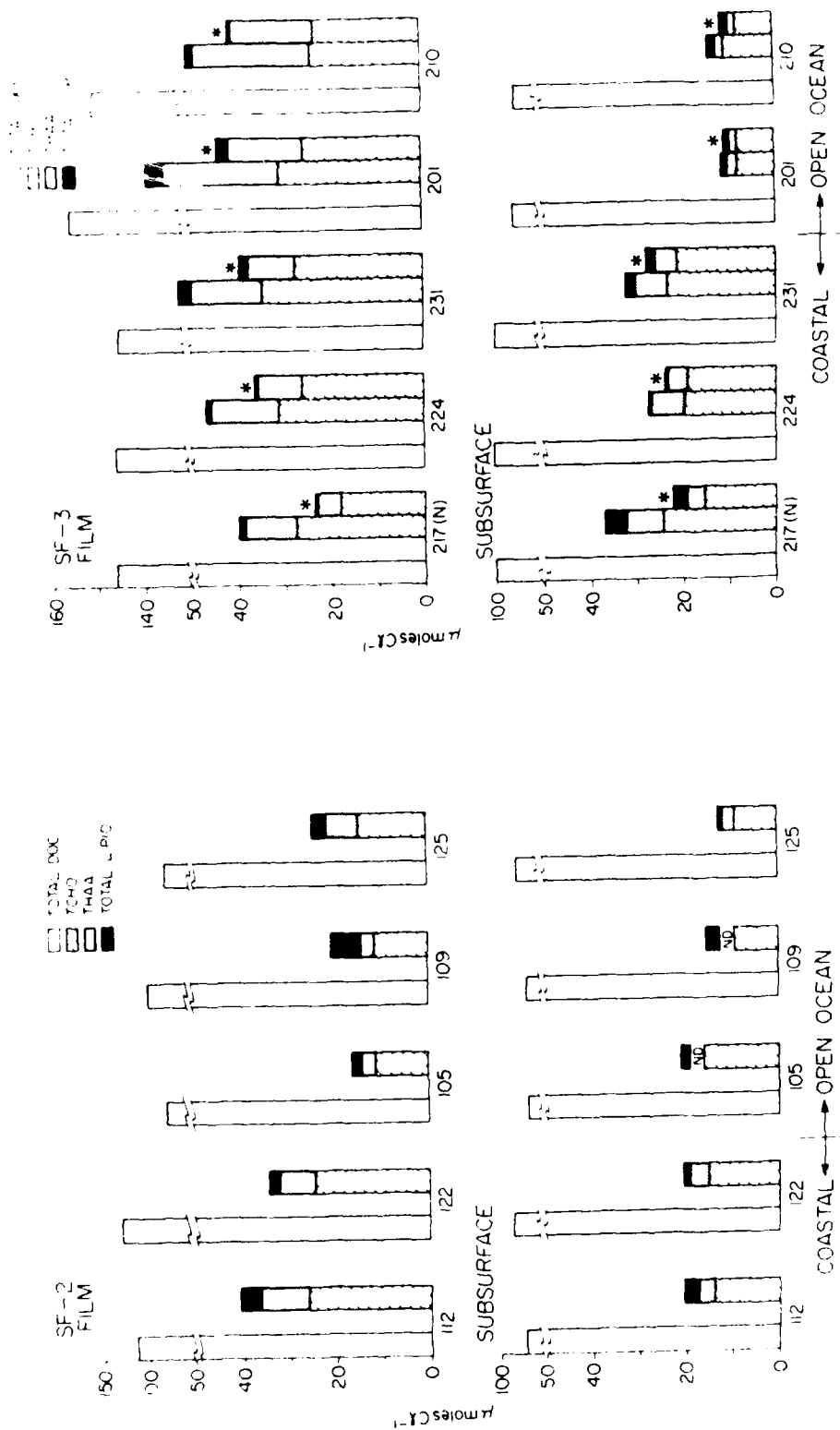


Figure 2. Components of DOC in $\mu\text{moles C l}^{-1}$. Cruise SF-2: Event 112 = Station 3; 122 = 4; 105 = 1; 109 = 9; 125 = 5. Cruise SF-3: 217 (night) = 2; 224 = 2; 231 = 3; 201 = 1. Asterisks (*) = components passing a $1 \mu\text{m}$ glass fiber filter and retained by a $0.2 \mu\text{m}$ polycarbonate filter. Taken from Williams et al. (1986)

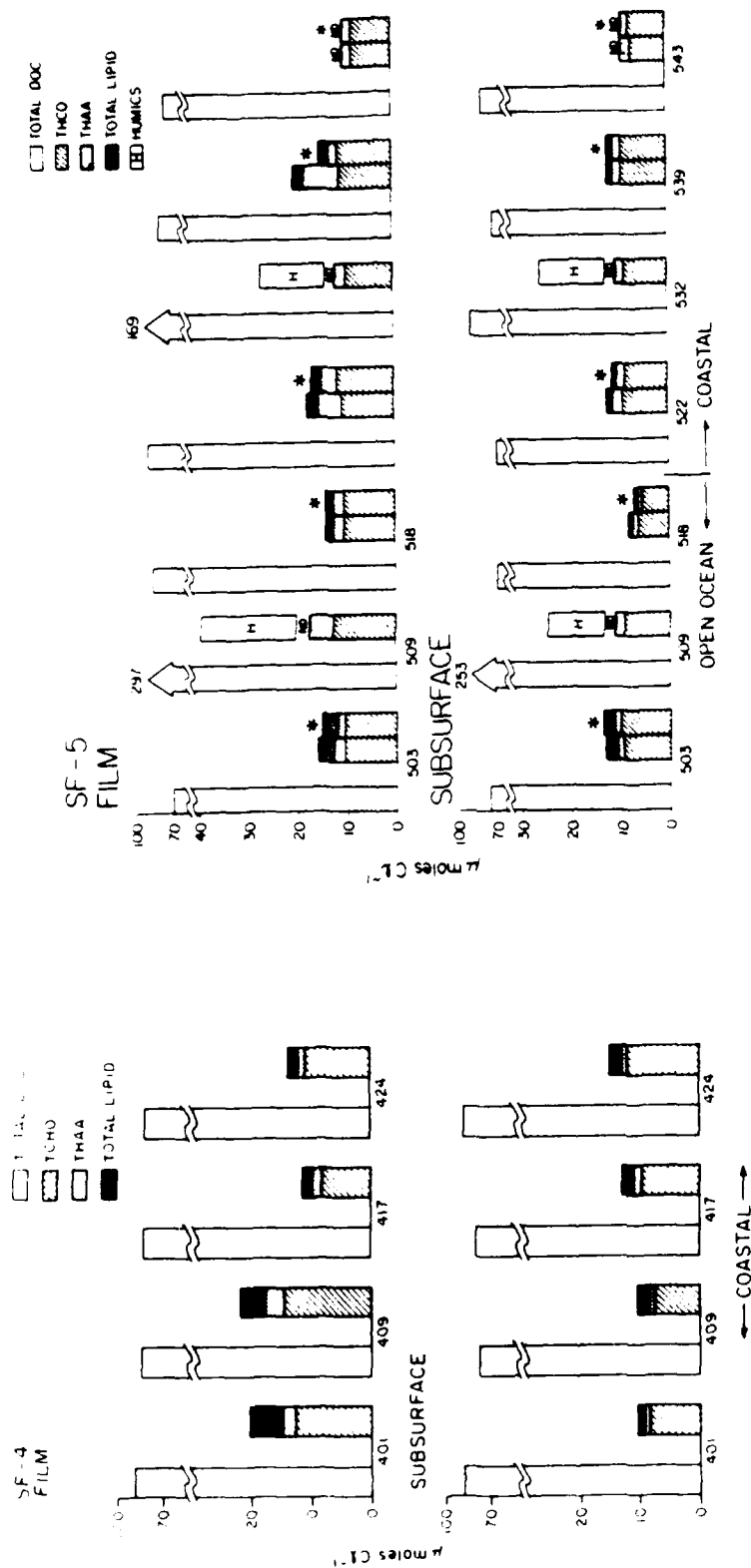


Figure 3. Components of DOC in $\mu\text{moles C l}^{-1}$. Cruises SF-4: Event 401 = Station 1; 409 = 4; 417 = 6; 424 = 8. Cruise SF-5: 503 = 2; 509 = 2; 518 = 2; 522 = 4; 532 = 5; 539 = 6; 543 = 7. Asterisks (*) same as in Figure 2.

Cruise SF-5) are applicable to the four Samples (Events 503, 518, 522 and 539) used to compile the percent THAA, TCHO and TL in Table 1. The extraordinarily high DOC content of the film samples 509 and 532 are considered atypical (see Table 2).

There are large variations in the THAA, TCHO and TL contents of both films and subsurface waters and, in general, these three components have higher concentrations in films than in the corresponding subsurface waters. These large variations are not surprising, considering that each event represents one film patch sampled on one particular day on one particular cruise. Ratios of TCHO/THAA are consistently greater in subsurface waters, and there is a wider range in the concentration of THAA than of TCHO between film samples, whether from open-ocean or coastal waters.

These differences in the microlayer and subsurface water compositions of protein and carbohydrate are probably related to differences in the surface activity of polymers containing amino acids and carbohydrates, and to interactions between surface-active molecules and particles (Henrichs and Williams, 1985). Although TCHO and THAA are positively correlated, this correlation is not stronger than that of either quantity to DOC, indicating no specific association between proteins and carbohydrates (i.e., "proteoglycan" or "glycoprotein"; Baier *et al*, 1974) for the major part of THAA and TCHO. There are negligible amounts of hydrolyzable amino acids associated with humic material isolated from bulk surface seawater on XAD-2 (styrene-divinylbenzene copolymer) resins (Bada *et al*, 1982; Ho *et al*, 1983), but greater than 50% of the THAA were isolated on Sep-Pak C₁₈ (octadecyl-silica adduct) cartridges (Ho *et al*, 1983). Both of these adsorbants will extract "humic-type" materials from seawater provided these materials have sufficient hydrophobic character. Short chain polysaccharides and polypeptides, per se, are not extracted by Sep-Pak C₁₈ or XAD-2 resins, yet Sep-Pak C₁₈ will remove up to ~40% of the DOC, including >50% of the THAA from bulk surface seawater (Ho *et al*, 1983; Mills *et al*, 1982). This suggests that a significant fraction of the THAA in surface seawater is not simple protein, but consists of polypeptides attached to non-polar moieties (e.g., lipoproteins, glycolipids).

The hexane-soluble, dissolved total lipid content of both films (Table 1) and subsurface waters (Figures 2 and 3) averaged about 4% of the DOC. An additional 1-3% dichloromethane-soluble material (includes pigments and more polar lipids) was also present in the films (Table 2)

Table 2. Chemical and biological properties of surface films. Mean values from Cruises SF-1,2,3,4,5.

Property	Coastal			
	Open Ocean (SF-2,3,5)	(SF-1)	(SF-2,3)	(SF-5) (SF-4)
NO_3^- - $\mu\text{moles l}^{-1}$.16	5.2	.05	.05 .27
NH_4^+ - "	.37	.59	.26	.24 .36
Chl-a - $\mu\text{g l}^{-1}$.09	1.3	.45	.21 .30
ATP - "	.13	1.6	.41	.14 .13
DOC - $\mu\text{moles l}^{-1}$	103	106	121	102 86
DON - "	7.5	12.4	8.2	5.5 6.1
POC - "	2.7	5.7	.32	18 1.2
PON - "	.6	.6	.3	1.8 .1

Table 2 (cont.). Chemical and biological properties of surface films. Mean values from Cruises SF-1,2,3,4,5.

Property	Open Ocean		Coastal	
	(SF-2,3,5)	(SF-1)	(SF-2,3)	(SF-5) (SF-4)
Total bacteria $\mu\text{g C l}^{-1}$	2.76	8.44	9.89	.82 4.43
Bacterial heterotrophy Turnover time of glutamic acid - h	135 (SF-5)	--	14 (SF-3)	96 115
Microplankton $\mu\text{g C l}^{-1}$	24 (SF-2,3)	--	24	-- --
Primary productivity $\mu\text{g C l}^{-1} \text{ h}^{-1}$	1.3 (SF-2,3)	--	3.3	-- --
Dissolved free amino acids - $\mu\text{moles l}^{-1}$	78 (SF-3,5)	--	115 (SF-3)	62 80
Total lipid - $\mu\text{moles C l}^{-1}$ as stearic acid				
Hexane soluble	2.7	--	2.2	2.0 3.6
CH_2Cl_2 soluble	.7		1.5	4.9 2.2

but was not included in Table 1 and Figures 2 and 3. Although the lipid content of films is relatively low, it may be of sufficient magnitude to influence the physical properties (force-area, surface potential-area isotherms) of natural films. This effect is illustrated in Figure 4, where the lowest n-octadecanol to collagen (a glycoprotein) ratio approximates the upper limit of the weight percent of lipid carbon relative to the total DOC in natural films (Van Vleet and Williams, 1983).

Kattner *et al* (1985) measured dissolved protein (bovine serum albumin equivalents), carbohydrate (glucose equivalents) and lipid (total fatty acids) in films and subsurface waters (.25, 1 and 5 m) collected in the North Sea, 3-6 miles from Helgoland. They collected 8 replicate samples on one day (07/26/77) from a "non-slicked" area ($\gamma_f = 2.7 - 4.4 \text{ mNm}^{-1}$) and 10 and 4 replicate samples on a second day (07/28/77) in a "slicked" area ($\gamma_f = 12-35 \text{ mNm}^{-1}$). Kattner *et al* (1985) used a rotating drum surface skimmer to collect samples, and did not measure DOC -- hence direct comparison of their results with this work is subject to these constraints, plus the fact that their measured film pressures in and out of film patches were considerably higher than those measured off Baja California and Southern California ($0.5-1.5 \text{ mNm}^{-1}$ out of films and $1.5-12 \text{ mNm}^{-1}$ in films). However, there were important similarities and differences between both studies. The sum of THAA, free amino acid, THCO and TL carbon (Kattner *et al*, 1985) varied from 35 to 60 $\mu\text{moles C l}^{-1}$ versus 10 to 60 $\mu\text{moles C l}^{-1}$ (this work). Using average DOC values of 100 $\mu\text{moles C l}^{-1}$ (this work), the percentage composition of THAA, THCO and TL (Kattner *et al*, 1985) is estimated to be about 20, 20 and 5%, respectively, for the "non-slicked" samples; and 20, 30 and 5%, respectively, for the "slicked" areas, resulting in the identification of about 50% of the organic components by classes (compared to 26% for this work). A DOC concentration of 200 $\mu\text{moles C l}^{-1}$ would obviously result in similar percent compositions for both studies. Kattner *et al* (1985) also found that THAA nitrogen averaged 24% of the total DON (compared to 23%, this work). The most significant results from Kattner *et al* (1985) are the near constant THCO contents of replicate film samples at each site, higher ratios of THAA to THCO in all samples compared to this work, and only slightly elevated concentrations of THAA plus THCO plus TL in the "slicked" versus the "non-slicked" areas. Thus, the results of Kattner *et al* (1985) give evidence for uniformity in the chemical composition of replicate film samples taken over a period of several hours in one area versus the much wider scatter in composition for discrete

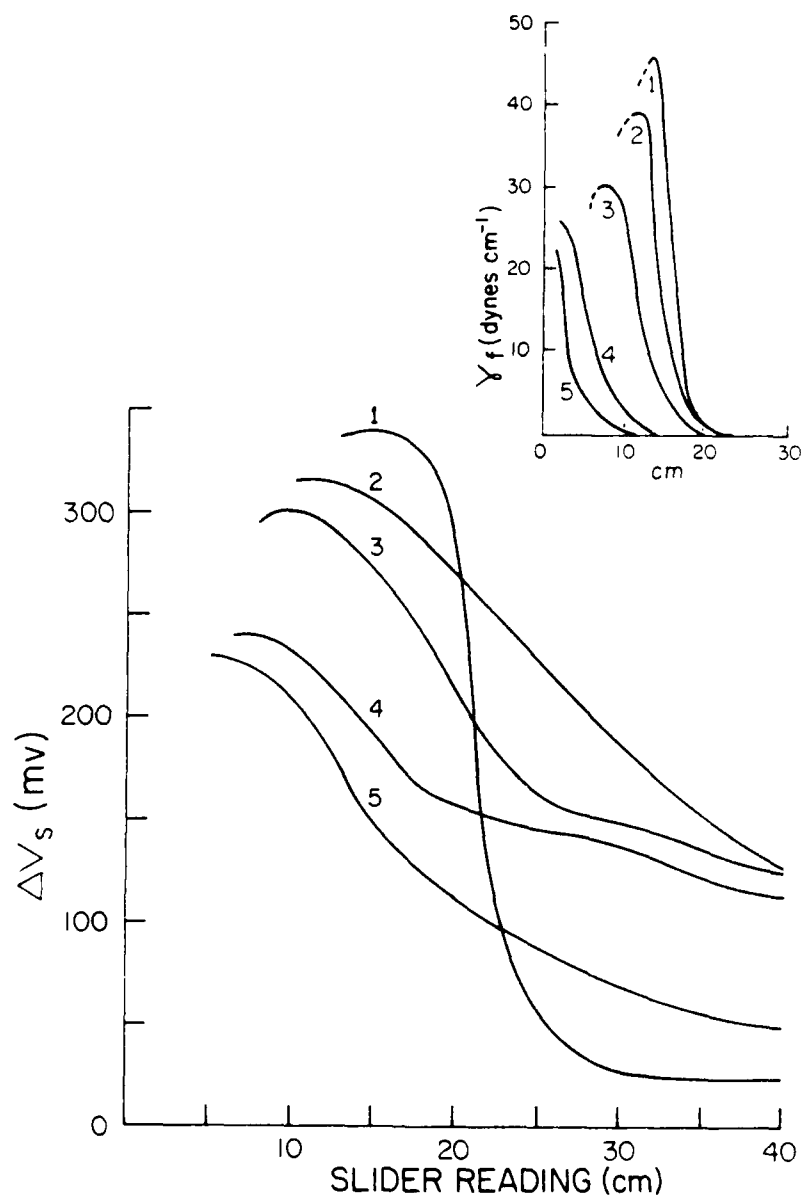


Figure 4. Surface potential (ΔV_s) and film pressure (γ_f , inset) vs. slider reading (cm) for varying amounts of n-octadecanol mixed with 4.7×10^{-4} μ moles of collagen. Molar ratios, weight ratios and weight percent of octadecanol are, respectively: curve 1 = pure octadecanol; curve 2 = 390, 0.2, 45; curve 3 = 195, 0.41, 22.5; curve 4 = 39, 0.082, 4.5; curve 5 = pure collagen. Dashed lines at high compression (inset) indicate that the film broke at these points. Compression curves were run in the order 1, 5, 4, 3, 2 on the same UV-irradiated, organic carbon-free seawater samples scraped clean between runs, and are corrected for blank values taken before each run. High initial ΔV_s values at 40 cm for curves 2, 3, and 4 are due to formation of protein "films" from "soluble" collagen components between runs. Taken from Van Vleet and Williams (1983).

samples taken under diverse conditions as reported in this paper.

The average dissolved lipid content (as the sum of fatty acids) measured by Kattner *et al* (1985) was 5% (compared to 4% from this work for hexane soluble total dissolved lipid, presumed to be composed primarily of fatty acids). In addition, Kattner and Brockman (1978) and Kattner *et al* (1983) have described the fatty acid composition of lipid material extracted from films and subsurface waters. The principle dissolved fatty acids in both films and subsurface waters were the saturated, myristic, palmitic and stearic acids, and the monounsaturated, palmitoleic and oleic acids (see also Marty and Saliot, 1974; and Marty *et al*, 1979). These are the main saturated and monounsaturated fatty acids derived from marine organisms and dissolved in bulk seawater (Williams, 1965; Kattner *et al*, 1983). The polyunsaturated C₁₆, C₁₈, C₂₀ and C₂₂ fatty acids present in marine organisms will be oxidized rapidly by photochemical reactions, and hence will have short half-lives in the surface microlayer.

II. Particulate protein carbohydrate and lipid

This will not be discussed in any detail (see Williams *et al*, 1986). A carbon balance for POC in films and the corresponding subsurface waters is depicted in Figure 5 for Cruises SF-2 and -3 (Williams *et al*, 1986). The sum of particulate (>1 μ m in diameter) THAA, THCO and TL carbon accounted for, on average, 50% (15-114%), and microplankton plus bacterial carbon 16% of the total POC, whereas particulate THAA nitrogen averaged 30% of the total PON. These high fractions of unidentified constituents in the PON of many film and subsurface water samples is perplexing, since up to 100% of the PON in suspended particles collected throughout the water column off Southern California was derived from amino acid nitrogen (Siezen and Mague, 1978). Particle formation in films by aggregation and photochemically-induced polymerization of DON components may be a major source of this unidentified material.

The effects of increased biological activity in surface waters on the overall physical characteristics and chemical composition of surface films, as deduced from THAA, THCO and TL compositions, is not as significant as might be expected. At several stations off Baja California, the open-ocean films in oligotrophic waters were richer in proteins and carbohydrate-containing organic matter than films collected in eutrophic coastal waters. Some chemical and biological properties of films

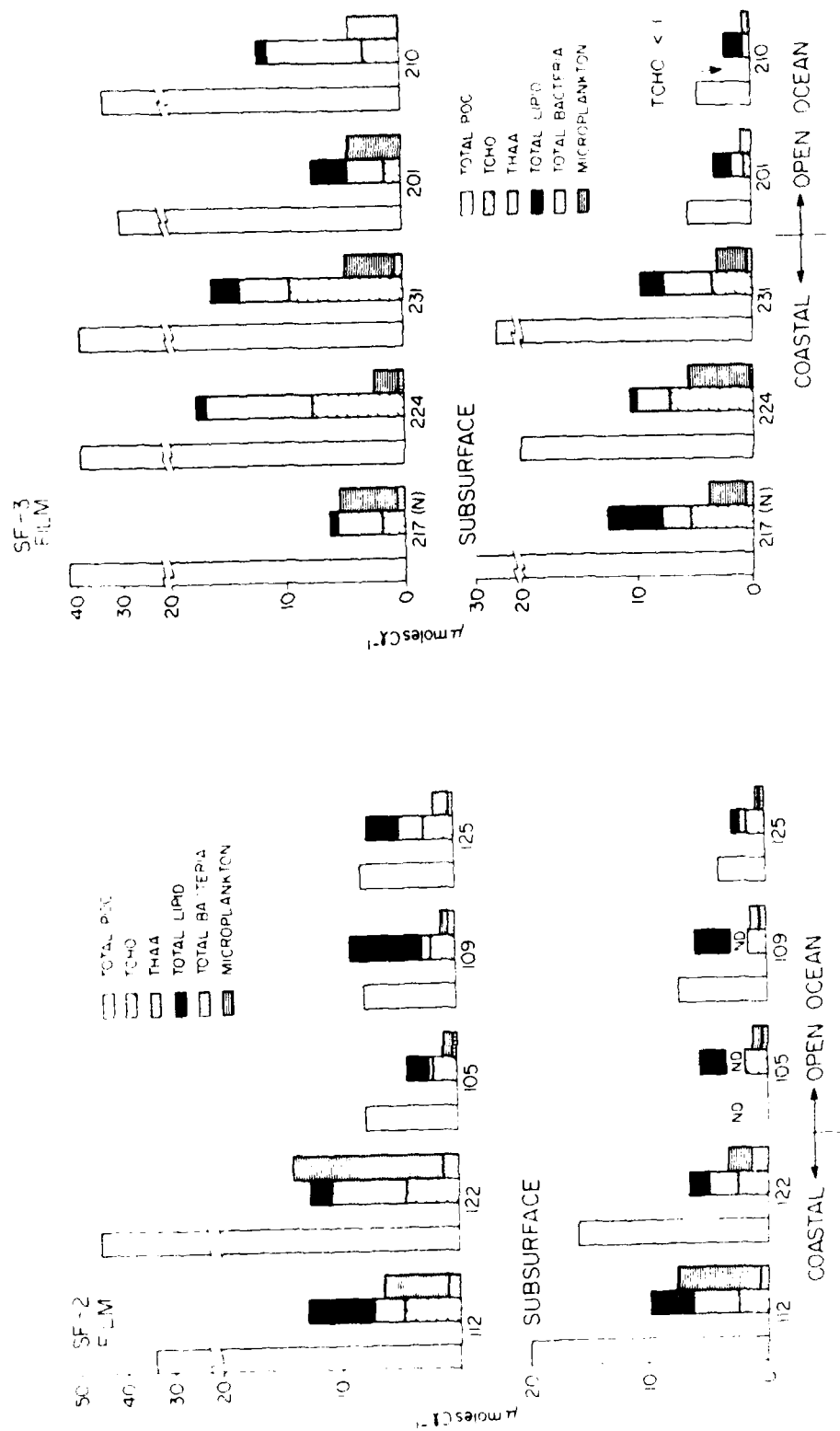


Figure 5. Components of POC in $\mu\text{moles C l}^{-1}$. Events same as in Figure 2. Total bacteria are those passing a $35 \mu\text{m}$ Nitex net and retained by a $0.2 \mu\text{m}$ polycarbonate filter. Taken from Williams, et al. (1986).

from Cruises SF-1 through SF-5 are summarized in Table 2. These cruises encompassed highly eutrophic (SF-1), moderately eutrophic (SF-2,-3), mesotrophic (SF-4), and near oligotrophic (SF-5, El Niño conditions) coastal waters, and oligotrophic (SF-2,-3,-5) "open-ocean" waters. Between the open-ocean and coastal regimes the main differences (Table 2) were slower turnover times of amino acids, reduced primary productivity and lower chlorophyll-a concentrations in the open-ocean films. Total dissolved organic carbon and nitrogen do not necessarily reflect biological activity in the underlying waters, and, in fact, DOC is not significantly correlated with any other parameter (Williams *et al*, 1986). In effect, the chemical character of natural sea surface films is pretty much the same in coastal and open ocean areas when considering the major organic constituents at a non-molecular level. This suggests that there is a ubiquitous, background concentration of relatively refractory, surface active, organic compounds in the surface microlayer upon which is superimposed varying amounts of labile constituents derived from dynamic biological processes occurring in the underlying water or in the microlayer itself. Thus, the organic composition of the surface microlayer reflects past biological histories of moving water masses combined with local biological events.

III. Amino acid composition

Compositional differences in dissolved free amino acids (FAA), dissolved THAA, and particulate hydrolyzable amino acids (PAA) could reflect such microlayer processes as fractionation of proteinaceous compounds between films and the subsurface waters, specific bacterial heterotrophic degradation reactions, excretion of FAA by surface microplankton, and exchange rates of surface active proteins or polypeptide-containing compounds between films and the underlying water. Figures 6 and 7 depict the mole fractions of the major amino acids identified in the dissolved and particulate organic components of films and the corresponding 5-10 cm subsurface waters (Cruises SF-2,-3,-5). The analytical procedures are described in Henrichs and Williams (1985) and Williams *et al* (1986). The amino acids proline and hydroxyproline are not analyzed by this technique; lysine and ornithine are not included due to erratic analytical precision; and glutamine, asparagine, histidine and tryptophane are destroyed during acid hydrolysis (therefore not present in THAA results) and were not included with the FAA.

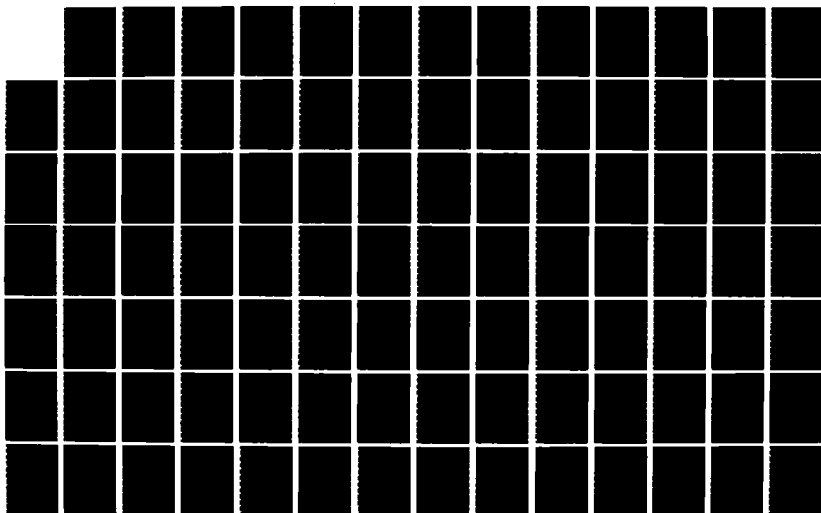
AD-A175 172

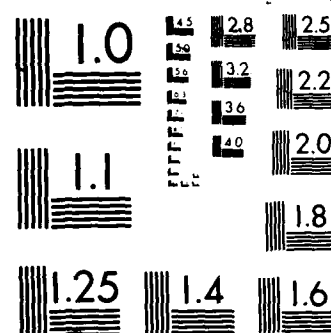
ONRL WORKSHOP PROCEEDINGS - ROLE OF SURFACTANT FILMS ON 2/3
THE INTERFACIAL P. (U) OFFICE OF NAVAL RESEARCH LONDON
(ENGLAND) F L HERR ET AL 21 NOV 86 ONRL-C-11-86

UNCLASSIFIED

F/G 8/10

NL





PHOTOCOPY RESOLUTION TEST CHART

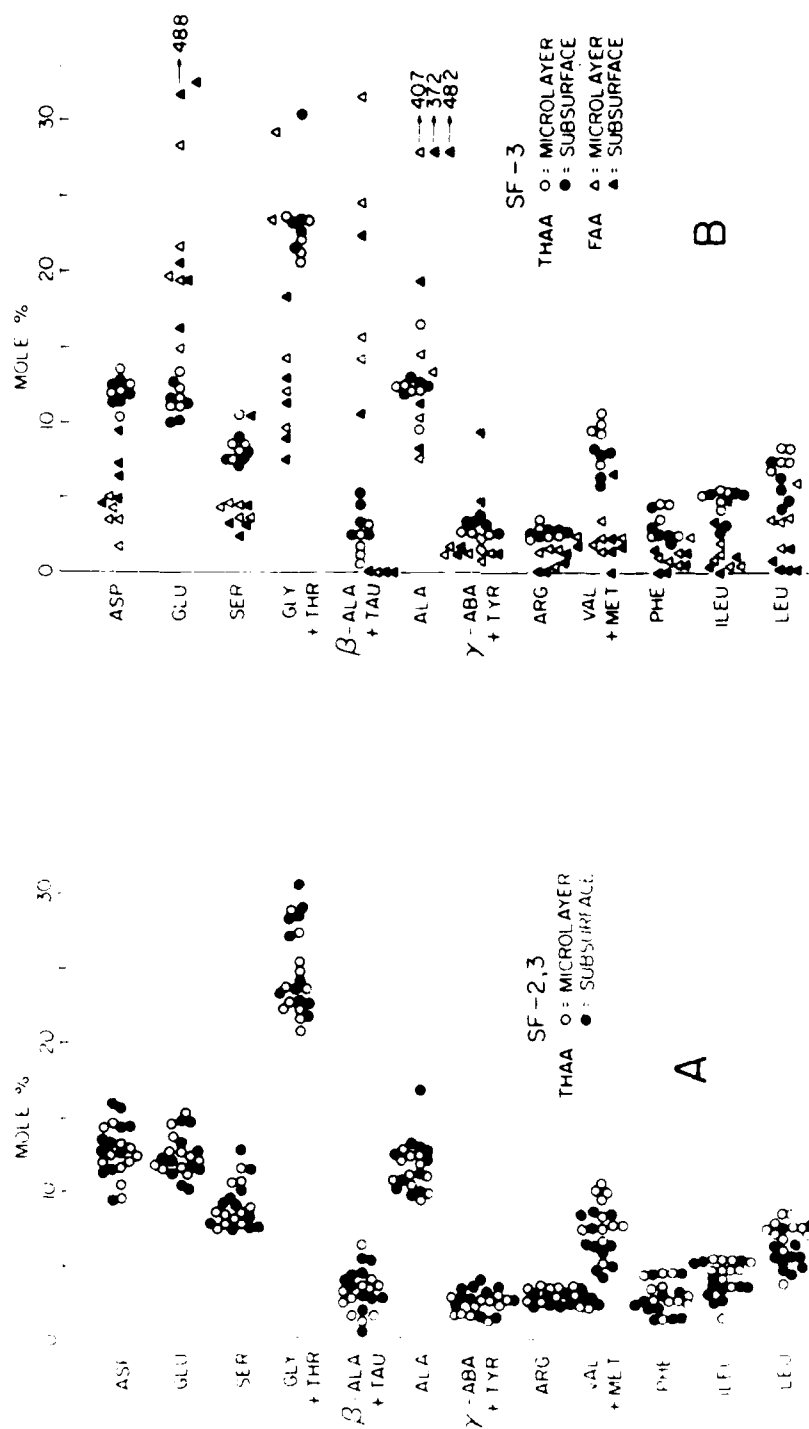


Figure 6. Mole percent composition of dissolved total hydrolyzable (THAA) and dissolved free (FAA) amino acids in films and subsurface waters. Cruise SF-2, -3. Each point is one sample. Arrows denote values of off-scale points. ASP = aspartic acid, GLU = glutamic acid, SER = serine, GLY = glycine, THR = threonine, β -ALA = β -alanine, TAU = taurine, ALA = alanine, γ -ABA = γ -aminobutyric acid, TYR = tyrosine, ARG = arginine, VAL = valine, MET = methionine, PHE = phenylalanine, ILEU = isoleucine, LEU = leucine.

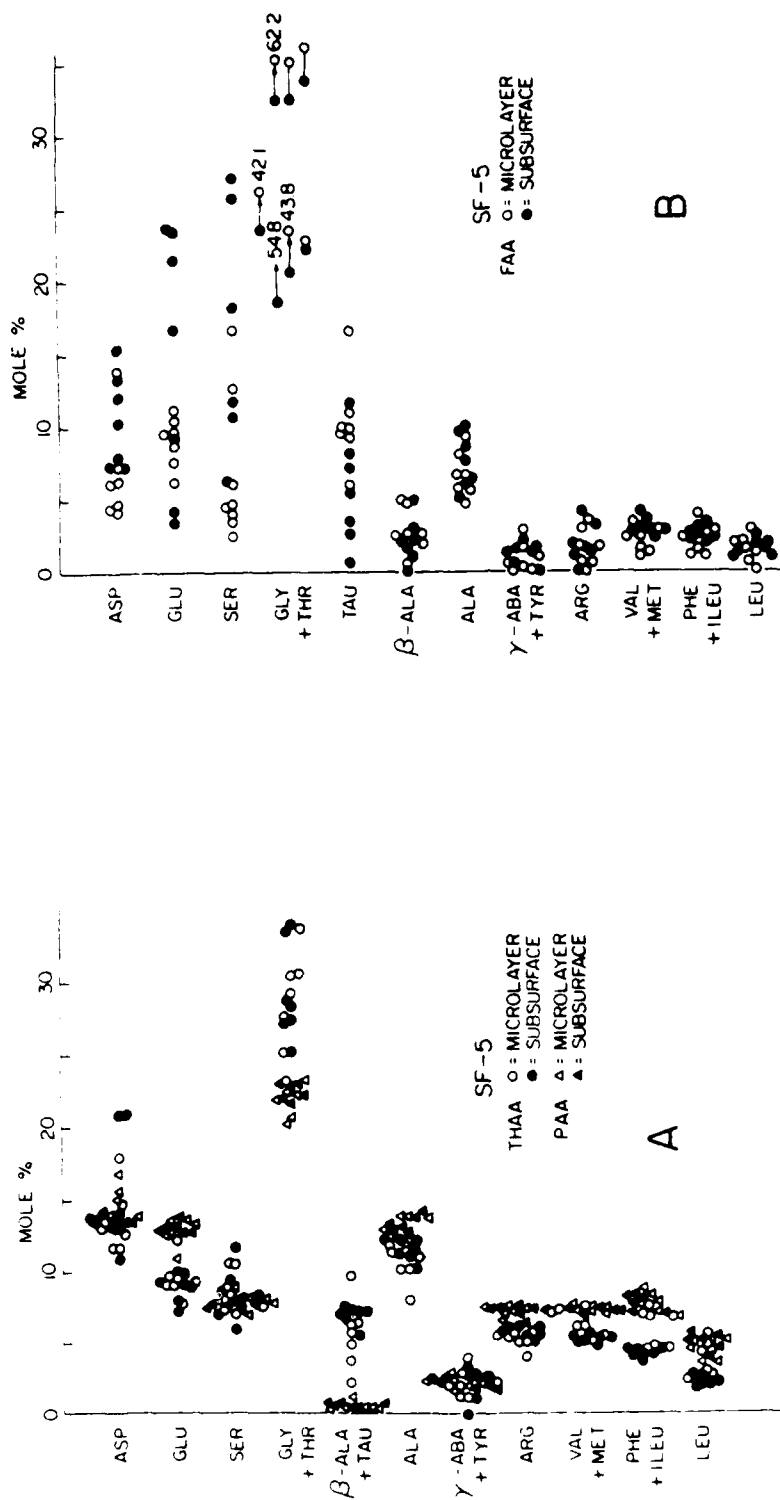


Figure 7. Mole percent composition of THAA, particulate hydrolyzable amino acids (PAA) and FAA, Cruise SF-5. Arrows denote values of off-scale points.

The dissolved ($<1.0\ \mu\text{m}$) THAA composition of all surface film and subsurface water samples was similar (Cruises SF-2,-3,-5), despite concentration ranges of more than an order of magnitude (Figures 6A and 7A). There was relatively less glutamic acid and more β -alanine + taurine in the SF-5 samples, possibly from the enzymatic decarboxylation of glutamic acid to give β -alanine. This similarity in THAA indicates no major *in situ* contributions to the microlayer of THAA with unique amino acid compositions (e.g., bacterial cell walls high in glutamic acid), or significant fractionation of surface-active organic compounds having dissimilar polypeptide components between subsurface waters and the microlayer. The results (as expected) support a common, ubiquitous source of THAA to the microlayer, regardless of location or the level of biological activity in the underlying water.

The molar composition of the FAA (Figures 6B and 7B) showed differences between cruises, between films and subsurface waters, and between samples (individual points on the figures). There was a very high mole percent of free glycine + threonine in subsurface waters on Cruise SF-5, which was not found in either the THAA or the particulate amino acids (PAA). Conversely, on Cruise SF-3, the mole percent of free glycine + threonine was low in films and subsurface waters compared to its molar composition in THAA. Reasons for these differences are not known, but could be related to phytoplankton excretion of soluble metabolites (diatoms were predominant in surface waters during the El Niño conditions on Cruise SF-5; dinoflagellates on Cruises SF-2 and -3). There was also considerable scatter in the values for glutamic acid, serine and aspartic acid for Cruise SF-5 (Figure 7B), primarily a result of wide scatter in the molar percentages of these three FAA in the films. For Cruise SF-3 (Figure 6B), the mole percent of free aspartic acid and serine were lower and glutamic acid higher than in the THAA, and there were no obvious variations in molar composition between films and subsurface waters. These diverse results for FAA compositions are essentially signatures of various biochemical processes taking place in the films and subsurface waters (e.g., bacterial heterotrophy, enzymatic hydrolysis of THAA, excretions from living and lysed organisms).

The molar composition of PAA ($<35\ \mu\text{m}$; $>1.0\ \mu\text{m}$) shows remarkably little variation between films and subsurface waters or between samples (Figure 7A, Cruise SF-5), especially considering the significant and diverse bacterial and microplankton contributions to both films and subsurface waters. Although there are several

differences in the molar compositions of THAA and PAA, mainly a higher mole percent of glutamic acid and a corresponding lower percentage of β -alanine + taurine in the PAA, these two amino acid pools reflect the overall uniformity in the composition of the major combined amino acids in all marine organisms.

A close correspondence between the THAA composition of original films and new films generated in situ onto a film-free surface is shown in Figure 8A. These new films were generated in the film containment tube described below by removing the original film with screens, allowing new films to form over a 1 to 5 minute waiting period, and sampling again with screens. Figure 8B represents one such experiment, depicting strip chart tracings (from the HPLC amino acid analyzer) for THAA in an original and newly-formed film. There was a lower total concentration of THAA in the new film, but its specific amino acid and molar composition was nearly identical to the original film. The corresponding FAA compositions (Figure 8A) showed considerable scatter in the mole percentages of glutamic acid, serine, glycine + threonine, and a large molar fraction of β -alanine + taurine -- not unlike the FAA compositions in Figure 6B and 7B.

These film-formation experiments showed that the hydrolyzable amino acid components of original and newly-formed films were essentially identical, but did not give any clues to the surfactant nature or structure of the actual compounds involved.

In situ surface potentials, film pressures, and film formation studies

The surface potential (V_s or ΔV_s , measured in terms of Volta potentials, Gaines, 1966) of an organic monolayer is defined, for our purposes, as the difference in the measured potential between a "clean" seawater surface and the same seawater surface covered (or partially covered) by an organic film. If an insoluble monolayer with a permanent dipole is spread on seawater, then the potential difference at the interface will be a resultant of the average dipole moment of the monolayer and electrostatic interactions of ionized film molecules with the cations and anions in seawater. For example, V_s values for monomolecular films of n-octadecanol, n-octadecanoic acid, and n-octadecane spread on organic carbon-free seawater at pH 8.2 and measured as noncompressed, close-packed monolayers are 338, -5 and 0 millivolts, respectively (Van Vleet and Williams, 1983). Natural organic sea-surface films may or may not exist as monolayers and are composed

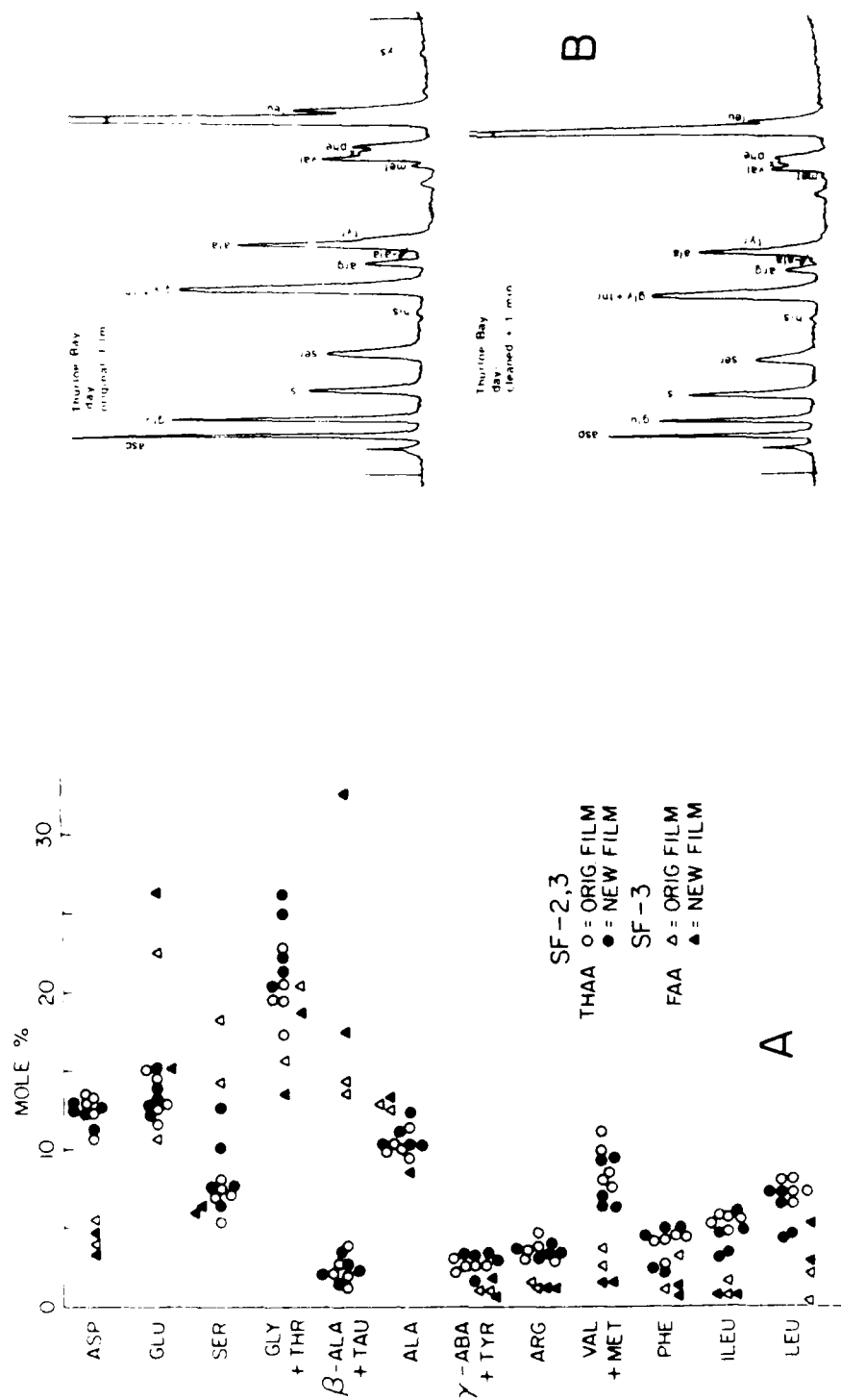


Figure 8. THAA and FAA in film formation experiments. A. Mole percent composition of THAA and FAA in the original, in situ films and in newly-formed films generated onto a cleaned surface after 1 to 5 min standing. B. Strip chart record of THAA spectra in an original and newly-formed film after 1 min film-formation; Cruise SF-2, Station 3. The THAA contents of the original and new films were 3.7 and 1.9 $\mu\text{mol l}^{-1}$, respectively. Taken from Williams et al. (1986)

of mixtures of complex, unidentified molecules. Thus, V_s measurements are useful primarily for detecting the presence or absence of films, following their formation, alteration and disappearance, and relating various "types" of films to specific physical, chemical and biological parameters.

Surface film pressure (γ_f) is defined as being equal to the difference in surface tension between "clean" seawater ($\sim 73 \text{ mNm}^{-1}$) and seawater covered (or partially covered) by an organic film.

In situ surface potentials were measured using an ²⁴¹Am ionizing electrode coupled with a Ag-AgCl reference electrode, and film pressures using spreading oils (see Williams *et al.*, 1980, 1986 and references therein). Note that V_s measurements are approximately 10 times more sensitive than the corresponding γ_f values in detecting the presence of organic films. V_s measurements were made from an electric motor-driven catamaran using either a teflon-coated, 48 cm diameter (ID) innertube (SF-2,-3,-4) or a 75 x 60 cm open-ended wooden box (SF-1) as floating film-containment devices (Williams *et al.*, 1980, 1982, 1986). The corresponding γ_f measurements were made using the wooden toothpick-piston oil technique of Barger *et al.* (1974) such that the piston oils did not impact the V_s measurements.

V_s values for coastal and open-ocean films measured at 36 locations (Cruises SF-1 through SF-4) varied from -10 to 635 mv with most values falling between 200 and 400 mv (the value of -10 mv was measured during a bloom of pelagic crabs and may be a result of excreted saturated fatty acids). These potentials encompass V_s values determined in the laboratory for known biological compounds (lipids, proteins, polysaccharides, humic-type material; Jarvis *et al.*, 1967; Van Vleet and Williams, 1983) and natural sea-surface films (Jarvis *et al.*, 1967; Jarvis, 1967) spread on seawater. A plot of V_s versus γ_f for 25 in situ measurements (Figure 9), where V_s and γ_f were considered to represent the same film patch, shows considerable scatter. The regression of V_s on γ_f is significant ($r = 0.66$) only if the three V_s values >500 mv are excluded -- with no justification, however. It is obviously impossible to infer the chemical composition of natural films on the basis of their V_s and γ_f values, but changes observed in V_s from one location to another and in repetitive measurements within the same film patch suggest that film composition is not necessarily isotropic and that film "thickness" is not the sole factor in determining the in situ variability of V_s .

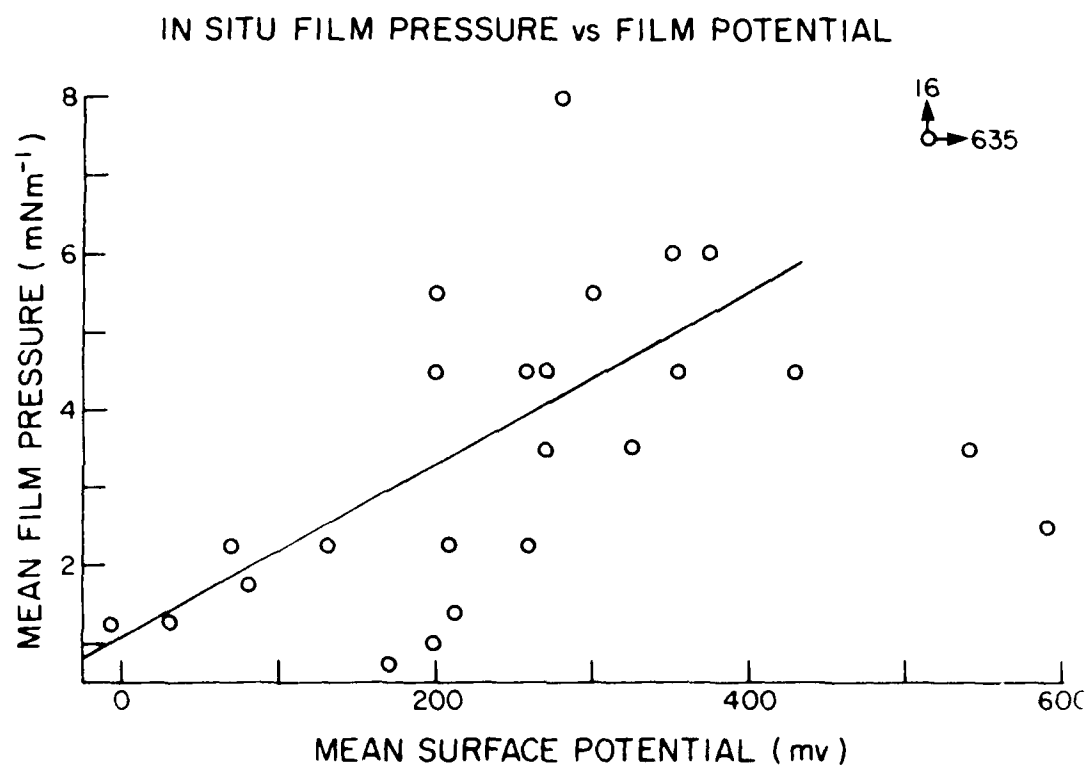


Figure 9. Mean in situ film pressures (each point is mean of spreading oil ranges; e.g., $\gamma_f = 4$ for $\gamma_f = 3-5$) versus mean in situ surface potentials (mean = baseline V_s averaged from strip chart records; e.g., see Figure 10, Event 225). Arrows denote values of off-scale points. The data are from Cruises SF-1, -2, -3, -4. The regression line ($y = 0.86 + 0.012x$; $r = 0.664$) does not include the three V_s values >500 mv.

The difficulties involved in using film-containment devices ("film-in-a-box" problem) to obtain V_s values representative of the true surface potentials are evident from tracings of the original strip chart records (Figure 10). These tracings show wide, periodic fluctuations in V_s for the original *in situ* films, presumably due to compression and dilation of the trapped films. Non-fluctuating baselines were only found in very heavy slicks (kelp beds, tidal convergences, protected bays, etc.), or with newly-formed films.

Representative film-formation experiments are also depicted in Figure 10 (see also Williams *et al*, 1980). The original trapped films were removed with paper towels (SF-1) or a circular screen (SF-2,-3) and V_s values for newly-formed films measured after standing and, in several cases, subsequently bubbling 10 cm below the surface with organic carbon-free air (35 cm³ min⁻¹, bubble diameters = ~0.3 mm at the frit).

Film-formation rates measured during the first 2 minutes after cleaning were 2-50 times greater than those measured from 2 minutes on. This can be seen graphically in Fig. 10 (Events 237-A and 225-A). In fact, even faster formation rates must occur during the initial 10-15 seconds it takes to deploy the electrode after cleaning the surface. The final V_s attained after the initial cleaning and waiting for 2-16 minutes was equal to or 10 mV less than the original baseline V_s in only three runs. It is apparent from Fig. 10 that the original, baseline V_s values are slowly approached with time in some cases (Events 237-A, 225-Aa and 6-SB), while in other cases (Events 109-A and 118-A), there are no measurable increases in V_s , at least during the initial 3-4 minutes. Whether or not baseline V_s values would ever be attained during longer waiting periods is not known. Re-establishment of the original *in situ* film with its microplanktonic, bacterial and detrital organic components and atmospheric inputs cannot take place in a trapped film over short time intervals (<1 hour), and there is no contribution from adjacent films spreading over the freshly cleaned surface when using the film-containment devices. The principal source of organic matter in these newly formed films (in the absence of bubble transport) is dissolved (and colloidal) surface active material in the subsurface waters being carried to the interface by eddy diffusion.

Bubbling tended to increase V_s values above those obtained by standing. V_s after bubbling during Event 6-SB increased to approximately the same value as that of the original film, but increased only slightly during Event

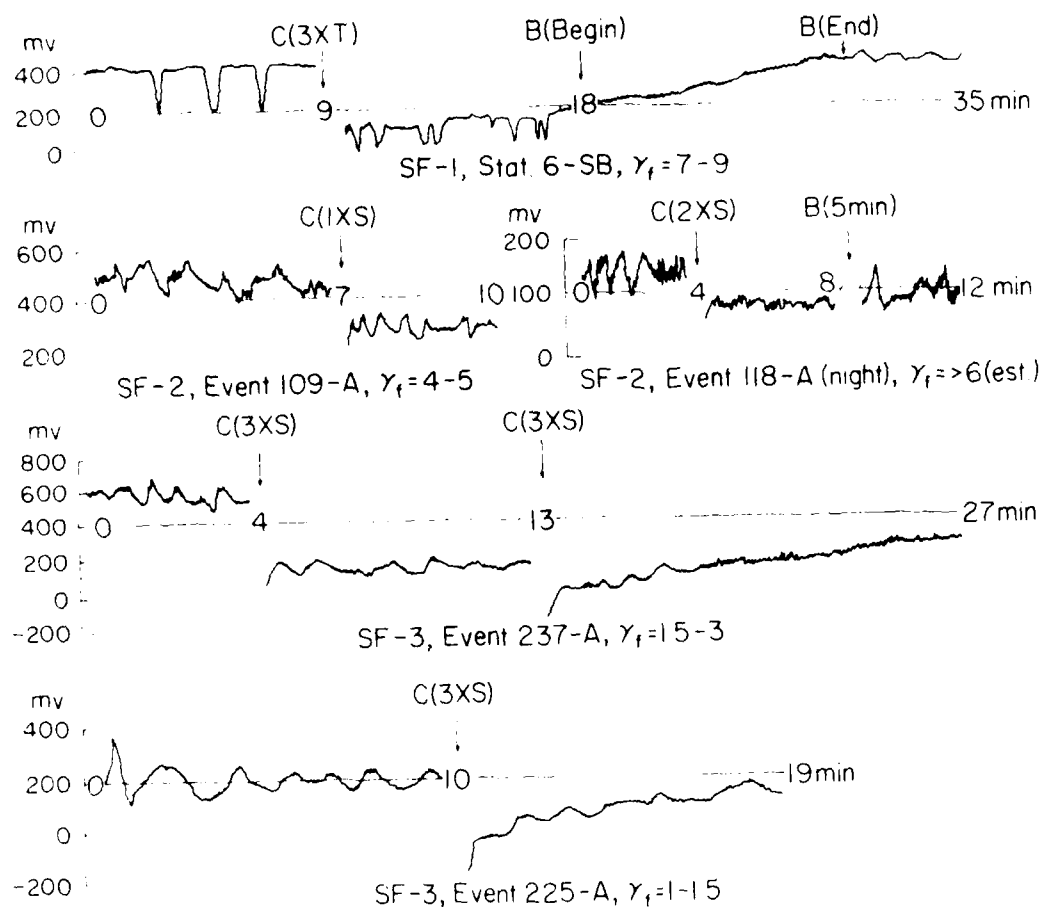


Figure 10. Transcriptions of strip chart records of in situ surface potential (V_s) measurements; including the corresponding surface film pressures (γ_f). The tracings on the left part of each record are for the original, in situ films. C = cleaned with paper towels (T) or a metal screen (S) where X is the number of replicate cleanings. B = bubbling. Taken from Williams et al. (1986).

118-A. Selective bubble scavenging of organic components having low V_s values could account for this latter result.

A summary of film-formation rates obtained under quiescent conditions (no bubbling), compiled from laboratory experiments using a Langmuir trough or 72 l aquarium (Van Vleet and Williams, 1983), and from *in situ* measurements with trapped films (SF-1,-2,-3,-4) are plotted in Figure 11. This plot illustrates the wide diversity of the *in situ* film formation rates.

Jarvis (1967) observed that V_s increased 30-120 mV when discrete samples of surface (0-10 cm) seawater from the Bay of Panama were bubbled for 30 minutes at rates of 26-200 bubbles min^{-1} (bubbles approximately 6 mm in diameter were generated from untreated ambient air). These V_s increases are of the same order as reported here, in other *in situ* samples (Williams *et al.*, 1980), and in discrete samples of SIO Pier seawater (Van Vleet and Williams, 1983). Direct comparisons, however, between V_s results from *in situ* and discrete sample experiments are not necessarily justified since there is a greater volume of seawater potentially available for bubble scavenging during *in situ* measurements where, in addition, turbulent mixing occurs.

These *in situ* film formation experiments show that new films are formed relatively rapidly in eutrophic coastal waters and more slowly in oligotrophic, open-ocean waters. Judging solely from surface potential measurements, the newly formed films may or may not attain potentials equal to those of the original films. Even considering the constraints associated with "film-in-a-box" measurements, it is clear that film-free surfaces in the ocean do not exist except during elevated sea states, and that new films will form in a matter of seconds to minutes where original films have been blown away.

Discussion

It has been pointed out (Hunter and Liss, 1981; Williams *et al.*, 1986) that the average amount of "excess" dissolved organic matter in a 250 μm thick surface film relative to the concentration of dissolved organic matter in the corresponding subsurface water is usually insufficient to form an unbroken monomolecular film (e.g., stearic acid or albumin) if distributed isotropically on the surface. Assuming a mean enrichment of DOC (film minus 10 cm) of 36 $\mu\text{moles C l}^{-1}$ or 36 mmoles C m^{-3}

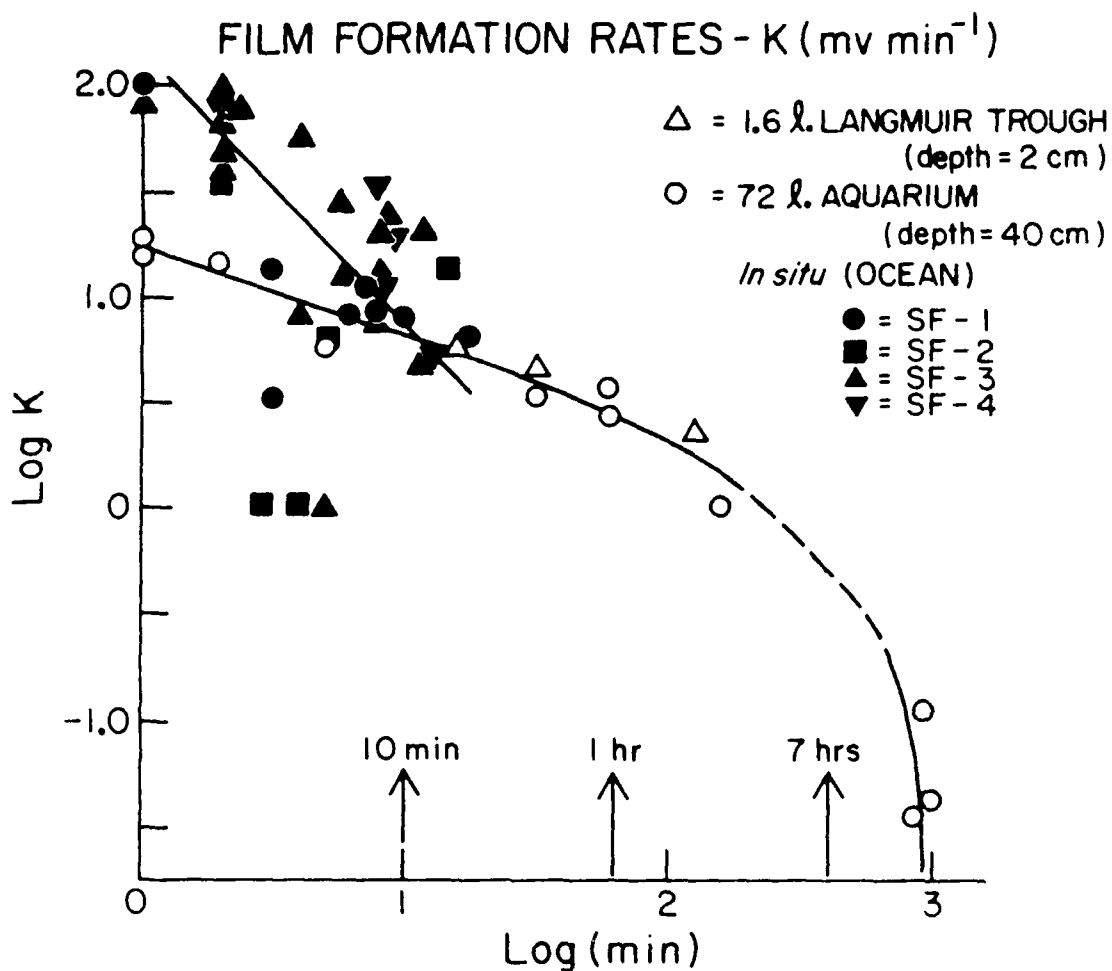


Figure 11. Film formation rates, K ($\text{mV} \cdot \text{min}^{-1}$) vs. formation times (min). Langmuir trough and aquarium points represent films formed from a clean (wiped) surface after standing undisturbed (no mechanical stirring or bubbling). Seawater was collected from Scripps Institution of Oceanography pier and transferred directly to trough or aquarium (see Van Vleet and Williams, 1983). *In situ* (ocean) experiments were performed as described by Williams *et al.* (1980; 1986), and represent data from Cruises SF-1, -2, -3, -4. The lines are drawn arbitrarily.

(Cruises SF-2 and -3; Williams et al., 1986), and a film thickness of 250 μm , then the surface "excess" of DOC is 9×10^{-3} mmole C m^{-2} or 108 $\mu\text{g C m}^{-2}$ (250×10^{-6} times 36). This excess surface DOC, if it were composed entirely of stearic acid or albumin, would cover 7 or 22% of the surface, where monomolecular films of stearic acid and albumin are equivalent to 1600 and 500 $\mu\text{g C m}^{-2}$, respectively (Williams, 1965).

Natural monolayers, however, are not necessarily mimicked by stearic acid or albumin. They are composed of heterogeneous mixtures of surface active compounds whose steric and electrostatic properties may widely differ, resulting in multi-component molecular films having dynamic conformations at the interface. Compaction of scattered monomolecular film patches by wind or their generation along convergences (Langmuir cells, internal waves, wakes) will form visible slicks which must include mono- and polymolecular films and associated, thicker microlayers containing "excess" dissolved organic molecules. Within this system, there must also be continuous exchange (sorption and desorption) of surface active organic molecules between the two layers, as well as conformational changes in the monolayer due to the folding and unfolding of long chain molecules. This is a dynamic situation at the interface where monolayers are forming and dispersing, and surface active organic molecules are entering and leaving the microenvironment. Conceivably, an interrupted or non-continuous monolayer could produce an apparently uniform "slick" by cumulative capillary wave damping.

We have seen that combined amino acids, sugars and fatty acids constitute about 30% of the dissolved organic carbon in the microlayer, humic-type condensates perhaps another 20%, with the remainder completely unknown. Few measurements exist for divining the molecular properties of these unknown compounds; i.e., molecular weights or sizes, conformation at the interface, or interactions with water molecules and dissolved ions.

Barger and Means (1985) have estimated molecular weights and coefficients of compressibility of natural film components by modeling films as two-dimensional gases using force-area isotherms measured on films collected in the Atlantic Ocean and Chesapeake Bay. Using a modified van der Waals equation of state and coefficients determined from force-area isotherms of known compounds, they estimated molecular weights ranging from 1800 ± 700 (Atlantic screen samples) to 2300 ± 900 (Chesapeake Bay screen samples) with values as high as 3700 ± 1200 in Atlantic deep water. In comparison, ultrafiltration of

dissolved organic carbon (Carlson, 1985) in surface seawater from the Gulf of Maine and North Atlantic gave the following "molecular weight" distributions of DOC; 66% <1000 and 34% >1000, with 6% >30,000 and 1% >100,000.

Barger and Means (1985) also postulated structural criteria for film components which would satisfy their force-area isotherms. These contain large oxygenated hydrophilic head groups and long hydrophilic tails (e.g., sucrose monomyristate and polyoxyethylene dodecanol). These criteria (big heads and small tails) characterize many naturally-occurring lipoproteins, lipopolysaccharides, glycoproteins, proteoglycans and glycolipids, all of which should be present in the microlayer at one time or another. Marine humic substances have been assigned many hypothetical structures, including condensates of amino acids/sugars/lipids (Gagosian and Stuermer, 1977) and photochemically-oxidized triglycerides (Harvey and Boran, 1985). The point is that naturally-occurring lipoprotein- and lipopolysaccharide-type compounds, and/or unbonded (free) lipids probably determine the basic physical-chemical characteristics of surface monolayers (force-area, potential-area isotherms), with the "humic" substances, other unidentified condensates, and low molecular weight, polar compounds constituting the bulk of the more soluble organic compounds within the microlayer. This makes it imperative to obtain analytical data for the various lipid classes (phospholipids, wax esters, triglycerides, hydrocarbons, free fatty acids) and their oxidation products in both films and subsurface waters.

Attractive interactions between constituent molecules in sea surface monolayers, and between these molecules and the associated water molecules in the microlayer include long range "hydrophilic interactions" between non-polar groups (Israelachvili and Pashley, 1982), van der Waals dispersion forces, and hydrogen-bonding. Ice-like, clathrate water structures induced by polarization from monomolecular films have been postulated by Alpers *et al.* (1982), Hühnerfuss and Alpers (1983) and Hühnerfuss *et al.* (1984) to explain an anomalous dispersion regime at 1.43 GHz in airborne microwave radiometer measurements. These clathrate structures were calculated to be <190 μm in thickness from *in situ* experiments with oleyl alcohol monolayers spread on seawater, and were implicated in wave damping by known monomolecular films. Thick, crude-oil films (nonpolar) on the ocean do not give this 1.43 GHz signature (Hühnerfuss *et al.*, 1986). It is not clear, however, what microwave signatures would be observed for natural sea slicks.

Summary

1. The molecular structure of the organic components of sea-surface films is virtually unknown. On average, only 26% of the total dissolved, and 50% of the total particulate organic carbon can be attributed to carbohydrate-, amino acid- or fatty acid-containing compounds.

2. Striking changes in the gross chemical composition of natural films and the corresponding subsurface waters are not observed between coastal, eutrophic waters and open-ocean, oligotrophic regimes. This implies a ubiquitous source of organic film constituents, derived from both past and current biological events occurring in the water column.

3. New films form rapidly from subsurface waters when the original films are removed. The amino acid composition of both the new films and original ones are nearly identical. This identity, however, gives no clues to the molecular structures of the surface-active compounds involved.

4. Excess organic matter in the microlayer relative to its concentration in subsurface waters is normally insufficient to form continuous, ordered, monomolecular films at the surface. Visible slicks result from compaction of scattered monomolecular film patches by wind and tides, from compression of surface active organic matter along convergences and from the cumulative effects of an anisotropic monolayer inhibiting capillary wave formation.

Acknowledgements

Thanks are due to the many people involved in this program (see Williams et al., 1986). I am especially grateful to K. J. Robertson for assistance with laboratory analyses and sample collections on Cruises SF-4 and SF-5, to the Officers and Crew of the R/V New Horizon, and to M. A. Ogle for preparation of this manuscript. Work on Cruise SF-5 was facilitated by Diplomatic Note 302322 from the Secretaria de Relaciones Exteriores, Government of Mexico. Support was provided by NSF grants OCE77-26178, OCE79-25942 and OCE82-00158.

References

- Alpers, W., C.B. Hans-Juergen, W.D. Garrett, and H. Hühnerfuss. 1982. The effect of monomolecular surface films on the microwave brightness temperature of the sea surface. *Int. J. Remote Sensing*, **3**: 457-474.
- Bada, J.J., E. Hoopes, and M.-S. Ho. 1982. Combined amino acids in Pacific Ocean waters. *Earth Planet. Sci. Lett.*, **58**: 276-284.
- Baier, R.E., D.W. Groupil, S. Perlmutter, and R. King. 1974. Dominant chemical composition of sea surface films, natural slicks, and foams. *J. Rech. Atmos.*, **8**: 571-600.
- Barger, W.R., and J.C. Means. 1985. Clues to the structure of marine organic material from the study of physical properties of surface films. In: Marine and Estuarine Geochemistry, A.C. Sigleo and A. Hattori (Eds.), Lewis Publishers, Inc., Chelsea, MI, pp. 47-67.
- Barger, W.R., W.H. Daniel, and W.D. Garrett. 1974. Surface chemical properties of banded sea slicks. *Deep-Sea Res.*, **21**: 83-89.
- Carlucci, A.F., D.B. Craven, and S.M. Henrichs. 1985. Surface film microheterotrophs: amino acid metabolism and solar radiation effects on their activities. *Mar. Biol.*, **85**: 13-22.
- Carlucci, A.F., D.B. Craven, K.J. Robertson, and P.M. Williams. 1986. Surface-film microbial populations: diel amino acid metabolism, carbon utilization, and growth rates. *Mar. Biol.* (in press).
- Carlson, D.J., M.L. Braun, and T.H. Mague. 1985. Molecular weight distribution of dissolved organic materials in seawater determined by ultrafiltration: a re-examination. *Mar. Chem.*, **16**: 155-173.
- Gagosian, R.B., and D.H. Stuermer. 1977. The cycling of biogenic compounds and their diagenetically transformed products in seawater. *Mar. Chem.*, **5**: 605-632.
- Gaines, G.L. 1966. Insoluble Monolayers at Liquid Gas Interfaces. Interscience, New York and London, 386 p.

- Harvey, G.R., and D.A. Boran. 1985. Geochemistry of humic substances in seawater. In: Humic Substances in Soil, Sediment, and Water. Geochemistry, Isolation and Characterization, G.R. Aiken, D.M. McKnight and R.L. Wershaw (Eds.), John Wiley and Sons, New York, pp. 233-247.
- Henrichs, S.M., and P.M. Williams. 1985. Dissolved and particulate amino acids and carbohydrates in the sea surface microlayer. *Mar. Chem.*, 17: 141-163.
- Ho, M.-S., J. Bada, Y. Zuopeng, and L. Deming. 1983. Amino acid compositions and enantiomeric ratios of humic-like substances extracted from fossils and seawater by Sep-Pak C₁₈ and Amerlite XAD-2 resins. In: Aquatic and Terrestrial Humic Materials, R.F. Christman and E.T. Gjessing (Eds.), Ann Arbor Science, Ann Arbor, Michigan, pp. 429-441.
- Horrigan, S.G., Carlucci, A.F., and P.M. Williams. 1981. Light inhibition of nitrification in sea-surface films. *J. Mar. Res.*, 39: 557-565.
- Hühnerfuss, H., and W. Alpers. 1983. Molecular aspects of the system water/monomolecular surface film and the occurrence of a new anomalous dispersion regime at 1.43 GHz. *J. Phys. Chem.*, 87: 5251-5258.
- Hühnerfuss, H., W.D. Garrett, and F.E. Hoge. 1986. The discrimination between crude-oil spills and monomolecular sea slicks by an airborne lidar. *Int. J. Remote Sensing*, 7: 137-150.
- Hühnerfuss, H., P. Lange, and W. Walter. 1984. Wave damping by monomolecular surface films and their chemical structure. Part II: Variation of the hydrophilic part of the film molecules including natural substances. *J. Mar. Res.*, 43: 737-759.
- Hunter, K.A., and P.S. Liss. 1981. Organic sea surface films. In: Marine Organic Chemistry, E.K. Duursma and R. Dawson (Eds.), Elsevier, Amsterdam, pp. 259-298.
- Israelachvili, J., and R. Pashley. 1982. The hydrophobic interaction is long range, decaying exponentially with distance. *Nature*, 300: 341-342.
- Jarvis, N.L. 1967. Adsorption of surface-active material at the sea-air interface. *Limnol. Oceanogr.*, 12: 213-222.

- Jarvis, N.L., W.D. Garrett, M.A. Scheiman, and C.O. Timmons. 1967. Surface chemical characterization of surface-active material in seawater. *Limnol. Oceanogr.*, 12: 88-96.
- Kattner, G., and U.H. Brockmann. 1978. Fatty acid composition of dissolved and particulate matter in surface films. *Mar. Chem.*, 6: 233-241.
- Kattner, G., G. Gercken, and K.-D. Hammer. 1983. Development of lipids during a spring plankton bloom in the northern North Sea. II. Dissolved lipids and fatty acids. *Mar. Chem.*, 14: 163-173.
- Kattner, G., K. Nagel, K. Eberlein, and K.-D. Hammer. 1985. Components of natural surface microlayers and subsurface water. *Oceanologica Acta*, 8: 175-182.
- Lee, R.F., and P.M. Williams. 1974. Copepod "slick" in the northwest Pacific Ocean. *Naturwiss.*, 61: 505-506.
- Marty, J.-C., and A. Saliot. 1974. Etude chimique comparee du film de surface et de l'eau de mer sous-jacente: acides gras. *J. Rech. Atmos.*, 8: 563-570.
- Marty, J.-C., A. Saliot, P. Buat-Menard, R. Chesselet, and K.A. Hunter. 1979. Relationship between the lipid composition of marine aerosols, the sea surface microlayer, and subsurface water. *J. Geophys. Res.*, 84: 5707-5716.
- Mills, G.L., A.K. Hanson, Jr., and J.G. Quinn. 1982. Chemical studies of copper-organic complexes isolated from estuarine waters using C₁₈ reverse-phase liquid chromatography. *Mar. Chem.*, 11: 355-379.
- Siezen, R.J., and T.H. Mague. 1978. Amino acids in suspended particulate matter from oceanic and coastal waters of the Pacific. *Mar. Chem.*, 6: 215-231.
- Van Vleet, E.S., and P.M. Williams. 1983. Surface potential and film pressure measurements in seawater systems. *Limnol. Oceanogr.*, 18: 401-414.
- Williams, P.M. 1965. Fatty acids derived from lipids of marine origin. *J. Fish. Res. Bd. Can.*, 22: 1107-1122.
- Williams, P.M., E.S. Van Vleet, and C.R. Booth. 1980. In situ measurements of sea-surface potentials. *J. Mar.*

Res., 38: 193-204.

Williams, P.M., A.F. Carlucci, S.M. Henrichs, E.S. Van Vleet, S.G. Horrigan, F.M.H. Reid, and K.J. Robertson. 1986. Chemical and microbiological studies of sea-surface films in the southern Gulf of California and off the west coast of Baja California. Mar. Chem. (in press).

Williams, P.M., D.R. Long, C.C. Price, K.J. Robertson, and E.S. Van Vleet. 1982. A mobile platform for studying sea surface films. Deep-Sea Res., 29: 641-646.

THE CHEMISTRY OF NEAR-SURFACE SEAWATER*

Peter S. Liss

School of Environmental Sciences
University of East Anglia
Norwich, NR4 7TJ, U.K.

ABSTRACT

The top few hundred micrometres of the sea (often called the surface microlayer) is a difficult part of the oceans to study. The depth of the region is almost impossible to define in a meaningful way, and microlayer thicknesses are by default specified in terms of what the various sampling devices appear to collect. The organic composition of the microlayer is poorly characterized and its study suffers from similar problems to analogous work in bulk seawater. Some dissolved constituents in the microlayer appear to show small enrichments in concentration over subsurface waters, although such enrichments now seem smaller than was previously thought to be the case. Particulate material, on the other hand, does show significant microlayer enrichments.

INTRODUCTION

Although near-surface waters are acknowledged to be a very important zone with respect to chemical processes in the oceans, the chemistry of these waters has received rather little discussion. For this and other reasons discussed later, our knowledge in this area is still somewhat rudimentary. In the present account some aspects of the topic will be discussed. No attempt has been made to be comprehensive; several review papers have appeared in recent years of which the most relevant in the present context include those by MacIntyre (1974a,b), Liss (1975), Wangersky (1976), Hunter and Liss (1981), Hardy (1982), and Lion (1984). Topics are dealt with in the form of questions. This correctly implies that subjects selected for inclusion are ones for which significant uncertainties still exists.

* An extended version of this paper will appear in Dynamic Processes in the Chemistry of the Upper Ocean (ed. by J.D. Burton et al.), Plenum, 1986.

HOW THICK IS THE SEA SURFACE REGION?

The answer to this question is about as indefinite as that to the query "How long is a piece of string?" If one is dealing with such phenomena as ion rejection, interfacial double layers, or true monolayers the answer is several nanometres. However, for the oceanographically important processes of, for example, gas exchange or heat conduction then about 100 μm is probably the relevant thickness. These very different depth scales are elegantly illustrated in Fig. 1, which is taken from MacIntyre (1974a). It should be noted that in Fig. 1 the vertical axis is logarithmic and, as MacIntyre points out, continuing the depth scale to include the deepest ocean trenches would extend it by less than a factor of two. He remarks that in terms of processes the sea surface region may prove as rich a field for research as the deeper half of the "logarithmic" ocean.

Thus, the only answer to the question posed above is that it depends on the properties one is interested in. Since this chapter is about the chemistry of near-surface seawater, here it is the thickness of water required in order to obtain chemical information. Obviously, chemists would like to be able to analyse material from as near the interface as possible. However, the most widely used samplers collect material down to depths of tens to hundreds of micrometres from the surface, so that most of the presently available information on chemical composition is for this thickness of the sea surface. The term 'sea surface microlayer' is often used to describe samples harvested in this depth range. There are two sampling techniques which appear to collect thinner layers, but their utility is rather limited. These, together with the more conventional "microlayer" samplers, are discussed in the next section.

HOW IS THE SEA-SURFACE REGION SAMPLED?

The first practical device for sampling the sea surface microlayer was devised by Garrett (1965). It consists of a mesh screen of metal or plastic wires to which the near-surface water adheres and is drained into a sample bottle for subsequent chemical analysis. With this type of device the top 100-300 μm are collected, and reasonably large volumes of water (hundreds of millilitres) can be harvested. Garrett screens have proved the most popular of the microlayer samplers so far invented. Other devices, collecting similar thicknesses and volumes, which have been found useful include a rotating ceramic drum (Harvey, 1966) and a glass plate (harvey and Burzell, 1972). Since they can harvest reasonably large volumes, sophisticated chemical analysis of the water is possible, and these

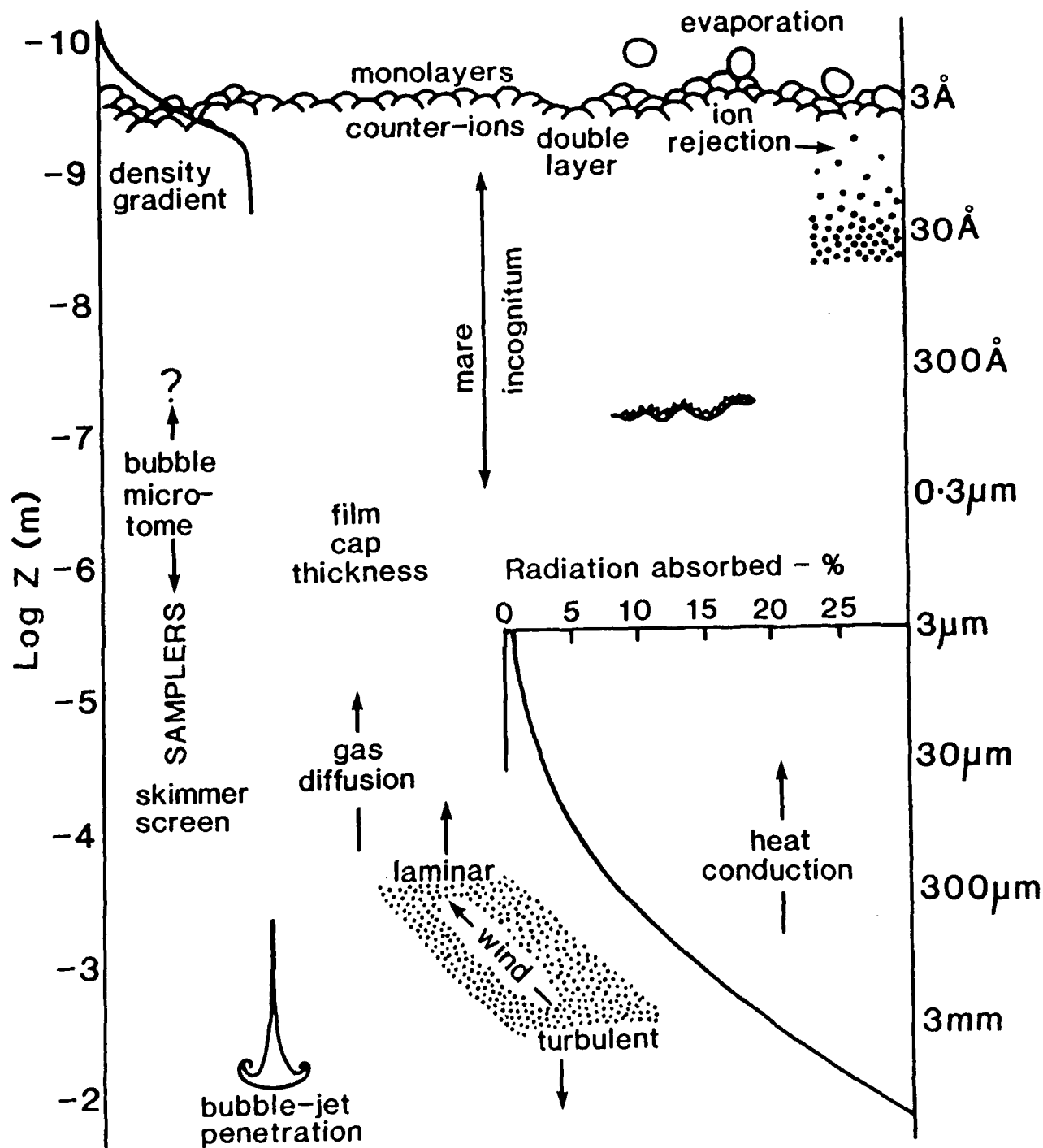


FIG. 1. Depth range of processes occurring in the top millimetres of the ocean surface (from MacIntyre, 1947a).

"microlayer" samples have so far been the mainstay of research into the chemical composition of near-surface seawater.

A cryogenic device, in which a slice of water about 1 mm thick is frozen onto a flat plate collector cooled with liquid nitrogen, has been described by Hamilton and Clifton (1979). Although not widely used, it has found application for the collection of microlayer samples for dissolved trace gas analysis (Turner and Liss, 1985). Clearly, more conventional samplers in which the water is exposed to the atmosphere after collection are unsatisfactory for this type of work.

Layers nominally substantially thinner than those harvested by the samplers described above have been obtained by collecting the aerosol formed when artificially-produced bubbles burst at the sea surface. The bubble acts as a microtome and is thought to peel off a layer from the sea surface whose thickness is 0.05% of the diameter of the bursting bubble (MacIntyre, 1968). For a 1 mm bubble this corresponds to a "cut" of approximately 0.5 μm ; i.e. two orders of magnitude thinner than can be achieved with the more traditional "microlayer" samplers. A practical realisation of this idea has been described by Fasching et al. (1974) and is called by them a Bubble Interfacial Microlayer Sampler (BIMS). With this device it is possible to collect tens of millilitres of water, so that quite detailed chemical analysis is possible. The device does suffer from a number of problems, including the need to deploy it under only the calmest of sea states, and high blanks (measured with the bubbler switched "off") particularly in the analysis of trace substances. More fundamental problems arise since the bubbles scavenge material from the subsurface water during their rise to the interface, and from the possibility of fractionation occurring during the actual bursting process. All in all, it would seem that the BIMS is more likely to successfully mimic and collect naturally produced marine aerosol than to sample an undisturbed slice of the order of 1 μm thickness from the sea surface.

The sampling device which appears to harvest the thinnest layers is the germanium prism described by Baier et al. (1974). This relies on the traditional Langmuir and Blodgett technique of using a hydrophilic material to collect monolayers from water surfaces. The thickness sampled appears to be approximately 30 nm when the collected material is in the dry state. It has been argued by Hunter and Liss (1981) that in the wet state (as at the sea surface) the material will be considerably expanded, possibly reaching dimensions of up to 1 μm . With such thin layers and considering the small dimensions of the sampling prism, it is

inevitable that only very small sample volumes are collected, so that the analysis which can be performed is strictly limited. In fact, by making the prism of germanium it is possible to obtain infra-red spectra of the adsorbed material directly, and this allows some of the major organic functional groups to be identified.

Further details of the samplers discussed above, as well as others not mentioned, are to be found in several of the reviews listed in the Introduction to this paper. An article specifically devoted to sea surface samplers is that by Garrett and Duce (1980).

WHAT IS THE ORGANIC CHEMICAL COMPOSITION OF MATERIAL FROM NEAR THE SEA SURFACE?

In early work only lipid-type material was analysed (Garrett, 1967), so that it was widely accepted that the organic matter in the microlayer was largely "dry" surfactants (straight chain largely saturated hydrocarbons with a hydrophilic head group). By straightforward mass balance arguments it can be shown that lipids represent, at the most, only 10% of the total organic matter (Liss, 1975).

Infra-red analysis of the thinner layers harvested by the germanium prism technique indicates the presence of mainly polysaccharide and polypeptide chains, fixed to the sea surface by occasional hydrophobic functional groups (Baier et al., 1974). Material of this type is often referred to as "wet" surfactant.

The past decade has seen little further fundamental advance in our knowledge of the organic chemistry of the sea surface. Characterisation of this material is at least as difficult as the analogous problem in bulk seawater, indeed there are many reasons for thinking that the organic material in the microlayer and the bulk water organics are rather similar in nature. For many years considerable efforts have been made to elucidate the organic chemistry of subsurface seawater, but these studies have only recently begun to yield information on possible pathways to the formation of marine humic materials as well as to its structure (Harvey et al., 1983). Much of this work is likely to be directly applicable to similar studies of microlayer organics, so that significant steps forward can be expected in the near future.

WHAT SUBSTANCES OCCUR AT ELEVATED CONCENTRATIONS IN THE SEA SURFACE MICROLAYER?

Early studies of the sea surface microlayer seemed

to indicate that, relative to bulk seawater, it was enriched substantially with respect to many components, e.g. total dissolved and particulate organics, bacteria and other microorganisms, pesticides and PCBs, trace metals, and plant nutrients (Liss, 1975). However, this assessment was based on very few analyses and, as more data have become available, the range of enriched substances and their degree of enrichment have both decreased. For example, Chapman and Liss (1981) found little or no significant microlayer enrichment for any of the plant nutrients in a range of samples collected in U.K. coastal waters. These authors suggested that the apparent enrichments of nutrients found by others may have been due to depleted concentrations in the subsurface, relative to the microlayer, water rather than true microlayer enrichments. Carlson (1983) has compiled measurements of dissolved organic carbon (DOC) in microlayer and bulk seawater and these are shown in Fig. 2. Most points plot close to the 1:1 line indicating that substantial microlayer enrichment for DOC is the exception rather than the rule.

Small but significant enrichments for particular fractions of the total organics are found. For example, measurements of ultra-violet absorbance, a measure of phenolic compounds, all plot above the 1:1 line, as shown in Fig. 3. Furthermore, for this particular class of compounds there is a clear relationship between degrees of enrichment and the presence or absence of visible slicks on the surface (Carlson, 1982).

One of the clearest examples of microlayer enrichment is shown by particulate organic carbon (POC). Carlson (1983) summarises data he has collected from estuarine, coastal and oceanic regions (his Table 1) and in all cases the microlayer is enriched in POC, the extent of the enrichment (ratio of microlayer to bulk sea-water concentrations) varying from 1.36 to 38.4. A plausible case can be made for the idea that the reason why POC always shows microlayer enrichment whereas DOC generally does not is that the surface active fraction of the DOC in bulk seawater achieves a lowering of its free energy by adsorbing onto particulate material. The particles are scavenged by bubbles and transported to the sea surface by them; the adsorbed surface-active organic matter then helps the particles to remain in the microlayer.

REFERENCES

- Baier, R.E., Goupil, D.W., Perlmutter, S., and King, R., 1974, Dominant chemical composition of sea surface films, natural slicks, and foams, J. Rech. Atmos., 8:571.

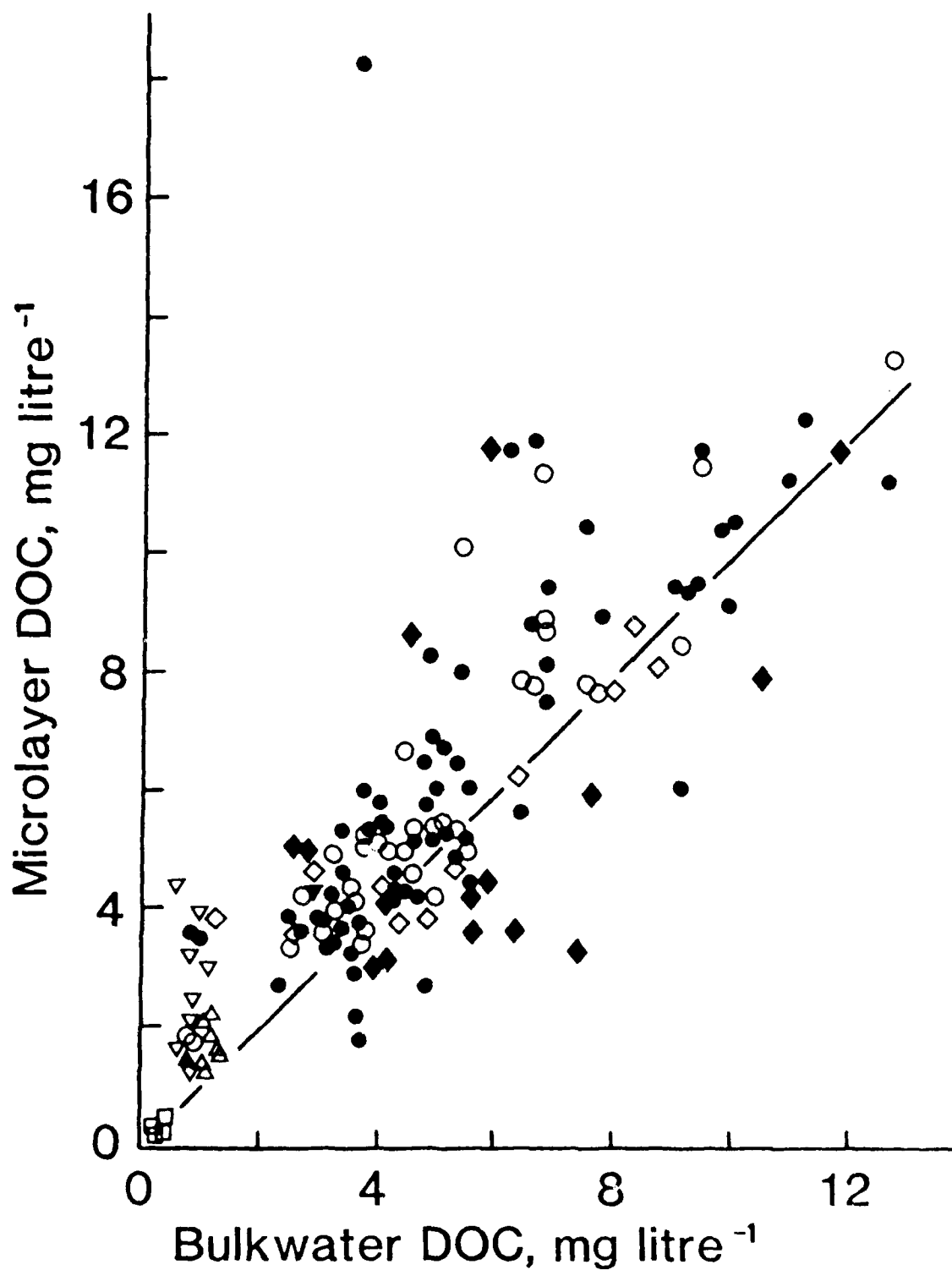


Fig. 2. Compilation of reported concentration of dissolved organic carbon (DOC) in the microlayer and bulk seawater (from Carlson, 1983). Broken line indicates equal concentrations in both samples.

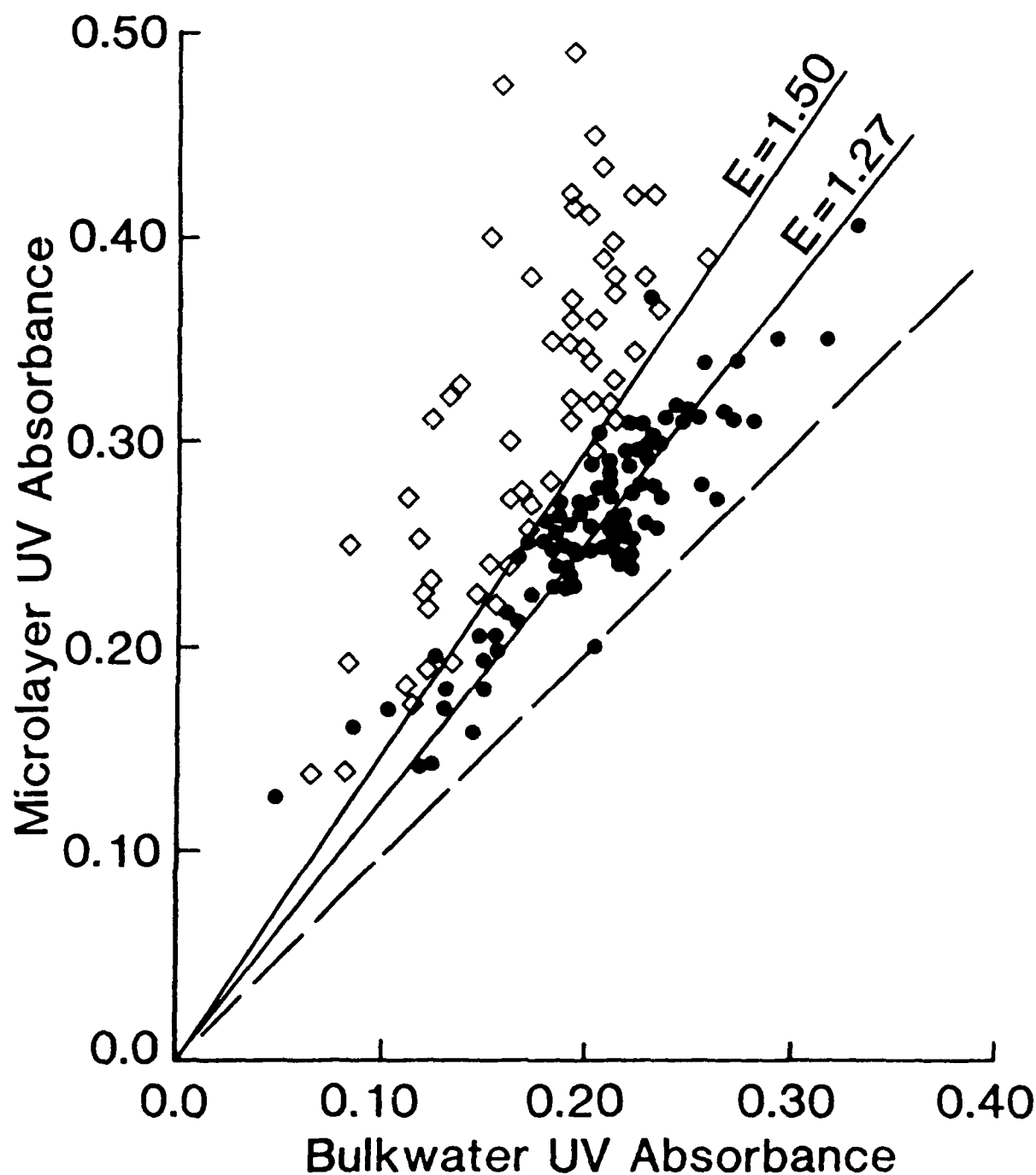


Fig. 3 Microlayer ultra-violet absorbance (280 nm) against that of bulk seawater (from Carlson, 1982). Dashed line indicates equal absorbance in both samples. Line of slope 1.27 ($r^2=0.99$, including 0,0) denotes mean enrichment of clean-surface samples in terms of ultra-violet absorbance. Line representing enrichment of 1.50 approximates boundary between clean and slicked samples. Lowest absorbances (<0.10) of bulk seawater are from waters of salinity $>33^{\circ}/_{\text{oo}}$. ● - Clean surfaces; ◇ - Slicked surfaces. Several slicked surfaces had absorbances >0.50 .

- Carlson, D.J., 1982, Surface microlayer phenolic enrichments indicate sea surface slicks, Nature, Lond., 296:426.
- Carlson, D.J., 1983, Dissolved organic materials in surface microlayers: Temporal and spatial variability and relation to sea state, Limnol. Oceanogr., 28:415.
- Chapman, P., and Liss, P.S., 1981, The sea surface microlayer: Measurements of dissolved iodine species and nutrients in coastal waters, Limnol. Oceanogr., 26:387.
- Fasching, J.L., Courant, R.A., Duce, R.A., and Piotrowicz, S.R., 1974, A new surface microlayer sampler utilizing the bubble microtome, J. Rech. Atmos., 8:650.
- Garrett, W.D., 1965, Collection of slick-forming materials from the sea surface, Limnol. Oceanogr., 10:602.
- Garrett, W.D., 1967, The organic chemical composition of the ocean surface, Deep-Sea Res., 14:221.
- Garrett, W.D., and Duce, R.A., 1980, Surface microlayer samplers, in: "Air-Sea Interaction: Instruments and Methods", F. Dobson, L. Hasse and R. Davis, eds, pp.471-490, Plenum Press, New York.
- Hamilton, E.I., and Clifton, R.J., 1979, Techniques for sampling the air-sea interface for estuarine and coastal waters, Limnol. Oceanogr., 24:188.
- Hardy, J.T., 1982, The sea surface microlayer: Biology, chemistry and anthropogenic enrichment, Prog. Oceanogr., 11:307.
- Harvey, G.R., Boran, A.D., Chesal, L.A., and Tokar, J.M., 1983, The structure of marine fulvic and humic acids, Mar. Chem., 12:119.
- Harvey, G.W., 1966, Microlayer collection from the sea surface: A new method and initial results, Limnol. Oceanogr., 11:608.
- Harvey, G.W., and Burzell, L.A., 1972, A simple microlayer method for small samples, Limnol. Oceanogr., 17:156.
- Hunter, K.A., and Liss, P.S., 1981, Organic sea surface films, in: "Marine Organic Chemistry", E.K. Duursma and R. Dawson, eds, pp.259-298, Elsevier, Amsterdam.

- Lion, L.W., 1984, The surface of the ocean, in: "The Handbook of Environmental Chemistry", Volume 1, Part C, O. Hutzinger, ed., pp.79-104, Springer-Verlag, Berlin.
- Liss, P.S., 1975, Chemistry of the sea surface microlayer, in: "Chemical Oceanography", Second edition, Volume 2, J.P. Riley and G. Skirrow, eds, pp.193-243, Academic Press, London.
- MacIntyre, F., 1968, Bubbles: A boundary-layer "microtome" for micron-thick samples of a liquid surface, J.Phys.Chem., 72:589.
- MacIntyre, F., 1974a, Chemical fractionation and sea-surface microlayer processes, in: "The Sea, Volume 5, Marine Chemistry", E.D. Goldberg, ed., pp.245-299, Wiley-Interscience, New York.
- MacIntyre, F., 1974b, The top millimeter of the ocean, Scient.Amer., 230:62.
- Turner, S.M., and Liss, P.S., 1985, Measurements of various sulphur gases in a coastal marine environment, J.Atmos.Chem., 2:223.
- Wangersky, P.J., 1976, The surface film as a physical environment, Ann.Rev.Ecol.Systematics, 7:161.

The molecular structure of the system water/monomolecular
surface film and its influence on water waves.

Heinrich Hühnerfuss

Institut für Organische Chemie der Universität Hamburg,
Martin-Luther-King-Platz 6, 2000 Hamburg 13, F.R. Germany

Werner Alpers

Fachbereich Physik/Elektrotechnik der Universität Bremen,
D-2800 Bremen 33, F.R. Germany

1. Introduction

In the years 1975 and 1979, two large-scale international experiments with well-defined man-made monomolecular sea slicks were performed on the North Sea¹⁻¹⁰⁾. The investigations aimed at finding a correlation between the molecular structure of the surface films and their influence on water waves and on the signals of various active and passive remote sensors. It turned out that the data obtained during these two experiments could only be interpreted by assuming strong interactions between the surface film and the adjacent water layer⁹⁾. However, in spite of this insight it was not yet possible to reach the ambitious goal of finding a correlation between the molecular structure of the film molecules and their influence on water waves and on the electromagnetic signals of remote sensors. This problem could only be solved after having performed very extensive laboratory measurements including surface viscosity, surface potential, relaxation, phase shift, and wind-wave-tunnel measurements.

In this paper, these recent and partly unpublished laboratory measurements will be reviewed. The importance of these results for interpreting wave damping by sea slicks will be discussed briefly. The modification of the signals of remote sensors by sea slicks will be reported by Alpers and Hühnerfuss separately.

2. The interaction between the monolayer and the vicinal water layer

In the first part of this paper, experimental evidence will be presented which supports the hypothesis that strong interactions between the monolayer and the adjacent water layer ("vicinal water layer") occur.

2.1. Surface viscosity measurements¹¹⁻¹³⁾

The surface viscosity measurements have been performed by means of the canal method which has been described in a recent paper by Hühnerfuss¹¹⁾. The main conclusion to be drawn from these measurements are as following:

a.) as shown in Table I, the surface viscosity increases with increasing chain length in the homologous series dodecanol, tetradecanol, hexadecanol and octadecanol. This result is in line with the hypothesis that the degree of hydrogen-bond formation strictly depends on the hydrophobicity of the film molecules and increases with increasing alkyl chain length, which implies a corresponding increase in viscosity within this layer.

Furthermore, an optimum interaction between the hydrophobic alkyl chains of the film-forming substance appears to be vital for an optimum interaction between surface film and water. In line with this hypothesis, the sterically hindered oleyl alcohol surface film exhibits a considerably lower surface viscosity than the corresponding saturated octadecanol film.

Table I : Limiting surface viscosity values of the homologous saturated long chain alcohol surface films and one unsaturated oleyl alcohol monolayer after relaxation having been attained. The data, which were approximated against time and against $W = 0.2$ cm, were corrected for the area loss, which is caused by relaxation effects, according to equation (63) of ref.¹³⁾, i.e., no correction term for the drag effect was included (spreading solvents ethanol and heptane; $T = 293$ K), surface pressure difference $20 \times 10^{-3} \text{ N m}^{-1}$).

substance	surface viscosity [mPa s m]		
	ethanol	heptane	lit. values
dodecanol	0.033 ± 0.003	0.028 ± 0.004	-
tetradecanol	0.420 ± 0.130	0.140 ± 0.040	1.1*
hexadecanol	0.560 ± 0.210	0.210 ± 0.030	0.85*/0.03**
octadecanol	1.08 ± 0.22	0.210 ± 0.090	0.17*
Z-9-octadecen-1-ol ("oleyl alcohol")	0.071 ± 0.024	-	-

* torsion pendulum method

** canal method

b. The surface viscosity values show a distinct spreading solvent dependence: the general impression is that the long chain alcohols exhibit significantly lower surface viscosity values, when heptane is used as spreading solvent. This result is in line with the assumption that heptane molecules are included between the long alcohol alkyl chains thus preventing the film-forming molecules from an optimum interaction, which must necessarily lead to less intensive hydrophobic interactions with the adjacent water layer and, consequently, to lower surface viscosities.

In order to investigate the "hypothesis of optimum hydrophobic interaction", which is assumed to be the crucial parameter for surface viscosity, systematic investigations with various carboxylic acid ester derivatives were performed. Carboxylic acid esters are of particular interest because of their widespread occurrence in natural surface films. Most investigations devoted to the analysis of biogenic surface films describe the fatty acid composition of such sea slicks (see e.g.^{14,15}), and literature cited therein).

In a first set of experiments α - and ω -bromo-derivatives of hexadecanoic acid methyl ester were investigated¹²⁾. The results are summarized in Table II. In comparison to the unsubstituted hexadecanoic acid methyl ester, the α -bromo-derivative gives rise to a considerable sterical hindrance and, as a consequence, the surface viscosity

Table II: Limiting surface viscosity values of long chain carboxylic acid ester derivatives after relaxation having been attained. The data, which were approximated against time and against $W = 0.2$ cm, were corrected for the area loss, which is caused by relaxation effects, according to equation (63) of ref.¹³⁾, i.e., no correction term for a drag effect was included (spreading solvent ethanol, $T = 293$ K, surface pressure difference $10 \times 10^{-3} \text{ N m}^{-1}$ and $15 \times 10^{-3} \text{ N m}^{-1}$, respectively).

substance	surface viscosity mPa s m	
	$10 \times 10^{-3} \text{ Nm}^{-1}$	$15 \times 10^{-3} \text{ Nm}^{-1}$
hexadecanoic acid methyl ester	0.193 ± 0.053	-----
α -Br-hexadecanoic acid methyl ester	0.0063 ± 0.0007	-----
ω -Br-hexadecanoic acid methyl ester	0.136 ± 0.053	-----
hexadecanoic acid ethyl ester	-----	0.220 ± 0.096
tetradecyl-butyrolacton	-----	0.041 ± 0.004

value is significantly reduced. The sterical hindrance of the ω -bromo-derivative is not so pronounced compared to the α -bromo-compound. Hence the surface viscosity of ω -bromo-hexadecanoic acid methyl ester approaches the value of the unsubstituted ester, although it remains slightly lower.

In conclusion, the above results are in line with the "hypothesis of optimum hydrophobic interaction" and with the assumption that the hydrophobic alkyl chain always induces a more or less pronounced hydrogen-bond formation ("structure former"), which implies an increase in surface viscosity. However, the role of the hydrophilic part of surface-active compounds needs some further investigations: for this reason another set of experiments was performed during which the hydrophobic alkyl chain was kept constant, while the hydrophilic character was systematically increased by gradual prolongation of the ethoxyl-group of ethoxylated hexadecanol¹³⁾.

The results, which are summarized in Table III, show that an increasing hydrophilic character appears to lead to a decrease of the surface viscosity. At first glance, this effect seems to be astonishing, because it is generally accepted that increasing hydrophilic character implies increasing interaction with adjacent water molecules.

However, these hydrophilic interactions are, although of high energy, only of

Table III: Limiting surface viscosity values of ethoxylated hexadecanol derivatives and of an ammonium compound after relaxation having been attained. The data, which were approximated against time and against $W = 0.2$ cm, were corrected for the area loss, which is caused by relaxation effects, according to equation (63) of ref.¹³⁾, i.e., no correction for a drag effect was included (spreading solvent ethanol, $T = 293$ K, surface pressure difference 20×10^{-3} N m⁻¹).

substance	surf. viscosity [mPa s m]
	20×10^{-3} N m ⁻¹
hexadecanol	0.560 ± 0.210
mono-(ethylenglycol)-mono-hexadecyl ether	0.196 ± 0.001
di-(ethylenglycol)-mono-hexadecyl ether	0.051 ± 0.018
tri-(ethylenglycol)-mono-hexadecyl ether	0.043 ± 0.012
hexadecyl-tri-methyl ammonium bromide	0.045 ± 0.003

short range character. In contrast to this short range effect hydrophobic interactions are assumed to be of long-range character. Therefore, the surface viscosity values summarized in Table III can only be understood, if it is considered that the "structure promoting effect" of the hydrophobic alkyl chain is partly disturbed by different structural arrangements induced by the hydrophilic head group, which in all leads to a lower surface viscosity.

For further details the reader should refer to the two recent papers by Hühnerfuss^{12,13)}.

2.2. Passive microwave measurements^{9,10,16)}

An extensive report on the passive microwave measurements will be given in the paper by Alpers and Hühnerfuss. In this paper, only those data will be mentioned briefly, which support the conclusions drawn from the surface viscosity measurements: in the presence of an oleyl alcohol surface film an increase in the relaxation time of the water molecules within the upper water layer by an order of magnitude has been observed. While the relaxation time of pure water is known to be $\tau_0 = 1.19 \times 10^{-11}$ s, in the presence of an oleyl alcohol slick a relaxation time $\tau_s = 1.11 \times 10^{-10}$ s was determined ($T = 287.2$ K). These values and the weighted average of the free activation enthalpy $\Delta G = 6.53$ kJ/mol reflect an increase in hydrogen bond formation, as sche-

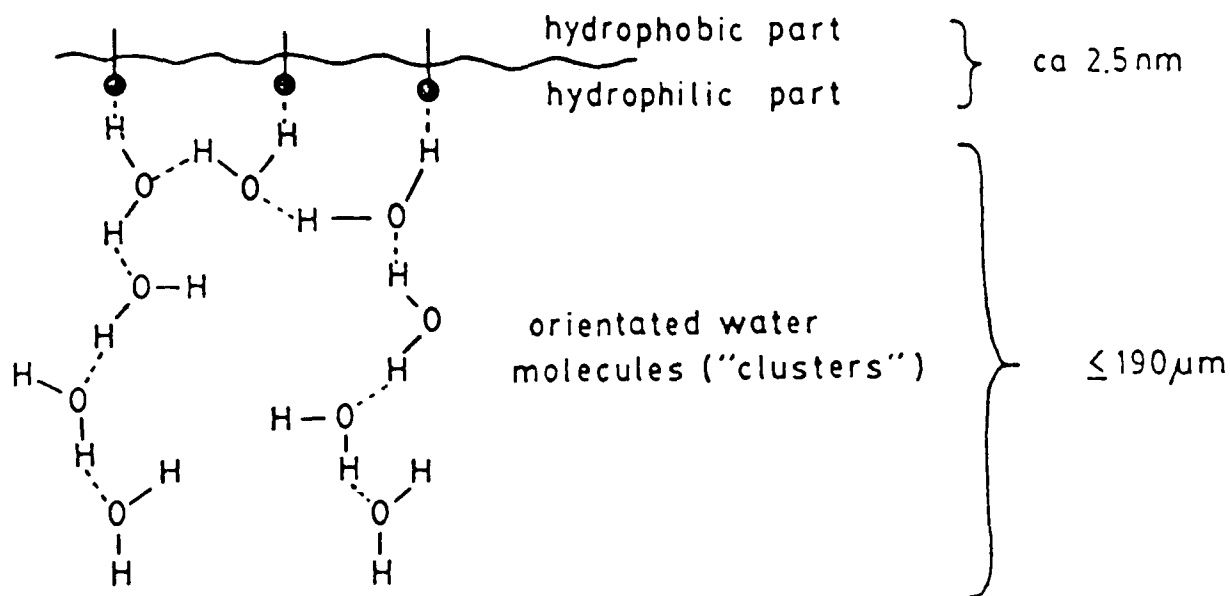


Figure 1 : Interaction between a monomolecular surface film, consisting of a hydrophobic and a hydrophilic part, and the adjacent water molecules.

matically depicted in Figure 10, and the formation of icelike clathrate structures with $\text{O} \cdots \text{O}$ distances of $r = 5.8 \times 10^{-10} \text{ m}$, where the strength of these structures decreases exponentially with depth.

For more details the reader should refer to the paper by Alpers and Hühnerfuss.

2.3. Surface potential measurements^{13,17)}

The surface potential measurements have been performed by means of the "ionizing electrode method", which has been described in two recent papers by Hühnerfuss^{13,17)}.

During a first set of measurements the contribution of the hydrophobic chain to the polarization effect within the upper water layer was investigated by comparing a compound with saturated alkyl chain (octadecanol (ODA)) and a compound with unsaturated alkyl chain (Z-9-octadecen-1-ol (OLA)). The surface potential values, which are summarized in Figure 2, are in line with the above "hypothesis of optimum hydrophobic interaction": the values obtained in the presence of ODA generally are about twice as large as those of the unsaturated OLA, which exhibits considerable sterical hindrances due to the Z-configured double bond of the alkyl chain (Figure 2). Obviously, sterical hindrance, which prevents the molecules from an optimum hydrophobic interaction, leads to a decrease of the polarization effect.

This conclusion is further supported by a comparison of the surface potential data measured by applying two different spreading solvents, ethanol and heptane: as already concluded from the surface viscosity data (section 2.1), heptane molecules may be included in the monolayer, whereas ethanol seems to be easily dissolved in the subphase. With regard to the octadecanol monolayer at low surface pressures these different characteristics of the two spreading solvents result in remarkably lower surface potential values when spread from heptane compared to the corresponding ethanol spreading solvent data (Figure 2). At first glance this appears to be an astonishing effect, because at low surface pressures the

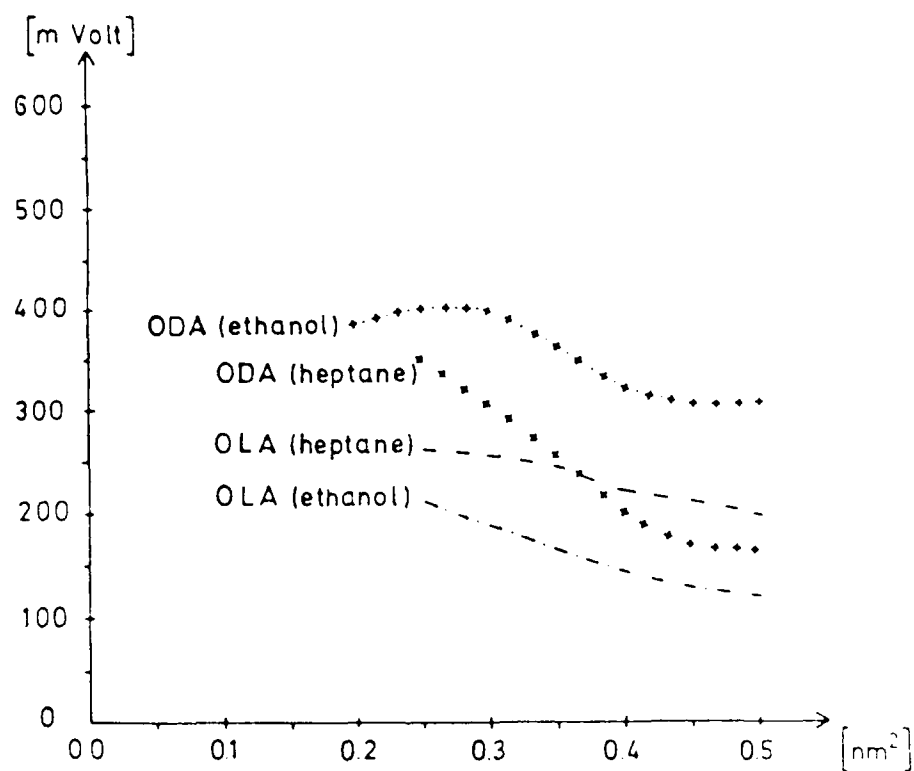


Figure 2: Surface potential values [millivolts] vs. area/molecule [nm^2] of an unsaturated long chain alcohol, Z-9-octadecen-1-ol (OLA), and a saturated alcohol, octadecanol (ODA), surface film. The data are given for the application of both ethanol and heptane spreading solvents.

concentration of the octadecanol molecules ought to be so low that it should not make much difference whether or not heptane molecules are present. This assumption, however, is based upon an "ideal-gas-like status", i.e. it is provided that the molecules do not interact between each other at low pressures. But this is not valid for octadecanol molecules: an analysis of the total area covered by a low pressure octadecanol surface film by means of the extremely sensitive surface potential sensor revealed that the film is very inhomogeneous when spread from ethanol. This implies that the octadecanol molecules form islands rather than being distributed homogeneously. Thus, when spread from heptane solvent, these islands are easily broken by including heptane molecules, and consequently, the average surface potential is lower, because the heptane molecules prevent the alkyl chains from an optimum interaction.

However, when compressing the octadecanol surface film, which was spread from heptane, the solvent molecules are squeezed out more and more, and the surface potential values are approaching the values determined for the ethanol spreading solvent case (Figure 2).

Furthermore, it is interesting to note that this "squeezing-out effect" of heptane molecules appears to be less pronounced in the presence of OLA monolayers. Because at the start of compression of the unsaturated alkyl chains which are in a state of

heptane molecules seems to be left although compressing the surface film, and, consequently, the dependence of the surface potential on the available area/molecule is less intensive in the case of OLA films compared to ODA monolayers (Figure 2). The inclusion of heptane molecules into the free "holes" of the sterically hindered OLA film even seems to give rise to a better mutual interaction between the hydrophobic chains of the OLA molecules, as can be tentatively concluded from the larger surface potential values of the OLA (heptane)-curve compared to the OLA (ethanol)-curve of Figure 2.

During another set of experiments the surface potential values of saturated alcohols were compared with their respective ethoxylated derivatives, in order to investigate the contribution of increasing hydrophilic character to the polarization effect. The results, which are summarized in Figure 3, reveal a more complex influence of the homologous series of ethoxylated alcohols on the surface potential than encountered in the presence of long chain alcohols: the general impression is that the ethoxylated alcohols exhibit a larger surface potential than the alcohols. This holds, in particular, at low surface pressures, while at higher surface pressures the values become more comparable.

The different characteristics of long chain alcohols and their poly-ethoxylated derivatives can be understood as follows:

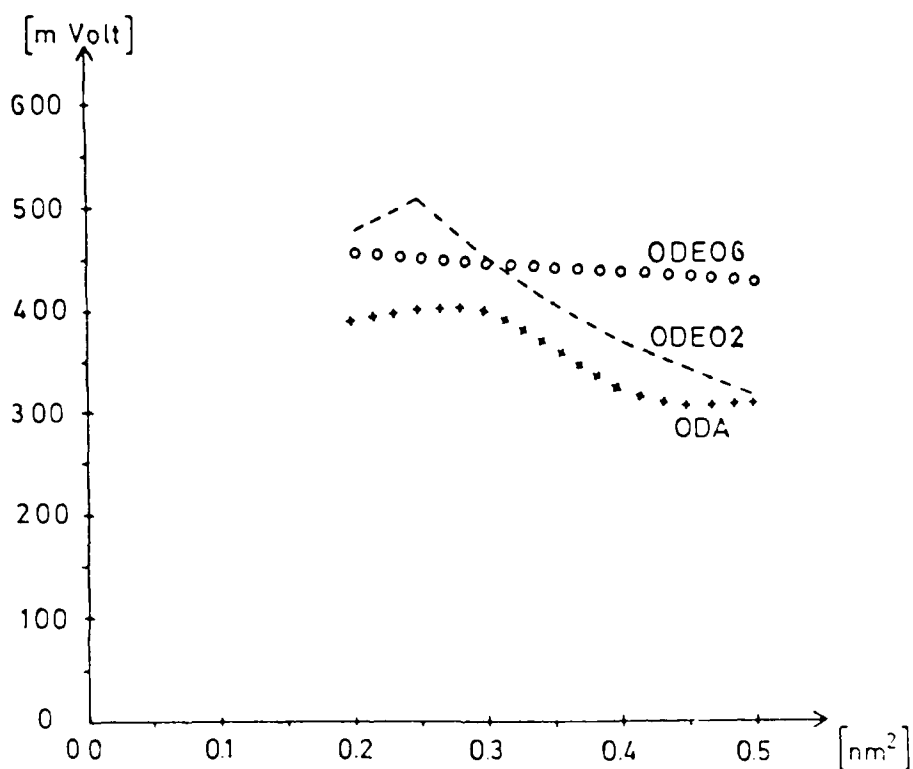


Figure 3: Surface potential values [millivolts] vs. area/molecule [nm^2] of an octadecanol (ODA) and two ethoxylated long chain alcohol surface films, di-(ethylenglycol)-mono-octadecyl ether (ODE02), and hexa-(ethylenglycol)-mono-octadecyl ether (ODE06), which were spread from ethanol spreading solvent.

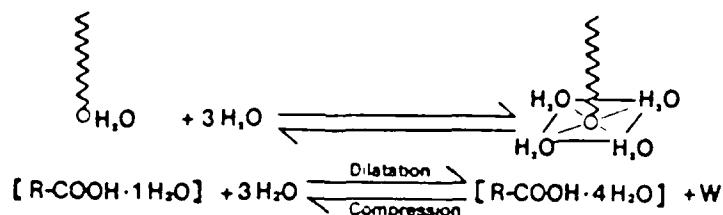


Figure 4: The hydration equilibrium of an alkyl carboxylic acid film on the water surface.

at low surface pressures water complexes can be formed by the hydrophilic head group as schematically depicted in Figure 4. Compression of the surface film to smaller areas must necessarily lead to dehydration (see Figure 4). Monomolecular coverage is theoretically achieved at 0.185 nm^2 , which is consistent with the necessary area for the saturated alkyl chain. At this compression status the water complex can at most contain one water molecule¹³⁾, and the long alkyl chains are positioned so close to each other that strong hydrophobic interactions are dominant.

With regard to poly-ethoxylated alcohols more hydrophilic positions are available within each molecule, which are able to form water complexes, and thus it is conceivable that at lower surface pressures the hydrophilic hydration term contributes more intensely to the surface potential than in the case of long chain alcohols. As a consequence, polyethoxylated

alcohols exhibit considerably larger surface potential values at low surface pressures than the corresponding alcohols (see Figure 3). However, although the hydrophilic hydration term plays a minor role at higher surface pressures, it still contributes to the surface potential such that in total larger values are measured also in the presence of compressed ethoxylated alcohols compared to compressed unsubstituted alcohols (see Figure 3).

In conclusion, depending on the hydrophilic character of the head group of the alcohols and ethoxylated alcohols, respectively, the hydrophilic hydration and the hydrophobic hydration contribute to the surface potential in a different manner: at low surface pressures hydrophilic hydration becomes dominant provided that the head group is of very hydrophilic character, while at high surface pressures the hydrophobic hydration is dominant, if no sterical hindrances prevent the molecules from undergoing optimum hydrophobic interactions.

This partly additive and partly antagonistic character of the hydrophobic and the hydrophilic hydration terms has been investigated further by determining the surface potentials in the presence of surface-active substances with varying hydrophilic head groups: in Figure 5 three substances are compared, which cannot achieve considerable hydrophobic interactions because of their unsaturated alkyl chains, tri-olein (TOLG), sorbitane-monoleate (SPAN), and 2-9-octadecen-1-oic acid (OLS). It should

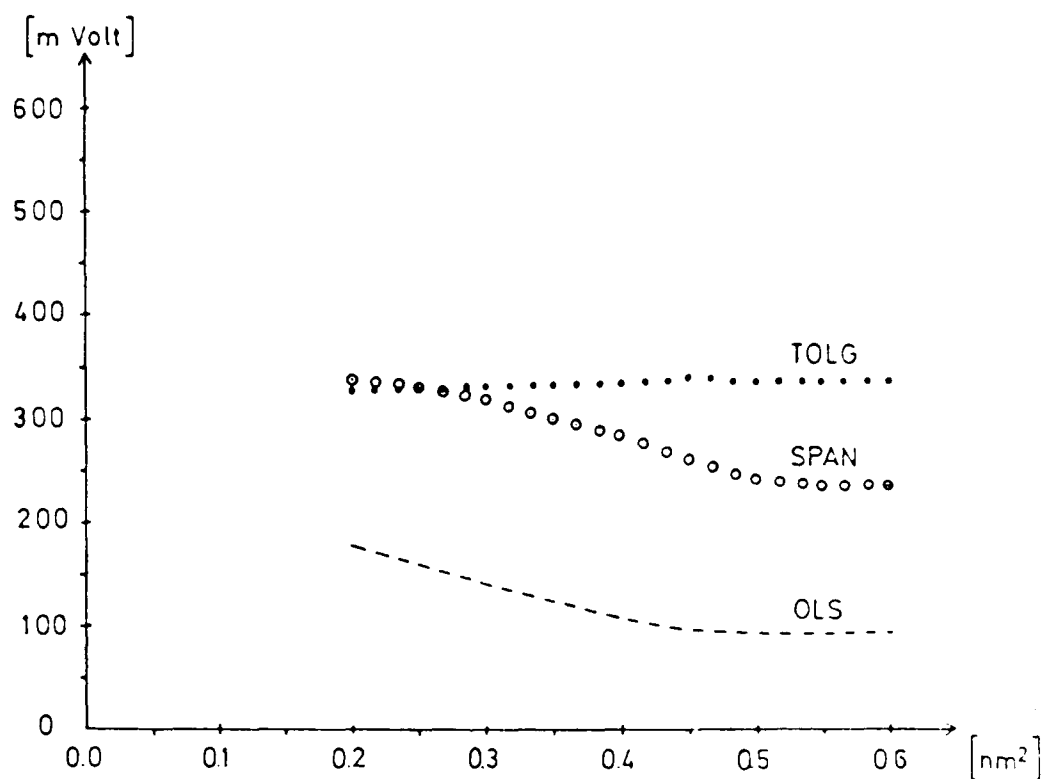


Figure 5: Surface potential values [millivolts] vs. area/molecule [nm^2] of three surface-active substances with unsaturated alkyl chains and different hydrophilic character, tri-olein (TOLG), sorbitane-mono-oleate (SPAN), and Z-9-octadecen-1-oic acid (OLS), which were spread from ethanol spreading solvent.

be noted that SPAN has been included in this investigation in spite of its only "technical purity" , because the physico-chemical characteristics of SPAN are similar to those of natural sea slicks. In the case of TOLG and SPAN relatively strong hydrophilic hydration is induced, which gives rise to large surface potential values even at low surface pressures. Because of the low hydrophobic interaction term at high surface pressures only a slight increase in the surface potential is observed in the presence of SPAN, when compressing the surface film, and in the presence of TOLG even a slight decrease (!) of the surface potential is measured.

If not only the hydrophobic term, but also the hydrophilic term is low, relatively low surface potential values are obtained both at compressed and dilated film status. This is exemplarily shown for OLS (Figure 5). The low hydrophilic hydration ability of the carboxylic acid head group, may be due to possible direct hydrogen-bond formation between the functional groups, which in this case can be accomplished without intervening hydrogen-bonded water molecules¹³⁾.

Additional experimental results including carboxylic acid ester derivatives and ammonium compounds can be found in the papers by Hühnerfuss^{13,17)}.

3. Monomolecular surface films under dynamic conditions

On an undulating water surface, monomolecular surface films will be compressed and dilated, i.e., the optimum arrangement of the film molecules will be disturbed periodically, and concentration gradients and thus surface tension gradients will be induced. According to the Marangoni wave theory, which will be extensively discussed by Lombardini and by Lucassen-Reynders, these surface tension gradients give rise to longitudinal "stream flows" as schematically depicted in Figure 6. The magnitude of these "stream flows" decreases exponentially with depth. However, prior to the beginning of this work no experimental approach for verifying the occurrence of surface tension gradients on gravity water waves had been described in the literature, and thus, novel experimental methods had to be developed.

3.1. Dynamic surface potential and phase shift measurements^{13,18-20)}

Wave-induced compression and dilation of a monomolecular surface film are expected to lead to concentration gradients, which in turn give rise to a surface tension and surface potential gradient. Continuous surface potential measurements above a film-covered wavy water surface thus are expected to reveal periodic surface potential variations. This phenomenon has been taken advantage of in the present work.

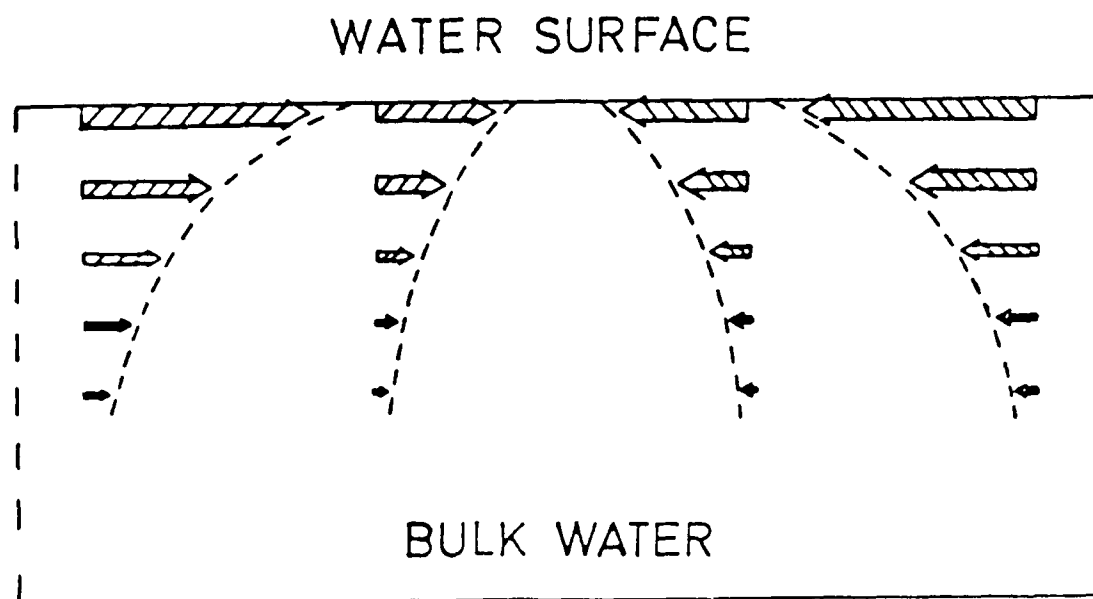


Figure 6: Liquid motion caused by a longitudinal wave. Note that in an actual wave, the wavelength is very much larger than the penetration depth.

The measurements were performed in the wind-wave tunnel of the University Hamburg (26 m long, 1 m wide, and 0.5 m deep) which is equipped with a hydraulically driven wave flap.

Our approach to measuring the surface contraction and extension of a film on an undulating water surface involves a direct measurement of the electrical surface potential of the film by a dynamic "wave following" procedure. As outlined in section 2 previously reported measurements of surface potentials were performed under static condi-

tions using either the air ionization electrode or the vibrating electrode method. The advantage of the former was substantiated above.

In order to measure the surface potential over a wavy water surface, our surface potential probe - originally designed for static laboratory measurements in our Langmuir-trough as described above - was mounted on a wave follower¹⁸⁾ so that it remained a fixed distance above the film-covered undulating water surface.

In order to localize the maximum compression and dilation zone - measured by the surface potential probe - with respect to the position on the water wave, conventional wave staff measurements were performed simultaneously by resistance wave gauges of the Danish Hydraulic Institute, Horsholm (Denmark). The output of the surface potential probe was correlated to the output of the wave gauge placed next to and at the same position, with regard to the length of the channel, of the surface potential probe.

Figure 7 shows a typical measurement using the wave follower mounted surface potential probe for a 1 Hz flap generated wave (wavelength = 1.56 m; wave height = 2 cm). The trace exhibits the expected jump in surface potential with the arrival of the film. The wave-induced surface potential fluctuations also increase significantly in the presence of the film. Another notable characteristic of the curve depict-

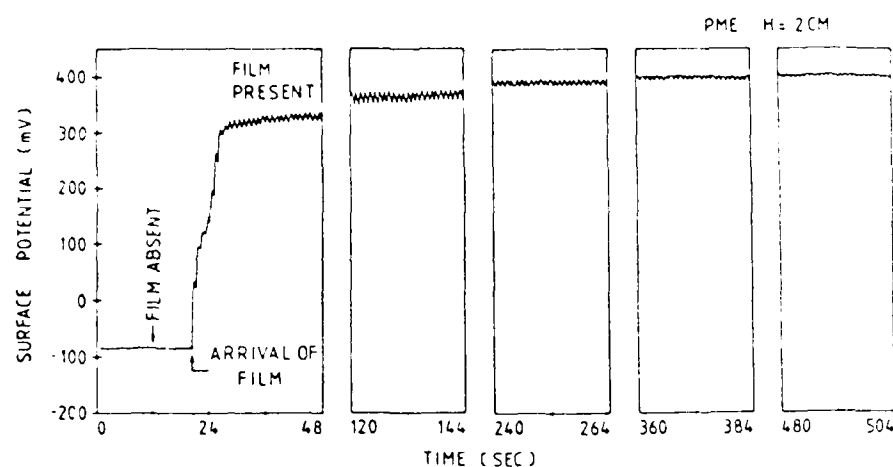


Figure 7: Typical surface potential trace for hexadecanoic acid methyl ester (PME) showing response to 1 Hz water wave of 2 cm height.

ed in Figure 7 is the decrease of the surface potential fluctuations in time, i.e., the film molecules experience a "relaxation". This effect can be easily understood in the light of the relaxation characteristics of monomolecular surface films discussed below.

In order to assure that the relaxation effect was not due to a gradual fouling of the surface potential probe, the probe was cleaned in the middle of a run. The probe output returned to the precleaned form after a few seconds.

The data obtained in the presence of various surface active compounds support the hypothesis that surface tension gradients are induced in monolayers by propagating gravity waves.

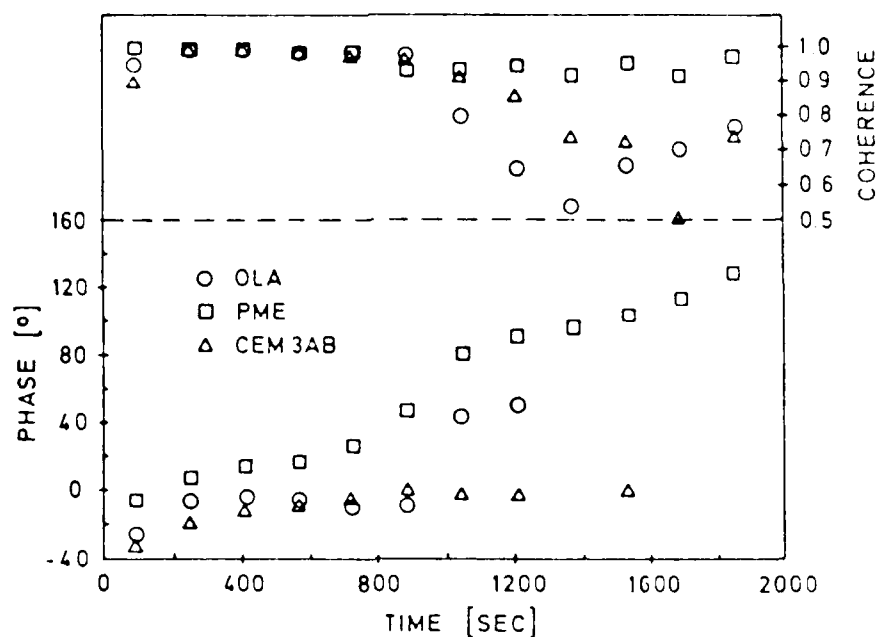


Figure 8: Phase angles between the hydrodynamic surface area variation and the area of surface potential variation of OLA (circles), PME (squares), and CEM3AB (triangles). Phase and coherence refer to a comparison of the surface potential output to that of a fixed wave height gauge.

In addition, the data allow the determination of the zones of maximum compression and dilatation on the backward and forward side of the propagating gravity water wave. Therefore, concurrently to the spectral peak measurements, the surface potential output was correlated with the output of a fixed wave height gauge placed next to and at the same "fetch" (= wave propagation distance) of the surface potential probe. In Figure 8 ,

the curves in the lower part show the phase relationship, and in the upper part the corresponding coherences of the transfer function between the wave height gauge and the surface potential probe. We have arbitrarily plotted only the phase values up to where the coherence dropped to 0.5 .

An extensive discussion on the phase shift and its importance for interpreting wave attenuation by monolayers can be found in Hühnerfuss et al.^{20,21)}.

3.2. Relaxation measurements²¹⁾

The microwave relaxation measurements supplied valuable insight into the interaction characteristics between surface film and the vicinal water layer and into the molecular structure of the interacting system. However, the relaxation time $\tau_s = 1.11 \times 10^{-10}$ s obtained in the presence of the surface film is still considerably shorter than the inverse angular wave frequency ω^{-1} and, consequently, the relaxation behaviour of the water molecules cannot be the key for the viscous film-induced wave damping effect.

Therefore, the relaxation effects in monomolecular surface films were investigated, in particular with regard to the time scales of the relaxation process and their potential contribution to the viscous damping term.

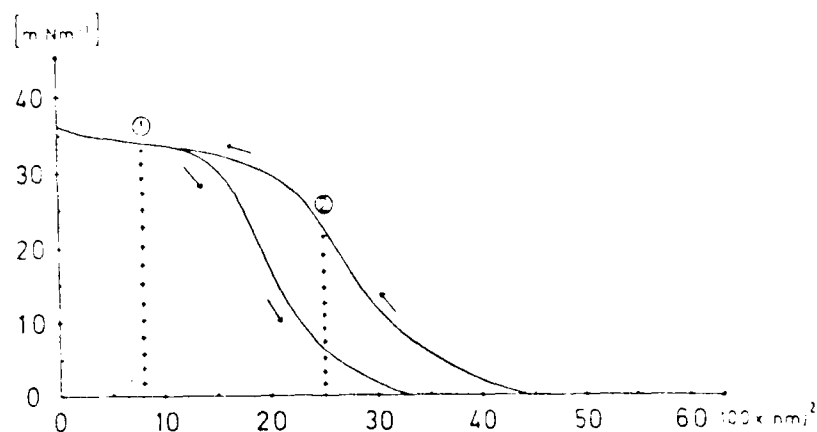


Figure 9 : Surface pressure $[\text{mNm}^{-1}]$ plotted vs. area/molecule $[100 \times \text{nm}^2]$. Compression and dilatation curve (indicated by \rightarrow) of an Z-9-octadecen-1-ol ("oleyl alcohol") surface film measured in an automatically working Langmuir-trough. Point 1 indicates a constant area of $0.08 \text{ nm}^2/\text{molecule}$, at which compression was stopped and the time dependence of surface pressure decrease was measured. The second set of relaxation measurements was performed at point 2 at $0.25 \text{ nm}^2/\text{molecule}$.

The measurements were performed in an automatically working Langmuir-trough Type A, Fa. Lauda, Lauda (F.R. Germany). The compression and dilatation curve of 9-octadecen-1-ol, Z-isomer, (oleyl alcohol) measured at 288 K (velocity v_{comp} and v_{dil} were $0.016 \text{ nm}^2/\text{molecule} \cdot \text{min}$) is shown in Figure 9. The relaxation process was investigated by compressing the surface film to monomolecular coverage at $0.25 \text{ nm}^2/\text{molecule}$

(point 2 in Figure 9), keeping the surface film material within this constant area and measuring the time dependence of the surface pressure decrease. The experiment was repeated by compressing the film until partial collapse to $0.08 \text{ nm}^2/\text{molecule}$ (point 1 in Figure 9), which is supposed to occur at the ocean surface at higher wind velocities. These measurements were performed at 288, 298, 303, and 308 K.

The spreading solvent was ethanol, which was redistilled over a bubble-cap column. In connection with investigations on spreading solvent effects on the physicochemical properties of monolayers, the measurements at $0.08 \text{ nm}^2/\text{molecule}$ were also performed applying heptane as spreading solvent.

As an example for the results obtained two set of curves determined at a constant area of $0.08 \text{ nm}^2/\text{molecule}$ are shown: Figure 10 depicts the time dependence of the surface pressure decrease of an Z-9-octadecen-1-ol surface film, which was spread from ethanol solution, and Figure 11 shows the results obtained, when applying heptane as spreading solvent. The data, which were measured at a constant compression area of $0.25 \text{ nm}^2/\text{molecule}$, were qualitatively similar to those in Figure 10 (spreading solvent ethanol).

The relaxation time τ_{comp} is defined as the time, after which the surface pressure dropped to $1/e$ (i.e. 37 %) of the difference between the initial surface pressure F_{comp} after stopping the compression, and the equilibrium surface pressure F_{eq} . The relaxation times calculated from the

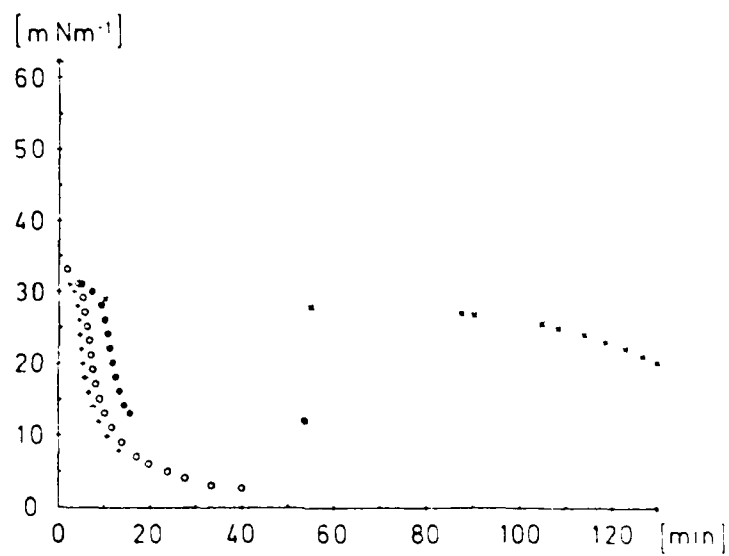


Figure 10: Time dependence of surface pressure decrease at 288 K (oooo), 293 K (●●●●), 303 K (++++), and 308 K (xxxx). The measurements were performed at a constant area of $0.08 \text{ nm}^2/\text{molecule}$ (point 1 in Figure 9), using ethanol as spreading solvent.

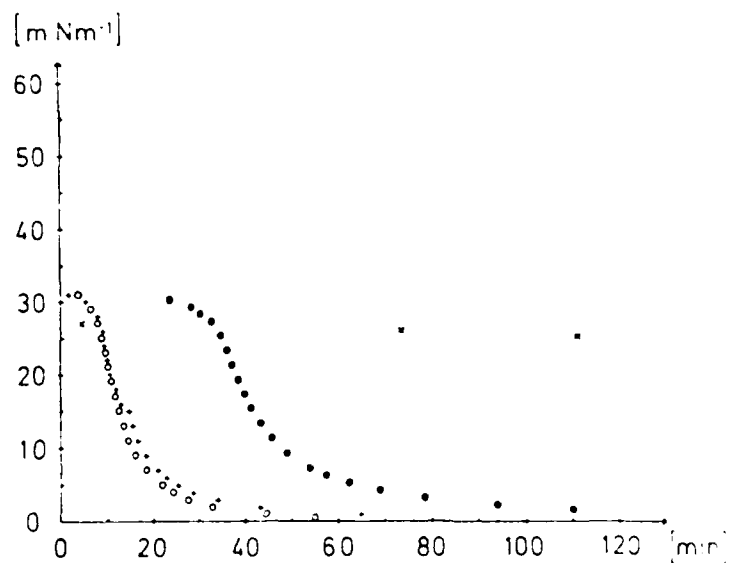


Figure 11: Time dependence of surface pressure decrease at 288 K (oooo), 298 K (••••), 303 K (++++), and 303 K (xxxx). The measurements were performed at a constant area of $0.03 \text{ nm}^2/\text{molecule}$ (point 1 in Figure 9), using heptane as spreading solvent.

Table IV: The relaxation time τ_{comp} calculated from
Figures 10 and 11.

Spreading solvent	Temperature [K]	Relaxation time [min]
Ethanol	288	9.6 ± 0.5
	298	11.7 ± 0.9
	303	7.5 ± 0.5
	308	148 ± 6
Heptane	288	13.8 ± 1
	298	45 ± 3
	303	16.2 ± 1
	308	192 ± 8

curves of Figures 10 and 11 are summarized in Table IV.

Each measurement was repeated three to five times, until the necessary reproducibility of the relaxation time τ_{comp} was achieved. At $\tau_{\text{comp}} < 10$ min a deviation $\delta\tau$ of ± 0.5 min, at $\tau_{\text{comp}} \approx 10 - 20$ min a deviation of ± 1 min, at $\tau_{\text{comp}} \approx 20 - 50$ min a deviation of ± 3 min, $\tau_{\text{comp}} \approx 50 - 100$ min a deviation of ± 5 min, and at $\tau_{\text{comp}} > 100$ min a deviation of ± 10 min was tolerated. The $\delta\tau$ values of the averaged relaxation times are also given in Table IV.

The above results clearly reveal a thermal anomaly at 303 K: The velocity of surface pressure decrease becomes smaller with increasing temperature at 298 and 308 K (Figures 10 and 11), which results in an increasing relaxation time (Table IV). However, at 303 K a significantly faster decrease of surface pressure is observed compared to 288 and 298 K, corresponding with a decrease of the relaxation time. It would be beyond the scope of this paper to discuss this thermal anomaly effect and its implication for biological processes, and , therefore, the reader should refer to the papers by Hühnerfuss and Walter²¹⁾ and by Hühnerfuss¹³⁾.

4. The Marangoni wave phenomenon

The theory of the Marangoni wave phenomenon will be discussed in subsequent papers by Lombardini and by Lucassen-Reynders. The results presented in this paper show that the assumptions which form the basis for the Marangoni wave theory are realistic:

- gravity waves are generating surface tension gradients within a film-covered water surface,
- strong interactions between the monolayer and the vicinal water layer were observed, which are depending on the hydrophilic and hydrophobic hydration terms,

- the time scale of the relaxation effect due to rearrangement processes of the film molecules is significantly larger than the inverse angular wave frequency ω^{-1} ,
- the phase difference between the hydrodynamic compression zone and the zone of maximum concentration of the film molecules can be determined.

Based upon these results, it was possible to calculate the theoretical wave damping curves by means of the Marangoni wave theory and to compare these results with wave damping curves determined experimentally by wind-wave-tunnel measurements. Presently, this comparison has been undertaken for about 60 to 70 chemical compounds. In all cases, the accordance between theoretical and experimental curves is astonishingly well. As an example, the results are given for the homologous series of saturated long chain alcohols (Figure 12) and for the ethoxylated hexadecanol-derivatives (Figure 13). Recently, Hühnerfuss et al. could show that the modification of wind wave spectra by monomolecular sea slicks can also be explained by means of the Marangoni wave phenomenon²²⁾.

In conclusion, the experimental evidence presented in this paper and the additional result, which will be presented by Lombardini, clearly show that the wave damping effect by sea slicks is fully understood both for mechanically and for wind generated water waves.

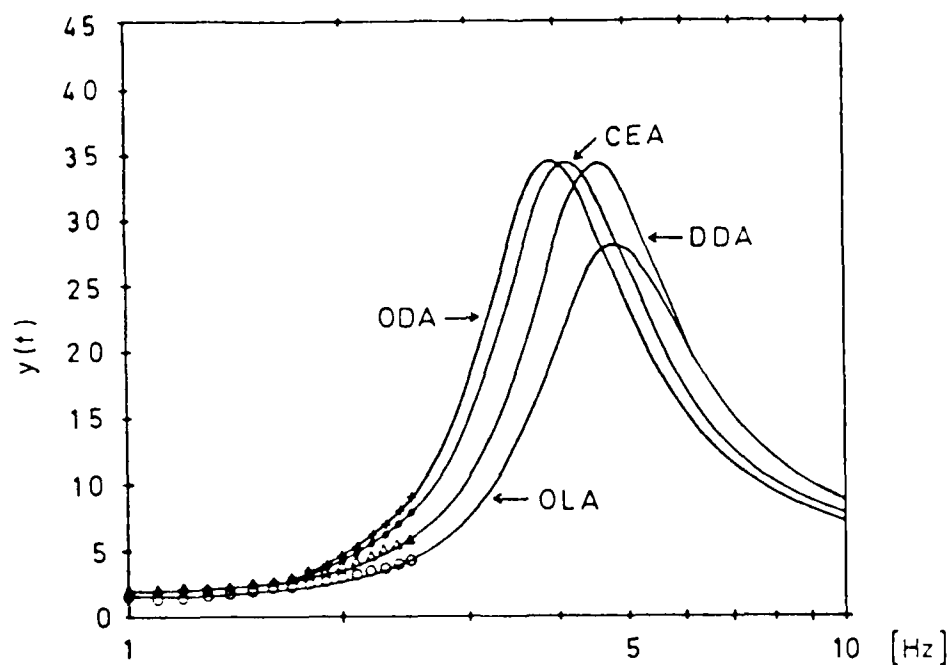


Figure 12: Wave damping ratio $y(f)$ vs. frequency [Hz]. The experimentally determined values are indicated by the following symbols: $\Delta\Delta\Delta\Delta$ dodecanol (DDA), $\circ\circ\circ\circ$ Z-9-octadecen-1-ol (OLA), $\bullet\bullet\bullet\bullet$ hexadecanol (CEA), $++++$ octadecanol (ODA). The solid lines represent the respective theoretical curves.

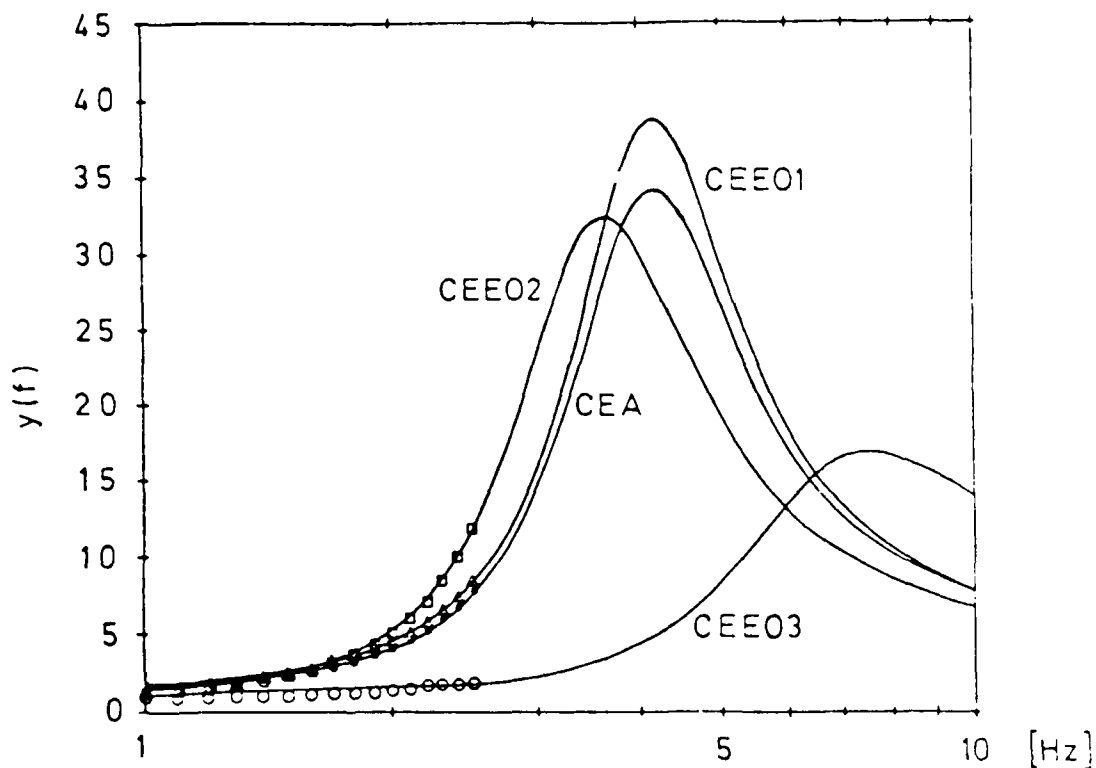


Figure 13: Wave damping ratio $y(f)$ vs. frequency [Hz]. The experimentally determined values are indicated by the following symbols: $\bullet\bullet\bullet\bullet$ hexadecanol (CEA), $\Delta\Delta\Delta$ mono-(ethylenglycol)-mono-hexadecyl ether (CEE01), $\square\square\square$ di-(ethylenglycol)-mono-hexadecyl ether (CEE02), $\circ\circ\circ\circ$ tri-(ethylenglycol)-mono-hexadecyl ether (CEE03).

5. References

1. HÖHNERFUSS, H., AND GARRETT, W.D.,
J.Geophys.Res., 86, 439 (1981).
2. HÖHNERFUSS, H., ALPERS, W., AND JONES, W.L.,
Radio Sci., 13, 979 (1978).
3. HÖHNERFUSS, H., ALPERS, W., JONES, W.L., LANGE, P., AND
RICHTER, K., J.Geophys.Res., 86, 429 (1981).
4. HÖHNERFUSS, H., ALPERS, W., GARRETT, W.D., LANGE, P.A.,
AND STOLTE, S., J.Geophys.Res., 88, 9809 (1983).
5. HÖHNERFUSS, H., ALPERS, W., CROSS, A., GARRETT, W.D.,
KELLER, W.C., LANGE, P.A., PLANT, W.J., SCHLUDE, F.,
AND SCHULER, D.L., J.Geophys.Res., 88, 9817 (1983).
6. HÖHNERFUSS, H., AND ALPERS, W.,
Proceedings of the 1982 International Geoscience and Remote
Sensing Symposium (IGARSS '82), Vol. I, TP-4, 2.1. (1982).
7. HÖHNERFUSS, H., LANGE, P., SCHLUDE, F., AND GARRETT, W.D.,
Proceedings of the 1984 International Geoscience and
Remote Sensing Symposium (IGARSS '84), Vol. II, 715 (1984).
8. HÖHNERFUSS, H., GARRETT, W.D., AND HOGE, F.E.,
Int.J.Remote Sensing, 7, 137 (1986).
9. ALPERS, W., BLUME, H.-J., GARRETT, W.D., AND HÖHNERFUSS, H.,
Int.J.Remote Sensing, 3, 457 (1982).
10. BLUME, H.-J. C., HÖHNERFUSS, H., AND ALPERS, W.,
IEEE Trans.Geosci.Remote Sensing, GE-21, 295 (1983).
11. HÖHNERFUSS, H.,
J.Colloid Interface Sci., 107, 84 (1985).
12. HÖHNERFUSS, H.,
J.Colloid Interface Sci., submitted for publication (1986a).

13. HÖHNERFUSS, H.,
"The molecular structure of the system water/monomolecular
surface film and its influence on water wave damping",
Habilitation-thesis, University of Hamburg, 238 pp. (1986).
14. KATTNER, G.G., AND BROCKMANN, U.H.,
Mar.Chem., 6, 233 (1978).
15. BROCKMANN, U., KATTNER, G., HENTZSCHEL, G., WANDSCHNEIDER, K.,
JUNGE, H.D., AND HÖHNERFUSS, H., Mar.Biol. (Berlin), 135 (1976).
16. HÖHNERFUSS, H., AND ALPERS, W.,
J.Phys.Chem., 87, 5251 (1983).
17. HÖHNERFUSS, H.,
J.Colloid Interface Sci., submitted for publication (1986b).
18. LANGE, P.A., AND HÖHNERFUSS, H.,
J.Phys.Oceanogr., 14, 1620 (1984).
19. HÖHNERFUSS, H., LANGE, P.A., AND WALTER, W.,
J.Colloid Interface Sci., 108, 430 (1985).
20. HÖHNERFUSS, H., LANGE, P.A., AND WALTER, W.,
J.Colloid Interface Sci., 108, 442 (1985).
21. HÖHNERFUSS, H., AND WALTER, W.,
J.Colloid Interface Sci., 97, 476 (1984).
22. HÖHNERFUSS, H., ALPERS, W., LANGE, P.A., AND WALTER, W.,
J.Geophys.Res., submitted for publication (1986).

MAXIMUM OF DAMPING RATIO IN RIPPLED WATER COVERED BY MONOMOLECULAR FILMS

Pietro Paolo Lombardini
Istituto di Cosmogeofisica, Torino, Italy

Extensive theoretical and experimental work has been done relative to the damping of capillary waves in presence of adsorption and spreading films ¹. Recently, this work has been extended to the lower part of the short-gravity region ². We have dedicated the last decade to the exploration of the entire short-gravity band (1 - 20 Hz).

The ratios of damping of short gravity waves in presence and in absence of surface films, plotted vs. frequency, give origin to diagrams having cuspidate shape.

Fig. 1 shows plots measured for four different films: 1 - methyl palmitate; 2 - cetyl alcohol; 3 - oleic alcohol; 4 - Triton X100. The three first samples are insoluble films, the fourth soluble film. Clearly, the maxima are all well marked, and the maxima of insoluble films prevail by at least one order of magnitude. The two parameters of each maximum, frequency and damping ratio of maximum, are characteristics of the substance composing the film, and univocally related to the rheological parameters, elasticity coefficient and diffusional frequency.

These results have a theoretical justification ³.

Theoretical basis

I shall refer to the classical book of V.G. Levich "Physico-Chemical Hydrodynamics" and re-write two basic equations from the section entitled "Damping of capillary waves by surface-active substances", equations 121-18, 121-19.

$$(\rho\Omega^2 + \sigma k^3 + \sigma k^3 + 2\rho\Omega k^2)A - j(\rho k g - \sigma k^3 - 2\rho\Omega k^2)B = 0$$

$$j(2\rho\Omega k^2 + E k^3)A + (\rho\Omega^2 - 2\rho k^2 \rho l + E k^2 l)B = 0 \quad (1)$$

where: ρ liquid density, ν kinematic viscosity, σ surface tension, E viscoelasticity modulus, g acceleration of gravity, k wave number, $\Omega = \sqrt{k^3 \rho l / \eta}$, Ω complex frequency, η viscosity damping.

Satisfaction of both conditions requires vanishing of the determinant of the coefficients, from which one may extract the following equation:

$$\Omega^4 + 2\delta\Omega^3 + (1+a_1)\omega^2\Omega^2 + (a_1-a_2)\omega^4 = 0 \quad (2)$$

where:

$$a_1 = E\kappa^2\sqrt{\eta}/\rho\omega\sqrt{\eta} \quad a_2 = E\kappa^3/\rho\omega^2 \quad (3)$$

Equation (2) admits two solutions⁵: the Laplace solution,

$$\Omega_L = \pm (j\omega - \delta \frac{1-(a_2\omega^4/2\delta\Omega^3)}{1-a_1}) \quad (4)$$

accompanied by the dispersion relation:

$$\omega = \sqrt{\sigma\kappa^3/\rho + g\kappa} \quad (5)$$

and the Marangoni solution,

$$\Omega_M = \pm (E^2\kappa^4/\rho^2\eta)^{1/2} \quad (6)$$

For the case of adsorption films we shall assume that thermodynamic equilibrium exists within the sub surface.

Note that:

$$E = \frac{\partial\sigma}{\partial(\ln A_s)} = - \frac{\partial\sigma}{\partial(\ln \Gamma)} \frac{d(\ln \Gamma)}{d(\ln A_s)} = -\epsilon_0 \frac{d(\ln \Gamma)}{d(\ln A_s)} \quad (7)$$

where ϵ_0 is the elasticity coefficient of the film, A_s the element of surface area, and Γ the surface film concentration. The second factor of the medium term measures adsorption and desorption variations during the surface expansions and compressions due to waving. Taking into account the diffusion process and defining the diffusional frequency,

$$\omega_D = D \left(\frac{dc}{d\Gamma} \right)^2 \quad (8)$$

where c is the bulk concentration of the solution, function of z , and D the diffusion coefficient, it results,

$$\frac{d(\ln r)}{d(\ln A_s)} = \frac{1+\tau+j\tau}{1+2\tau+\tau^2} \quad (9)$$

where,

$$\tau = \sqrt{\frac{\omega_D}{2\omega}} \quad (10)$$

We may then write,

$$E = E_0(\cos\phi + j \sin\phi) \quad (11)$$

where,

$$E_0 = \epsilon_0 / \sqrt{1+2\tau+2\tau^2} \quad (12)$$

and,

$$\phi = \arctan\left(\frac{\tau}{1+\tau}\right) \quad (13)$$

From (10), moving ω from zero to infinity ϕ passes from 45° to 0° . We will use in Laplace formula (4) the approximation $\Omega = j\omega$ and get,

$$\omega_L = j\omega - \delta \frac{1-a_1\omega/2\delta}{1-a_1} \quad (14)$$

The real part of the second term on the right side of (14) divided by δ , represents the damping ratio y_L .

Setting,

$$X_0 = \epsilon_0 \kappa^2 / \rho \sqrt{2\eta\omega^3} \quad Y_0 = \epsilon_0 \kappa / 4\rho\eta\omega \quad (15)$$

we obtain,

$$y_L = \frac{1+2\tau+2\tau^2-X_0+Y_0(X_0+\tau)}{1+2\tau+2\tau^2-2X_0+2X_0^2} \quad (16)$$

Plotted in terms of frequency, equation (16) exhibits the cuspidate shape of curve 4 in Fig. 1.

Let now pass to the Marangoni solution. It may be written,

$$\Omega_M = \left(\frac{E_0^2 \kappa^2}{\rho^2 \eta}\right)^{1/2} \exp(j\psi) \quad (17)$$

where,

$$\psi = \frac{2}{3} (\phi + 180^\circ) \quad (18)$$

For soluble films ψ is confined between 120° and 150° . Clearly the real and imaginary part of Ω_M are of the same order. This corresponds to a damping which is very high, and removes any physical interest to the Marangoni wave for soluble films.

In the case of insoluble films, in-lieu of the diffusion process, which is valid for adsorption films, we invoke an analogous process, occurring however above the interface, where a packaging density distribution c_p , function of z , is assumed. This concept, which we will call "directional packaging" and which also requires thermodynamic equilibrium, involves a structural parameter D_p , having the dimensions of a diffusion coefficient.

Setting,

$$\tau = \sqrt{D_p \left(\frac{dc_p}{dz} \right)^2} / 2\omega = \sqrt{\frac{\omega D_p}{2\omega}} \quad (19)$$

we get in this case,

$$E = \epsilon_0 (1 - 2\tau + 2\tau^2)^{-1/2} \exp(j\phi) \quad (20)$$

where,

$$\phi = \arctan\left(\frac{-\tau}{1-\tau}\right) \quad (21)$$

In this case, while ω moves from zero to infinity, ϕ passes from 225° to 360° . Thus, will use in Laplace expression (4) the approximation $\Omega = -j\omega$ and obtain,

$$\Omega_L = j\omega - \delta \frac{1 + j \frac{a_2 \omega}{2\delta}}{1 - a_1} \quad (22)$$

The real part of the second term on the right side, divided by δ leads to the damping ratio,

$$\gamma_L = \frac{1 - 2\tau + 2\tau^2 - X_0 + Y_0(X_0 + \tau)}{1 - 2\tau + 2\tau^2 - 2X_0 + 2X_0^2} \quad (23)$$

Plotted in terms of frequency the equation exhibits the cuspidate shape of curves 1, 2 and 3 of Fig. 1.

When $X_0 = 1/2$ and $\tau = 1/2$ equation (23) goes to infinity

For understanding the Marangoni solution it is convenient to subdivide the range ϕ in two sectors: $225^\circ - 315^\circ$ and $315^\circ - 360^\circ$.

In the first sector,

$$\psi = \frac{2}{3}(450^\circ - \phi) \quad (24)$$

and in the second sector,

$$\psi = \frac{2}{3}(\phi - 180^\circ) \quad (25)$$

Fig. 2 presents an overall picture of the behavior of both solutions for the condition $\epsilon_0 = 9.7$ and $\omega_D = 19.0$. The figure displays four curves: a and b show Laplace and Marangoni dispersion laws, respectively, the wavenumber κ appearing on the ordinate at the left side of the figure; curves c and d feature the damping ratios y_L and

$$y_M = (E_0^2 \kappa^4 / \rho^2 \eta)^{1/3} \cos \psi / \delta \quad (26)$$

reported on the ordinate at the right side.

Note that at the frequency f curves a and b intersect indicating a tight coupling between the two modes. The effect of coupling is that of removing from the picture both Laplace pole and Marangoni zero, and introducing instead a maximum according to (23) evaluated with the proper value of ω_D of the film. This maximum derives from the need for an identity of motion for both modes at the same frequency f_m , identity which may be written

$$y_L = y_M \quad (27)$$

Fig. 3 shows how y_L and y_M vary as a function of τ in the case of a film of oleic alcohol ($\epsilon_0 = 9.7$, $\omega_D = 9.6$).

In conclusion, in the case of insoluble films for frequencies far apart from f_m the Laplace mode predominates because the Marangoni wave is too much damped. Getting closer to f_m the outcome of coupling is an attenuation computable with equation (23).

Equations (16) and (23) offer a complete description of the damping ratios for both soluble and insoluble films. The substances composing the film are described by the coordinates of the peak of the curves, and they are uniquely related to the rheological parameters ϵ_0 and η . The passage from one set of parameters to the other is given graphically in Fig. 4, which shows the loci of cusp ordinate as a function of the frequency of maximum.

Methods of measurement

Measurements of damping ratio have been performed in the short-gravity wave frequency band.

In the laboratory, cleaning problems can be minimized using small tanks. We used a 15 liters tank, 81 cm long, 22 cm wide and 10 cm deep.

Two different methods have been utilized, according to frequency, the semilog method and the resonance method.

In the semilog method a mechanical wave-maker (loudspeaker plus vertical Teflon wedge-shaped blade) oriented transversally to the tank plunges rhythmically into the water creating small, monochromatic, rigorously transversal waves. Attenuation, α_m (cm^{-1}) is measured taking care that the reflected wave does not interfere with the source. Measured damping δ_m is derived from the attenuation coefficient with the relation,

$$\delta_m = \alpha_m v_g \quad (28)$$

where v_g is the group velocity. The damping ratio is calculated with the formula,

$$y = \delta_m / 2\pi\kappa^2 \quad (29)$$

In the resonance method the wave-marker is a horizontal metal wing oriented transversally to the tank and moved rhythmically in air toward and away above the water surface. The liquid waves are created by pneumatic pulsations. The tank is excited in conditions of resonance and damping is measured in term of relaxation time, according to the rule,

$$\delta = T/2 \quad (30)$$

where T measures the time interval between the instant in which the wave excitation is discontinued and that in which the wave amplitude becomes $1/e$ of its initial value.

The amplitude of the waves is measured using a specially built capacitive probe sensitive to differences of level of the water surface of the order of 1 micrometer, calibrated versus a Cahn R.H. electrobalance.

It is estimated that using these step-by-step methods the overall error in the measurements of damping ratios was kept below $\pm 5\%$.

Dynamic methods of measurement are also available. They are all based upon confrontation of wave spectra. Spectra of wind-excited waves on a film-covered water surface, $S(f)_f$, and analogous spectra measured on a purely viscous water under the same wind excitation, $S(f)_o$, lead to the damping ratio sought for, because of the formula ⁹,

$$\gamma(f) = S(f)_o / S(f)_f \quad (31)$$

We have used this method utilizing a novel wave probe ⁹, capable of measuring the high frequency range of the sea spectrum on an absolute, self calibrating scale. The basic concept of our probe is a Teflon-coated wire (Goubau-line). The lower end of this wire, which is held straight vertically, is dipped in the water, while the other end is fed by a microwave, X band, source. The microwave energy travels downwards confined to a close proximity of the coated wire, and the contact with the water acts as a short circuit, giving origin to reflected waves. The standing wave pattern is uniquely determined by the contact with the water. Changes in height of the water surface correspond to changes in phase angle. This is accurately measured in a computer and the measurement is accomplished with an error of few micrometers.

Spectra of a sea rippled by a gentle breeze were obtained mounting the apparatus on board of a small boat. In this mounting the Goubau line was hanging from the bow as a plumb line. The obtained spectra followed rather faithfully the slope predicted by Phillips, for the dynamic equilibrium range of the sea spectrum. In Fig. 5 a) is shown a spectrum of clean water, and in Fig. 5 b) the spectrum obtained after having poured in the water, upwind of the probe, 200 cc of a 10% solution of oleic alcohol in Hexane. Performing point by point the division between spectral data in a) and b) a curve is obtained similar to curve 3 of Fig. 1.

A similar experiment has been performed by Dr. Hohnertuss in Hamburg using a wind tank. Fig. 6 shows his results for the case of oleic alcohol: upper curve-clean water; lower curve-presence of film.

Finally, the peculiar response of damping versus frequency shown above may also be observed using a multi-frequency radar, viewing a sea area covered by a film. This is possible because the radar return of a rippled sea is mainly due to Bragg back-scattering. Hence the effect of the presence of a film will bring fourth a decrease of sea echo proportional to the damping pertaining to the liquid wavelength in Bragg resonance with the radio wave. The wave number of this component is given by the formula,

$$\kappa = 2K \cos \theta \quad (32)$$

where θ is the grazing angle between the radar and the horizon, and K the radar wave number.

We note that when the radar cell is not uniformly covered by the film the decrease of echo will be lesser than that given by the theoretical damping ratio, y . Let F be the filling factor of the radar cell, $F = 1$ meaning that the film covers uniformly the area of the cell. The effective damping ratio, y_e , is given by,

$$y_e = (1 - F + F/y)^{-1} \quad (33)$$

The relationship between y_e and y is shown in Fig.7 which refers to a film of oleic alcohol. The upper curve in Fig. 7 corresponds to a coverage of 100%, the lower curves to coverages of 99%, 90%, 75% and 50%, respectively.

On the basis of the previous considerations, we have carried out an experiment using a radar system which utilizes two frequencies: S band ($\lambda = 9.8$ cm), X band ($\lambda = 3.2$ cm) and vertical polarization ¹⁰. An important feature of the system is that the radar cell at both frequencies is the same, and equal to $7.5 \times 0.02 D \text{ m}^2$, where D is the target distance in meters. At grazing incidence, the frequencies of the liquid waves in Bragg resonance are about 6 Hz for the S band and 11 Hz for the X band. In our experiment we created an extended spot of film on the surface of the sea by depositing a total of 1 liter of oleic alcohol at a distance of approximately 0.3 Km from the radar, which was operating on the shore. A light breeze blowing seaward was assuring ripples on a calm surface. Using photometric intensities on the PPI we have computed $y_e = 15.6$ for the S band and $y_e = 6.9$ for the X band as indicated in Fig.7. From this data one gets $F = 93\%$.

Concluding remarks

From the developments of the previous pages it appears clearly that a solid basis exists for the development of remote sensing techniques capable of uniquely identifying the presence of films distributed over the ocean surface, independently of their nature.

Measurements of damping ratio of short-gravity waves as a function of frequency via Bragg backscattering of radar waves suggest the possibility of observations in local, medium and even planetary scale from space.

The possibility exists that these techniques, involving structural parameters, e.g. surface visco-elasticity, may lead to the characterization of thermodynamic surface properties related to the substances forming the film.

R E F E R E N C E S

- 1 - M.Van den Tempel, E.H.Lucassen-Reynders "Relaxation processes at fluid interfaces" Advan.Colloid Interface Sci.
Vol. 18, p.281, Elsevier Sci.Pub.Co. Amsterdam, 1983
- 2 - H.Huehnerfuss, P.Lange, W.Walter. Jour.Marine Research, 40, 1982, p.209; 42, 1984, p.737
- 3 - R.Cini,P.P.Lombardini, J.Colloid Interface Sci. 65, 1978, p.387
- 4 - V.G.Levich "Physico-Chemical Hydrodynamics", Prentice Hall, Englewood Cliffs, N.J. 1962
- 5 - P.P.Lombardini, F.Piazzese, R.Cini. Nuovo Cimento C 5, 1982, p.256
- 6 - R.Cini, P.P.Lombardini. J.Colloid Interface Sci. 81, 1981, p.125
- 7 - P.Pavese "Proximity linear transducer for the study of short-gravity waves in a tank" (in Italian) Internal Report No 40-1980, Istituto Cosmogeofisica, Torino, 1980
- 8 - R.Cini, P.P.Lombardini, H.Huehnerfuss. Int.J.Remote Sensing, 4, 1983, P.101
- 9 - B.Fiscella, P.P.Lombardini, P.Pavese Nuovo Cimento C, 5, 1982, p.247
- 10 - B.Fiscella, P.P.Lombardini, P.Trivero, P.Pavese, R.Cini. Nuovo Cimento C 8, 1985, p.175

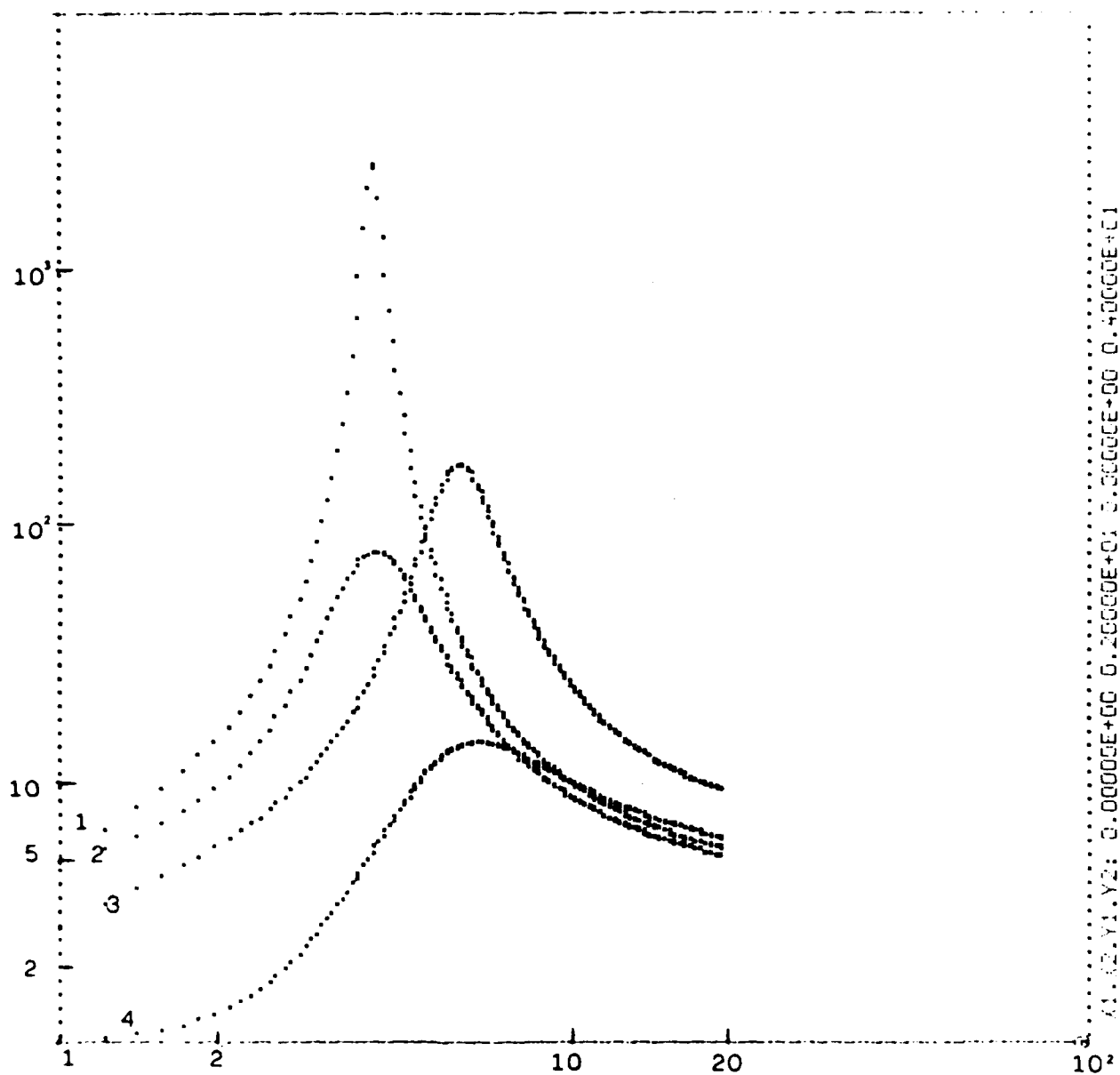


Fig. 1 Curves of damping ratio for:
 1 - methyl palmitate
 2 - cetyl alcohol
 3 - oleic alcohol
 4 - Triton X 100

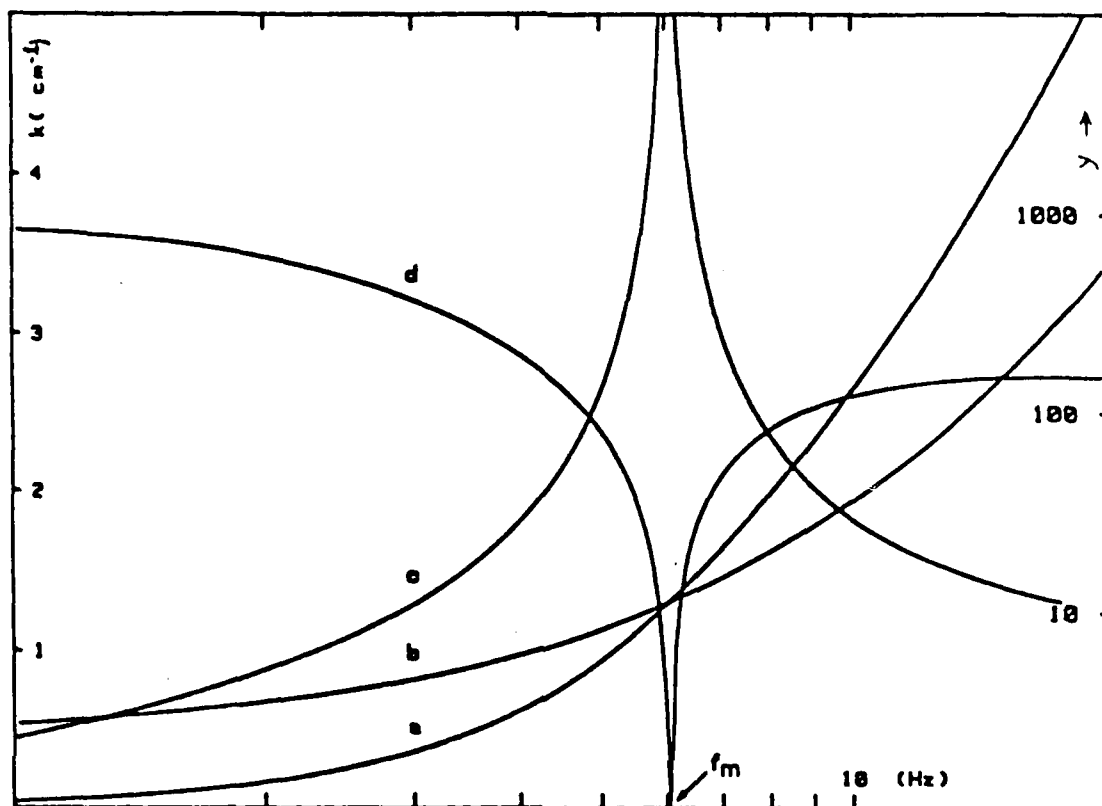


Fig. 2 Dispersion (a,b) and damping ratio (c,d) for $\epsilon_0 = 9.7$
and $\omega_D = 19.0$
a,c Laplace wave; b,d Marangoni wave

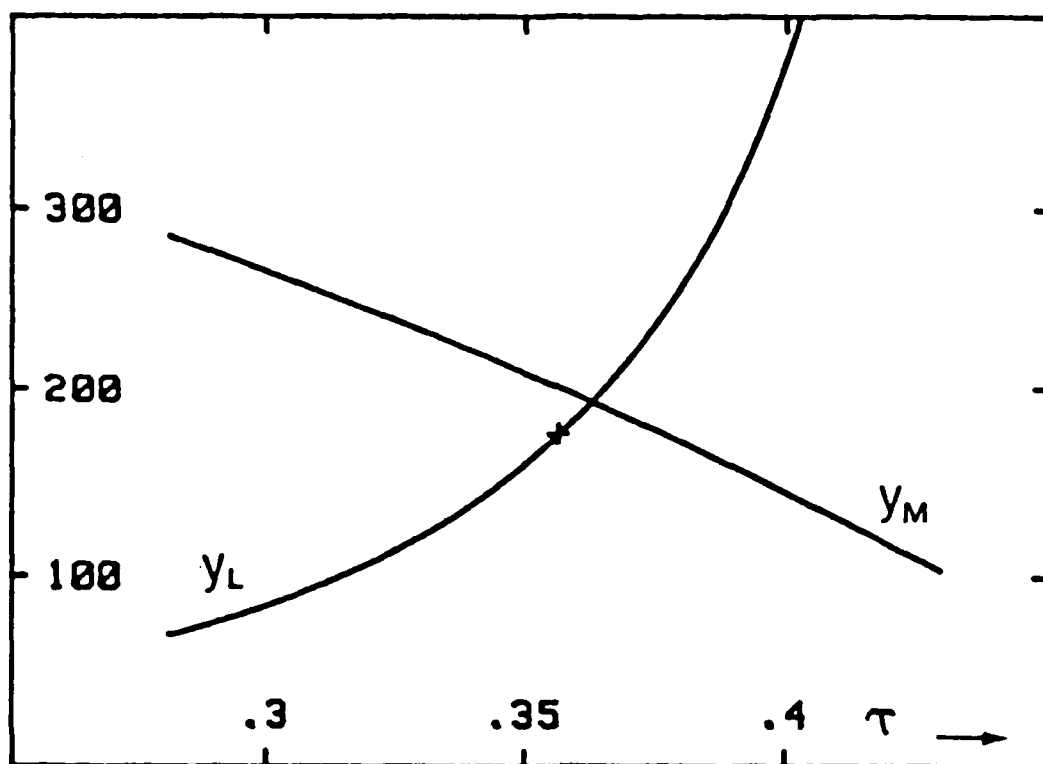


Fig. 3 y_L and y_M for varying τ . Point : experimental value for oleic alcohol

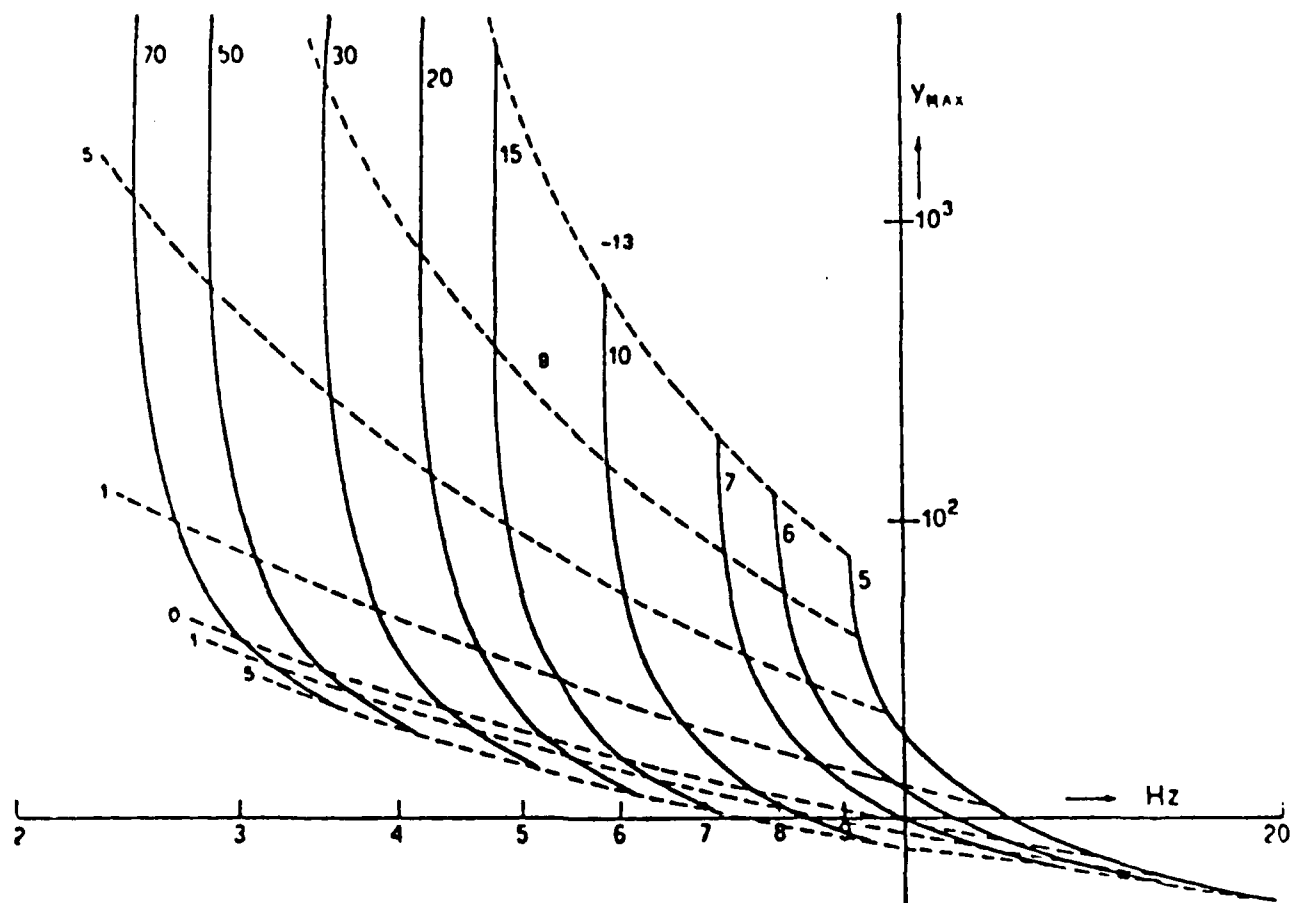


Fig. 4 Loci of maxima of damping ratio versus frequency of maximum. Dotted line indicates condition of $w_0=0$. Soluble films lie below, insoluble films lie above. Running parameters ϵ , and ω_D

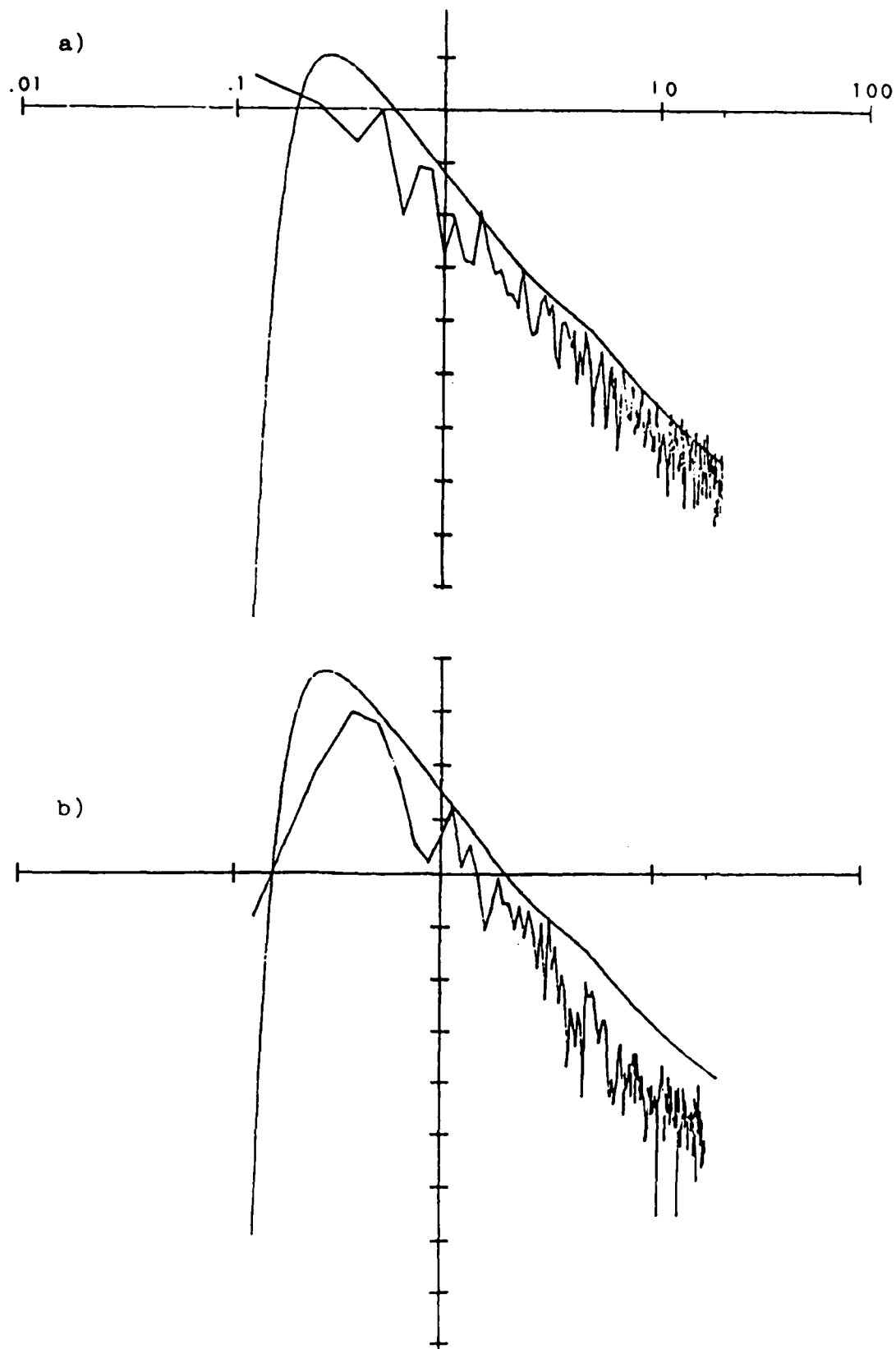


Fig. 5 Spectra observed in the Ligurian Sea:
a) observed in clean water
b) observed in presence of film (oleic alcohol)

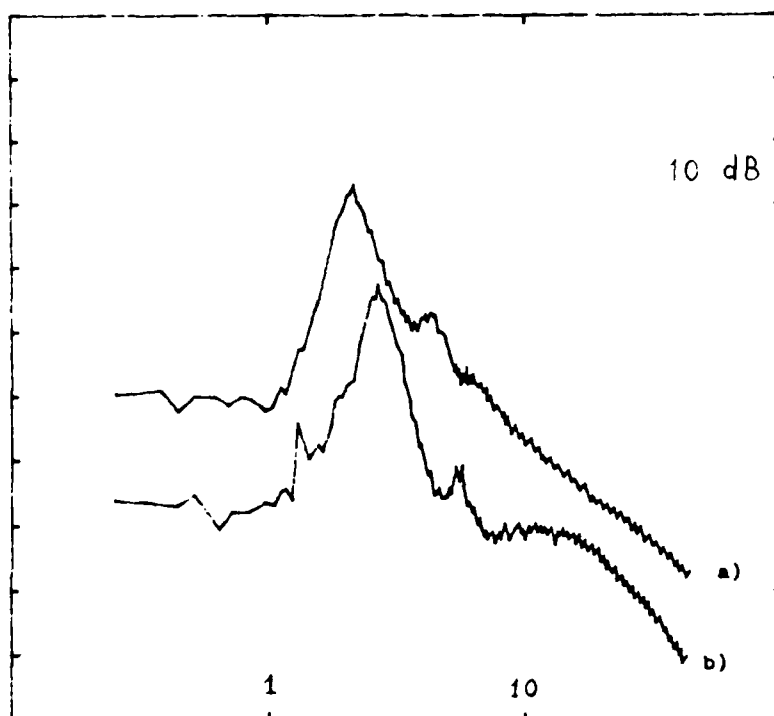


Fig. 6 Spectra observed in a tank: a) clean water,
b) presence of film (oleic alcohol)

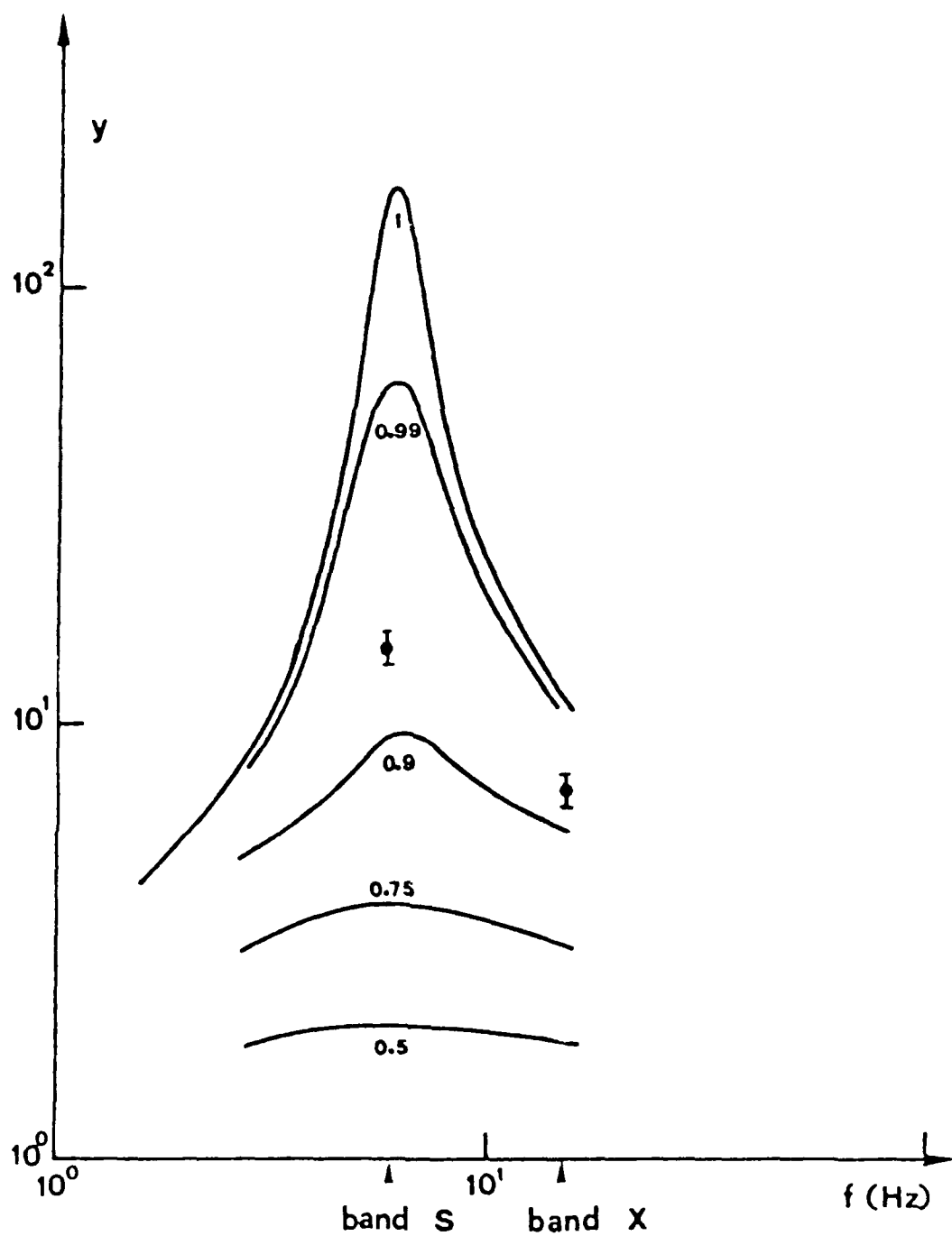


Fig. 7 Effective damping ratio for a choice of the filling factor F

E.H. Lucassen-Reynders
6, Kingsway
Heswall, Wirral
Merseyside L60 3SW
England

DYNAMIC PROPERTIES OF FILM-COVERED SURFACES

INTRODUCTION

The interests of marine investigators appear to overlap those of traditional surface and colloid chemists to some considerable degree. The former are more directly concerned with surface waves because of the effects of wave characteristics on surface roughness and, hence, on reflectivity as measured by remote sensing techniques. Surface chemists, on the other hand, are interested in surface waves in so far as they are relevant to, e.g., the stabilisation of the thin liquid layers separating emulsion droplets, and other applications of surface active materials. Both the remotely-sensed properties of the sea surface and the mechanical behaviour of many dispersed systems depend on the surface-chemical parameters that govern the propagation of surface waves.

This presentation will briefly review (i) the relevant characteristics of surface waves, and (ii) the physico-chemical variables most useful for understanding the effects of surface active materials on sea water.

SURFACE WAVES

Sea surface motions can be linked to three types of surface waves, distinguishable by the restoring forces which try to bring a disturbed surface back to its original position. Two obvious restoring forces working in the direction normal to the undisturbed sea surface are gravity and surface tension. These forces largely govern the transverse waves (1-5) known as gravity waves and capillary waves (or ripples), respectively. A third restoring force is the surface elasticity, which works in the tangential direction and largely governs the longitudinal waves also known as Marangoni waves. This type of wave was discovered much later (6), and requires the surface to have elastic properties. It is, therefore, never found on a clean surface but it does exist on film-covered surfaces where the surface tension can vary from place to place because of local contractions and expansions accompanying the wave motion. The surface elasticity results from the tendency of

areas with high surface tension to contract at the expense of areas with lower tension, and it is this tendency which produces the tangential restoring force.

Transverse and longitudinal waves generally coexist on the same surface because they are produced simultaneously by any mechanical means of wave generation. This remains the case even if wave generation is achieved by purely vertical or purely horizontal movement of, say, a barrier in the surface. Horizontal movement, like wind, will generally produce not only horizontal but also some vertical surface motion, and vertical barrier movement will also generate some horizontal surface motion. Vertical surface motion merely predominates in the transverse waves and horizontal surface motion in the longitudinal waves, without the other motion being quite absent in either case.

The distinction between the two wave types lies in their dispersion equations, which predict a different dependence of wavelength on wave frequency for each. The dispersion equations are derived by solving the hydrodynamic equations of motion in the liquid for the boundary conditions imposed by the surface. Specifically, any viscous stresses acting from within the liquid must be balanced by stresses due to gravity, surface tension and surface elasticity. A number of simplifying assumptions have to be made in the process (1-6), the most important of which are that (i) the wave amplitude is small compared to the wavelength, (ii) the energy of the wave motion is dissipated by viscous friction in the liquid, and (iii) viscosity and density of the liquid keep their bulk values right up to the surface.

The main results of this hydrodynamic wave theory are contained in the dispersion equations, which are independent physically significant solutions of the general equations. On water and other low-viscosity liquids, the transverse waves are only lightly damped and their wavelength is to very good approximation given by Kelvin's equation, derived as early as 1871:

$$\rho g k_T + \sigma k_T^3 \approx \rho \omega^2 \quad (1)$$

(see List of Symbols). Thus the long waves ($k \ll [\rho g / \sigma]^{\frac{1}{2}}$) generated at low frequency and dominated by gravity have wavenumbers increasing with ω^2 , while the wavenumbers of the shorter capillary waves dominated by surface tension at high frequency only increase with $\omega^{2/3}$. For water, the transition between the two regimes lies at a wavelength of about 1 cm.

The longitudinal waves, on the other hand, are mainly governed by the surface dilational modulus, \mathcal{E} , which combines surface elasticity and surface viscosity, as defined by analogy with a three-dimensional compression modulus:

$$\mathcal{E} = d\sigma/d \ln A \quad (2)$$

The dispersion relation of these waves was not derived until 1968 (6) and it reveals a frequency dependence intermediate between gravity waves and capillary waves:

$$k_L^4 \approx \eta \rho \omega^3 / i \mathcal{E}^2 \quad (3)$$

Both Eqs (1) and (3) are approximate, in the sense that elasticity terms were neglected in Eq (1) and surface tension/gravity terms in Eq (3). The errors made are very small (4,7), reflecting the fact that transverse waves are very largely dominated by surface tension and gravity, and longitudinal waves by surface elasticity. The corollary of this is that, while ripples can be used to obtain information on surface tension, the longitudinal waves are eminently suitable as a tool for measuring the surface dilational modulus, \mathcal{E} . In fact, much of the information on the viscoelastic surface properties to be discussed in the next section has been obtained through the study of longitudinal waves, as reviewed elsewhere (8).

Another approximation implied in Eqs (2) and (3) is that the surface's resistance against shear deformation is ignored: \mathcal{E} as defined in Eq (2) measures the elastic and viscous resistance against isotropic changes in area, not against changes in shape, of a surface element. The latter resistance can be expressed in the surface shear viscosity, a much-investigated parameter (9), but experimental evidence surveyed elsewhere (8) indicates that the numerical values of it are generally much smaller than those of the surface dilational viscosity embodied in \mathcal{E} .

A major difference between the transverse waves described by Eq (1) and the longitudinal ones of Eq (3) is that damping is far more pronounced for the latter than for the former. Damping can be expressed in a complex value of the wavenumber k :

$$k = \kappa + i\beta \quad (4)$$

where the imaginary component β is the damping coefficient, i.e., the relative decrease of wave amplitude with increasing distance from the wave source. As can readily be seen from Eq (3) for real values of \mathcal{E} , i.e., for purely elastic surfaces, the damping coefficient β of longitudinal waves is always of the same order of magnitude as the wavenumber κ :

$$\beta/\kappa = \sqrt{2} - 1 \approx 0.4 \quad (\text{for } \mathcal{E} \text{ real}) \quad (5)$$

This implies very heavy damping, leading to an almost

vanishing amplitude after the very first wave cycle. For transverse waves, on the other hand, the hydrodynamic theory predicts that on a clean water surface the ratio of damping coefficient to wavenumber is given by Stokes' equation:

$$\beta/k = 4\eta(\kappa^3/\rho^2g)^{1/2} \lll 1 \quad (6)$$

for gravity waves, and

$$\beta/k = \frac{4}{3}\eta(\kappa/\rho\sigma)^{1/2} \ll 1 \quad (7)$$

for capillary ripples. Eq (6) means that β/k is less than 0.001 for all gravity waves on clean water, i.e., the wave amplitude is reduced by less than 0.6% with each wave cycle. The damping ratio decreases with increasing wavelength because of the factor $\lambda^{-3/2}$, and is only 0.00002 for 1 m waves. Ship wakes, producing waves of this order of magnitude, are thus essentially undamped given the low value of the viscosity η , and can remain visible for many miles on clean stretches of sea surface.

These low amounts of damping (somewhat higher for capillary waves, but with β/k from Eq (7) still below 0.01 as long as $\lambda > 0.15$ cm) were neglected in the derivation of Eq (1). The effect of surface elasticity, as caused by adsorbed or spread films, on this low damping can be quite considerable. Such films only have to result in relatively low modulus values in order to increase damping by several hundred percent. Figure 1 illustrates this for 1 mm capillary waves. Three aspects of this effect of surface elasticity may at first sight seem surprising:

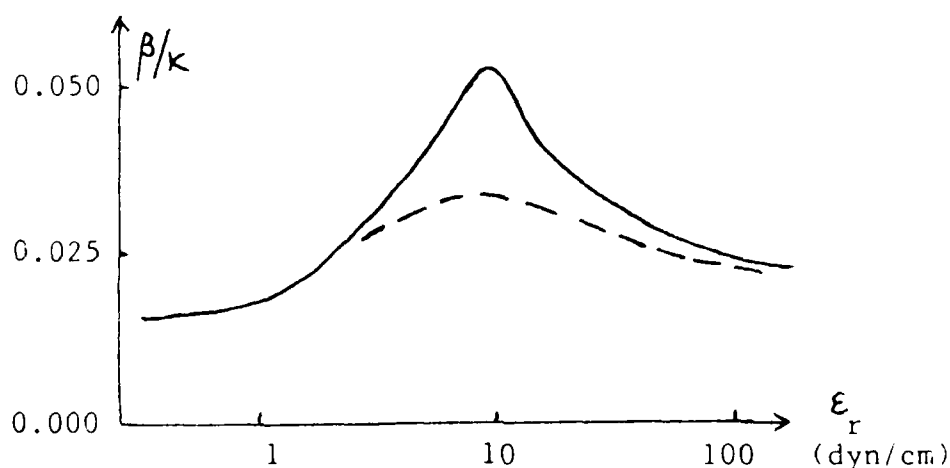


Figure 1. Effect of surface elasticity on damping ratio of 1 mm capillary waves. Solid line: purely elastic surface. Dashed line: viscoelastic surface. Data from Reference 2.

(i) The effect is not largest for the highest elasticities, but passes through a maximum at an intermediate elasticity value which depends on the wavelength. This maximum is connected with the ability of an elastic surface to carry two kinds of waves, i.e., not only the transverse wave in question but also the longitudinal one (4-7). In fact, the maximum is always found at the elasticity value for which the wavelength as calculated from Eq (3) is near - although not equal to (10) - the wavelength of the transverse wave. Thus the maximum in damping is reminiscent of resonance-like damping in electrical and mechanical circuits.

(ii) The introduction of surface dilational viscosity, at given values of the surface dilational elasticity, decreases rather than increases the maximum damping. This is because in the hydrodynamic theory all damping is caused by liquid motion underneath the surface. All the surface can do is modify such liquid motion through the boundary conditions. Surface dilational viscosity tends to short-circuit the surface tension gradients and, thereby, make the surface behave more like a clean surface, i.e., it decreases the damping maximum.

(iii) Surface elasticity causes a maximum in damping not only for capillary ripples but also for gravity waves. Indeed, the maximum damping relative to that for the clean surface increases steeply with increasing wavelength, as shown in Figure 2. Thus the damping of

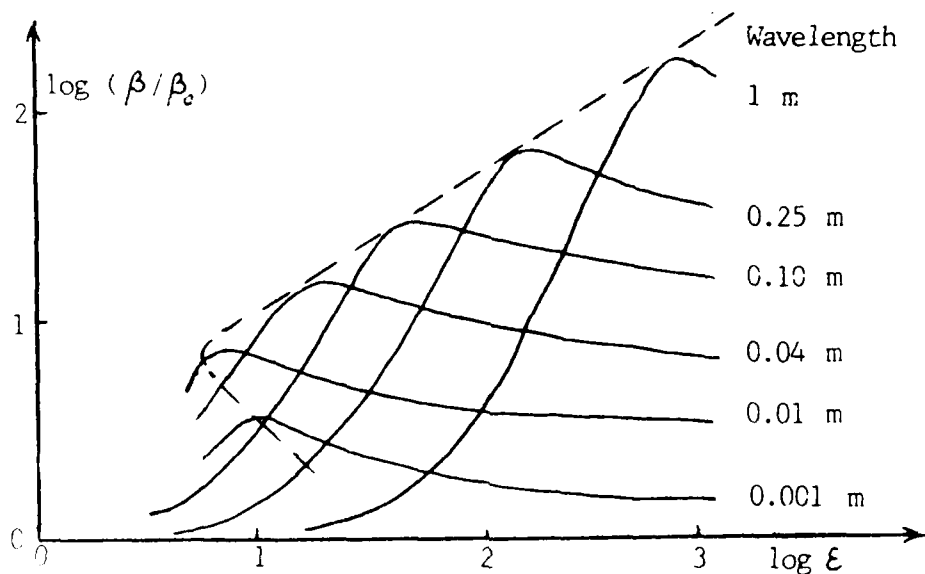


Figure 2. Increased damping of gravity and capillary waves caused by surface elasticity, ϵ (zero surface viscosity). β_0 is the damping coefficient for the clean surface as given by Eqs (6), (7). Dashed line: locus of maxima. Data from Reference 7.

gravity waves does depend very sensitively on surface properties, even though their wavelength does not. This is because the wavelength depends mainly on the normal boundary condition, in which the surface tension force can be swamped by the gravitational force; damping depends mainly on the forces in the tangential direction, where there is no gravity to swamp the surface elasticity force.

Ample experimental evidence for both transverse and longitudinal waves on clean and film-covered surfaces has confirmed the validity of the hydrodynamic wave theory (1-8). The basic assumptions listed earlier on can, therefore, be taken as sound. An interesting side effect of this conclusion follows from the third of these assumptions. Bulk viscosities remaining unaltered in the uppermost liquid layers are incompatible with the notion of thick layers of "structured" water bound to surface films. According to some suggestions, layers of tightly-anchored water might extend to depths of more than 100 μm below the surface in some cases (11). Anomalous physical properties over such distances should produce anomalous wave damping. Experimental data confirming the wave theory in its present state, therefore, lend no support to the notion of such layers.

This leaves us with the following main conclusions on the characteristics of surface waves as affected by surface properties:

- (i) the surface dilational modulus defined in Eq (2) is the most important variable governing the damping of both gravity waves and ripples. Maximum damping is obtained at intermediate values of the surface elasticity and zero values of the surface viscosity.
- (ii) the surface tension governs only the wavelength of ripples, i.e., waves shorter than 1 cm.

Quantitatively, the effect of surface films on wave motion thus depends on the numerical values of surface tension, surface elasticity and surface viscosity. The next section will consider these variables in somewhat more detail.

SURFACE TENSION AND SURFACE DILATIONAL MODULUS

The primary effect of organic film on a water surface is a drop in surface tension, by an amount which depends on the surface excess concentration. Although it may be convenient to think of the organic material on the surface as a two-dimensional gas, exerting a surface pressure equal to the drop in surface tension, it must be emphasised that surface films hardly ever obey the two-dimensional analog of the ideal gas law.

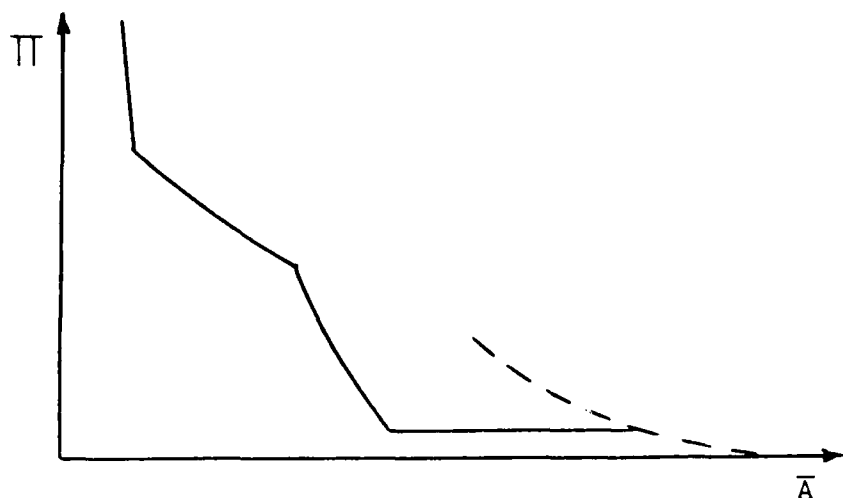


Figure 3. Schematic surface pressure (Π) vs molar area (\bar{A}) curves. Dashed line: ideal gas, Eq (8). Drawn line: many real systems.

$$\Pi \bar{A} = RT \quad (\text{ideal gas}) \quad (8)$$

Deviations from this simple equation of state are usually extreme and start at very low surface pressures, as indicated in Figure 3. Surface active materials known from technological applications and biological systems show a wide variety of surface behaviour, as reviewed elsewhere (12), and can reduce the surface tension of water by a factor of up to three. The surface tension of sea water under natural conditions is unlikely to be reduced to the same degree and, therefore, can be taken as always of the same order of magnitude. Too little is known about the chemical nature of the sea-surface enrichment for any classification of its Π - \bar{A} curves to be possible as yet (13,14).

As to the surface dilational modulus, ϵ , it is only under simplifying conditions that this parameter is determined completely by the equilibrium surface equation of state, and given by a limiting value ϵ_0 defined as:

$$\epsilon_0 = (d\Pi / d \ln \Gamma)_{eq} \quad (9)$$

This implies purely elastic surface behaviour, i.e., zero surface viscosity. Such simple behaviour is found when two conditions are met: (i) the variations in surface tension resulting from local variations in Γ should be instantaneous, and (ii) the total amount of surface excess material (ΓA) should be constant, i.e., diffusional interchange between surface and adjacent water layers should be negligible. The latter condition is obviously satisfied if the film material is insoluble in water. The condition does not require total lack of solubility, however, merely lack of solubility in the time scale of the experiment. The time scale of surface waves is the inverse wave frequency ($1/\omega$ sec), and "insoluble monolayer behaviour" is observed whenever the rate of diffusion is too low to have a measurable effect

on (ΓA) in $1/\omega$ sec. As a result, surface active materials that are readily soluble in times longer than $1/\omega$ sec will form monolayers that behave as if insoluble towards surface waves with frequency ω . For instance, solutions of octanoic acid were found to show insoluble monolayer behaviour, with a surface elasticity described by Eq (9) and zero surface viscosity, towards 200 Hz capillary ripples (15). At not too high concentrations, the same behaviour was observed for decanoic acid solutions at wave frequencies as low as 1 Hz, with measured modulus values up to 70 dyn/cm (16).

Figure 4 illustrates the elasticity values that can be calculated for some simple equations of state. Values at given surface tension are seen to vary considerably, but in all cases the values needed for maximum damping of waves of up to 0.1 m are within easy reach. These elasticities are obtained for simple monomolecular adsorption, at concentrations far below those giving visible films or slicks.

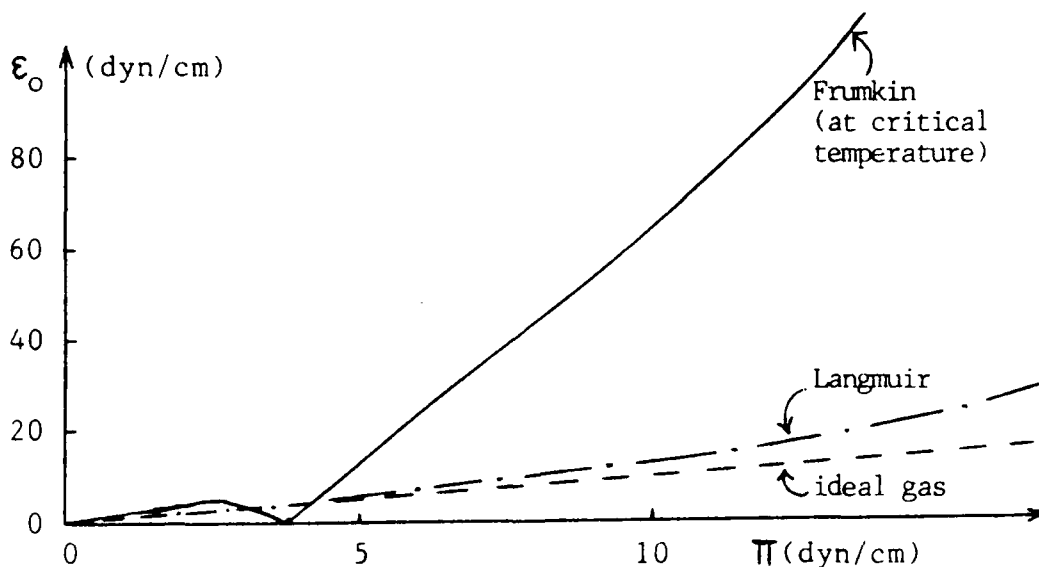


Figure 4. Limiting elasticity values ϵ_0 as a function of surface pressure Π for various equations of state. (Calculations for film material with limiting area of $0.2 \text{ nm}^2/\text{molecule}$.)

Such purely elastic surface behaviour, with ϵ given by Eq (9) and zero viscosity, is restricted to a limited range of frequencies. Outside this range, either of the two above conditions is no longer satisfied. This means that the time scale of the surface wave ($1/\omega$) is no longer incommensurate with the time scales of all relaxation phenomena that can take place in or near the surface. Under the heading of "relaxation phenomena" comes any spontaneous process occurring after a disturbance and leading to a re-equilibration of the surface tension, e.g., a rearrangement in the surface or transport of material to/from it. Since such a process

always involves dissipation of energy, one can formally express the result in terms of a viscosity, which in our case of area disturbance by surface waves is the surface dilational viscosity. Any relaxation process capable of altering the surface tension within a time of $1/\omega$ sec will cause a time lag between the fluctuations in σ and those in surface area, A . In other words, the modulus as defined in Eq (2) is no longer a real number but a complex one, with a real part representing elastic energy stored in the surface and an imaginary part reflecting viscous loss:

$$\epsilon = \epsilon_r + i\epsilon_i = \epsilon_r + i\omega\eta_d \quad (10)$$

Both contributions are measurable, e.g., by applying Eq (3) to measured properties of longitudinal waves, and the results of such measurements have been reviewed (17,18).

The most obvious and general relaxation mechanism for films of sufficient solubility is diffusional transport to/from adjacent water layers. The theory of it in the case of surface waves is now more or less fully established and confirmed by experiment (2-8, 15-18). Apart from rendering the surface viscoelastic, this mechanism also reduces the absolute value of the modulus, because it short-circuits the surface tension gradients. For this reason, very soluble monolayers never reach the moderate elasticity values needed for the maximum wave damping illustrated in Figure 1.

It should be stressed that the effect of diffusion on the modulus depends as much on time scale as on film solubility. Therefore, the effect will always be more pronounced for gravity waves than for capillary ripples. An illuminating example may be calculated from theory applied to a system resembling some of the decanoic acid solutions for which ripple damping has been measured (15). To 1 mm capillary ripples (high frequency) such a solution may present an almost perfectly elastic surface, with $|\epsilon| = 0.9\epsilon_0$ and negligible viscosity. From the point of view of 1 m gravity waves (much lower frequency), however, the same solution with the same surface film would be viscoelastic with a much reduced modulus of less than $0.2\epsilon_0$.

Diffusional interchange is only one of a number of possible relaxation mechanisms, and the frequency spectrum of the modulus will generally show more than one range of viscoelastic behaviour, as depicted in Figure 5. Each range is centred round the frequency corresponding to the characteristic time of a relaxation process, and measured modulus spectra can be used to obtain information on these processes. The most interesting relaxation processes apart from diffusion probably are those caused by rearrangements in the surface. These can range from very fast reorientation of single small molecules to the much slower formation of

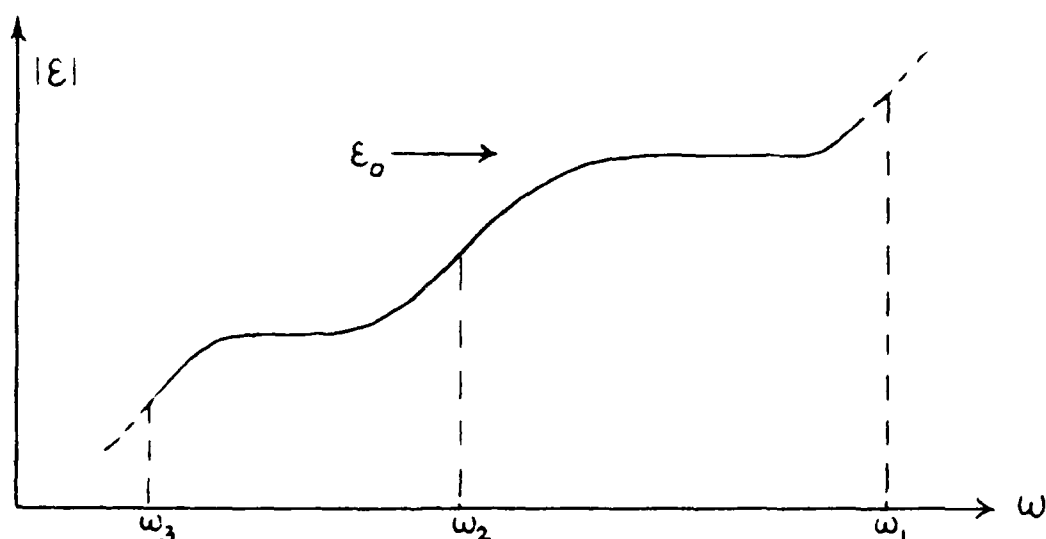


Figure 5. Schematic frequency spectrum of surface dilational modulus. $\omega_1, \omega_2 \dots$ are frequencies corresponding to characteristic times of relaxation processes ($\tau_i = 1/\omega_i$).

new surface phases and cooperative structures involving either many small molecules or single large ones. The former will show up in the behaviour of very high frequency ripples, e.g., in the kHz region (19), and the latter only at frequencies in the mHz range or lower (17,18).

To sum up, the main points of this section are that both the surface elasticity and the surface viscosity show wide ranges of variation. These variations are caused both by differences in equilibrium equation of state of surface films (see Figure 4) and by the occurrence of relaxation processes under dynamic conditions (see Figure 5). As a result, numerical values of elasticity and viscosity are meaningful only at the frequency for which they are measured. In comparison to the measured variations in surface elasticity, the possible variations in the surface tension appear to be of minor importance.

CONCLUSIONS

The major conclusions on the effects of organic films on surface waves can be summarised in the following points:

- (i) Organic films can have large effects on surface waves by modifying flow patterns in the liquid through the boundary conditions.
- (ii) The film parameter with the greatest effect on wave damping is the surface dilational modulus, which combines surface elasticity with surface viscosity. Damping is most increased by moderate values of the elasticity, but surface viscosity leads to a decrease in maximum damping. Surface tension determines only the wavelength of capillary ripples.

(iii) The maximum relative increase in wave damping caused by surface elasticity is larger for gravity waves than for capillary ripples, but the elasticity values required are also larger.

(iv) Surface shear viscosity so far has been found to be of minor importance in comparison to surface dilational viscosity.

LIST OF SYMBOLS

A	area of surface element
\bar{A}	area per molecule of film material
g	gravitational constant
i	$= \sqrt{-1}$
k	complex wavenumber
k_L	wavenumber of longitudinal wave
k_T	wavenumber of transverse wave
R	gas constant
T	absolute temperature
β	(distance) damping coefficient ($=$ imaginary part of k)
Γ	surface excess concentration ($=1/\bar{A}$)
ϵ	(complex) surface dilational modulus
ϵ_r	real (elastic) part of ϵ
ϵ_i	imaginary (viscous) part of ϵ
η	bulk viscosity
η_d	surface dilational viscosity ($=\epsilon_i/\omega$)
κ	real part of complex wavenumber
λ	wavelength ($=2\pi/\kappa$)
Π	surface pressure ($=\sigma^{\text{water}} - \sigma^{\text{film}}$)
ρ	bulk density
σ	surface tension
τ	characteristic time of relaxation process
ω	wave frequency

REFERENCES

1. R. Dorrestein, Proc. Koninkl. Ned. Acad. Wetenschappen, B54, 260, 350 (1951)
2. R.S. Hansen, J.A. Mann, J. Appl. Phys., 35, 152 (1964)
3. M. van den Tempel, R.P. van de Riet, J. Chem. Phys., 42, 2769 (1965)
4. E.H. Lucassen-Reynders, J. Lucassen, Adv. Colloid Interface Sci., 2, 347 (1969)
5. R.S. Hansen, J. Ahmad, Progr. Surface Membr. Sci., 4, 1 (1971)
6. J. Lucassen, Trans. Faraday Soc., 64, 2221, 2230 (1968)
7. J. Lucassen, J. Colloid Interface Sci., 85, 52 (1982)
8. E.H. Lucassen-Reynders, "Physical Chemistry of Surfactant Action", p.173 (Dekker, New York, 1981)
9. H. Hühnerfuss, this Workshop (1986)
10. Y. Rabin, this Workshop (1986)
11. ONR Workshop (October 1984) p.26

12. E.H. Lucassen-Reynders, "Physical Chemistry of Surfactant Action", p.1 (Dekker, New York, 1981)
13. P. Williams, this Workshop (1986)
14. P.S. Liss, this Workshop (1986)
15. J. Lucassen, R.S. Hansen, J. Colloid Interface Sci., 23, 219 (1967)
16. J. Lucassen, M. van den Tempel, J. Colloid Interface Sci., 41, 491 (1972)
17. M. van den Tempel, E.H. Lucassen-Reynders, Adv. Colloid Interface Sci., 18, 281 (1983)
18. E.H. Lucassen-Reynders, Proc. Vith International conference on Surface Active Substances, Bad Stuer, GDR, 1985
19. J.A. Mann, this Workshop (1986).

DAMPING OF SHORT WAVES BY INSOLUBLE SURFACE FILMS

by

Kristian Dysthe*
Center for Studies of Nonlinear Dynamics**
La Jolla Institute
3252 Holiday Court, Suite 208
La Jolla, California 92037

and

Yitzhak Rabin
Department of Chemical Physics
Weizmann Institute of Science
Rehovot, Israel 76100

* Permanent Address: Institute of Mathematical and Physical Sciences,
Department of Physics, University of Tromsø,
Tromsø, Norway

** Affiliated with the University of California, San Diego

Introduction

The phenomenon of wave damping by thin films (monolayers) of surfactants has been known since ancient times (for historical notes, see Scott, 1978) and the basic hydrodynamic mechanism behind it is now well understood (Dorrenstein, 1951).

In view of the recent interest in the above problem, which is related to the possibility of acoustic noise reduction by the presence of such monolayers, we have constructed a simplified hydrodynamic model of the wave damping process and investigated its consequences. While our results were reported in a more general form by other authors (Van Der Tempel and Van De Riet, 1965; Lucassen-Reynders and Lucassen, 1969), we feel that the simplicity of our presentation and the insight provided by the analysis in terms of a mechanical analogue, are both appealing and useful.

We have applied our model to the analysis of the experimental data (Garret and Zisman, 1970) on wave damping by monolayers of linear polymers. Somewhat surprisingly, the results are in excellent agreement with experiment, indicating that the simple hydrodynamic theory is sufficient if the temporal variation produced by the wave is much faster than the relaxation processes associated with the monolayer (as is probably true in the case of polymeric monolayers and wave frequencies in the 60 Hz range).

Another, more indirect mechanism for wave damping by monolayers, appears in the context of wind-generation of waves, where experimental observations (Fitzgerald, 1963) indicate that the generation of short waves is suppressed for friction velocities below a critical value of 25 m/sec. Following Gottfried and Jameson (1968) we have analyzed the growth rate of waves as a function of their wavenumber, and investigated its dependence on the friction velocity and film compressibility, using experimental data for the growth rate in the absence of the film (Larson and Wright, 1975), and our theoretical model for the film-induced damping rate. The results are in qualitative agreement with Fitzgerald's experiments. There still remains some uncertainty with regard to field experiments (see Hühnerfuss and Garrett, 1981), where experimental sea slicks of different kinds have been used. It is claimed that films with a high equilibrium spreading pressure π_e (greater than 30 dyne/cm) are more effective in damping the capillary waves than those with a lower π_e . In view of the practical implications (choice of films and method of spreading) it is very important that the reason for this be understood. Work

along these lines is now in progress.

Derivation of Damping Rate

Consider a plane surface wave in the small amplitude approximation (*i.e.*, amplitude small compared to wavelength).

Let ω be its angular frequency and k its wavenumber, and assume a "deep" fluid (*i.e.*, a depth of more than half a wavelength).

The planar motion is taken to be in the x - z plane, with the x -axis in the direction of wave propagation, and the z -axis pointing vertically upwards with $z = 0$ at the equilibrium position of the surface.

The fluid velocity, $u_0 = \{u_0, w_0\}$ and surface elevation ζ are given by

$$u_0 = a \omega e^{kz} \cos \theta, \quad w_0 = a \omega e^{kz} \sin \theta \quad (1)$$

$$\zeta = a \cos \theta \quad (2)$$

where $\theta = kx - \omega t$, and a is the elevation amplitude. (Note that this is a potential flow, *i.e.*, $\nabla \cdot u_0 = 0$ and $\nabla \times u_0 = 0$).

In the absence of dissipation the dispersion relation is given by the expression

$$\omega^2 = \omega_k^2 = gk + \frac{\sigma}{\rho} k^3 \quad (3)$$

where g is the acceleration due to gravity, ρ is the density of the fluid, and σ the surface tension.

Taking dissipation into account, the above wave characteristics are still essentially correct, except that a small wave damping is introduced in Equation (3), and the flow (1) is modified in a boundary layer of thickness $\delta = (2\nu/\omega)^{1/2}$ below the surface (here ν is the kinematic viscosity)—the so called viscous shear layer (Landau and Lifschitz, 1959).

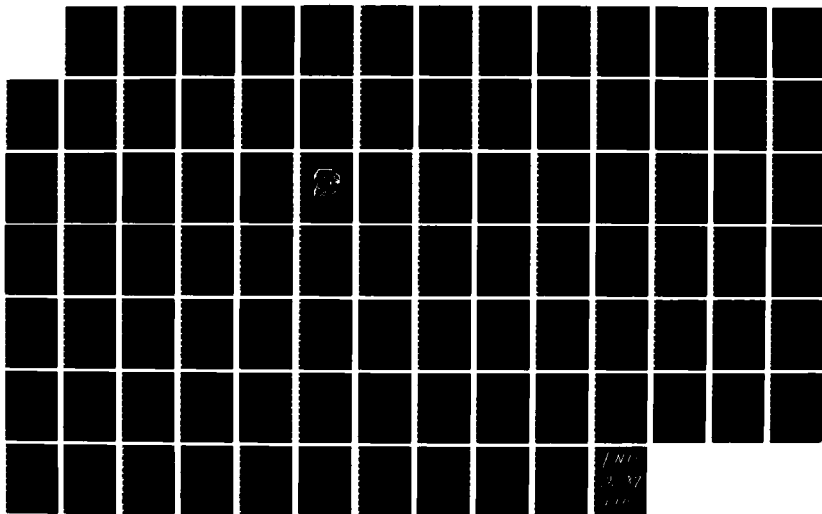
In the following arguments we shall make use of the fact that $k\delta \ll 1$, *i.e.*, the thickness of the boundary layer is small compared with the wavelength; in fact, $k\delta$ varies from 0.02 for 10 cm gravity waves to 0.14 for 0.1 cm capillary waves. This seems to be true for all interesting applications, and without further notice we shall proceed to neglect terms of relative order of magnitude $(k\delta)^2$.

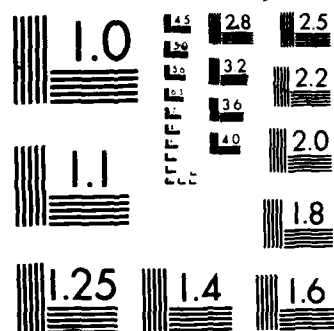
AD-A175 172 ONRL WORKSHOP PROCEEDINGS - ROLE OF SURFACTANT FILMS ON 1/3
THE INTERFACIAL P (U) OFFICE OF NAVAL RESEARCH LONDON
(ENGLAND) F L HERR ET AL 21 NOV 86 ONRL-C-11-86

UNCLASSIFIED

F/G 8/10

NL





We denote the total fluid velocity by $V = \{V, W\}$ and write $V = u_0 + u$. The vorticity, Ω , aligned in the y -direction, is given in terms of the relative velocity u (relative to the bulk velocity u_0 below the surface layer) by

$$\Omega = \frac{\partial u}{\partial z} . \quad (4)$$

The vorticity is produced at the surface; in the absence of a surface film it results from the need to balance the potential flow (Equation (1)) contribution to the tangential stress there, $\partial u_0 / \partial z + \partial w_0 / \partial x = \partial u / \partial z$. It is transmitted into the boundary layer by viscous "diffusion:"

$$\frac{\partial \Omega}{\partial t} = \nu \frac{\partial^2 \Omega}{\partial z^2} . \quad (5)$$

Note that to this approximation both u and w satisfy Equation (5). The relevant solution of Equation (5) gives Ω and u as

$$u = B e^{z/\delta} e^{i(\theta - z/\delta)} + c.c. , \quad (6)$$

and

$$\Omega = \frac{B(1-i)}{\delta} e^{z/\delta} e^{i(\theta - z/\delta)} + c.c. ,$$

Here B is determined by the tangential stress condition at the surface. Where there is no surface film, the stress to be balanced at the surface, $\nu \rho (\partial u_0 / \partial z + \partial w_0 / \partial x) = 2\nu \rho \omega k a \cos \theta$, is very feeble, producing an excess velocity u in the boundary layer of the order $(k \delta) u_0$. In this case the rate of energy dissipation in the boundary layer scales like $\nu \rho \delta \overline{(u/\delta)^2}$ (the bar implies averaging over a wave period) which is found to be a factor $k \delta$ lower than the bulk dissipation rate \dot{Q}_0 calculated from the flow field Equation (1) (Phillips, 1977)

$$\dot{Q}_0 = 2\nu \rho k \omega^2 a^2 = 4\nu k^2 E . \quad (7)$$

Here E is the mean energy density (per unit surface area) $\rho \omega^2 a^2 / (2k)$ in the wave. Thus, in the absence of a surface film, the damping of the wave is due to viscous dissipation in the bulk giving $\dot{E} = -\dot{Q}_0$. The temporal rate of damping, γ_0 , then becomes

$$\gamma_0 = 2\nu k^2 , \quad (8)$$

which is a classical result due to Stokes (1845).

In the presence of an insoluble surface film this picture changes rather drastically. The surface film has elastic properties, meaning that the surface tension, σ , varies with the molecular area A (area per surfactant molecule). A nonuniform horizontal displacement $\xi(x, t)$ of the film (in the x -direction) gives a tangential stress (in the linear approximation)

$$\frac{\partial \sigma}{\partial x} = \frac{1}{C_s} \frac{\partial^2 \xi}{\partial x^2} ; \quad (9)$$

where $C_s = -\frac{1}{A_0} \left. \frac{dA}{d\pi} \right|_0$ is the compressibility of the film at some unperturbed value A_0 of A , and π is the film "pressure" $\sigma_w - \sigma$, where σ_w and σ are the surface tensions of the pure fluid and the film-covered surface respectively (Gaines, 1966). Now, in the absence of any response in the boundary layer, the contraction and expansion of the surface implied by Equation (1) is $\xi_0 = -a \sin \theta$ which gives a surface stress of $-(k^2 a / C_s) \sin \theta$. This should be compared to the potential flow contribution to the viscous stress at the surface, $2\nu \rho k a \omega \cos \theta$. The ratio of the amplitudes of these expressions is $2\nu \rho C_s \frac{\omega}{k}$ which, except for the "gaseous" regime (see Gaines, 1966) where C_s is very large, is a small number.

The conclusion to be drawn from the above estimate is that, in contrast to the case of no surface film, $|\partial u_0 / \partial x + \partial w_0 / \partial x| \ll |\partial u / \partial z|$, so that the balance of stresses at the surface is between the elastic stress induced in the film and the viscous stress due to the shear in the boundary layer.

The equation expressing the continuity of tangential stress through the surface becomes

$$\nu \rho \frac{\partial u}{\partial z} = \frac{1}{C_s} \frac{\partial^2 \xi}{\partial x^2} , \quad (10)$$

where the left-hand side can be written as the rate of change of horizontal momentum in the motion relative to the bulk, i.e., $\partial P / \partial t$ with $P = \int_{-\infty}^0 \rho u \, dz$.

The relative velocity u is now of the same order of magnitude as the bulk velocity. The dissipation in the shear layer scales like $\nu \rho \delta (u / \delta)^2$, exceeding that in the bulk by a factor $(k \delta)^{-1}$. To calculate the damping rate of the surface wave, we therefore proceed to calculate the rate of dissipation \dot{Q} in the shear layer (Phillips, 1977),

$$\dot{Q} = \nu \rho \int_{-\infty}^0 \overline{\Omega^2} dz = \frac{2\nu\rho}{\delta} |B|^2, \quad (11)$$

where we have used Equation (6). Notice that in writing down the expression for \dot{Q} we have neglected a term of relative order $k\delta$ coming from the product $\overline{\frac{\partial u_0}{\partial z} \frac{\partial u}{\partial z}}$.

A relation between the complex amplitude, B , and the real amplitude of elevation, a , is found from (10) by noting that $\frac{\partial \xi}{\partial t} = u_0 + u$:

$$B = \frac{i-1}{1-\beta-i} \cdot \frac{\omega a}{2}, \quad (12)$$

where we have introduced the dimensionless quantity β defined by

$$\beta = \frac{2\nu\rho C_s \omega}{k^2 \delta} = \sqrt{2\nu\rho C_s} \omega^{1/2} k^{-2}, \quad (13)$$

which varies from $\beta \rightarrow \infty$ in the absence of the film to $\beta \rightarrow 0$ for an incompressible monolayer. Inserting (12) into (11) we obtain

$$\dot{Q} = 2E \frac{\frac{\nu k^2}{k\delta}}{(1-\beta)^2 + 1}. \quad (14)$$

The damping rate, γ , is (to leading order in $k\delta$) given by

$$\gamma = \frac{\frac{\nu k^2}{k\delta}}{(1-\beta)^2 + 1} = \frac{(\nu k^2 \omega/2)^{1/2}}{(1-\beta)^2 + 1}, \quad (15)$$

which exceeds the contribution from the bulk dissipation (cf. γ_0 given by Equation (8)) by a factor $(k\delta)^{-1}$.

In order to obtain an expression for the dissipation rate that contains contributions from both the shear layer and the bulk, one must carry out the standard linear analysis of the Navier-Stokes equations and use the corresponding boundary conditions on the normal and tangential stresses at the surface. The details are not presented here. They can be found, e.g., in the review paper by Lucassen-Reynders and Lucassen (1969). The dispersion relation can be written

$$\left[1 - \frac{\omega_k^2}{\omega^2} + i(k\delta)^2 \right] \left[\frac{m}{k} - i \frac{2\rho v C_s \omega}{k} \left(1 + \frac{m^2}{k^2} \right) \right] \quad (16)$$

$$= \left[\frac{\omega_k^2}{\omega^2} - i \frac{m}{k} (k\delta)^2 \right] \left[-1 + i \frac{2\rho v C_s \omega}{k} \right],$$

where $m = k(1-i)((k\delta)^{-2} + i/2)^{1/2}$ and ω_k is given by Equation (1). This can be shown to be identical to that given by Van Der Tempel and Van De Riet (1965).

We now exploit the fact that $k\delta$ is a small number. If in Equation (16) we neglect terms of relative order of magnitude $(k\delta)^2$, except for terms where $(k\delta)^2$ is multiplied by C_s (which becomes large in the limit of a gaseous film) we obtain

$$\frac{\omega^2}{\omega_k^2} = 1 + k\delta \frac{1 - 2i\beta k\delta}{\beta - 1 + i}, \quad (17)$$

which easily lends itself to iteration. In the "gaseous" limit (when $\beta \gg (k\delta)^{-1}$) we have

$$\omega = \omega_k - 2i v k^2 \quad (18)$$

in accordance with (8) ($-\gamma_0$ is the imaginary part of ω). When $\beta \ll (k\delta)^{-1}$ we have

$$\omega = \omega_k - \left[\frac{v k^2 \omega_k}{2} \right]^{1/2} \frac{1 - \beta + i}{(\beta - 1)^2 + 1}, \quad (19)$$

which agrees with Equation (15), and confirms that our simpleminded derivation contains the relevant physical effects.

Mechanical Analogue—Discussion

The tangential stress condition (10) can be recast into the form

$$\frac{\partial P}{\partial t} = \frac{\partial \sigma}{\partial x} = \frac{1}{C_s} \frac{\partial^2 \xi}{\partial x^2} \quad (20)$$

where P is the excess horizontal fluid momentum per unit surface area due to the boundary layer:

$$P = \rho \int_{-\infty}^0 u \, dz = \frac{\rho \delta}{2} (1+i) B e^{i\theta} + c.c. \quad (21)$$

Further:

$$\begin{aligned}\frac{\partial P}{\partial t} &= \rho v \left. \frac{\partial u}{\partial z} \right|_0 = \frac{\rho v}{\delta} (1-i) B e^{i\theta} + c.c. \\ &= \frac{\rho v}{\delta} \left[u_s + \frac{1}{\omega} \frac{\partial u_s}{\partial t} \right],\end{aligned}\quad (22)$$

where u_s is the excess surface velocity. Thus the rate of change of the excess fluid momentum consists of one friction-like term

$$\frac{\rho v}{\delta} u_s \quad (23)$$

and one acceleration-like term

$$\frac{\rho v}{\delta \omega} \frac{\partial u_s}{\partial t} = \frac{1}{2} \rho \delta \frac{\partial u_s}{\partial t}, \quad (24)$$

where $\frac{1}{2} \rho \delta$ is half the mass per unit area in the boundary layer. From (22) it is also seen that while the two terms have *equal amplitudes*, they are 90° out of phase. This property, which does not seem to have an analogue in a discrete mechanical system, is a consequence of the fact that (due to Equation (5)) the viscous force and the inertial force balance each other throughout the depth of the boundary layer.

We write (20) in the form

$$\frac{1}{2} \rho \delta \ddot{\chi} + \frac{\rho v}{\delta} \dot{\chi} = \frac{\partial \sigma}{\partial x} = -\frac{k^2}{C_s} (\chi + \chi_0) \quad (25)$$

where χ is the excess displacement of the film (i.e., $\dot{\chi} = u_s$) and χ_0 is the displacement of the bulk (i.e., $\dot{\chi}_0 = u_{0s}$).

Formally, this is the equation of a driven damped mechanical oscillator of mass $\frac{1}{2} \rho \delta$ and spring constant k^2/C_s .

We first look into the free motion of the oscillator in the absence of the driving term (i.e., the bulk motion of the surface wave). This corresponds to a nearly longitudinal elastic wave-mode in the film and the accompanying shear layer.

The dispersion relation for the mode is readily found from (25) to be

$$\omega^2 = \frac{k^2(1-i)}{\sqrt{2} v \rho C_s}, \quad (26)$$

which is seen to be heavily damped (this is again a consequence of the fact that friction forces balance the inertial forces throughout the accompanying shear layer).

Taking ω to be real, we solve (26) with respect to $k = k_L + i\alpha_L$ and obtain

$$k_L^2 = \left[\frac{1}{2} + \frac{\sqrt{2}}{4} \right] C_s (\nu \rho^2 \omega^3)^{1/4}$$

$$\alpha_L = (\sqrt{2} - 1) k_L . \quad (27)$$

These are exactly the longitudinal mode solutions which were derived and experimentally verified by Lucassen (1968).

The dispersion relation (26), which can be recast in the form $\beta = 1 - i$, is found to be the lowest order approximation in $k \delta$ to a more exact relation that can be obtained from Equation (17). It should be noted that the wave-mode is longitudinal in the sense that the horizontal displacement amplitude dominates the vertical by a factor of order $k \delta$ (as can be seen from the condition of incompressibility). We also remark that $k \delta$ (for this wave-mode) scales like $(\nu)^{1/4} (\rho C_s)^{1/4} \omega^{1/4}$, which is small for reasonably dense monolayers.

Returning to the driven oscillator (25) we first observe that it dissipates energy at an average rate

$$\frac{\rho \nu}{\delta} \overline{\dot{\chi}^2} = \overline{\dot{\chi} \frac{\partial \sigma}{\partial x}} , \quad (28)$$

which is readily shown to be identical to \dot{Q} calculated in Equation (14).

Let us now address the question of the mean energy flow in the system consisting of the film, the shear layer, and the bulk motions.

We remark that, on the average, no work is done by or on the film. This is an obvious consequence of our model, which does not allow for energy sources or sinks in the film. Mathematically, this is expressed as

$$\overline{(\dot{\chi}_0 + \dot{\chi}) \frac{\partial \sigma}{\partial x}} = 0 \quad (29)$$

where $\dot{\chi} \frac{\partial \sigma}{\partial x}$ can be interpreted as the rate of work that the film is doing on the shear layer, while $-\dot{\chi}_0 \frac{\partial \sigma}{\partial x}$ is the rate at which work is delivered by the bulk motion. Notice

that χ_0 and χ are out of phase: at maximum damping ($\beta = 1$) the phase difference is $\pi/4$; at maximum horizontal film displacement ($\beta = 2$), it is $\pi/2$.

For the driven oscillator (25) the ratio between the amplitude of the driven motion, χ_{\max} , and the amplitude of the drive, $\chi_{0\max} = a$, is given by $2^{1/2}((1 - \beta)^2 + 1)^{-1/2}$. This has a maximum of $2^{1/2}$ for $\beta = 1$. As a function of frequency, this ratio has two maxima of $2^{1/2}$ ($\beta = 1$) and one relative minimum at $\omega = 2.6\omega_0$ (where ω_0 is the frequency corresponding to minimum phase velocity). The bimodal character of this relation comes from the fact that β as a function of ω has a minimum of $3.7(g\rho^3\sigma^5v^4)^{1/4}C_s$, for $\omega = 2.6\omega_0$.

The horizontal displacement of the film, $\chi_0 + \chi$, has an amplitude given by

$$\frac{a\beta}{[(1 - \beta)^2 + 1]^{1/2}} \quad (30)$$

which has a maximum of $2^{1/2}a$ for $\beta = 2$.

The motion of the film particles is given by the total displacements of the surface*:

$$\text{Vertical: } \zeta_0 = a \cos \theta$$





$$\text{Horizontal: } \chi_0 + \chi = \frac{a\beta}{1 + (\beta - 1)^2} ((1 - \beta) \sin \theta + \cos \theta)$$

It is seen from the latter expression that for very dense films ($C_s \ll 1$), and not too low frequencies so that $\beta \ll 1$, the surface film does not move horizontally.

This result was already anticipated by Reynolds (1880), and was derived by Levich (1941). The fact that the horizontal displacement has a maximum of $2^{1/2}a$ between the dense ($\beta \ll 1$) and gaseous ($\beta \gg 1$) regimes, namely for $\beta = 2$, seems to have gone unnoticed.

In the table below we have listed the horizontal film velocity, the excess velocity (over that of the bulk), and the displacement amplitude, together with the growth rate and orbit of the film particles.

*There is also an excess elevation ζ . It is, however, of order $a \pm \delta$.

TABLE 1				
β	0	1	2	∞
γ	$(\gamma_0 \omega)^{1/2}/4$	$(\gamma_0 \omega)^{1/2}/2$	$(\gamma_0 \omega)^{1/2}/4$	γ_0
Horizontal film velocity	0	$\omega a \cos(\theta - \frac{\pi}{2})$	$2^{1/2} \omega a \cos(\theta - \frac{\pi}{4})$	$\omega a \cos \theta$
Excess film velocity	$\omega a \cos(\theta + \pi)$	$2^{1/2} \omega a \cos(\theta + \frac{3\pi}{4})$	$\omega a \cos(\theta - \frac{\pi}{2})$	0
Horizontal film displacement amplitude	0	a	$2^{1/2} a$	a
Orbit of particle on film				

Going back to Equation (15) we remark that γ has a maximum of $(\nu k^2 \omega/2)^{1/2}$ for $\beta = 1$, which is twice the value for an inextensible monolayer ($\beta = 0$). Intuitively one might expect the maximum damping to occur for this latter case, where the film acts like an inextensible membrane, near which the wave produces a strong shear-layer, dissipating its energy. The rate of dissipation does indeed depend on the "strength" of the shear, or vorticity, in the layer. Since the structure of this layer (see Equation (6)) is independent of film compressibility, what matters is the amplitude of the excess velocity u at the surface which is readily found to be

$$u_{\max} = \frac{2 \omega a}{[(1 - \beta)^2 + 1]^{1/2}} \quad (31)$$

It is seen that u_{\max} has indeed a maximum of $2^{1/2} a \omega$ for $\beta = 1$, which should be compared to $a \omega$ for $\beta = 0$. Since the rate of dissipation is quadratic in u_{\max} , the somewhat counter-intuitive result for the damping rates mentioned above follows.

Let us finally discuss an explanation given by Lucassen for the maximum in the damping coefficient. He relates this effect to a sort of linear resonance between the two basic wave modes of the system: the capillary gravity-wave on the one hand, and the

longitudinal wave (Equation (27)) on the other. Such linear resonance between distinct wave-modes propagating in a system is well known from several fields of physics. However, while for essentially undamped waves the interaction is expected to take place where the frequencies and phase velocities (or wavenumbers) are coinciding or nearly coinciding, no such simple relation is expected to hold in the case of heavily damped modes (such as the longitudinal wave).

Indeed, the ratio between the wavenumber k of the capillary-gravity wave, and that of the longitudinal mode, k_L , at maximum damping is readily found (from Equation (27) and the condition $\beta = 1$) to be $\frac{2}{(1 + 2^{1/2})^{1/2}} \approx 1.29$.

Viscoelastic Effects

So far we have focused on the case where the wave damping characteristics of the surface film can be fully described in terms of its elastic properties, *i.e.*, the real coefficient C_s . For many insoluble monolayers this seems to be a realistic approximation.

Surface films may, however, exhibit a "surface dilatational viscosity" due to relaxation processes. These may be of two kinds. First, during rapid oscillation (compression and expansion) of the surface, the value of the surface tension σ may be different from that measured with the surface at rest. This effect, which has been observed (for a thorough discussion see Lucassen-Reynders and Lucassen, 1969) for spread monolayers of long chain molecules is apparently connected with the reorientation processes of the absorbed molecules at the surface. Another relaxation process is that of diffusional interchange between surface and bulk during contraction and expansion of the surface.

In both cases, the effect can be formally included in the treatment given in the previous section, by a generalization of Equation (9), writing

$$\frac{\partial \sigma}{\partial x} = \left[e_s + \eta_s \frac{\partial}{\partial t} \right] \frac{\partial^2 \xi}{\partial x^2}, \quad (32)$$

where e_s is the surface dilatational elasticity, and η_s is a surface dilatational viscosity, both

of which, in general, depend on frequency.

While it is not clear how η_d is related to measured surface properties, for the first kind of relaxation effect mentioned above it is a relatively simple exercise to show that for a wave of frequency ω , we have in the case of diffusional relaxation process,

$$\epsilon_d = \frac{1}{C_s} \frac{1 + \theta}{1 + 2\theta + 2\theta^2},$$

and

$$\eta_d = -\frac{1}{\omega C_s} \frac{\theta}{1 + 2\theta + 2\theta^2}, \quad (33)$$

where $\theta = -A^2 \frac{dc}{dA} \left(\frac{D}{2\omega} \right)^{1/2}$, c is the bulk concentration, and D the diffusion coefficient of the surfactant.

When $\theta \ll 1$, the relaxation time is much longer than the wave period and we have $\eta_d = 0$ and $\epsilon_d = C_s^{-1}$, so that the soluble surfactant acts as if it was insoluble.

Wave Damping—Numerical Results

In the following we want to take a closer look at the predictions of the simple theory (essentially that of Dorrenstein) neglecting dilational viscosity in the film.

Since the wave damping depends rather critically on the value of the parameter β , in Figure 1 we plot the ratio of β/C_s (note that by Equation (13), β is proportional to C_s) as a function of frequency ω . It is seen that for gravity waves one has a $\omega^{-3/2}$ dependence, while for capillary waves there is a weak $\omega^{1/6}$ dependence. There is a minimum for β at $\omega = 2.6\omega_0$, where ω_0 corresponds to the minimum of the phase velocity.

We note especially that in the range of angular frequencies between 10^2 and 10^3 the ratio β/C_s is within 7% of the value 7.4. As we pointed out previously, the damping rate, as a function of C_s , has a maximum for $\beta = 1$. Thus we should expect that for the frequency range $10^2 - 10^3$ where $\beta/C_s \approx 7.4$, an optimal damping would occur for C_s around $(7.4)^{-1} = 0.135$.

This is demonstrated in Figures 2 and 3 where γ/γ_0 is shown as function of ω for different values of C_s . The fact that the graphs run more or less parallel in this frequency

domain is due to the insignificant variation of β here.

Figures 4 and 5 show γ/γ_0 as a function of the wave length λ for different values of C_s . The uncorrected (by γ_0 dependence of the damping rate γ on the wavelength λ) is given in Figure 6. In summary we find that:

1. There is an optimum film compressibility of $C_s \approx 0.14$ cm/dyne for the capillary waves ($\omega \sim 10^2 - 10^3$)
2. For gravity waves the maximum relative damping, γ/γ_0 , at a particular film compressibility, C_{s1} occurs for a wave length

$$\lambda \approx 5.7 [\rho v^4 g^3 C_s]^{-1/3},$$

or $\lambda \approx 0.58 C_s^{-1/3}$ (C_s in cm/dyne). Thus to have maximum relative damping of a 23 cm wave we need $C_s \approx 10^{-2}$, while for a 10 cm wave $C_s \approx 0.03$.

Comparison with Experimental Data

There exists a lot of experimental data on wave damping by surface films (see, e.g., Lucassen-Reyders and Lucassen, 1969; Davies and Vose, 1965; Garrett and Zisman, 1970), and on the whole there is satisfactory agreement between these data, and the simple hydrodynamical theory presented in the previous sections.

Garrett and Zisman (1970) have investigated the damping of capillary waves with absorbed insoluble monolayers of surface-active linear polymers. They observed a highly complex variation of the damping rate as a function of molecular area A (Figure 7), and indicate (page 1804 in their paper) that the simple hydrodynamical theory of Dorrenstein is unable to predict this complex behavior.

They are of course right in the sense that the simple theory takes the elastic film property (i.e., C_s) as given. C_s is derived from the relation between the equilibrium surface pressure π and the molecular area A . In their paper Garrett and Zisman determine experimentally both the π vs. A curve and the corresponding damping curve.

In order to check whether the hydrodynamic theory can reproduce the complex features of the Garrett-Zisman results, we have fitted a smooth π vs. A curve to their experimental points (spline function) and from this obtained a numerical value for C_s for each value of A . This value was used to determine β , which is then substituted into a formula for the spatial damping rate, $\kappa = \gamma/v_g$ (v_g is the group velocity) derived from

Equation (17). Figure 8 shows the corresponding variation in surface pressure π , β , and the spatial damping rate.

As can be seen from comparison with Figure 7 (Figure 4 in Garrett and Zisman, 1970), the variations in π are quite similar. Since π is obviously a very sensitive function of the slope of the π vs. A curve (which is proportional to C_s^{-1}) hardly a better agreement could have been expected.

Suppression of Wind-Generated Waves by a Film

In the preceding sections we have seen how the damping of shorter surface waves may be strongly enhanced by the presence of a surface film.

The calming effect of such films on wind-generated waves has been noted in the literature with references going back to Pliny (77 C.E.) and Plutarch (95 C.E.). In modern times, two major revivals of interest in the subject seem to have occurred in the last quarter of the eighteenth century, initiated by Benjamin Franklin, and the last two decades of the nineteenth century, with contributions from people like Reynolds and Lamb. An interesting account of the historical development of the subject is given by J. C. Scott (1977).

Experimental work on the effect of a surface film on wind-generated waves seems to have started with Benjamin Franklin who carried out a series of experiments on ponds and lakes in England. Well known is his description of how a teaspoonful of oil had the effect of making a pond of half an acre in Clapham Common: "As smooth as a looking glass."

Fitzgerald (1963) carried out an experiment on wind generation of waves with and without surface films. He used a film of cetyl alcohol, and measured the wind stress τ_0 at the surface. He found that for a friction velocity u_{*c}

$$u_{*c} = (\tau_0 / \rho_{\text{atm}})^{1/2}$$

exceeding 25 cm/sec, short waves (2-3 cm) would start growing, and for smaller velocities the waves would be suppressed.

Gottfredt and Jamexon (1968) investigated theoretically how the surface film would affect the growth rate of the wind generated waves. For this purpose they used the Miles theory of wind wave-generation modified to describe the case where the critical layer

(i.e., where the wind velocity is equal to the phase velocity of the wave) occurs in the transition region just outside the laminar sublayer. They demonstrate that to a good approximation the growth rate of a given frequency component ω is given by the growth rate $\beta(\omega)$ in the absence of film, minus the damping rate $\gamma(\omega)$ due to the film. The calculated growth rate $\beta(\omega)$, is not entirely accurate, as it does not take into account the shear flow in the upper part of the water. Even if this wind induced current is rather shallow (a few millimeters) its effect on the short waves ($\lambda \leq 1$ cm) may still be of significance.

Rather accurate measurements of the wind-induced growth rates of waves have been conducted by Larson and Wright (1975) in the short wave regime (λ from 7 to 0.7 cm).

Valenzuela (1976) and Kawai (1979) analyzed the stability with different models of the wind induced shear flow in the water. Both obtained results in fair agreement with the experimental results of Larson and Wright.

Kawai (1979) also conducted experiments showing that the first waves to appear after the wind has been "switched on" are those whose wavelength corresponds to the maximum growth rate.

To get some idea of the threshold wind velocity necessary to produce short waves in the presence of a film, we have used the following procedure:

1. We fit a smooth curve to the experimental points of Larson and Wright (see Figure 13) giving us $\beta(k)$.
2. The damping rate in the absence of wind, $\gamma(k)$, as given by Equation (15), is subtracted from $\beta(k)$ to give an estimate of the net growth rate.

We remark that in calculating the damping rate according to Equation (15) we have used $\omega = \omega_k(k)$ (see Equation (3)). This is not quite accurate, because the dispersion characteristics of the growing waves differ somewhat from Equation (3), due to the shear flow.

Both the calculations of Gottfredi and Jameson (1968) and the estimate outlined above (see Figures 9-12) indicate that the threshold for wind generation of short capillary-gravity waves, in terms of the friction velocity u_{*c} , is somewhere near 25 cm/sec. This is in good agreement with the experimental observations of Fitzgerald (1963).

An earlier experiment by Keulegan (1951) was done in a wind tunnel with water in the presence of soap. He claims that waves could be suppressed up to $u_{*c} \leq 60$ cm/sec, which is greatly in excess of Fitzgerald's figure. Since soap is soluble it is possible that the concentration (at least in a layer $\geq \delta$) would be high enough to drastically increase the fluid viscosity. Since the wave damping is proportional to $v^{1/2}$ a factor of increase of nearly 6 would be necessary to explain Keuligan's figure.

Acknowledgement

This work was supported in part by DARPA through ORINCON Corporation, under NOSC contract No. N66001-85-D-0026/0008.

References

1. B. Franklin, Letter to Dr. Browrigg, 7 November 1773, *The Works of Benjamin Franklin*, edited by J. Bigelow, Vol. 6 (G.P. Putnam and Sons, New York, 1904).
2. O. Reynolds, Brit. Ass. Rep. (1880), cited in *Lamb's Hydrodynamics*.
3. V.G. Levich, *Acta Physicichim. U.S.S.R.* 14, 307-321 (1941); *Physicochemical Hydrodynamics*, Chap. XI (Prentice-Hall, New Jersey, 1962).
4. R. Dorrenstein, *Proc. Acad. Sci. Amst. B*54, 260-350 (1951).
5. L.D. Landau and E.M. Lifshitz, *Fluid Mechanics* (Pergamon, London, 1959).
6. H. Lamb, *Hydrodynamics*, 6th Ed. (Dover, New York, 1932).
7. G.L. Gaines, *Insoluble Monolayers at Liquid-Gas Interfaces* (Interscience, New York, 1966).
8. J.T. Davies and R.W. Vose, *Proc. Roy. Soc. A*286, 218 (1965).
9. M. Van Der Tempel and R.P. Van De Riet, *J. Chem. Phys.* 42, 2769 (1965).
10. J.C. Scott, *Hist. Technol.* 3, 163 (1978).
11. E.H. Lucassen-Reynders and J. Lucassen, *Advan. Colloid Interface Sci.* 2, 347 (1969).
12. O.M. Phillips, *The Dynamics of the Upper Ocean* (Cambridge Univ. Press, Cambridge, 1966).
13. J. Lucassen, *Trans. Faraday Soc.* 64, 2221-2230 (1968).
14. W.D. Garrett and W.A. Zismann, *J. Phys. Chem.* 74, 1796 (1970).
15. T.R. Larson and J.W. Wright, *J. Fluid Mech.* 70, 417 (1975).
16. S. Kawai, *J. Fluid Mech.* 93, 661 (1979).
17. J.C. Gottifredi and G.J. Jameson, *J. Fluid Mech.* 32, 609 (1968).
18. G.H. Keulegan, *J. Res. Nat. Bur. Stanol.* 46, 358 (1951).
19. L.M. Fitzgerald, *Aust. J. Phys.* 16, 475 (1963).
20. H. Hühnerfuss and W.D. Garrett, *J. Geophys. Res.* 86, 439 (1981).
21. G.R. Valaniadis, *J. Fluid Mech.* 76, 229 (1976).

Figure Captions

1. The ratio β/C_s (in cm/dyne) is plotted vs. the wave frequency ω (in radian/sec).
2. Plot of the normalized (w.r.t. the free-surface value) damping rate γ/γ_0 as a function of ω (in radian/sec) for values of the compressibility C_s in the range 0.02–0.15 cm/dyne.
3. Same as Figure 2, for $0.15 \leq C_s \leq 10$ cm/dyne.
4. Same as Figure 2, with the frequency ω replaced by the wavelength λ (in cm).
5. Same as Figure 3, with ω replaced by λ .
6. Plot of the normalized damping rate γ (in radian/sec) as a function of the wavelength λ (in cm), for values of C_s in the range 0.02–10 cm/dyne.
7. Wave damping behaviour of polydimethylsiloxane heptadecamer monolayer on water (taken from Garrett and Zisman, 1970).
8. The (dimensionless) parameter β and the spatial damping rate κ (in radian/cm) are plotted vs. the area A per surfactant molecule (in $\text{\AA}^2/\text{molecule}$), using a fit to the π vs. A curve taken from Figure 7, and substituting the resulting compressibility into the hydrodynamic theory, Equations (13) and (17).
9. The growth rate $\beta - \gamma$ (in radian/sec) of a wind-generated wave is plotted vs. the wavenumber k (in radian/sec) for different values of the compressibility C_s (in cm/dyne). The friction velocity is $u_{*a} = 124$ cm/sec.
10. Same as Figure 9, with $u_{*a} = 66$ cm/sec.
11. Same as Figure 9, with $u_{*a} = 27$ cm/sec.
12. Same as Figure 9, with $u_{*a} = 15$ cm/sec.
13. Correlation of growth rate β to wavenumber k , \blacksquare , \bullet , Δ , \square , \circ , converted from Figure 8 of Larson and Wright (1975); \times results of this study for the initial wavelets. Friction velocities in the air u_{*a} at atm measured at the fully developed stage are given in cm/sec. (From S. Kawal, 1979).

Figure 1

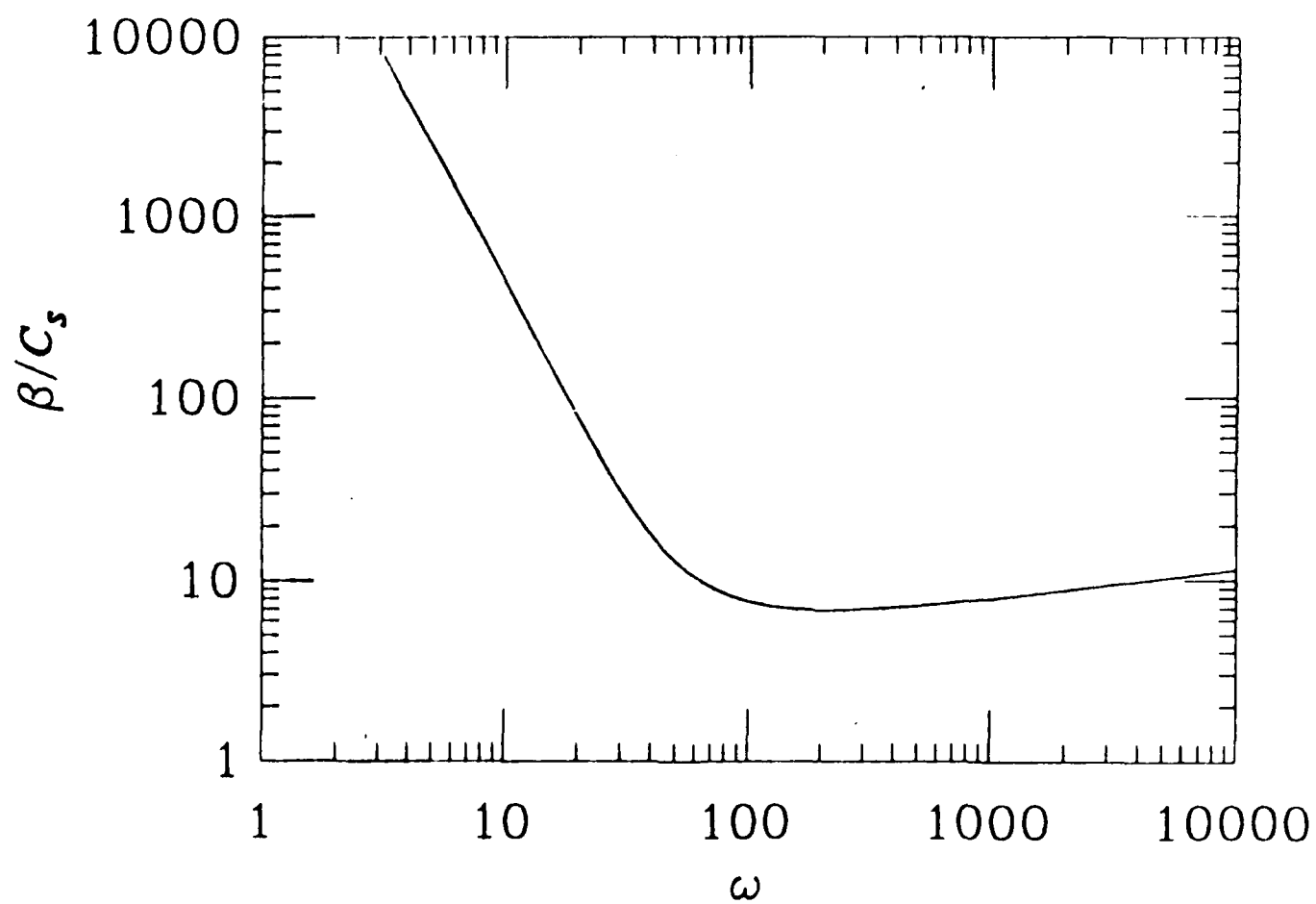


Figure 2

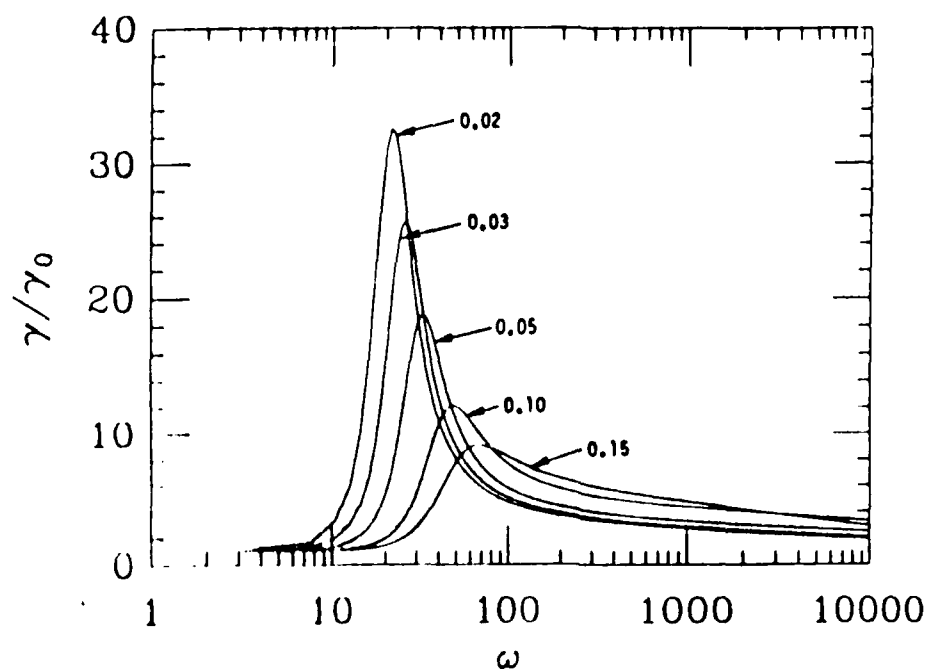


Figure 3

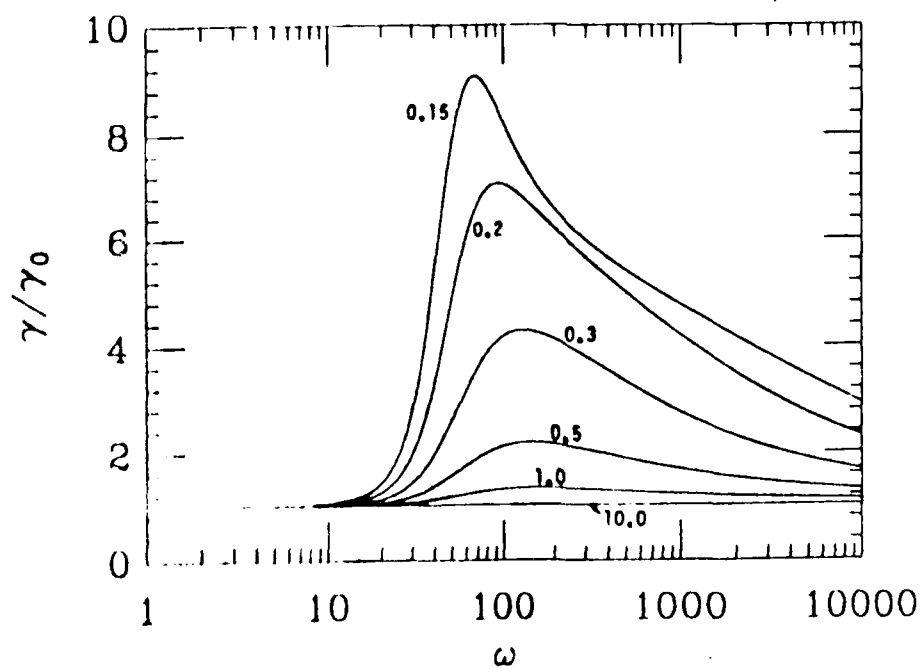


Figure 4

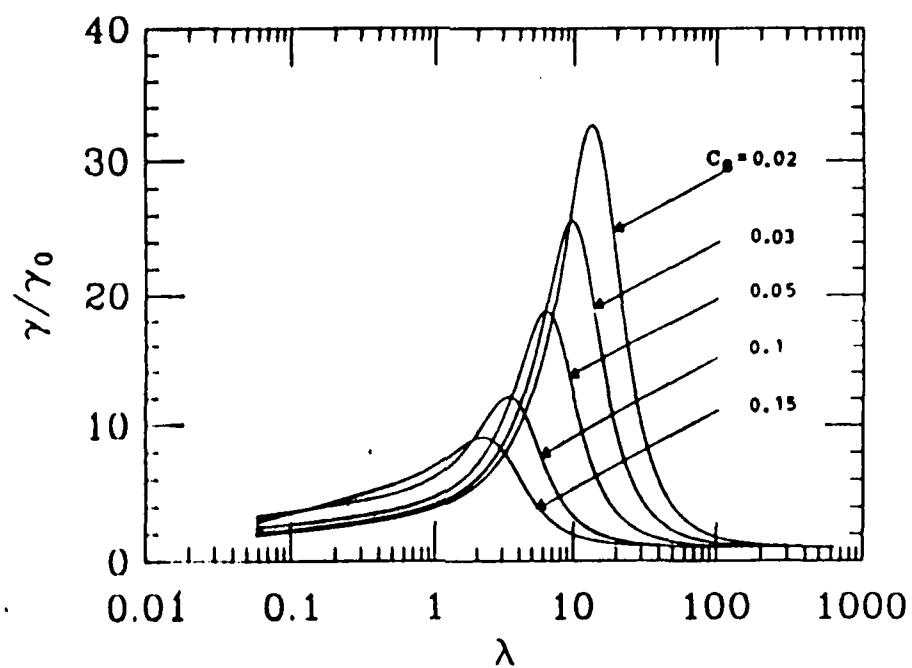


Figure 5

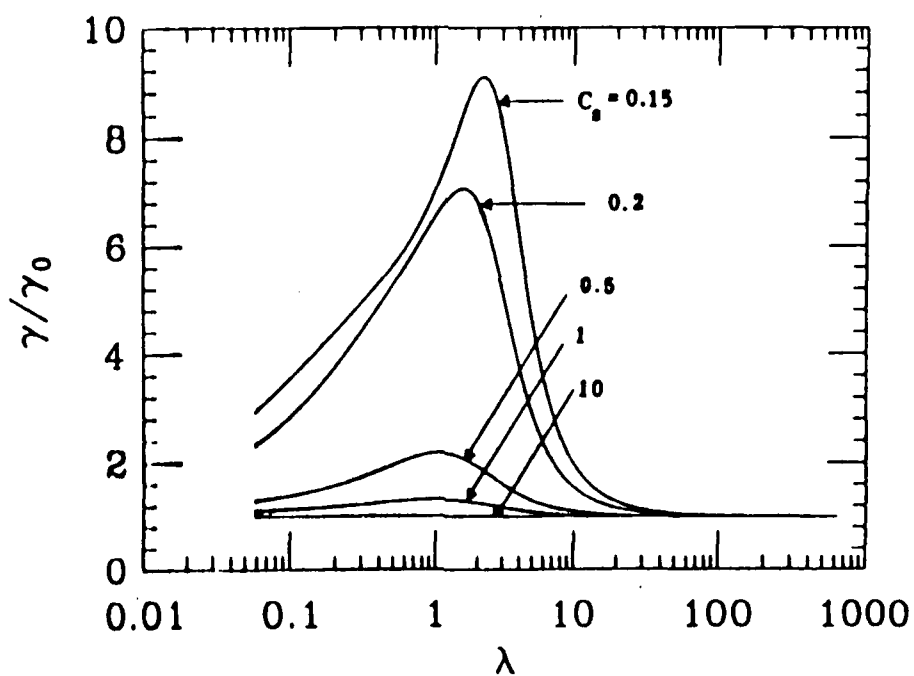


Figure 6

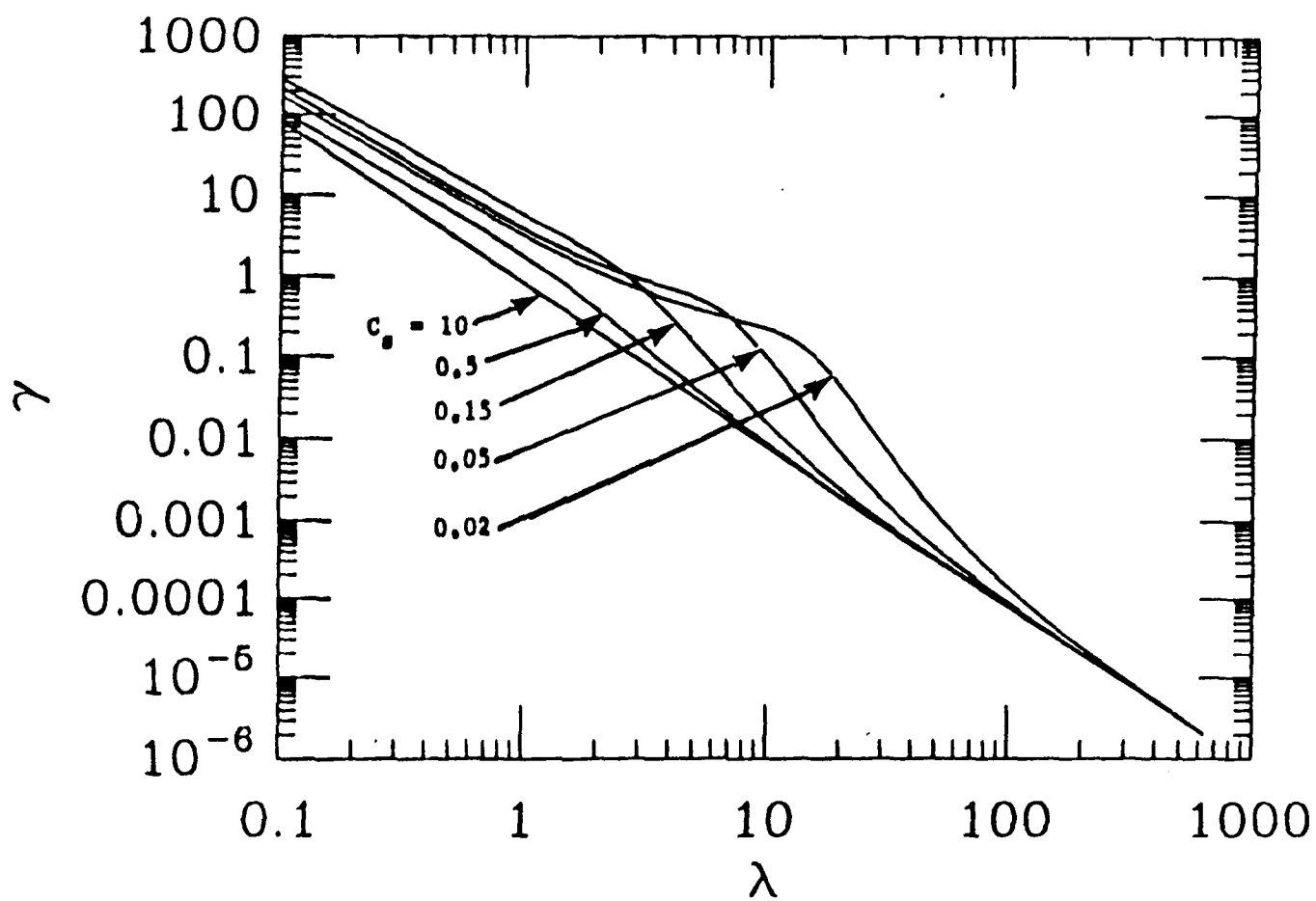


Figure 7

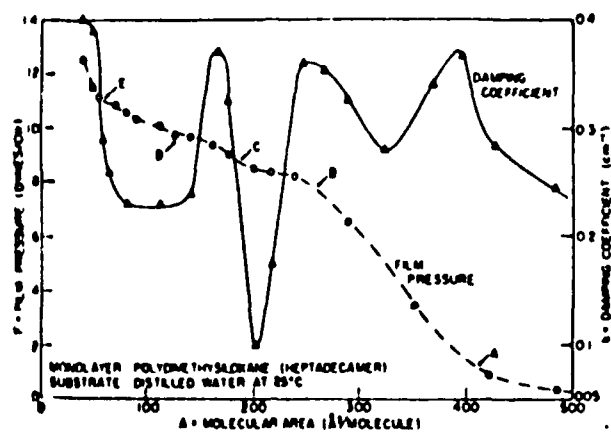


Figure 4. Wave damping behavior of polydimethylsiloxane heptadecamer at 60 cps.

Figure 8

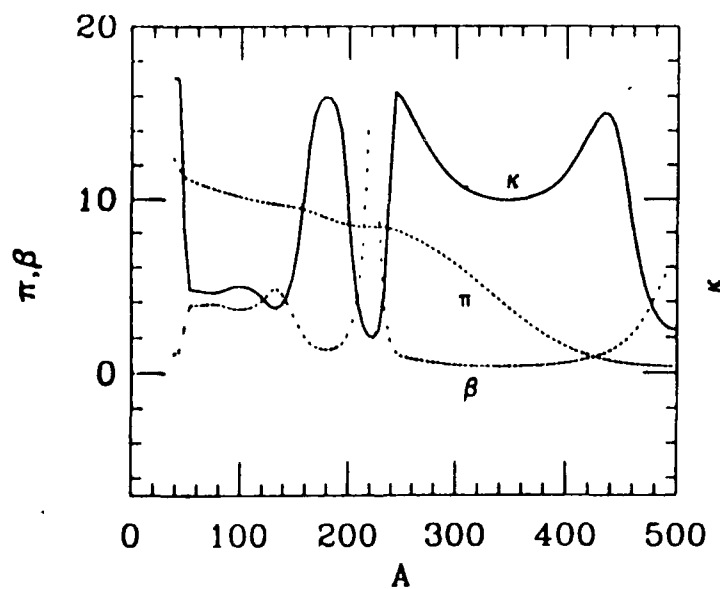


Figure 9

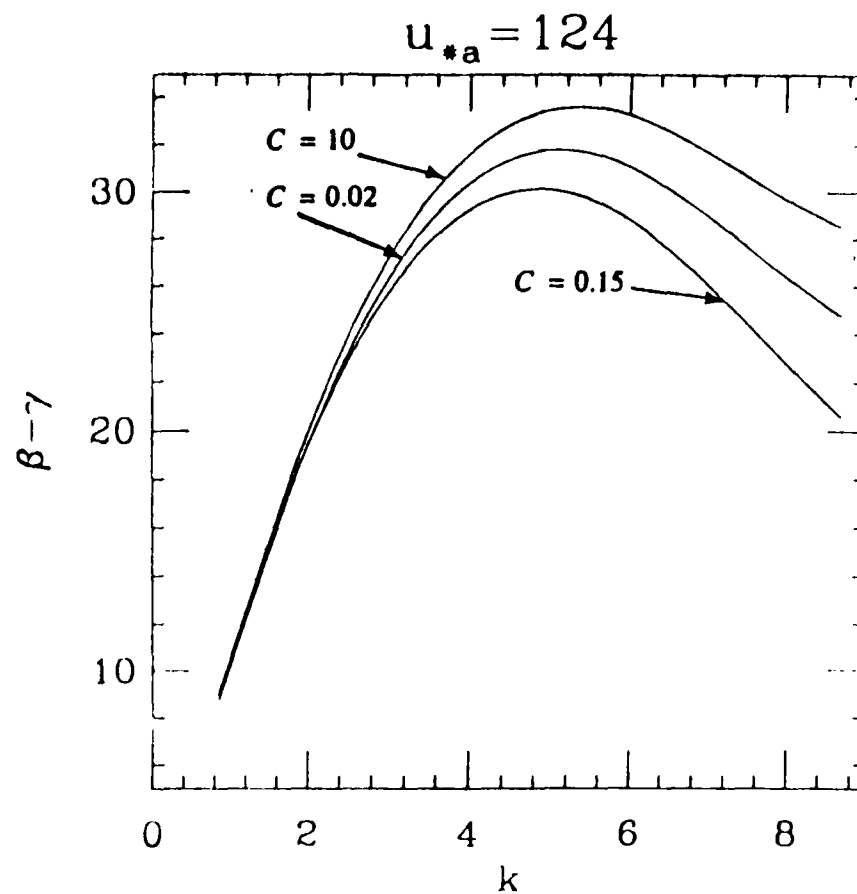


Figure 10

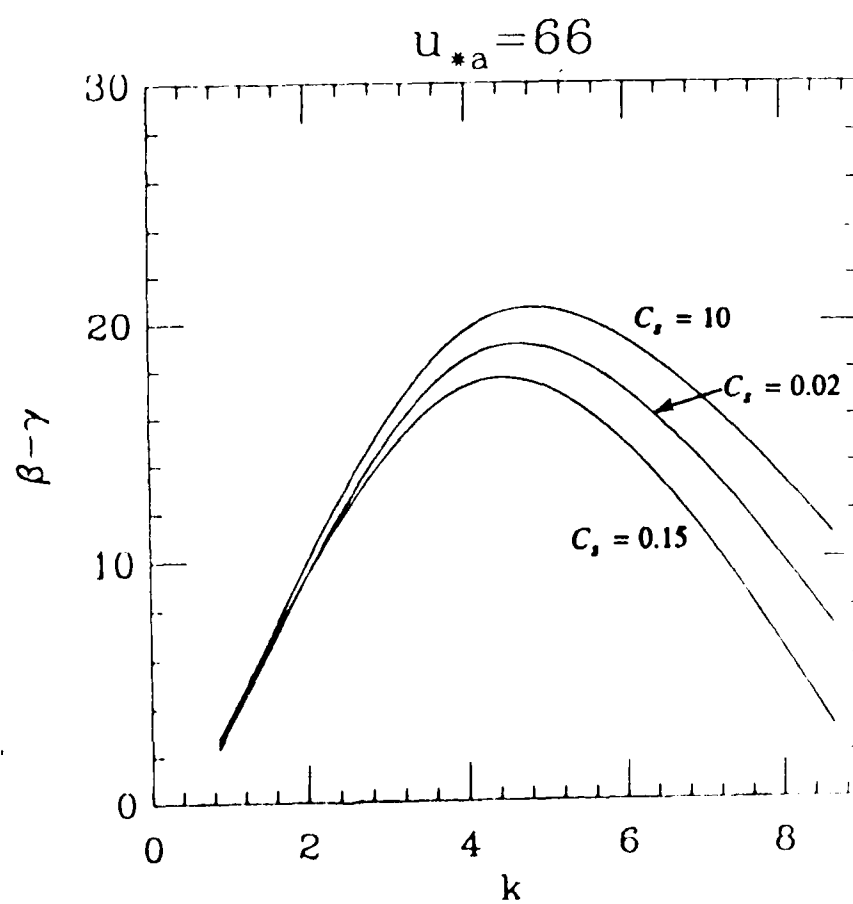


Figure 11

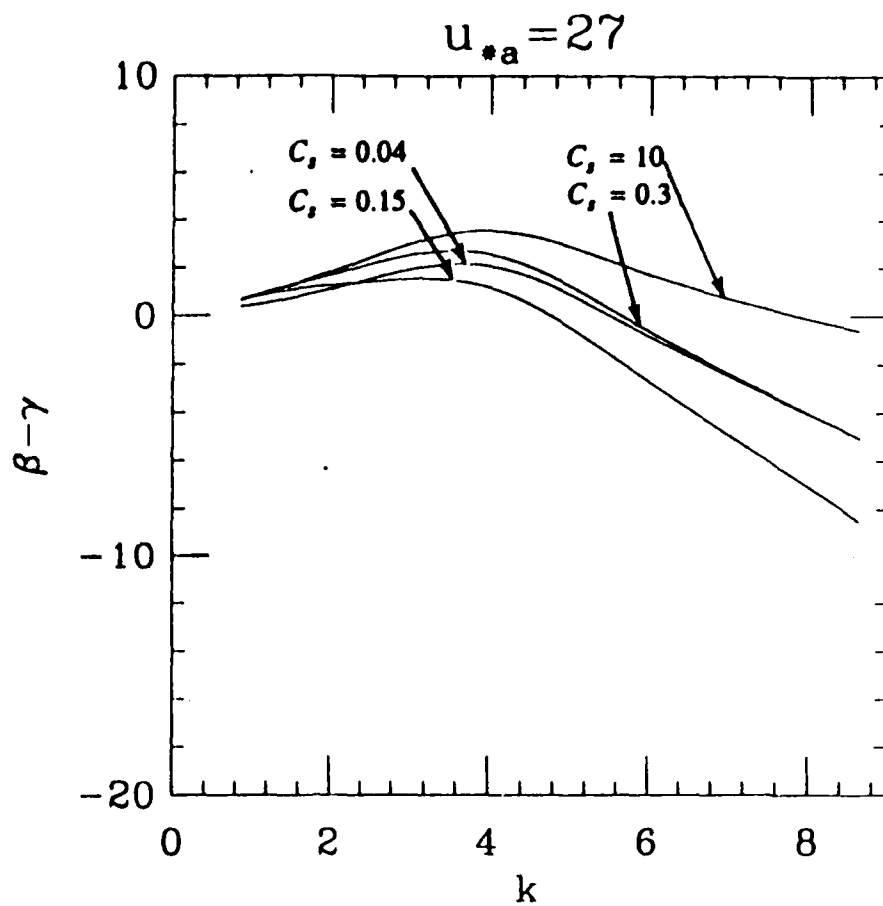


Figure 12

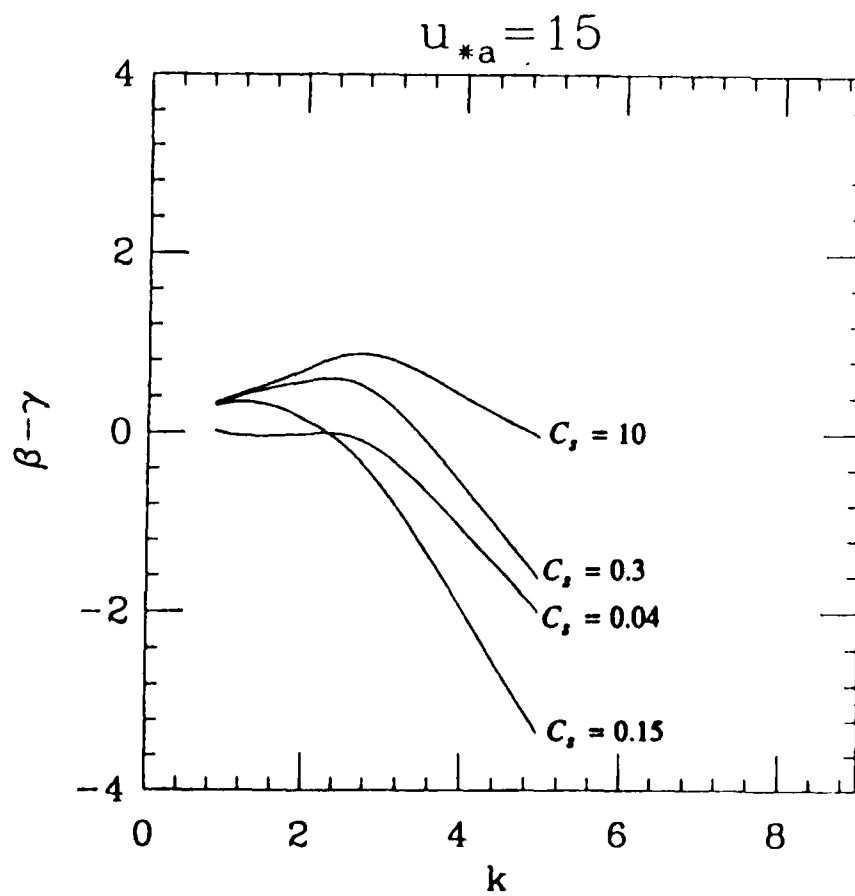


Figure 13

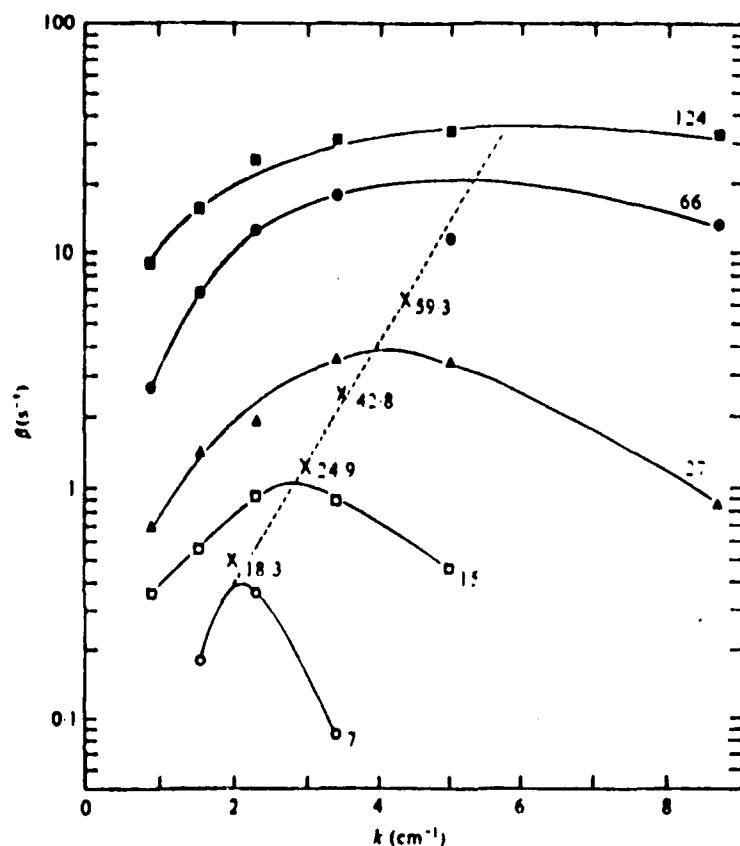


FIGURE 13. Correlation of growth rate β to wavenumber k . ■, ●, △, □, ○, converted from figure 8 of Larson & Wright (1978); x, results of this study for the initial wavelets. Friction velocities in the air $u_{0a,u}$ measured at the fully developed stage are given in cm s^{-1} .

(From S. Kawai (1979))

ACOUSTIC and CAPILLARY WAVE SENSING OF THE MARINE MICROLAYER

John F. Vesecky and Richard G. Johnson

Center for Radar Astronomy, STAR Laboratory
Electrical Engineering Dept., Stanford University

I. INTRODUCTION

Methods of studying the marine microlayer using high-frequency acoustic waves and short wavelength surface ripples are discussed. Acoustic sensing is by no means a new technology, but its application to the characterization of the marine microlayer offers an innovative approach to the study of this medium. Since this is a completely new way of studying the microlayer, many of the ideas which we present here are still only suggestions at this stage. Comments and suggestions are most welcome.

II. OBSERVATIONAL FUNDAMENTALS

Let's first review what is meant by the marine microlayer. Fig. 1 is a schematic diagram of the microlayer to the extent it is generally understood today. In our discussion, we will focus our attention broadly on the top millimeter of the ocean's surface. We particularly are interested in the surface active substances (surfactants) which affect the transfer of energy and material across the ocean's surface (e.g. gas, water vapor, momentum). Dry surfactants are described as oily or fatty surface molecules which consist of a hydrocarbon chain, the majority of which protrudes above the surface. These molecular chains are approximately 30 Å long and for most practical purposes, rest on the water's surface. Water molecules below the surfactant layer may be ordered by the surfactant to a depth of perhaps 100 Å. How much ordering actually occurs is a subject of controversy.

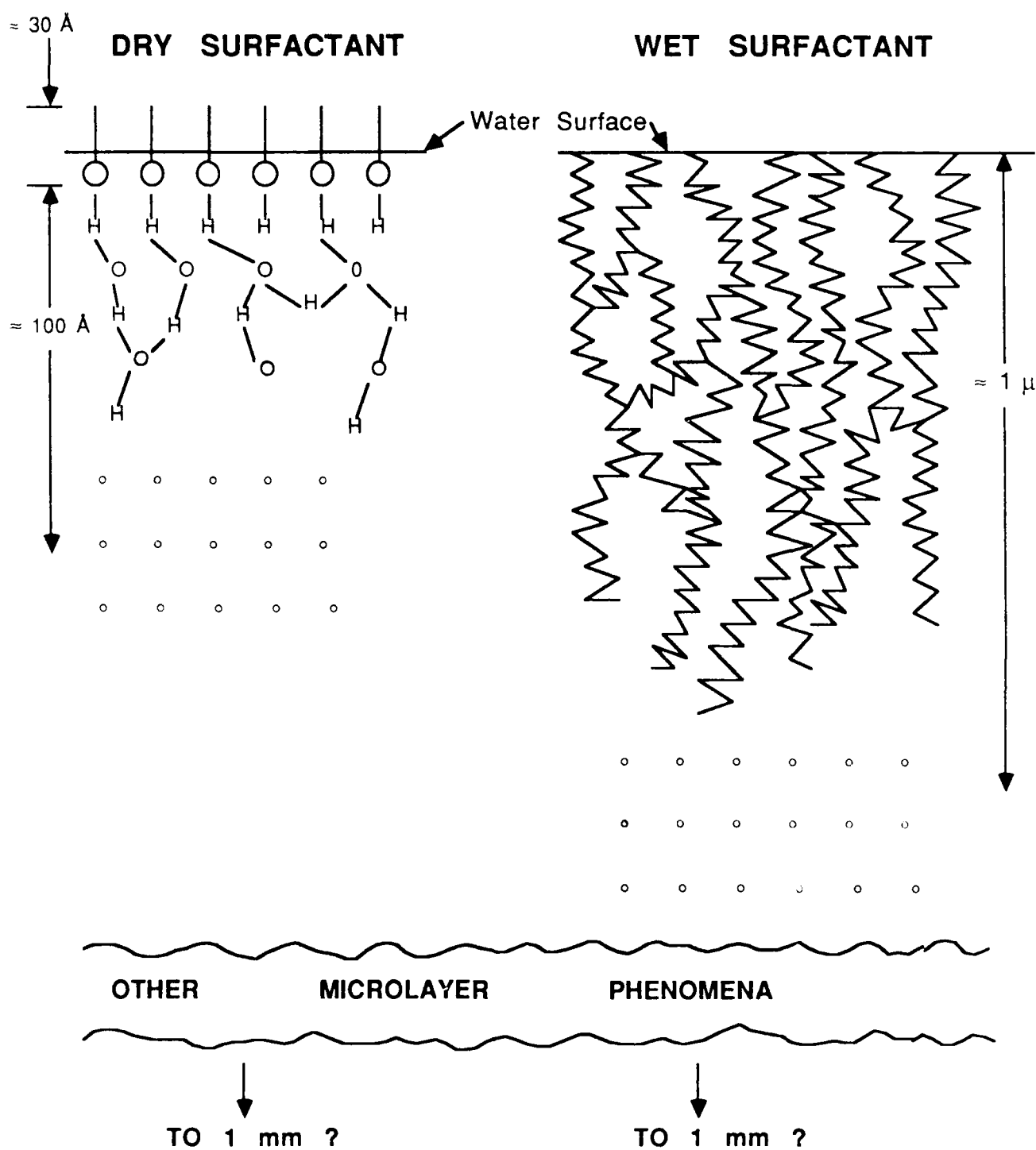


Fig. 1. Suggested schematic diagrams of two microlayer types.

Wet surfactants, which are much more abundant than those that are dry, typically extend to a depth of approximately one micron. These proteinaceous surface molecules comprise a broad group of substances which largely rest beneath the water's surface or protrude only to a minute degree.

Because the scale of the surface layer is so small, we propose the use of very high frequency acoustic waves to study its characteristics. **Remember that the wavelength of a 3 GHz acoustic wave in water is the same as that of green light.** While high acoustic frequencies offer high resolution, they also imply very high attenuation. This seriously limits the range (distance from source to object) over which an acoustic sensor can operate. A compromise will be required to balance the tradeoff between resolution and range. This is illustrated in Fig. 2. In this figure, the range and resolution are plotted for high frequency acoustic waves in water. As frequency increases, the resolution increases; but the range decreases. We think this approach will provide additional information on the elastic properties of the microlayer as well as insight into its structure and the extent of its influence on the water beneath it.

III. OBSERVATIONAL CONCEPTS USING MHZ. AND GHZ. ACOUSTIC WAVES

A. Summary of Concepts

Numerous acoustic techniques could be used to study the ocean microlayer. Each of these has its distinctive advantages and disadvantages; some produce horizontal structure information in images while others produce quantitative measurements of vertical structure without images. Many of these techniques are related and combinations of techniques could be useful. In this report we discuss several promising possibilities. We summarized these below in order of presentation.

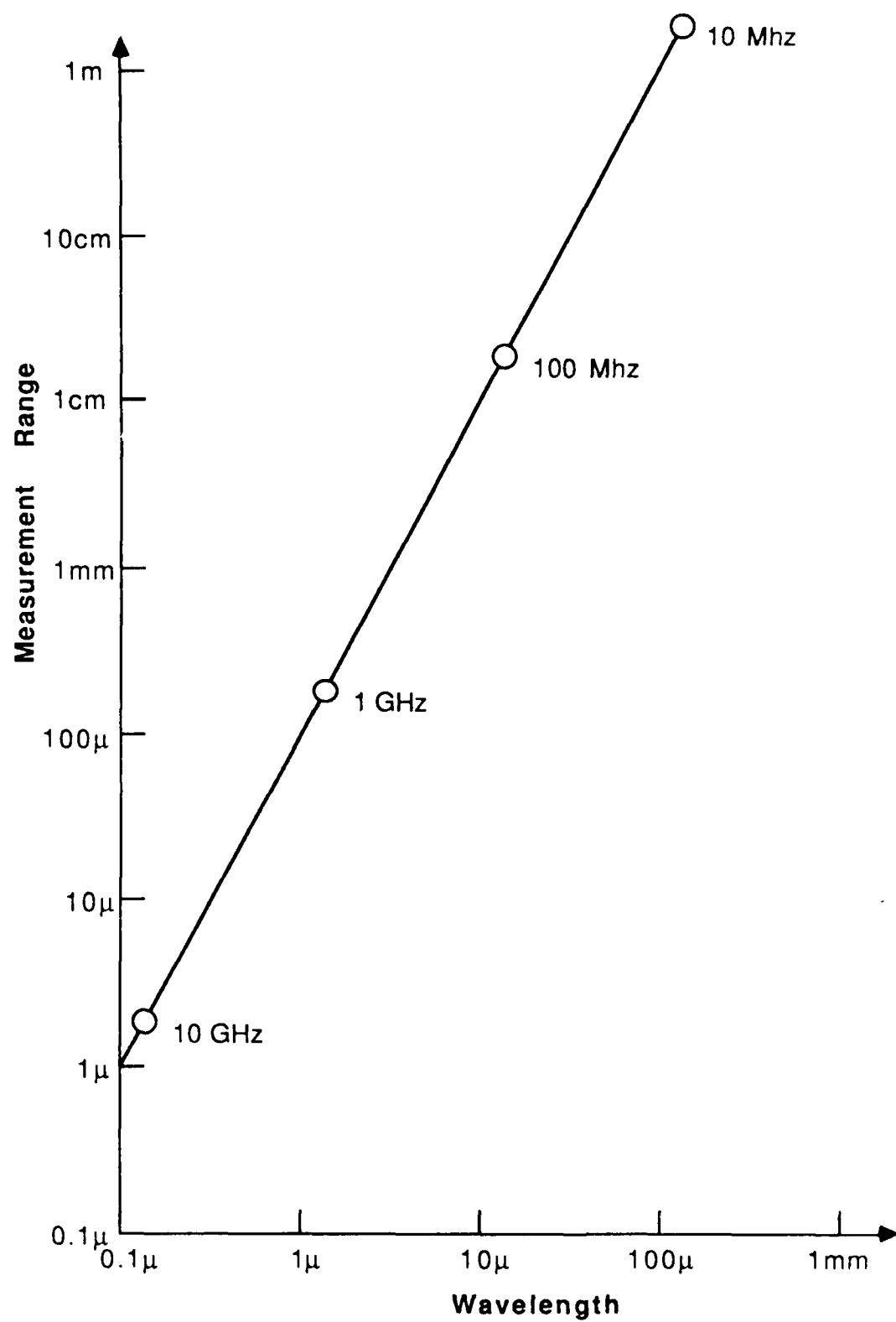


Fig. 2 Range and wavelength of high frequency acoustic waves

- **ACOUSTIC MICROSCOPY** - imaging of microlayer with acoustic wave backscatter
- **ACOUSTIC METROLOGY** - acoustic wave interference yields quantitative microlayer information, no images
- **INTERFACIAL and WAVEGUIDE MODE WAVES** - acoustic wave propagation in and near the microlayer yields quantitative information
- **NORMAL INCIDENCE, TRANSMISSION & REFLECTION** - quantitative microlayer information from standing wave observations
- **VIBRATIONAL MODES OF SURFACE FILM MEMBRANE** - microlayer membrane probing via observation of vibrational modes
- **RIPPLE WAVE OBSERVATIONS** - excitation of surface ripples yields microlayer information via observation of damping & wavelength

B. Acoustic Microscopy

1. Operating principles

We report on acoustic microscopy first because it sets the stage for subsequent discussions, i.e. the order of the topics is not a priority order. Acoustic microscopy is relatively new and has found its first applications within medicine (sonography) and the electronic microchip industry.

The basic idea is illustrated in Figure 3. First, an acoustic pulse is generated by a piezoelectric film, typically made of zinc oxide which efficiently converts about 50% of the applied electromagnetic energy into sound. As the figure below shows, attached to the film is a lens which focuses the energy through an acoustic transmission medium, such as water or liquid helium, at a specific focal point on or within the specimen. The lens frequently is made of a sapphire crystal with a spherical cavity for focusing purposes. To remind the reader of the size scale involved, these lenses are typically some tens of microns in diameter. As acoustic energy is pulsed through the lens, it is converted to a spherical wave at the liquid/crystal interface and focused on the specimen by diffraction. Upon striking the specimen, the acoustic energy is reflected back through the lens to the piezoelectric film which now functions as a detector. The power backscattered from the focal point is recorded and constitutes one picture

element (pixel) in the image of the specimen.

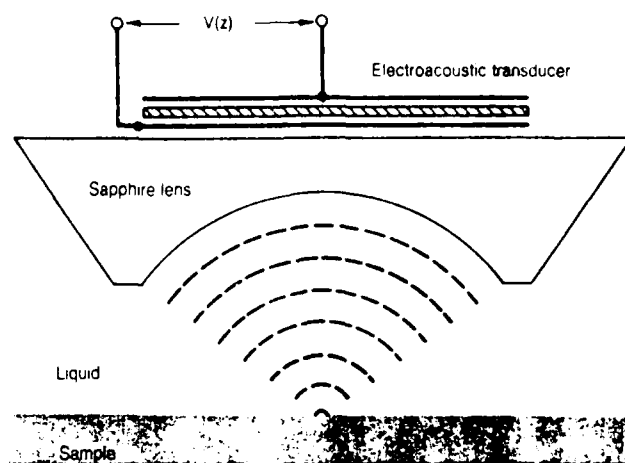


Fig. 3 Typical configuration for making acoustic microscopy measurements. The lens is a spherical cavity in sapphire (after Quate, 1985).

Previous research, such as that described in Quate's (1985) review, has determined that smooth surfaces with different elastic parameters will generate reflected signals that have a distinct characteristic for each material. By scanning the specimen in a raster pattern, an image area of 512 x 512 pixels can be covered in a few seconds. At each point within the area, typically 0.5 microns in diameter, response signals produce a visual image whose intensity of contrast is proportional to the acoustic reflection coefficient of the specimen at that point. When the image is viewed as a whole, the variation in intensity, from point to point, resolves the structure of changes in elastic properties of the specimen along the focal plane. Discontinuities are particularly evident.

Procedures similar to those described here are in commercial use today. For example, they are used to determine irregularities within electronic microchips, to locate calcium deposits in organs within the human body, and to measure the thickness of metallic platings. All measurements are made in a nondestructive manner and without invading the test subject. An example of high quality microscopy using water as the transmission medium is shown in Figure 4. The image of a bipolar transistor is clearly shown with connecting aluminum strips of 2 microns width.

2. Applications to the Microlayer

Laboratory studies of microlayers using acoustic microscopy may provide valuable information on the variations of elastic properties of surface films. Using appropriate focusing techniques, the film/air interface can be examined and the resulting image catalogued for a variety of film compositions. As with other applications of acoustic microscopy, the acoustic image reveals different features than does an optical image. Abrupt changes in the mechanical structure of the microlayer, similar to cracks in a solid specimen, would be particularly evident as would horizontal boundaries between different types of microlayer materials. This property is illustrated in Fig. 4. Thus acoustic micrographs of the ocean microlayer would show the horizontal structure of the microlayer as does an optical micrograph. This would be useful in observing the variety of objects imbedded in the microlayer as well as horizontal irregularities. One particularly interesting feature which would presumably be observed would be the presence and nature of cracks or faults (as one observes in crystalline solids) and how this faulting proceeds as a surface film is compressed.

In order to conduct meaningful laboratory studies of surface films, laboratory techniques would need to be developed which will accommodate these unique specimens. For example, the acoustic beam would probably have to be incident from below (rather than from above as is usually the case) so that gravity can be used to keep the film on the surface. That is, the geometry of Figure 3 would have to be turned upside down. An acoustic conducting medium must be selected which will not interfere or interact with the microlayer specimen. The ocean microlayer fits nicely into a common acoustic



Fig. 4. Image of a bipolar transistor produced using acoustic microscopy with water as the acoustic medium. The connecting lines made of aluminum are 2 microns wide (after Quate, 1985).

microscopy mode with the microlayer floating on water as the acoustic medium. A scanning technique would need to be devised which would keep the microlayer specimen fixed while the lens is moved in raster-like fashion. And finally, frequencies would need to be selected which would allow sufficient signal to noise ratio and resolve desired detail of the components found within the surface film specimen.

C. Acoustic Metrology

1. Operating principles

Fig. 5 shows a schematic drawing of a typical acoustic metrology system. First, we note that the sample specimen is not located at the focus of the acoustic beam formed by the lens. In this configuration there are two separate paths by which an acoustic signal travels from the lens to the specimen and back. There is a narrow central cone of acoustic rays which meet the transducer at near normal incidence. This is shown as the shaded area labeled "A." There is also a second path, labeled B, in which a wave strikes the sample surface obliquely, couples into an interfacial wave mode, travels along the interface, radiates out of the interfacial mode and finally returns to the sensor via an oblique path. The output of the system $V(z)$ is thus the phase coherent sum of the signals traveling via the two paths. The parameter z is the source to sensor distance measured along ray path A, but with z set to zero at the focal distance of the lens. As z is varied, $V(z)$ exhibits interference phenomena as the A and B signals change their relative phase. To couple into the interfacial wave (or out of it) the ray geometry must be such that a critical angle of incidence (θ_c) is exceeded. For a system whose critical angle is greater than the half-angle opening of the lens, no interfacial wave is excited and the resultant signal $V(z)$ is of the form $(\sin z)/z$, expected for simple focussing alone. This corresponds to the $\theta = 30^\circ$ curve in Fig. 6.

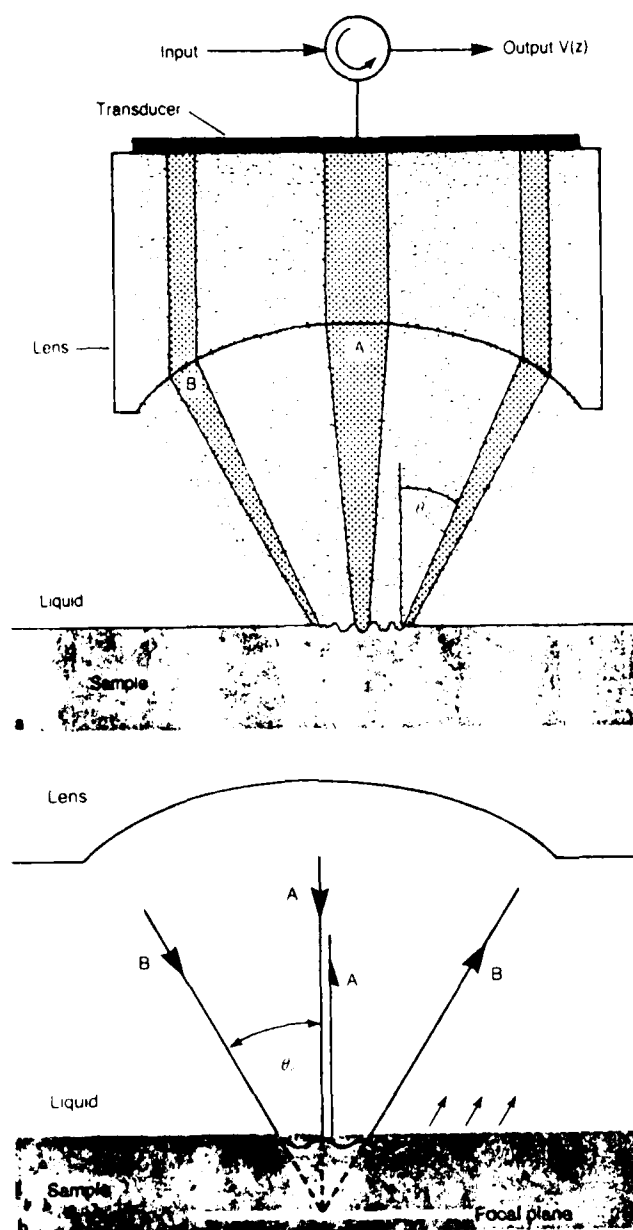


Fig. 5. The upper sketch shows the transducer-lens system emphasizing the central cone and the critical-angle cone. The lower sketch is a ray diagram showing the paths of the two acoustic signals that interfere at the transducer and generate the $V(z)$ curve (after Quate, 1985).

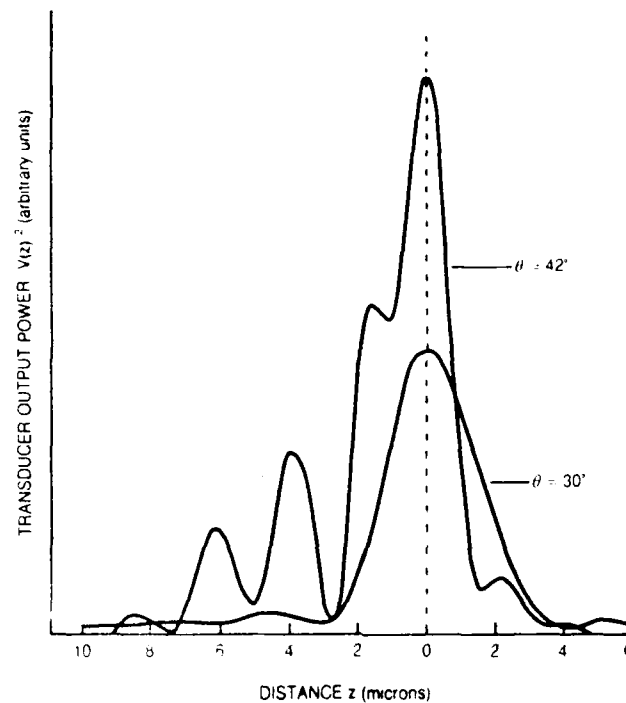


Fig. 6. Typical $V(z)$ curves of acoustic sensor response as the sensor to sample distance is varied. When the lens half angle θ is small, i.e. 30° , interfacial waves are excluded and the $\sin(z)/z$ or focussing curve results. When the opening angle of the lens exceeds the critical angle ($\theta > \theta_c$), the interfacial wave plays a role and interference effects occur as shown in the curve for $\theta = 42^\circ$ (after Quate, 1985).

When incoming radiation strikes the liquid/sample interface at an angle greater than the critical angle (θ_c), an interfacial wave (Rayleigh wave) can be excited which travels along the interface. As the interfacial wave propagates along the surface, it continually reradiates energy back into the liquid at the same critical angle. These reradiated components (leaky waves), can not be distinguished by the sensor from those reflected from the lens focal plane. When the leaky wave and the reflected acoustic wave are vectorially added in the transducer, a resultant detector signal containing interference fringes is produced (Fig. 6) whose amplitude and phase contain information about the

sample. The interpretation of this interference pattern $V(z)$ is an important part of the field of acoustic metrology.

We note that an acoustic microscopy image can be produced with $z \neq 0$. This was a great mystery before the role of interfacial waves was discovered. After much puzzlement it was realized that acoustic images produced with a sensor-sample spacing z other than at the focus ($z = 0$) could enhance the contrast of grain structure in the surface of an alloy (Atalar, 1979). Such 'out of focus' images may have a role in investigating the horizontal structure of microlayers.

2. Acoustic metrology technique

The variation of the transducer output voltage $V(z)$ with distance (z) from the lens to the sample surface has been defined as an Acoustic Material Signature (**AMS**). For a system whose critical angle (θ_c) is less than the half-angle opening of the lens, an interference pattern (consisting of the reflected longitudinal wave and reradiated leaky waves) results and $V(z)$ produces an AMS which is characterized by a series of deep voltage minima having periodic spacing Δz_N .

In Fig. 7 Weglein (1985) illustrates a typical transducer output voltage versus the lens-to-sample spacing, $V(z)$, curve. Notice that the curve contains three distinct regions; only the central portion contains the material-dependent information and it is this region that is referred to as the AMS. The portion to the left of the AMS is the $V(z)$ output observed at a distance z of less than one-half the focal length and is caused by acoustic beam fold-over. The portion to the right of the AMS is the $V(z)$ output observed at z values which are greater than the focal length and is dependent on the lens and liquid acoustic transmission medium.

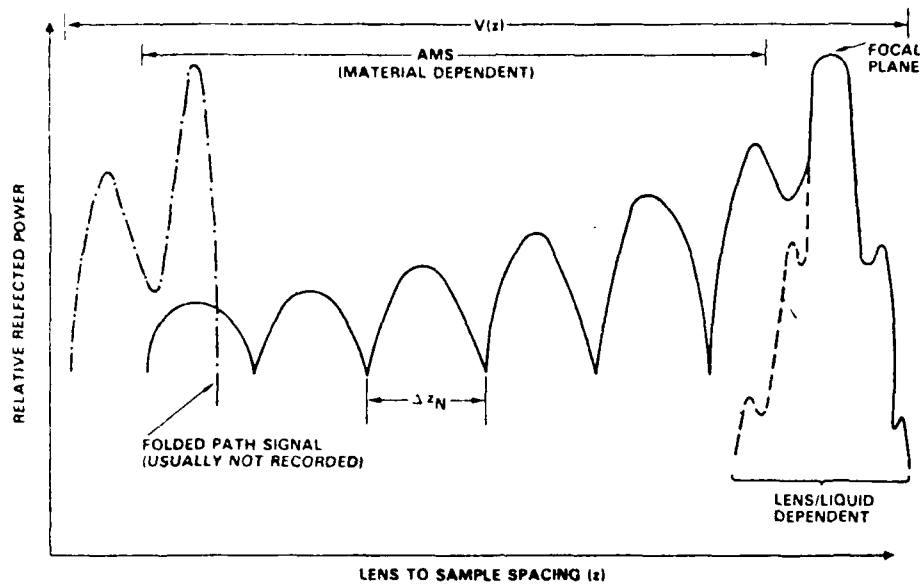


Fig. 7. Typical $V(z)$ curve showing the Acoustic Material Signature (AMS), after Weglein (1985).

The quantitative interpretation of the AMS depends on an understanding of acoustic wave propagation near the sample surface including surface wave modes. For solid samples the periodic spacing Δz_N depends on the Rayleigh surface wave velocity (C_r) of the specimen surface when C_r is sufficiently greater than the sound velocity in water C_w (where water is the acoustic transmission fluid between the lens and the specimen). For materials with C_r less than C_w , the spacing is found to depend on the incident longitudinal wave velocity. Equations which define the spacing Δz_N in terms of the measureable Rayleigh critical angle and wavelength are described by Parmon and Bertoni (1979). They have illustrated the AMS in terms of a ray model.

For solid samples Weglein (1985) has presented numerous case studies in which he demonstrated that the AMS contains both elastic and absorptive information that can be determined through the AMS period Δz_N , through the peak-to-valley amplitude ratio and through deviations from the nominal AMS

curve shown in Fig. 7. He has also shown that the use of low-frequency acoustic energy extends the AMS technique to higher propagating modes than Rayleigh waves. Both bulk longitudinal and Lamb wave modes have been observed. An example of such an acoustic material signature is shown in Fig. 8 for a sample in which a thin (8μ) layer of Copper resides on top of fused Quartz. Note how the AMS is affected by both the Rayleigh and longitudinal wave modes.

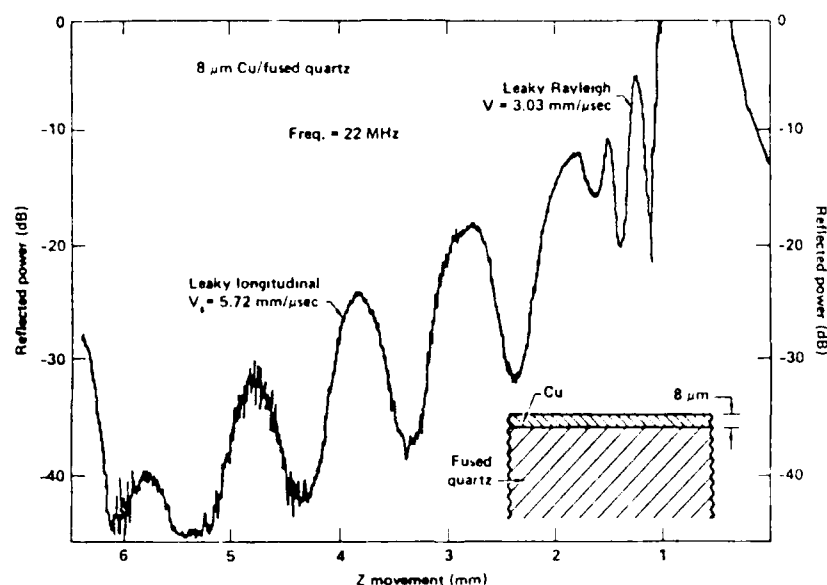


Fig. 8. Extended range Acoustic Material Signature showing both Rayleigh and longitudinal wave modes. The observation frequency was 22 MHz, after Weglein (1985).

Although a comprehensive interpretation of the excitation of these modes has not been completed, it is believed that further examination may permit significantly deeper specimen penetration than has been observed previously. The ocean microlayer is clearly not a solid. However, it has some properties similar to solids and it is likely that the interpretation techniques for solids noted here can, at least, be used for guidance in interpreting AMS's for microlayer samples. We discuss the interpretation question below.

3. Application to the microlayer

To apply the acoustic metrology technique to the marine microlayer we first need to invent a method of obtaining the AMS. As suggested above, we suspect this could be done simply by inverting the customary geometry of Fig. 3, i.e. putting the acoustic lens beneath the liquid surface pointing upward toward the microlayer on top of the liquid.

Since the acoustic wave propagation properties of the marine microlayer and adjacent water are not well known, no interpretation technique is presently available. What we can do is present and briefly discuss a possible hypothesis. Suppose that the atoms of the microlayer influence the water molecules immediately below the surface or extend themselves below the surface as suggested in Fig. 1. Further suppose that this influence creates a near surface region in which the mechanical properties of the are different from those of water including a different speed of acoustic wave propagation velocity. For example, if the influence of the microlayer molecules were to creat a layer of near surface water with mechanical properties somewhere between liquid water and ice, then one would expect a sound velocity somewhere between water (≈ 1500 m/s) and ice (≈ 4000 m/s). One would expect a significant effect in the AMS for acoustic frequencies such that the acoustic wavelength in water is at least several times the thickness of the anomalous layer. Depending on the details of the sound speed profile $C(z)$ near the surface a variety of wave modes could exist as with the Rayleigh wave modes discussed above for solid samples.

We think the best way to proceed with the interpretation is to obtain some experimental data and then try to interpret it. An initial hypothesis for interpretation would be by analogy with the case of solid samples as in Fig. 7 above. Another hypothesis for interpretation would be that discussed in the paragraph above. Having AMS data in hand for a known microlayer, such as oleyl alcohol, would suggest methods of interpretation.

It is our opinion that acoustic metrology holds great promise for investigating the marine microlayer. First, acoustic methods can sense mechanical properties of the microlayer on very small size scales, information which is vitally important in understanding the chemistry and physics of microlayers. Second, acoustic methods appear to be amenable to deployment at sea for obtaining in situ information on marine microlayers.

D. Interfacial and Waveguide Modes

1. Bistatic mode concept-advanced interference

The bistatic mode concept is based on acoustic metrology. The difference is that in the bistatic mode scheme the basic propagation effects are more fully explored in terms of experimental geometry and observables. The basic scheme is illustrated in Fig. 9 below.

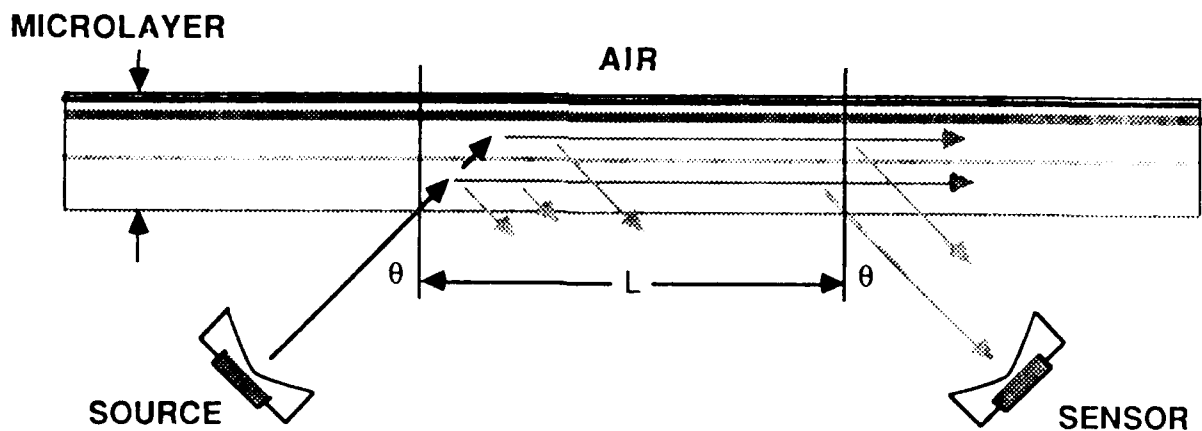


Fig. 9. Bistatic scheme for observing interfacial and waveguide modes propagating in the marine microlayer.

The source and sensor are separated which allows a wider range of observational geometries. Also a wider range of observables would be used than is normal in acoustic metrology. Interpretation of observed data would be done by identifying the several wave modes which could propagate acoustic energy from source to sensor and then studying the characteristics of the signals in each mode which are dependent on the structure of the microlayer. This scheme has elements in common with observations of the Earth's interior using seismic waves and observations of the Earth's ionosphere using radio waves. Below we discuss, in turn, **observables, variables, wave modes** and **interpretation**.

In this bistatic scheme signal amplitude, phase and direction of arrival can be observed as well as fluctuations in these quantities. All these data contain information on the propagation medium, i.e. the microlayer. Application of bistatic transmission schemes analogous to Fig. 9 have been used on much larger size scales with acoustic waves in the ocean (acoustic tomography) and with radio waves traveling through the solar corona (Tyler et al., 1981). The signals directly reflected from the surface or traveling horizontally between source and sensor could be used as references in measuring the observables mentioned.

A number of variables are in the hands of the experimenter in this scheme. Both wave frequency and experiment geometry are very important. The signal path could also be selected to some degree by using a directional source and/or sensor. A single source could also provide signals for several sensors to obtain information on the spatial variation of microlayer properties in the horizontal plane. The particular microlayer material being observed is another controllable variable. For example, different types of artificial microlayer material could be used, like oleyl alcohol or tetradecanol.

Since the structure of the microlayer is not well known, definitive models of acoustic wave propagation modes are likewise not well known. Nevertheless, there are several modes which are likely to be present based on experience with acoustic metrology of solid materials and theoretical

hypotheses. Rayleigh type, interfacial waves are commonly found to propagate along the interface between two media with different mechanical properties as are lateral waves (sometimes known as head or surface skimming bulk waves). One might also expect to find ducted waves in the microlayer medium if the influence of the surfactant molecules produces an appropriate variation of acoustic velocity with depth very near the surface.

Interpretation would be expected to rest upon observing a particular wave mode and then relating the signal observables to the characteristics of the medium which control propagation in that wave mode. Further, one can examine the variation of these observables, namely wave speed, amplitude, phase and direction of arrival with variables, such as frequency, which are under experimental control. For example, the cutoff frequency of a mode would be expected to be related to the thickness of the microlayer. Here thickness would refer to the layer in which acoustic wave propagation properties were different than ambient water. Rayleigh, lateral and ducted waves could all be interpreted in this way if they, in fact, exist in the microlayer. Fluctuations of the observables and interference between modes could also yield information. As mentioned above, these types of interpretation have been in use in geophysics for many years, albeit on a much larger scale, and much of our knowledge of the Earth's interior rests solely on such observations and interpretations.

E. Normal & oblique incidence-transmission & reflection

This method relies on the interference between an incident beam and a reflected beam to form a pattern of standing waves which would be observed in terms of strength, wavelength and position (phase). The idea is illustrated in Fig. 10 below. This scheme is a simple variant of the bistatic scheme in section D. above.

The incident beam and the energy scattered directly back from the surface would interfere to form presumably the strongest standing wave. Energy scattered from other levels in the microlayer would again interfere with the incident beam to form other standing waves of different strength and position. These several standing waves would be superposed and the resulting standing wave observed by the sensor. Interpretation would involve developing an

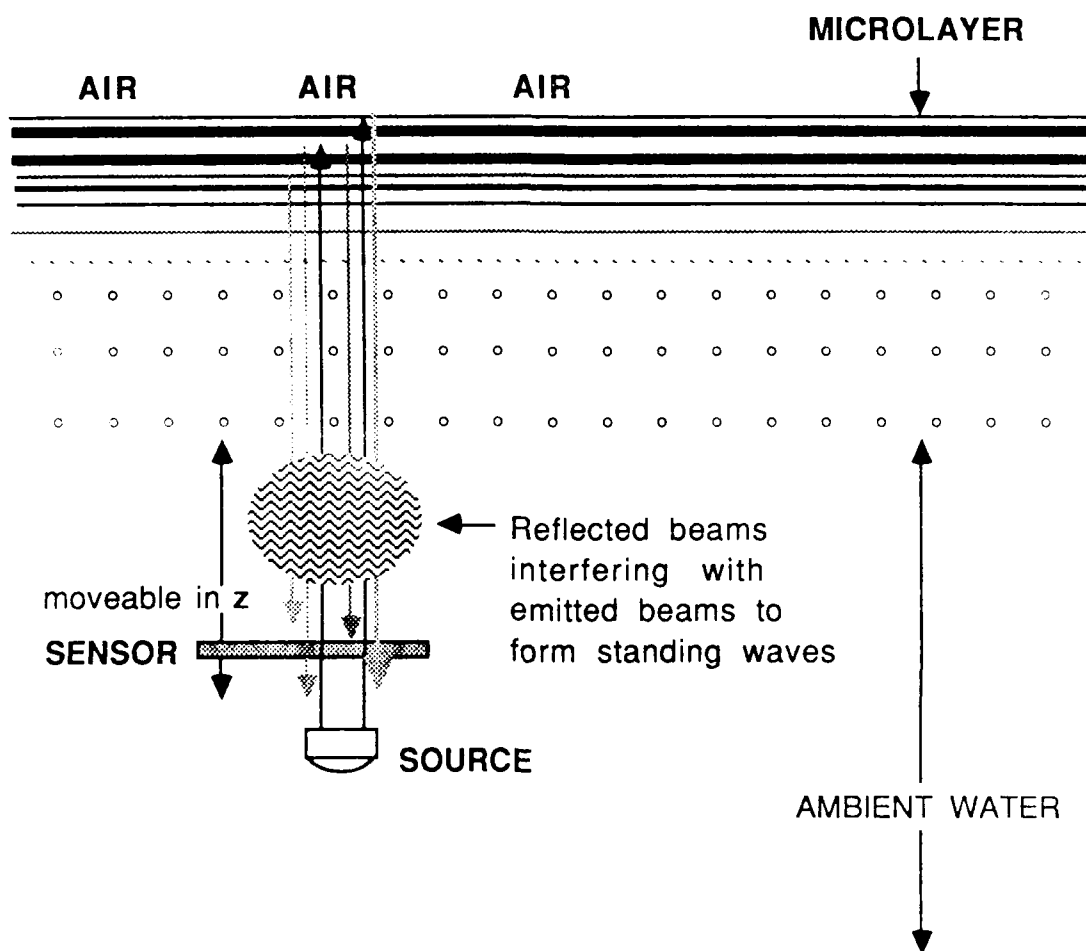


Fig. 10. Standing wave method for acoustic sensing of the microlayer. Sensor moves vertically to explore region of interference between incident and scattered waves.

hypothesis for microlayer structure, e.g. a series of scattering layers at varying levels. This hypothesis would then be used to construct a model with a number of parameters, such as the levels (z coordinate) and scattering strengths of the several layers. This model would then predict the standing wave to be observed. Prediction would be compared to observation with the goal of determining the parameters of the model and confirming or rejecting the hypothesis.

F. Acoustic drum scheme

This scheme exploits the variation of drum head vibrational modes with properties of the drum head material. This scheme is illustrated in Fig. 11 where a sample of the microlayer material is collected on a ring as in blowing soap bubbles. The thin membrane is excited and the vibrational modes observed. The characteristics of the vibrational modes are dependent on the mechanical characteristics of the microlayer material in the membrane. Thus observation of mode characteristics enables one to infer microlayer properties.

The microlayer material would be collected by dipping the ring through the ocean surface and withdrawing it in much the same way as microlayer samples are collected on a prism. The excitation could be done in several ways, for example by an air jet or by using electrostatic forces induced by applying an electric potential between the microlayer and the exciter.

Sensors to observe the motion of the drum head would be placed at several locations appropriate to the pertinent mode characteristics. These sensors would probably be electrostatic in character sensing the change in capacitance between the sensor and the microlayer. Although we have shown simple point sensors in Fig. 11, sensors of other shapes could be used, e.g. to average over an annulus at a given radial distance.

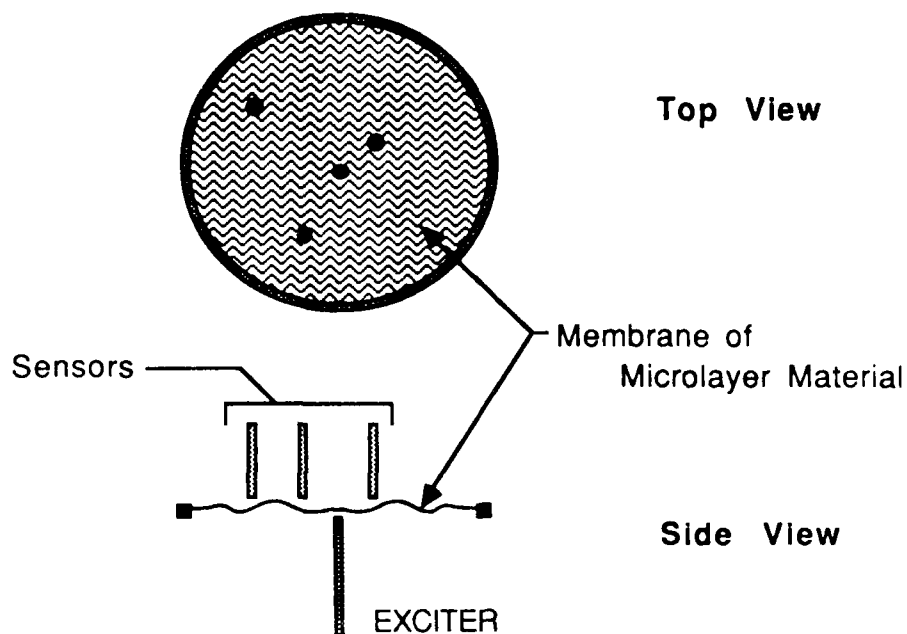


Fig. 11. Acoustic drum sensor for the marine microlayer. Exciter stimulates vibration of the drum head consisting of microlayer material. Sensors observe vibration modes which are dependent on properties of microlayer material.

Interpretation of the observational data would be in terms of the mode characteristics as the excitation frequency is varied. To give a simple example suppose the excitation frequency is varied until one obtains the displacement associated with a zeroth order radial mode. The excitation frequency and the size of the circular membrane then imply a mechanical wave propagation speed for the microlayer material. This speed then implies certain mechanical properties of the microlayer material. A satisfactory theory of mechanical wave propagation would be necessary for interpretation. While the theory of vibration of circular membranes is well in hand for a thin membrane of homogeneous material; e.g. see Croxton (1974) and Pennington

and Stetson (1968); it is presently unknown how well a sample of marine microlayer material would correspond to this simple model.

IV. GENERATION AND OBSERVATION OF RIPPLE WAVES

Perhaps one of the most appealing ways to sense marine microlayer is to observe the effects of the microlayer on short gravity-capillary ripples with wavelengths of the order of mm's to cm's. We point out that these short wavelength ripples form a crucial link between ocean surface films and remote sensing observations. Marine microlayers strongly damp such surface ripples and many remote sensing methods, such as synthetic aperture radar (SAR), respond primarily to the ocean surface roughness which these ripples constitute.

It is well known (Phillips, 1977 or Craper, 1984) that surface films such as the marine microlayer strongly damp surface ripples of the order of mm's to cm's and that the damping is dependent on the properties, concentration and temperature of the film. Further, the dependence of wavelength (λ) on frequency is also affected by surface films. In the study of wave propagation the dependence of wave properties on wave frequency is formalized in terms of the complex dispersion relation $k(\omega)$, where k is the complex wave number and $\omega = 2\pi f$, f being the wave frequency in Hz. The real part of $k(\omega)$ contains the dependence of wavelength on frequency $\lambda(\omega)$ as well as the dependence of group and phase speed on frequency. The imaginary part of $k(\omega)$ contains the dependence of the wave damping coefficient on frequency.

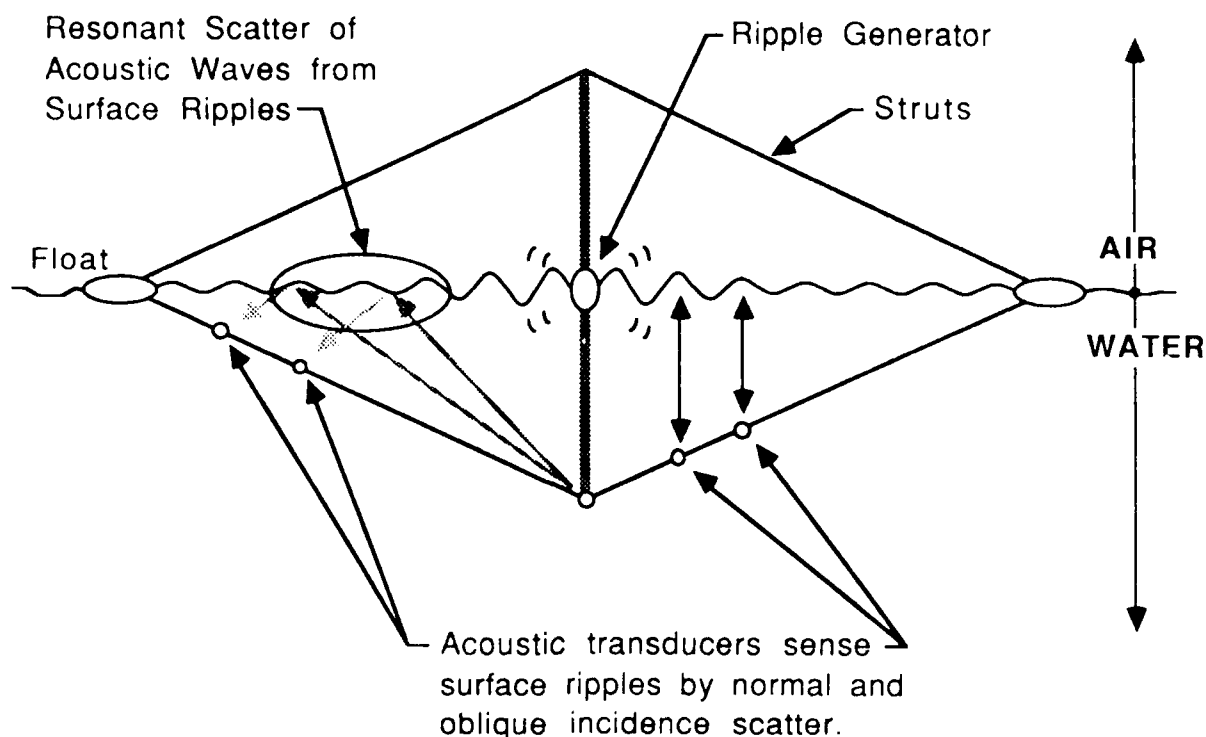


Fig. 12. Schematic view (in cross section) of a scheme to measure surface film properties by observing the dependence of wavelength and wave damping on frequency, i.e. the complex dispersion relation $k(\omega)$. The dispersion relation is dependent on surface film characteristics.

The observational part of this technique involves the generation of short wavelength ripples ($\lambda = \text{mm's to cm's}$) and then observing their wavelength, speed, damping, etc. at a number of frequencies, i.e. observing $k(\omega)$. There are a variety of techniques for generating ripple waves. For example, an electric motor driving a piston, a piezo-electric crystal and puffs of air blowing on the water surface have all been used. Selection of the best generation technique would involve consideration of the environment and power available on a small buoy as well as wave generation capabilities.

Observation of surface waves can likewise be done in a variety of ways. In the diagram we have shown a new techniques using short wavelength acoustic waves in water. Because the range is so short in this situation very short wavelength acoustic waves can be used as suggested in Fig. 2. At these short wavelengths highly directional beams can be generated using rather small devices, see Figs. 3 and 5. Normal incidence scatter of very short wavelength acoustic waves would supply information on the surface elevation which would in turn provide wave characteristics over a period of time, just a resistance wire wave gage does. The oblique incidence method relies on the strong scattering which has been shown to occur when the acoustic waves are resonant with the surface waves, i.e. the horizontal component of the wavenumber of the sensing acoustic waves matches the the wavenumber of the surface ripple waves. This resonant scatter is often referred to as "Bragg scatter" because of the analogy with Bragg scatter from a crystal lattice. In both normal and oblique incidence cases the doppler shift of the received signal can be used to obtain further information.

Interpretation depends on inferring microlayer properties from observaton of $k(\omega)$. The dispersion relation $k(\omega)$ depends on the presence of a surface film and its concentration, characteristics and temperature. The relationship between $k(\omega)$ and surface films has been studied in some detail, e.g. by Phillips (1977), Yermakof et al. (1980), Craper (1984) and Nelson (1985). These studies have all been with the 'forward' problem in mind, i.e. given a microlayer with certain characteristics, deduce $k(\omega)$. Here we are faced with the inverse problem of determining microlayer properties by observing $k(\omega)$. Very little work has been done on this inverse problem which is essential to successful measurement of microlayer properties by observing propagation of ripple waves. However, it seems clear that at least some basic microlayer properties could deduced from $k(\omega)$, in particular the presence of the microlayer (as opposed to clean water) and the surface tension.

V. SUMMARY and CONCLUSIONS

This report suggests several techniques for measuring the properties of the marine microlayer. All of them involve the use of high frequency acoustic waves in the tens of MHz to GHz range. In water, acoustic waves at such high frequencies have the very short wavelengths required to resolve the very small size scales of the microlayer. Below we list these suggested techniques with a very brief description. The list is in order of presentation above.

- **ACOUSTIC MICROSCOPY** - imaging of microlayer with acoustic wave backscatter
- **ACOUSTIC METROLOGY** - acoustic wave interference yields quantitative microlayer information, no images
- **INTERFACIAL and WAVEGUIDE MODE WAVES** - acoustic wave propagation in and near the microlayer yields quantitative information
- **NORMAL INCIDENCE, TRANSMISSION & REFLECTION** -quantitative microlayer information from standing wave observations
- **VIBRATIONAL MODES OF SURFACE FILM MEMBRANE** - microlayer membrane probing via observation of vibrational modes
- **RIPPLE WAVE OBSERVATIONS** - excitation of surface ripples yields microlayer information via observation of damping & wavelength

Although these techniques are still only suggestions at this stage, we think that two of them show particular promise for in situ (and laboratory) investigations of the marine microlayer. **Acoustic metrology** responds to the mechanical properties of the propagation medium on very small and localized size scales. This is just what is needed to investigate the physical structure of the marine microlayer. For example, this technique can probably resolve the issue of the depth to which the microlayer molecules influence the mechanical properties of the ambient ocean water. Further, acoustic metrology techniques appear to be adaptable to in situ ocean use. The application of acoustic metrology to investigation of the microlayer is new and will require significant research effort to bring to fruition. We think such an effort is worthwhile in view of the unique measurement capabilities of the technique.

The **ripple wave generation and observation technique** is less novel, but we think shows significant promise in terms of making basic measurements of the marine microlayer in situ. We believe the physics of the technique is soundly based and that a viable implementation of the method on a buoy is possible. The illustration and discussion of the method given here is necessarily brief and simple. Further research is likely to result in more clever schemes for generation and observation which can produce a robust and useful instrument for very basic measurements, e.g. surface tension. **We also point out that these short wavelength ripples form a crucial link between ocean surface films and remote sensing observations.** Marine microlayers strongly damp such surface ripples and many remote sensing methods, such as synthetic aperture radar (SAR), respond primarily to the ocean surface roughness which these ripples constitute.

ACKNOWLEDGEMENTS

The authors are grateful for financial support from the Office of Naval Research and the encouragement and advice of Dr. Frank Herr of ONR, Chemical Oceanography. *We are also grateful to our colleagues Professors Bert Auld, Ron Bracewell and Pierre Khuri-Yakub at Stanford University and to Professor Jay Mann of Case-Western Reserve for useful discussions and pointers.*

BIBLIOGRAPHY

This bibliography contains not only the references cited in the text, but also a number of other references which the reader may find helpful in delving deeper into the subjects of acoustic microscopy and metrology.

Atalar, Abdullah, Penetration Depth of the Scanning Acoustic Microscope, **IEEE Transactions on Sonics and Ultrasonics**, Vol. **SU-32**, No. 2, March 1985.

Atalar, A., A Physical Model for Acoustic Signatures, **Journal of Applied Physics**, Vol. **50**, No. 12, 8237, December 1979.

Atalar, A., C. F. Quate and H. K. Wickramasinghe, Phase Imaging in Reflection with the Acoustic Microscope, **Applied Physics Letters**, **31** (12), 15 December 1977.

Bertoni, H. L., Ray-optical evaluation of $V(z)$ in the reflection acoustic microscope, **IEEE Trans. Sonics & Ultrasonics**, **SU-31**, 2, March 1984.

Crapper, G. D., **Introduction to Water Waves**, Ellis Harwood, Chichester, 1984.

Croxton, C. A., **Introductory Eigenphysics**, Wiley, London, 1974.

Foster, John S. and Daniel Rugar, Low-Temperature Acoustic Microscopy, **IEEE Transactions on Sonics and Ultrasonics**, Vol. **SU-32**, No. 2, March 1985.

Hartwin, Eric O. and Frank L. Herr, "Chemistry and Biology of the Sea-Surface Interface, Relationships to Remote Sensing," Office of Naval Research Workshop", Sanibel, Florida, 23-25, October 1984.

Hoppe, Martin and Jurgen Bereiter-Hahn, Applications of Scanning Acoustic Microscopy--Survey and New Aspects, **IEEE Transactions on Sonics and Ultrasonics**, Vol. **SU-32**, No. 2, March 1985.

Hunter, K. A. and Peter S. Liss, Organic Sea Surface Films in **Marine Organic Chemistry**, edited by E. K. Duursma and R. Dawson, Elsevier Scientific Publishing Company, Amsterdam, 1981.

Islam, Mohammed N., Hermann A. Haus and John Melngailis, Bulk Radiation by Surface Acoustic Waves Propagating Under a Grating, **IEEE Transactions on Sonics and Ultrasonics**, Vol. SU-31, No. 2, March 1984.

Kessler, Lawrence, W., Acoustic Microscopy Commentary: SLAM and SAM, **IEEE Transactions on Sonics and Ultrasonics**, Vol. SU-32, No. 2, March 1985.

Lee, C. C., C. S. Tsai and X. Cheng, Complete Characterization of Thin- and Thick-Film Materials Using Wideband Reflection Acoustic Microscopy, **IEEE Transactions on Sonics and Ultrasonics**, Vol. SU-32, No. 2, March 1985.

Lemons, Ross A. and Calvin F. Quate, Acoustic Microscopy: Biomedical Applications, **Science**, Vol. 188, 30 May 1975.

Liang, Kenneth K., Gordon S. Kino and Butrus T. Khuri-Yakub, Material Characterization by the Inversion of $V(z)$, **IEEE Transactions on Sonics and Ultrasonics**, Vol. SU-32, No. 2, March 1985.

Lin, Zse-Cherng, Hua Lee and Glen Wade, Scanning Tomographic Acoustic Microscope: A Review, **IEEE Transactions on Sonics and Ultrasonics**, Vol. SU-32, No. 2, March 1985.

Nelson, D., "Suppression of Capillary Waves by Surface-Active Films", Tech. Rpt. JSR-85-206, Mitre Corp., 1820 Dolley Madison Blvd., McLean VA 22102, 1985.

Neubauer, Werner G., Ultrasonic Reflection of a Bounded Beam at Rayleigh and Critical Angles for a Plane Liquid-Solid Interface, **Journal of Applied Physics**, Vol. 44, No. 1, January 1973.

Parmon, W. and H. L. Bertoni, Ray Interpretation of the Material Signature in the Acoustic Microscope, **Electronics Letts.**, **15**, No. 21, 11 October 1979.

Pennington, K.S. and K.A. Stetson, **Scientific American**, Feb., 1968.

Phillips, O. M., **The Dynamics of the Upper Ocean** (2nd ed.), Cambridge Univ. Press, Cambridge, 1977.

Quate, C. F., Acoustic Microscopy: Recollections, **IEEE Transactions on Sonics and Ultrasonics**, Vol. **SU-32**, No. 2, March 1985.

Quate, Calvin F., Acoustic Microscopy, **Physics Today**, 1-8, August 1985.

Robinson, Enders A., Image Reconstruction in Exploration Geophysics, **IEEE Transactions on Sonics and Ultrasonics**, Vol. **Su-31**, No. 4, July 1984.

Schueler, Carl F., Hua Lee and Glen Wade, Fundamentals of Digital Ultrasonic Imaging, **IEEE Trans. Sonics & Ultrasonics**, Vol. **SU-31**, No. 4, July 1984.

Sinclair, D. A., I. R. Smith and S. D. Bennett, Elastic constants Measurement with a Digital Acoustic Microscope, **IEEE Transactions on Sonics and Ultrasonics**, Vol. **Su-31**, No. 4, July 1984.

Smith, Ian R., Robert A. Harvey and David J. Fathers, An Acoustic Microscope for Industrial Applications, **IEEE Transactions on Sonics and Ultrasonics**, Vol. **SU-32**, No. 2, March 1985.

Tyler, G. L., J. F. Vesecky, M. A. Plume, H. T. Howard, and A. Barnes, Radio wave scattering observations of the solar corona: first-order measurements of expansion velocity and turbulence spectrum using Viking and Mariner 10 spacecraft, **Astrophys. J.**, **249**, 318-332, 1981.

Weaver, Jonathan M. R., Michael G. Somekh, Andrew D. Briggs, Simon D. Peck and Christopher Ilett, Applications of the Scanning Reflection Acoustic Microscope to the Study of Materials Science, **IEEE Transactions on Sonics and Ultrasonics**, Vol. **SU-32**, No. 2, March 1986.

Weglein, Rolf D., Acoustic Micro-Metrology, **IEEE Transactions on Sonics and Ultrasonics**, Vol. SU-32, No. 2, March 1985.

Weglein, R. D., A Model for Predicting Acoustic Material Signatures, **Applied Physics Letters**, 34 (3), 1 February 1979.

Weglein, R. D. and R. G. Wilson, Image Resolution of the Scanning Acoustic Microscope, **Applied Physics Letters**, 31 (12), 15 December 1977.

Wilson, R. G. and R. D. Weglein, **Journal of Applied Physics**, 55, 3261, 1984.

Yermakov, S. A., Ye. N. Pelinovskiy and T. G. Talipova, Influence of surface films on changes in wind-wave spectra under the action of internal waves, **Izvestiya, Atm. & Ocean Phys.**, 16, 788-794, 1980.

On the Surface Response Properties of the Microlayer

J. Adin Mann, Jr.
Department of Chemical Engineering
Case Western Reserve University
Cleveland, OH 44106

ABSTRACT

The surface chemistry of the microlayer involves questions of structure, dynamics and function at both the microscopic and macroscopic levels. One ultimate goal is to understand the function of the microlayer in remote sensing applications. This essay builds on two tools for understanding structure and dynamics on the microscopic scale; Brownian dynamics and synchrotron generated x-ray scattering and reflection from the interface. The former is a simulation method from which structure and dynamic information can be estimated. In particular surface density distributions, isotherms and surface visco-elastic coefficients can be estimated. Behavior of polymer surfactants can be investigated. The x-ray techniques depend on the high brilliance of synchrotron sources to allow investigations of the surface structure of liquids and monolayers on the microscopic scale. These measurements and simulations yield information that is useful in understanding the molecular reasons for the magnitudes of surface tension and the surface visco-elastic coefficients determined experimentally. A tool for understanding the macroscopic behavior of the surface film is that of surface profile fluctuations. The theory of surface fluctuation spectroscopy is discussed for both the constant wave number case of capillary waves generated by thermal fluctuations and the constant frequency case for driven waves. The experimental design aspects are discussed for measuring surface fluctuation spectra and therefore the estimation of surface tension and the surface visco-elastic coefficients at the site of the ocean microlayer measurements. We conclude that an instrument can be developed for *ex situ* measurements; ship motion under conditions for which there is a sea film can be tolerated (calm seas, wind conditions of a few meters per second or less). The instrumentation can be adapted for *in situ* measurements in calm seas providing that a sufficiently stable boat or raft is available or can be designed. Active-control technology will be required to stabilize the measurement platform and optical components with respect to the surface of the sea. The light scattering technique will also measure surface velocity fields as well as the surface tension. The effect is similar to laser anemometry that depends on the detection of the motion of particles. Some of the obvious problems in implementing the *in situ* work are discussed. I invite the microlayer community and the remote sensing community to provide suggestions for the solutions of several practical problems discussed herein.

1.0. INTRODUCTION

Of the first one micrometer of a vertical water column in the ocean, the microlayer, only the top 1 to 10 nanometers (10\AA to 100\AA) can be considered the surface or near surface separating the liquid and gas phases. When bare of organic films, the transition region between the liquid and gas phases is only a few water molecules thick. Moreover, volume phase behavior obtains at depths beyond which the anisotropy of the interface (cylinder symmetry with the cylinder axis along the normal to the interface) no longer affects the liquid structure in the neighborhood of a test water molecule. This effect extends through 5 to 10 molecular distances so that water molecules about 5nm from the surface will appear to be in a homogeneous medium. Similar statements can be made when surfactants are adsorbed (or spread) at the interface.

Long-chain polymers can show surface effects beyond that range simply because the motion of different groups along a chain may be correlated by the existence of chemical bonds (the primary structure) along with non-bonding intra-molecular forces that lead to secondary structure. Thus polymer segments may be strongly adsorbed to the interface with loops formed by other segments that are not so strongly adsorbed. In an average sense, polymer adsorption involves a significantly larger interfacial region than when water molecules alone form an interface in liquid-vapor equilibrium. The scale does not change greatly for pure water when electrolytes are added; with polyelectrolytes adsorbed at the interface intermolecular and non-bonding intramolecular forces due to ionization can be modified greatly by the ionic strength of the solution and its pH.

It is also true that hydrodynamical effects of surface structure have a much longer range than 10nm into the water column; the first few micrometers (μm) show distortion of velocity fields as a result of the adsorption of surface-active molecules (surfactants) into the interface. In contrast to molecular properties of the interface, this effect is relatively easy to compute as the result of a boundary value problem. The mass, momentum and energy balances at the surface provide boundary conditions that along with certain continuity conditions for the fields that satisfy the volume equations of motion yields solutions that show explicitly the long-range, hydrodynamic effects of monolayer properties.

It is important to note that surface density, surface tension and surface visco-elastic properties must be known before much can be said about that part of the mechanical behavior of ocean waves that results from the microlayer. Moreover, it is well documented that beyond wave lengths of a few centimeters gravity dominates surface tension as a restoring force (gravity waves); surface tension dominates gravity for wavelengths below about 1mm (capillary ripples).

The experimental evidence developed in various studies of the ocean's surface by remote sensing argues that microlayer effects are important even for observation techniques that should be insensitive to the structure of capillary ripples. This apparent contradiction provides a strong motivation for investigating the structure, dynamics and function of the microlayer. In particular, this paper is an essay on the structure and dynamics of the interface that should be measured, with an emphasis on light scattering techniques and theoretical tools that can be useful in understanding the function of the microlayer in the context of remote sensing. Refer to my paper in Langmuir¹ for details that will not be repeated herein.

2.0. STRUCTURE

Think of the structure of the liquid vapor interface from the viewpoint of molecular density distributions; $\rho(\vec{x}, t)dV$ is the number (or the mass) of molecules at \vec{x} in a small volume dV . The density can be defined for each component, $\rho_i(\vec{x}, t)$ $i = 1, 2, \dots$ where by convention the first component will be water. Then by definition the excess of the given component, Γ_i , is defined by

$$\Gamma_i = \int_{-\infty}^{+\infty} (\rho_i(\vec{x}, t) - \rho_i^{\pm}) dz \quad (1)$$

where ρ_i^{\pm} is the density "far" from the interface. The concepts used here can be found in Adamson's textbook¹. In particular, the idea of a Gibbs surface is required. Since at some surface parallel to the interfacial region ρ_i^{+} switches to ρ_i^{-} , the integral, eq. (1) must depend on the location of that surface. The commonly used convention of taking $\Gamma_1 = 0$ as the definition of the Gibbs surface will be used herein; the excess of water is assumed to be zero. Recognize that the average $\rho_i(\vec{x}, t)$ is continuous through the interface although its gradients may be large there. This behavior has been studied by molecular dynamics, by statistical mechanical formulations, and now by x-ray reflectivity.

Since equation (1) is written as a function of time, the implication is that in some sense it is correct for non-equilibrium, dynamical systems. This is the case when the interfacial thickness is sufficiently small that the characteristic distance h_c in

$$\Gamma_i \cong \int_{-h_c}^{h_c} (\rho_i(\vec{x}, t) - \rho_i^{\pm}) dz \quad (2)$$

is small compared to the hydrodynamic length scale, e.g. λ_r , the ripple wave length. This is surely the case when $h_c \leq 10\text{nm}$ as is the situation for temperatures far from the critical temperature.

Similar formulas can be constructed for the surface tension or surface pressure and for the surface tension tensor. Thus it is possible to connect directly the continuum field variables of Γ_i, \vec{v}_i^s , the surface tension γ and the surface pressure tensor, Π .

It is also possible to construct formulas for the surface visco-elastic coefficients from general principles of statistical mechanics. Such connections provide a path for interpreting measurements of isotherms and visco-elastic coefficients as implying the existence of possible surface structures. For example, the magnitude of the dilational elastic modulus of a monolayer along with the isotherm can be taken as evidence that the monolayer is in a particular state, e.g. the solid state. However, such data is not sufficient to decide whether the monolayer is a two-dimensional crystal or a disordered solid.

I will briefly describe a theoretical tool that is valuable for connecting molecular structure to macroscopic variables and close this section by mentioning various experimental techniques for doing the same thing.

2.1. Molecular Structure by Theoretical Methods.

It is now possible to do useful simulations of the effects of molecular structure on the macroscopic properties of monomolecular films. The density distributions of surfactants can be estimated in detail including questions about thickness of the interfacial region when polymers are adsorbed. Conditions under which two-dimensional phase transitions might occur can be investigated. Tjatjopoulos^{2,3}, in this laboratory, determined how to integrate accurately (third order in space, second order in velocity) the Langevin equation, equation (3), for molecular force laws and realistic constraint potentials under a variety of conditions. While starting with various published algorithms, see references in 4,5,6, he greatly improved the accuracy by which trajectories are computed subject to constraints of various types. This is not the place to describe these technical details. However, a brief resume will hint at how these simulations have the potential of expanding our understanding of the structure and dynamics of the interface that the microlayer contains.

The trajectories for the phase space (the space of all positions and momenta) of the surfactant molecules are computed from coupled, ordinary differential equations of the form

$$M_i \frac{d\vec{v}_i}{dt} = -\sum_j \xi_{ij} \cdot \vec{v}_j + \vec{F}_i + \vec{F}_{i\Sigma} + \delta\vec{F}_i \quad (3a)$$

$$\frac{d\vec{x}_i}{dt} = \vec{v}_i \quad (3b)$$

In this equation M_i is the mass of the i th molecular fragment, \vec{v}_i is the velocity, ξ_{ij} the friction coefficient tensor, \vec{F}_i is the force that each fragment responds to as a result of contributions from every other fragment including intermolecular and intramolecular forces, $\vec{F}_{i\Sigma}$ is the force a fragment responds to due to the density gradient at the interface and finally $\delta\vec{F}_i$ is the fluctuating force caused by the background of water molecules. Another term accounting for external fields may be added but is not relevant to this essay.

At this time, a rather drastic approximation is made for the friction coefficient tensor, ξ_{ij} . The sum is replaced by either $6\pi\eta a$ (stick boundary condition) or $4\pi\eta a$ (no-stick) where a is the radius of the fragment and η the macroscopic viscosity of the solvent. Better approximations are known but the computations are far less efficient. The penalty is that macroscopic properties such as the surface diffusion coefficient and the surface viscosity coefficient will be poorly approximated; the results will be correct at least to order of magnitude. However, thermostatic properties do not suffer by this approximation.

The molecular structure of surfactants enters in the details of \vec{F}_i and $\vec{F}_{i\Sigma}$. It is practical to represent surfactant molecules as strings of beads of the sort developed in the simulation of polymer motion⁴. Our model for the interaction of surfactant molecules is considerably more detailed than Kox, et al⁵ and extends the model of van der Ploeg and Berendsen⁶ in several important ways. Firstly the integration algorithm is considerably improved, secondly the intermolecular and intramolecular potentials are now more realistic in my opinion and lastly, the potential that a molecular fragment

responds to near the interface is represented by a much more realistic potential³, described next.

In essence the potential that a polar group must respond to when moving toward the interface is zero until when within a few molecular dimensions of the interface, the fact that the gas phase provides fewer molecules interacting with the polar group generates a potential well. The potential well is shallow, only a few kT units deep. If the polar group moves toward the vapor phase it is repulsed by a barrier as should be expected. A non-polar hydrocarbon fragment behaves in the opposite way with a weak attractive well on the vapor side of the interface and a barrier to penetration into the polar phase. The model for this behavior allows adjustment of the height and location of each barrier and the depth and location of the potential wells.

In essence the hydrophilic-hydrophobic balance can be adjusted to provide realistic behavior of monolayers including adsorption-desorption and segment effects of polymer surfactants including looping away from the interface.

The following properties can be calculated from the trajectories $\{\vec{x}_i, \vec{v}_i\}$ collected after enough time steps have been computed in the simulation to reach equilibrium:

- a. One may plot and therefore study distinct states as the ensemble evolves in time. A proper graphical representation as for example, an isometric 3D projection, reveals the configurations that are favored. Are the chains kinked? Are there polymer loops out of the interface? How long do they persist? Does desorption occur? Are there slow changes in configuration?
- b. Isotherms can be computed. Conditions for phase transitions can be detected but unfortunately the states close to phase transitions involve fluctuations in structure larger than the control volume set in the simulation. The control volume is limited by the number of particles that can be followed in a given sequence of time steps. This limitation is imposed by the memory capacity of the computer and the number of time steps that can be executed within the limit of the CPU hours available.
- c. Various density functions can be computed that are useful for understanding structure; polar group distribution in the Gibbs surface, chain tilt, chain order parameters, distribution of various fragments along the normal,...
- d. X-ray diffraction structure factors and interference functions can be estimated.
- e. The surface pressure tensor and the two-dimensional elastic moduli can be estimated.

Certain dynamic quantities can also be estimated and they will be mentioned in a later section.

2.2. Molecular Structure by Experimental Methods

There is a lack of experimental methods for determining the molecular structure of monolayers and what "established" methods there are were described in my Langmuir paper¹. A new experimental method was recently suggested by Zare⁷ that could be useful in the study of microlayers. I will also briefly describe the x-ray (synchrotron source) technique developed by Pershan and Als-Nielsen⁸ since it is the only scattering technique that is capable of resolving monolayer structure on the scale of 0.1nm to 2nm.

The very high brilliance of synchrotron radiation can be used to advantage in measuring reflection and scattering properties of liquid interfaces and thereby resolve structure on the molecular scale. Pershan and Als-Nielsen⁸ measured the intensity of x-ray photons reflected by (octyloxy)cyanobiphenyl in the liquid state close to the isotropic/nematic liquid crystal phase transition. Their scans were to both sides of a characteristic wave number (1.989nm^{-1}) that corresponds to 0.5nm in direct space. They found that the x-ray reflectivity followed the Fresnel reflection law until the characteristic wave number was reached wherein deviations were found that could be related to structures in the interfacial region. More recently, Pershan¹⁰ has published on the x-ray reflectivity of water. They found that there was no special structures resolved close to the interface. Moreover, they estimated that the mean square elevation of the surface fluctuation was about 0.337nm. This number is consistent with light scattering results for photons of much longer wave lengths (514nm, 632.8nm).

In my opinion, our understanding of the microlayer structure could be enhanced by two studies involving synchrotron radiation. Firstly, the surface structure should be determined for aqueous solutions of electrolytes including native sea water free of surfactant. I anticipate that little if any structure will be found; the results should parallel the pure water measurements. The use of so-called structure makers and structure breakers are likely to be ineffective in changing the surface structure of water but the situation must be resolved experimentally. With this background, the reflectivity of microlayer samples will be most interesting to explore. Film balance experiments similar to the ones reported by Barger and Means⁹ can be done as x-ray reflectivity data is collected. That is, structure information can be gathered as a function of film density. Moreover, fluorescence yield measurements can be made as a function of the incident wave-length and incident angle of the x-ray beam. These data provide additional information about structure including information about near-neighbor distributions through EXAFS, for example.

In principle spectroscopy techniques such as Fourier transform infrared (FTIR) can give considerable structure information. However, even though impressive advances have been made, FTIR is still not sufficiently surface sensitive for investigating naturally occurring surface films. Similar comments obtain for other spectrometric techniques.

Zare⁷ has described an interesting new experiment that would use the very sensitive detection of capillary waves that is possible with optical interferometry. The idea is to illuminate a patch of surface with a beam from a tuneable laser. Just as in photo-acoustic spectroscopy, when the frequency of the incident light beam corresponds to quantum transitions in adsorbed molecules there will be absorption resulting in micro amounts of heat transferred to the interface. The result then is a change in the surface fluctuation amplitude which can be detected by a number of different methods. Since the incident beam can be pulsed, coherent detection methods can be used to improve the signal to noise ratio.

To my knowledge, this experiment has not been done by Zare's group but it is clear that it should be attempted using state of the art laser technology and capillary ripple interferometry.

3.0. DYNAMICS

3.1 Capillary Ripple Theory and Light Scattering.

There are several reviews of capillary ripple theory from the viewpoint of surface chemistry and they will only be cited herein.^{11,12,13,14} Several authors have attempted to develop the theory of these waves from the viewpoint of continuum mechanics¹¹ or "rational mechanics"; this approach will not be discussed. Rather, the emphasis will be on the amplitude function defining deviations away from a Gibbs surface.

Define the surface by the transformation

$$\Sigma \begin{cases} x = x \\ y = y \\ \zeta = \zeta(x, y, t) \end{cases} \quad (4)$$

It is Fourier components of this elevation, $\zeta(x, y, t)$, that are observed in the light scattering experiments from which estimates of the interfacial tension, γ , and also certain visco-elastic coefficients can be computed. The irradiance in the far field due to scattering is proportional to the square of the electric field which in turn depends on ζ through its Fourier components in wave number space. Moreover, it is the elevation that is determined in the method of forced capillary waves wherein what amounts to a Fourier decomposition in frequency space is analyzed. This duality

is worth developing just a bit farther so as to provide the context from which instruments can be designed to measure the surface tension of the ocean in situ.

First consider the light scattering experiment as shown in figure 1A. It is possible and necessary for any ocean experiment that the reflected beam be analyzed rather than the transmitted beam shown in figure 1A. The analysis of the reflected beam differs little from that of the transmitted beam and the differences are not important for this essay. Edwards et. al.¹⁵ and Lading et. al.¹⁶ and before them Hard et. al.¹⁷ have analyzed the spectrometer wherein the reflected beam is observed in the far field. The only point to recognize is that the geometry of the grating and the spatial filters determine the wave length of the ripple modes observed at the detector. Define the wave number $q = 2\pi/\lambda_{\text{ripple}}$ then the finite Fourier transformation of the elevation in a bounded patch of surface is

$$\zeta(x, y, t) = \sum_{\vec{q}} \zeta_{\vec{q}}(t) e^{i\vec{q} \cdot \vec{x}} \quad (5)$$

The autocorrelation function of the photocurrent generated by a square-law detector in the far field is^{15,16}

$$R_i(k_e, \tau) = \frac{1}{2} \int dq_x \int dq_y < \zeta_{\vec{q}}^*(0) \zeta_{\vec{q}}(\tau) > F^2(k_e - q_x, q_y) \quad (6)$$

where F is an instrument function that is sharply peaked at $k_e = q_x$ and $q_y = 0$ when the incident beam is of large cross section. Under practical conditions, F contributes an excess time damping over that expected from the autocorrelation function of the elevation,

$< \zeta_{\vec{q}}^*(t) \zeta_{\vec{q}}(t + \tau) >$. Fortunately the frequency of oscillations in

$R_i(k_e, \tau)$ and $< \zeta_{\vec{q}}^*(t) \zeta_{\vec{q}}(t + \tau) >$ for $q = k_e$ are nearly the same so that the surface tension can be accurately determined under field conditions even though the width of the spectrum is distorted. Moreover, the parameters in the function F which includes the beam diameter at the surface, the angle of incidence and the effective grating wave number as seen at the surface can all be estimated accurately. It has proven possible to determine corrections to both the apparent frequency, ω and mode damping frequency Γ . There are details that are better left to paper citations.^{15,16}

The relationship between $< \zeta_{\vec{q}}^*(0) \zeta_{\vec{q}}(\tau) >$ and the several visco - elastic coefficients of interest, including the surface tension and a complex dilational-type of elastic coefficient is determined by macroscopic equations of motion. Moreover, adsorption and other dynamics can also be determined for processes with characteristic

relaxation times in the frequency ranges probed by the spectrometer. These same coefficients are determined in the forced wave experiment wherein ω is fixed and real. Both the theory for the correlation function in time (constant q , complex ω) and the wave form in space (constant ω , complex q) begin with the equations of balance in the surface and the volume phases.

The computation of the response of an interface to either forced or natural fluctuations is based on the field equations of fluid mechanics which express conservation of mass, momentum and energy. Since the fluctuations considered are of small amplitude compared to the wave length, the linearized form is sufficient. In addition there are certain boundary conditions, such as the continuity of velocity at the interface, that must be involved in solving the equations of motion. The linearized balance equations are given next:

Surface:

$$\text{Mass} \quad \frac{\partial \Gamma_i}{\partial t} + \nabla_{\Sigma} \cdot \vec{\Gamma}_i \vec{v}_i^s = -n \cdot [\vec{J}_i] \quad (7)$$

for components 1, 2, ..., N

Momentum

$$\text{Normal component; } 0 = \gamma \left(\frac{\partial^2 \zeta}{\partial x^2} + \frac{\partial^2 \zeta}{\partial y^2} \right) - \hat{n} \cdot [\underline{P}] \cdot \hat{n} \quad (8)$$

$$\text{Projection onto the surface; } 0 = \nabla_{\Sigma} \cdot \underline{g} - \hat{n} \cdot [\underline{P}] \cdot \underline{U}_{\hat{n}} \quad (9)$$

Where Γ_i is the excess of the i^{th} component, \vec{v}_i^s is the velocity field on the surface, \vec{J}_i the volume flux and $[\vec{J}_i]$ the jump of the volume flux at the surface (the adsorption flux), \underline{P} is the pressure tensor in the volume phases and $[\underline{P}]$ its jump across the surface and $\underline{U}_{\hat{n}}$ projects the result onto the surface. Finally \underline{g} is the surface tension tensor.

Volume (one set for each phase):

$$\text{Mass; } \frac{\partial \rho_i}{\partial t} + \nabla \cdot \vec{J}_i = 0; \quad \nabla \cdot \vec{v} = 0 \quad (10)$$

$$\text{Momentum; } \rho \frac{\partial \vec{v}}{\partial t} = - \nabla \cdot \underline{P} + \rho \vec{f} \quad (11)$$

where \vec{J}_i is the volume flux of the i^{th} component and \vec{f} the volume force, (gravity, electric field, etc.). Convection is ignored in (10) but can be added without much complication.

It is not necessary to develop these equations in any detail for what is to come but several remarks are appropriate. Temperature gradients are excluded only because isothermal systems have been the special focus of the surface chemistry community; the effects of thermal gradients may need to be included in the formulation for *in situ* experiments on the ocean. The normal component of the momentum transport at the surface is a generalized form of the Laplace equation of capillarity². The surface pressure ($\Pi = \gamma_0 - \gamma$, γ_0 the surface tension for $\Gamma_i = 0$, $i = 2, 3 \dots$ with $\Gamma_1 \equiv 0$) is commonly measured in film balance experiments.^{1,2}

A constitutive equation must be set down relating the surface stress to the surface strain and time-rate-of-strain. In the linear response approximation and for cylinder waves moving in the x direction.

$$\sigma_{xx} = \Pi + (\bar{G} + \bar{K})u_{xx} + (\bar{\eta} + \bar{\zeta}) \dot{u}_{xx} \quad (12)$$

where by construction the deviation away from the uniform state characterized by Π and Γ constant everywhere is represented by the elastic coefficient $K_e = \bar{G} + \bar{K}$ and the viscosity coefficient $K_v = \bar{\eta} + \bar{\zeta}$. The coefficients \bar{G} and \bar{K} are the shear and dilational elastic moduli and $\bar{\eta}$, $\bar{\zeta}$ are the shear and dilational viscosity coefficients respectively. For isotropic systems this equation can be generalized to model the non-linear response of monolayers by taking \bar{G} , \bar{K} , $\bar{\eta}$ and $\bar{\zeta}$ as functions of the invariants of the strain and time-rate-of-strain; higher order terms in the strain \underline{u} and time-rate-of-strain $\underline{\dot{u}}$ can be telescoped to the first order terms in two-dimensions.

The monolayers found on the ocean and measured *ex situ* appear to be in expanded states for which $\bar{K} = \Gamma \frac{\partial \Pi}{\partial \Gamma}$ is of a modest magnitude; Barger and Means⁹ report 14-20d/cm. These monolayers are undoubtedly at best liquids so that the shear elastic coefficient, \bar{G} , is zero. Moreover, the state is likely such that $\bar{\eta}$ the shear viscosity of the monolayers is ignorable when compared to $\bar{\zeta}$, the dilational viscosity of the monolayer.

The Fourier transform in time of the constitutive equation gives

$$\hat{\sigma}_{xx} = (k_e - i\omega k_v) \hat{u}_{xx} \quad (13)$$

It is convenient to write

$$\hat{E} = k_e - i\omega k_v \quad (14)$$

as the complex surface visco-elastic coefficient. As the Lucassens have shown^{12,18}, considerable detail can be built into \hat{E} about monolayer relaxation processes including reorganization of the monolayer as well as exchange of material with the substrate. Some of these details are developed in Lucassens's paper in this volume and other results are given in citations therein and in review papers^{11,12,13,14,18}.

When q is constant so that $\langle \zeta_q(0) \zeta_q^*(\tau) \rangle$ is computed as in the light scattering experiment, the response function formulation provides a convenient pattern for solving the boundary value problem implicit in the physics of fluctuating interfaces. First the field equations are mapped from space-time variables to wave number-frequency variables by a Fourier transform on the space variables and a Laplace transform on the time variable according to

$$\tilde{\zeta} \equiv \tilde{\zeta}_q \dots = \int_0^\infty dt \int_{-\infty}^{+\infty} d\vec{x} e^{i\vec{q} \cdot \vec{x} - st} \dots \quad (15)$$

where s is the Laplace transform variable. The conversion to frequency is by the substitution $s \rightarrow i\omega$ at the appropriate point in the construction of the spectrum of the fluctuations. Note carefully that only the inplane space components are transformed, $\vec{x} = (x, y)$; z is not transformed.

The process can be illustrated by simplifying the problem slightly; assume that the instrument function is sharp enough that F is non-zero only when $q_x = k_e$ and $q_y = 0$. In that case cylinder waves, generated by thermal fluctuations, moving in the x direction are detected with amplitude $\zeta_{q_x}(t)$. The velocity field can then be written in terms of stream and potential functions, ψ and ϕ respectively. So far as I know, this is a new derivation of the response function but the results are the same as quoted in several references^{11,19}. Again for simplicity ignore monolayer effects so that only the generalized Laplace equation of capillarity is relevant. The generalization is easy but tedious; the appropriate

formulas are available in the literature, see references 11, 14, 19 and references therein.

When represented by the scalar functions ψ and ϕ , the components of the velocity field are

$$v_x = -\frac{\partial \phi}{\partial x} - \frac{\partial \psi}{\partial z} \text{ and } v_z = -\frac{\partial \phi}{\partial z} + \frac{\partial \psi}{\partial x} \quad (16)$$

Substitution into the continuity equation for the volume phase and the momentum balance gives the three equations $\nabla^2 \phi = 0$,

$\frac{\partial \psi}{\partial t} = \frac{\eta}{\rho} \nabla^2 \psi$ and $\rho \frac{\partial \phi}{\partial t} = \Delta P$ where ΔP is the pressure variation caused by the wave motion.

The approximation of incompressible flow gives, after transforming (only the space variable x is Fourier transformed, z is not transformed)

$$\frac{\partial^2 \tilde{\phi}}{\partial z^2} - q^2 \tilde{\phi} = 0 \quad (17)$$

with the boundary condition that $\lim_{z \rightarrow \infty} \tilde{\phi} = 0$

$$\phi = \tilde{\phi}(q, s) e^{qz}, \quad q > 0 \quad (18)$$

The equation for the stream function is

$$\frac{\partial \psi}{\partial t} = v \nabla^2 \psi; \quad v = \eta/\rho \quad (19)$$

So that with the boundary condition of $\lim_{z \rightarrow \infty} \tilde{\psi} = 0$ and the initial condition $\psi_q(z, 0) = 0$ the solution of the transformed equation

$$\psi_q(z, 0) = \frac{\eta}{\rho} \frac{\partial^2 \tilde{\psi}}{\partial z^2} - \left(\frac{\eta}{\rho} q^2 + s \right) \tilde{\psi} \quad (20)$$

is

$$\tilde{\psi} = \tilde{\psi}(q, s) e^{mz} \quad (21)$$

where
$$m = \sqrt{q^2 + \frac{s\rho}{\eta}}, \text{Re } m > 0 \quad (22)$$

so that m is the root with positive real part. Note that an initial condition of $\psi_q(z, 0) = 0$ was chosen. The rationale for this choice was discussed by Nelkin¹⁹. Finally the pressure drop, $\Delta\tilde{p}$ is given by

$$-\Phi_q(z, 0) + s\tilde{\Phi} = \frac{\Delta\tilde{p}}{\rho} \quad (23)$$

Again the initial condition $\Phi_q(z, 0) = 0$ is chosen for reasons cited in Nelkin¹⁹.

Substitution into the momentum balance equation for the surface assuming $\nabla \cdot \underline{\underline{g}} = 0$ for the a pure fluid followed by a Fourier-Laplace transform and substitution for $\tilde{\psi}$ and $\tilde{\Phi}$ gives

$$0 = -q^2 \gamma \tilde{\zeta} + \rho s \tilde{\varphi} + 2\eta(q^2 \tilde{\varphi} + i q m \tilde{\psi}) \quad (24)$$

and

$$0 = 2i q^2 \tilde{\varphi} - (q^2 + m^2) \tilde{\psi} \quad (25)$$

The most interesting aspect of the construction is the use of the continuity condition for the velocity field at the surface

$$\frac{\partial \zeta}{\partial t} = \hat{n} \cdot \vec{v} \Big|_0 = v_z|_0 \quad (26)$$

to generate the response function of the interface to thermal fluctuations. The Fourier-Laplace transform yields

$$s\tilde{\zeta} + q\tilde{\varphi} + i q \tilde{\psi} = \zeta_q(0) \quad (27)$$

This condition along with the two equations of momentum balance have the coefficients $\tilde{\zeta}$, $\tilde{\varphi}$ and $\tilde{\psi}$ in common so that the matrix equation is valid wherein

$$\begin{bmatrix} -q^2\gamma & (\rho s + 2\eta q^2) & 2i\eta q m \\ 0 & 2iq^2 & -(q^2 + m^2) \\ s & q & iq \end{bmatrix} \begin{bmatrix} \tilde{\zeta} \\ \tilde{\phi} \\ \tilde{\psi} \end{bmatrix} = \begin{bmatrix} 0 \\ 0 \\ \zeta_q(o) \end{bmatrix} \quad (28)$$

or with an obvious assignment of variable names

$$\tilde{M} \cdot \vec{\tilde{\zeta}} = \vec{\zeta}_q(o)$$

which is easily solved to give

$$\vec{\tilde{\zeta}} = \tilde{M}^{-1}(s) \vec{\zeta}_q(o) \quad (29)$$

In particular, $\tilde{\zeta}(t)$ can be calculated as

$$\tilde{\zeta} = (\tilde{M}^{-1}(s))_{13} \zeta_q(o) \quad (30)$$

so that for a time stationary process

$$\langle \zeta_q(o) \tilde{\zeta}(s) \rangle = (\tilde{M}^{-1}(s))_{13} \langle \zeta_q^2(o) \rangle \quad (31)$$

The inverse Laplace transform is the correlation function $\langle \zeta_q(o) \zeta_q(t) \rangle = L^{-1} \langle \zeta_q(o) \tilde{\zeta}(s) \rangle$ that is required for the interpretation of light scattering data through equation 6. The spectrum of the fluctuations can be computed directly from $\langle \zeta_q(o) \tilde{\zeta}(s) \rangle$ by

$$G(\omega) = \text{Imag} \{ (\tilde{M}^{-1}(s))_{13} \}_{s \leftarrow i\omega} \langle \zeta_q^2(o) \rangle \quad (32)$$

A somewhat different approach was taken by Hajiloo and Slattery²⁰ but fortunately their results are identical to that of reference 19 and herein. Recall that

$$(\tilde{M}^{-1}(s))_{13} = \frac{1}{D(s)} \quad (\text{Cofactor Matrix to } \tilde{M}_{13}) \quad (33)$$

where $D(s)$ is the determinant of \tilde{M} . Define the dimensionless group $Y = (\omega_o^2 \tau_o^2)$ where $\omega_o^2 = \frac{\gamma q^3}{\rho}$ (the Kelvin equation limit) and $\tau_o = 1/(2\nu q^2)$, then when $Y \gg 1$ as will be the case for the ocean surface

$$\langle \zeta_q(0) \zeta_q(\tau) \rangle = \langle \zeta_q^2(0) \rangle e^{-|\omega_q'' \tau|} \cos \omega_q' \tau \quad (34)$$

Moreover, taking $\hat{\omega} = \omega' + i\omega''$ then $\hat{\omega}_q$ is computable from the dispersion equation

$$\hat{D}(\hat{\omega}, q, \gamma, \dots) = 0 \quad (35)$$

where \hat{D} is computed from $D(s)$. When generalized to include k_e and k_v this relationship can be used to determine estimates of the two coefficients given $\hat{\omega}$, q and the density and viscosity numbers.

The experimental procedure for determining the visco-elastic coefficients and surface tension using the light scattering methodology is to

1. Determine $R_i(\tau)$ or its Fourier transform, figure 1.
2. Fit the correlogram which is $R_i(\tau)$ determined at regular intervals $0, \Delta t, 2\Delta t, \dots$ so as to determine the best estimate of $\hat{\omega}_m$ in

$$R_i(\tau) = A + B e^{-\omega_m'' \tau} \cos \omega_m' \tau \quad (36)$$

3. Correct for the instrumental effect which is largest for ω_m''

$$\omega_q'' \cong \omega_m'' - \frac{f}{\omega_m''} \quad (37)$$

and usually less than a .3% correction for ω_m'

4. Use the corrected frequency numbers to compute two coefficients from the complex dispersion equation. When a set $\{\hat{\omega}_q\}$ has been determined then the surface tension as well as k_e and k_v can be determined from (35).

When $Y \approx 1$ the fit must be made directly with the spectrum function or its inversion to the correlation function but this should not be necessary for determining the micro-layer properties.

Recently we have been exploring algorithms that fit the experimental correlation function directly to equation (6) using equation (34) and its generalization to a form consistent with equation (31). However, the integral eq. (6) must be approximated numerically and coded for efficient execution of the least squares procedure. I believe that this can be accomplished and provides a much better fit of the correlogram but the fit requires more computer time than the algorithm described above.

3.2. Capillary Ripple Theory and the Analysis of Generated Waves

When the surface profile is thought of as the sum of an ensemble of waves of small amplitude of differing frequencies and phases then

$$\zeta(x,t) = \sum_{\omega} \zeta_{\omega}(x) e^{i\omega t + \varphi} \quad (38)$$

The driven wave experiment involves a line source or a point source of excitation for one frequency so that

$$\zeta(x,t) = \zeta_{\omega}(0) e^{i(\hat{k}x - \omega t)} \quad (39)$$

where now $\hat{k} = k + i\alpha$. Where, again $k = 2\pi/\lambda_{\text{ripple}}$ and α is the space damping coefficient analogous to ω'' in the constant q analysis for the light scattering experiment. It is instructive to carry the analysis through formally, by defining the Fourier-Laplace operator as

$$\tilde{L}_{\omega} \dots = \int_{-\infty}^{+\infty} dt \int_0^{\infty} dx e^{i\omega t - kx} \dots \quad (40)$$

In the end you will conclude that the elevation function can be written formally as

$$\langle \zeta_{\omega}(0) \zeta_{\omega}(x) \rangle = \langle \zeta_{\omega}(0)^2 \rangle e^{-\alpha x} \cos kx \quad (41)$$

but $\langle \dots \rangle$ is not a thermal average. This is the function observed when the rms amplitude of plane waves is measured with distance from the source. Moreover, k and α are variables in a complex dispersion equation, $\hat{D}(\hat{k}, \omega, \gamma, \dots) = 0$ which also includes the surface visco-elastic coefficients k_e and k_v .

The standard deviation involves assuming that the various field variables, Φ, ψ etc are of the form $f(z) e^{i(\hat{k}x - \omega t)}$ and satisfy formulas derived from equations 7-11 along with continuity conditions. The first such construction that included both surface

visco-elastic coefficients as well as the adsorption-desorption flux was given by Hansen and Mann^{21,12,13,14}. The result is a dispersion equation.

4.0. EXPERIMENTAL TECHNIQUES FOR THE MICROLAYER.

The experimental techniques for generating capillary waves and the determination of accurate k and α numbers was reviewed most recently by Mann¹⁴. The experimental techniques for accurately measuring the correlation function of ripples generated by thermal fluctuations has been published by our group^{14,15,16,22,23} by Hard and his colleagues^{17,24}. A brief resume of the laser scattering instrument at Case will be useful.

Consider figure 1 where the upper schematic shows the Fourier optical transformations that are used to understand and design the spectrometer and the lower schematic shows one implementation.

First, a clean beam of Gaussian cross section illuminates the first key optical element, a grating with spacing that corresponds to perhaps a 100 cm^{-1} wave number. L1 and L2 combine to do two optical Fourier transforms; at the first plane, F1, the primary beam (zero order) and one higher order beam (the reference beam) is transmitted and optically transformed to a cosine distribution of light focused on the surface.

Capillary waves moving on the surface behave as a dynamic phase grating which modulates the imaged distribution of light. The modulation process due to propagating, damped surface ripples is detected after blocking the intense zero order beam at F2. L3 and the pinhole at the PMT is a convenience for eliminating optical flare. The modulation of the reference light beam is converted to a random photocurrent by the PMT from which the photocurrent autocorrelation function, R_1 , (or the spectrum) is computed. The correlogram is analyzed for surface visco-elastic effects through equation (6) and the theory developed in that section.

The optical signal to noise ratio can be improved by using an incident beam of smaller cross section but the corrections to the time damping coefficient are larger. The spectrometer can be designed so that a number of q values can be used by just shifting the order that is being transmitted as a reference beam. Many additional details will be found in the papers from the Case group.

Rather than reviewing these techniques in detail, I will comment on adapting this methodology to the micro-layer problem for both *in situ* and *ex situ* experiments.

4.1. Ex Situ Experiments

There is no doubt that microlayer "samples" can be brought back to our laboratories for careful measurements of the spectra of thermal fluctuations as a function of temperature and film compression. Various ocean sampling techniques are available for doing exactly that. The work of Barger and Means⁹ is a hint of the results that would come out of studies covering the frequency range from below 1 Hz to above 10 kHz. The surface film is composed of complex structures including natural polymers so that we should expect frequency dependent visco-elastic coefficients. In my opinion it is important to do this class of experiments and the results will be especially helpful when the analytical chemistry of the micro-layer is known.

In laboratory experiments under carefully controlled conditions, we can determine the surface tension to a fraction of a millinewton per meter (dyne/cm). The elastic modules can be determined to 10% or better and the surface viscosity to perhaps 20%. The accuracy of these visco-elastic coefficients can be improved in my opinion by refinement of the apparatus and the data processing algorithm.

Once we have enough information about the composition of the microlayer, then the visco-elastic coefficients and their frequency dependence can be studied using, for example the techniques of Brownian dynamics.

The larger problem of understanding how the microlayer affects remote sensing can then be modeled with considerable additional detail.

Remote laboratory experiments are not satisfactory since apparently the microlayer changes with time after sampling from the ocean surface. It is necessary to make these measurements very soon after sampling. However, the roll of the ship could interfere with the measurement of the scattered light from the fresh microlayer surface; a difficult problem has been the surface motion pumped by motion of the floor of the laboratory. Even when good optical benches (using passive isolation elements) are employed, low frequency (<100 Hz) surface waves can be bothersome. Fortunately, the center frequencies of the spectra to be measured on microlayer samples will be above 2kHz so that high-pass filtering of the signal from the photodetector will reduce the interference to a satisfactory level.

There is a new class of optical benches²⁵ that are stabilized by active control elements. Acceleration of the corners of the table are sensed and that signal drives control circuits that move the table enough to compensate for vibration. Such a device will stabilize the optical system well enough that *ex situ* experiments can be done in the relatively calm waters in which the sea films are collected. ('Breez' wind conditions; speeds of a few m/sec.)

Moreover, a second trick can be used to eliminate any remaining effects of ship motion. A stack of thin, stainless steel razor blades provide a good light trap to eliminate stray scattering from the bottom of the cell. When properly stacked and positioned in the cell so that the water level is within about 0.1mm of the blades, the low frequency waves that interfere with the laser beam scattering cannot develop.

The entire light scattering apparatus including the cell, the laser and actively controlled optical bench form a compact instrument of roughly 2' x 3' x 6". The electronics necessary to analyze the data includes a correlator interfaced to a micro computer. The Case Center for Complex Flows is working on a single board correlator which would take one slot in an IBM PC or one of the common clones. Presently, we use commercial correlators which amount to a hard-wired computer specialized for time series analysis.

After our experience at Case in building a compact, surface light scattering system based on the design described by Lading et al¹⁶, we believe that it is possible to build a system that will perform very well on a ship moving in fairly calm waters. It will be possible to determine surface properties of the microlayer accurately shortly after sampling. I expect that precision and accuracy will be comparable to the laboratory set-up; surface tension to better than .5d/cm and surface elasticity to better than 20%.

4.2. In Situ Experiments

The real challenge and real need is a device for the *in situ* measurement of sea film properties. I believe that it may be possible to do this using laser light scattering technology even though low frequency vibrations are a problem in laboratory experiments. Indeed, it may not be possible to attain the level of precision and accuracy that can be obtained in the laboratory.

Fortunately, the estimation of surface tension depends to first order on the frequency of the amplitude correlation function and that frequency is relatively easy to determine. The correlogram can be very noisy¹⁶ and still it is possible to estimate ω' to within a few percent. The time damping coefficient is more difficult to determine accurately and may be poorly estimated under experimental conditions where ω' can be closely estimated.

It is reasonable to set as an initial design goal the determination of γ , *in situ* to better than 10%. I doubt that we will be able to determine the time damping coefficient to better than 50% at first. It is likely that we can improve the operation of the system after some experience with the first version of the instrument. Our group does not have the experience to solve several obvious problems in developing the *in situ* system, e.g. the floating platform, but we understand that the community can help greatly.

The design problems that must be solved are numerous. It is crucial to control the geometry of incident and reflected beams carefully. That calls for a "stable" platform that follows the swells of a calm sea. The platform could be as simple as a pontoon structure or perhaps a catamaran type of boat carefully designed to provide active or passive "tracking" of the sea surface under calm conditions. (It might be possible to use a submerged platform if better stability could be obtained.) The EVIS²⁵ optical table is an example of active control in which the design goal was to vibration isolate the surface of the table. It is also possible to control such a table to keep a constant elevation with respect to "slow" changes in elevation above some surface. The spatial range over which such a device can operate is limited to a few centimeters but that may be enough.

It is clear from figure 1B that slow, rolling motion of the ocean surface with respect to the incident beam will cause the reference beam going through L3 to wander across the detector (PMT in figure 1). The situation is more difficult in that the primary beam which should be blocked at the F2 plane may flash through. However, this difficulty can be minimized by using an active control circuit to drive a mirror wherein the motion of the primary beam and reference beam are tracked to keep the reference beam on target. (The Case group has demonstrated such a device.) An optical control element will not affect the phase and amplitude relations between the reference and scattered beams which was determined at the surface.

Figure 1B represents only one optical arrangement; the optical paths can differ without changing the fundamental mechanism by which the spectrometer operates. Note that the focal lengths of L1 and L2 can be adjusted to give convenient working distances. We have used working distances out to about one meter with only relatively minor difficulties.

It may not be possible to control the position of the reference beam at the detector plane well enough for observing a stable photocurrent over the time period for collecting an averaged correlogram. However, there are two factors that we can use to optimize the process. Firstly, a time series collected over about 1 millisecond is enough to generate a correlogram but the signal to noise ratio will be poor and probably not useful but accumulation over a few seconds can give useful correlograms. We have found that even if there are gaps in the time series, as the reference beam moves out of the pinhole in front of the PMT (Figure 1), the correlogram averaged over a sufficiently long period (seconds) is not significantly distorted. Clearly, the gaps should be eliminated from the record. It is possible to detect motion of the reference beam and thereby start and stop the correlator by a trigger signal so that it is collecting data only while the beam is positioned properly. One can imagine using array detectors in schemes that will preserve the integrity of the time series.

We are considering other methods for measuring the surface fluctuations accurately:

- i A two-spot anemometer configuration has some potential. Capillary waves behave as a tracer particle in many ways.
- ii Drive the surface by an intense pulsed laser beam to generate ripples and observe the transit time of the capillary waves by either the light scattering spectrometer or a two-spot anemometer configuration.
- iii Laser scattering remotely detected without the reference beam for heterodyne detection of the scattered light.
- iv The use of Sun Glitter in an analysis scheme.

The spectrometer described by the Case group¹⁶ does detect and measure surface velocity fields. This was demonstrated some years ago in unpublished work done for NASA. If there is a velocity field perpendicular to the fringe pattern imaged by L1 and L2 down on the surface, then the spectrum of the photocurrent output will split according to

$$(\omega_0 \pm qv)^2 = \frac{\gamma}{\rho} q^3 Y_1 \quad (42)$$

where v is the speed of the surface flow, ω_0 the center frequency and Y_1 is a dimensionless group²¹. The width of the spectrum, controlled by volume viscosity and surface visco-elastic effects is sufficiently large that there is overlap of the spectra until a mean velocity of about 10 cm/sec is reached. Much larger velocity fields can be measured and the range of application can be to less than 1mm/sec. This may well be an effect that we will want to exploit in ocean work; the distortion to the spectrum must be taken into account when computing the surface tension and especially in estimating surface visco-elastic coefficients.

I remark that surface particles also scatter and their numbers cannot be controlled *in situ*. While their motion will be detected, they are much too large to have an effect on the signal due to the capillary waves. Such particles will contribute to a background signal that must be studied and understood.

There are other problems that must be solved for *in situ* work such as how to handle the laser source, power, enclosures for the equipment, etc. While I try not to underestimate these practical problems, I believe they can be solved.

5.0. CONCLUSIONS

I am confident that a laser spectrometer can be designed to work effectively *ex situ* on a ship in the open ocean. Active vibration isolation techniques can provide the stable platform for operation in calm and relatively calm seas. The time between collection and analysis is minimal. This will be an advantage in observing the effects of surfactant components that degrade over time.

The same isolation technology will also allow the driven wave experiment to be done on site along with the laser spectrometer. The apparatus could be designed to operate in the ultra-low frequency, long wave limit as well as the intermediate frequency range.

A manageable ensemble of instruments can be integrated so that the response functions of sea films can be studied over a very wide frequency range ($<.1\text{Hz}$, $>20\text{kHz}$) on site but *ex situ*.

In my opinion, laboratory experiments off site are still important in the development phase of the microlayer program and in providing data on mimic systems for comparison.

The interpretation of on site data will depend critically on the analytical chemistry of the microlayer reported by other groups. Moreover, from my viewpoint considerably more surface structure information will be required such as that derived from x-ray reflection and scattering techniques. Finally, Brownian dynamic simulations will help to understand the molecular basis of sea film structure and dynamics.

I believe that it is possible to adapt the Case group's light scattering techniques for *in situ* measurements. We should first try for the surface tension measurement which can be done even with much noise in the measured autocorrelation functions of the photocurrent.

A crucial step in developing the *in situ* measurement is the design of the boat or raft that will position the spectrometer with respect to the sea surface. We need help on that technology.

The Case group will study other optical methods for measuring the spectra of capillary waves. We invite our colleagues to suggest methods that might do the *in situ* measurement in a way that would be less sensitive to low frequency surface waves but sensitive to surface deformations that give information about surface tension and film visco-elastic response.

The microlayer program provides an unusual opportunity to combine the talents and knowledge of investigators from many disciplines to solve problems about the structure, dynamics and function of the microlayer specifically. In addition, I see the opportunity to work on surface structure and dynamics problems of very fundamental interest to the surface chemistry community.

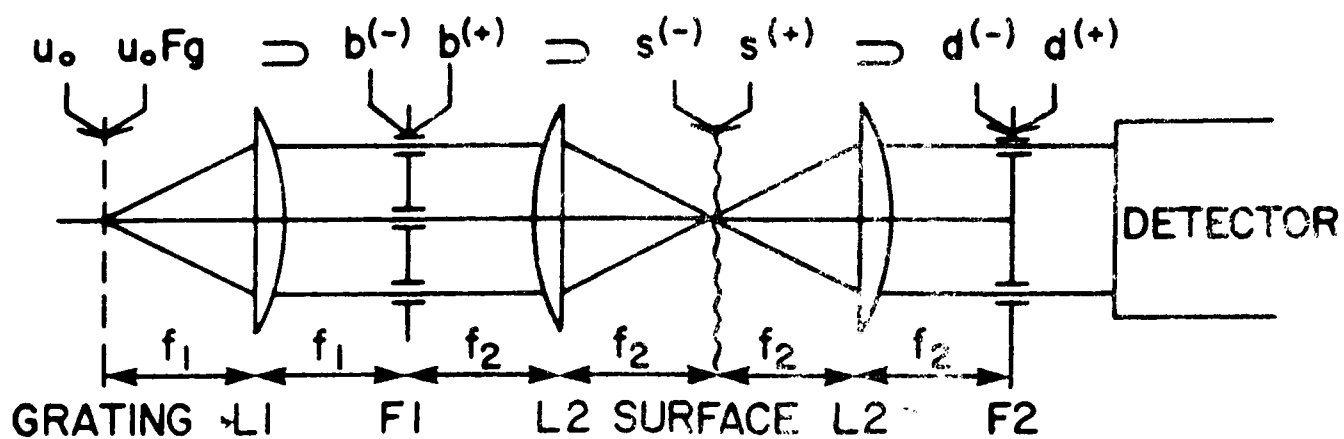
Acknowledgement

The work by the Case group on surface light scattering is being supported by the Office of Naval Research. The work on Brownian dynamics is being supported by the Office of Naval Research under a Selected Research Opportunities grant to CWRU. We acknowledge this support with gratitude.

References

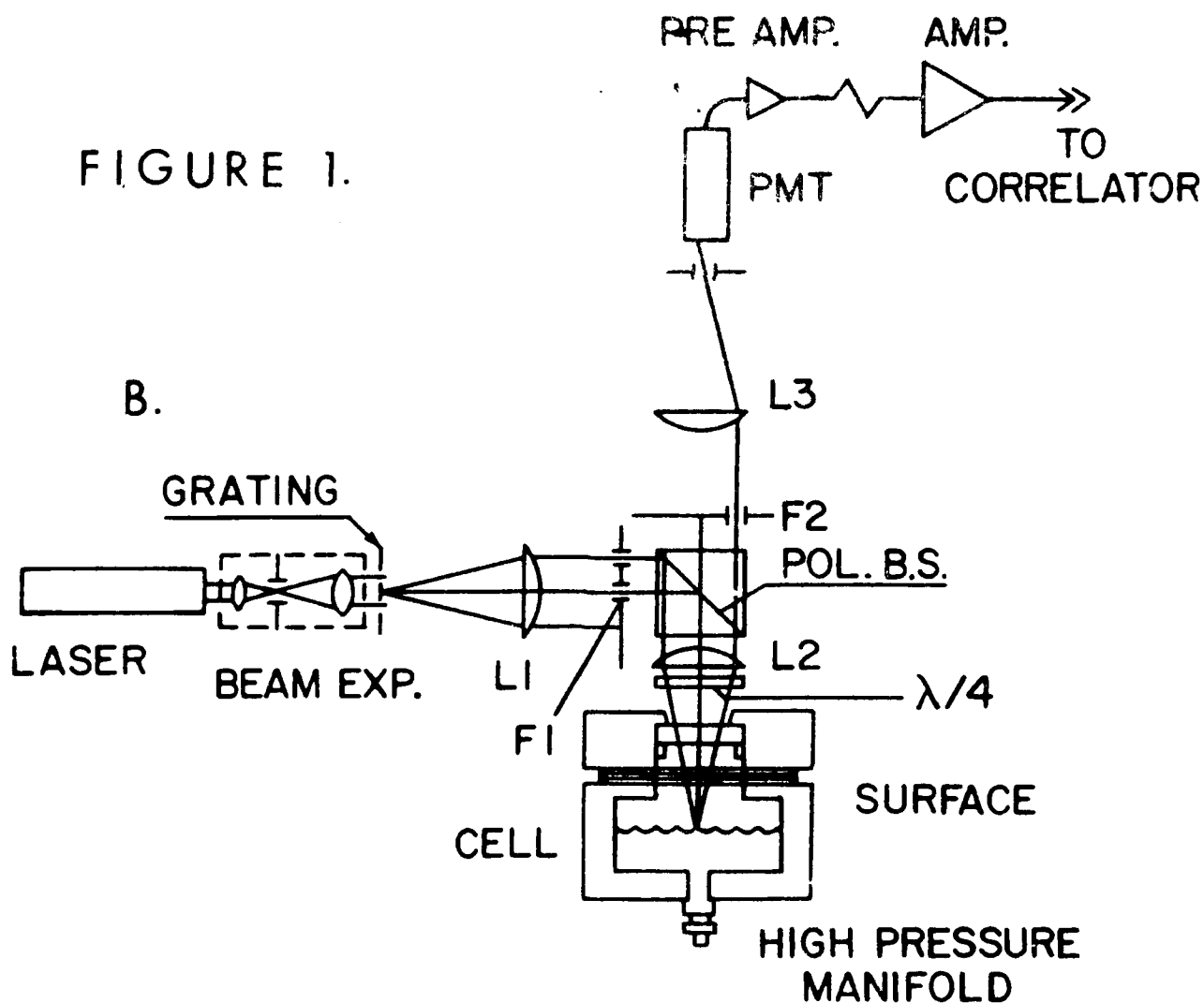
1. Mann, J. Adin, "Dynamics, Structure and Function of Interfacial Regions", *Langmuir*, 1985, 1, 10.
2. Adamson, A.W., "Physical Chemistry of Surfaces", 4th ed.; Wiley-Interscience: New York, 1982.
3. Tjatjopoulos, unpublished results for a Ph.D. thesis to be defended in 1986.
4. Baumgartner, A., *Ann. Rev. Phys. Chem.* 1984, 35, 419.
5. Kox, A.J., Michels, J.P.J. and Wiegel, F.w., *Nature*, 1980, 28, 317.
6. van der Ploeg, P. and Berendsen, H.J.C., *J. Chem. Phys.* 1982, 76(6), 3271 and *Molecular Physics* 1983, 49(1), 233.
7. Zare, R. private communication, spring 1986.
8. Pershan, P.S., Als-Nielsen, J. *Phys. Rev. Lett.* 1984, 52, 759.
9. Barger, W.R., Means, J.C., in "Marine and Estuarine Geochemistry", edited by Sigleo, A.C. and Hattori, A., Chapter 4; Lewis Publishers, Inc., Chelsea, MI, 1985.
10. Braslau, A., Deutsch, M., Pershan, P.S. Weiss, A.H., Als-Nielsen, J. and Bohr, J. *Phys Rev. Lett.* 1985, 54(2), 114.
11. Mann, J.A., Porzio K.C., *Int. Rev. Sci.: Phys. Chem.*, Ser. Two, 1975-1976, 1975, 7, 47.
12. Lucassen-Reynders, E.H. and Lucassen, J. *Advan. Colloid Interface Sci.* (1969), 2, 347.
13. Hansen, R.S. and Ahmad, J. *Progr. Surface Membrane Sci.* 1971, 4, 1.
14. Mann, J.A., *Surf. Colloid Sci.* 1984, 13, 145.
15. Edwards, R.V., Sirohi, R.s., Mann, J.A., Shih, L.B. and Lading, L. *Appl. Opt.*, 1982, 21, 3555.
16. Lading, L., Mann, J.A., Edwards, R.V., "Analysis of a Surface Scattering Spectrometer", submitted, preprints available.
17. Hard, S., Hamnerius, Y. and Nilsson, O. *J. Appl. Phys.* 1976, 47, 2433.

18. van den Tempel, M., Lucassen-Reynders, E.M., Adv. Colloid Interface Sci. 1983, 18, 281.
19. Nelkin, M., The Phys. of Fluids 1972, 15(10), 1985. Also see Bouchiat, M.A. and Meunier, J., J. Phys. (Paris) 1971, 32, 561.
20. Hajiloo, A. and Slattery, J.C., J. Colloid and Interface Sci. 1986, 112, 325.
21. Hansen, R.S. and Mann, J.A., J. Applied Phys. 1964, 35, 152.
22. Shih, L.B., Rev. Sci. Instruments, 1984, 55, 716.
23. Mann, J.A. and Edwards, R.V., Rev. Sci. Instruments, 1984, 55, 727.
24. Hard, S. and Neumann, R.D., J. Colloid and Interface Sci., 1981, 83, 315.
25. Turechek, J., Newport Corporation, EVIS Active Vibration Control System, 1986.



A.

FIGURE 1.



B.

Surface Film Chemistry Report

Organic Composition of Natural Films

The principal identifiable components of the dissolved and particulate phase (defined as passing or retained by 0.2 to 1.0 μm pore diameter filters) are primarily hydrolysis products (amino acids, carbohydrates, fatty acids) of the parent (unknown) constituent film molecules. These components, summed as organic carbon, account for only 25 to 50 percent of the total organic carbon in the microlayer just as is the case with bulk seawater. Aside from five amino acids, natural hydrocarbons and sterols, and urea, none of the naturally-occurring organic molecules in the sea surface microlayer have been identified or their stereochemistry at the interface determined. The total lipid content of microlayer organics is approximately 5 percent, less than that normally found in phyto- and zooplanktons. However, the presence of biopolymers with relatively low molecular weights (500-5000), such as lipoproteins and lipopolysaccharides, could well contribute to the physical chemical properties of the interface (film pressure, film potential, elasticity).

Sampling, Microlayer Enrichments and Slicks

A basic constraint in studies of sea surface chemistry is how to sample the material of interest. There is even uncertainty as to how to define what is of interest, i.e., the thickness of relevance to surface effects. Most devices sample a slice several hundred microns thick (screens, plates, skimmers). Langmuir-Blodgett techniques have been used and although the collected material is 10-30 μm thick in the dry state, when hydrated in seawater the thickness is probably near 1 μm . Inevitably much smaller volumes are collected than with the devices harvesting layers hundreds of microns thick so that the chemical analysis which can be performed is more limited (functional group identification by IR). Both classes of sampler certainly collect sub-surface water which dilutes any monomolecular film present at the air-sea interface. Collection of bubble-burst material similarly suffers from sub-surface scavenging by the rising bubbles, as well as from possible fractionation effects during bubble bursting at the sea surface.

By far the greatest number of reported chemical analyses of microlayer material has been on samples from the top several hundred microns of the oceans. Although the early literature gives the impression that many chemical species as well as bacteria and other microorganisms show enrichments in the microlayer relative to sub-surface concentrations, more recent data indicates enrichments which are often either considerably smaller or insignificant. Enrichments for bacteria, most plankton, dissolved organic carbon (DOC), nutrients and dissolved

trace metals are generally less by an order of magnitude and often much less. Particulate material does often show enrichments of an order of magnitude or greater, and this may well be due to adsorption of highly surface active material from the bulk water onto the particles and their transport to the interfacial region by bubbles and other processes.

Although the spatial and temporal variability of organic sea surface films has not been determined, only a relatively small part of the total surface area of the open ocean appears to be covered with films which are coherent enough to damp capillary waves and so give the surface a slicked appearance. This is almost certainly because of lack of availability of highly surface-active molecules (many of them may be adsorbed onto particles) and break-up and sinking of films under turbulent conditions. Thus, slick covered water is usually observed under calmer conditions and in areas of adequate supply of suitable organic material, either from natural biologically sources or from man-induced hydrocarbon inputs. Recent space shuttle sun-glint photography suggests that under certain conditions slicks are widespread in seas and coastal ocean areas.

Existing Sea Surface Measurement Methodologies

A. Surface Tension

Calibrated spreading oils

1. precision, ± 1 mN per meter
2. advantage: mobile and in situ
3. disadvantage: labor intensive

TOWARD (Tower Ocean Wave & Radar Dependence) instrument (Barger/Garrett)

1. accuracy ± 1 mN per meter
2. requires in situ calibration
3. is not in situ and is only semi-continuous (3 min. intervals)

B. Surface Potential

Measures dipole moment of oriented film-constituent molecules

1. Has been used in situ but with great difficulty
2. Actually detects surface film in gaseous state prior to change in compressibility from gas to liquid 2-D state, and prior to onset of wave damping and other film-induced modifications
3. Important as indicator of sub-critical surface-active material concentration

C. Hula Hoop Surface Concentration Method

Measures concentration (but not chemical character) of film-forming material actually at air-water interface at a point in time and space.

Is a measure of surface-area reduction required to form process modifying films (to point of phase change).

Labor intensive and difficult to use.

May be important as measure of film-forming potential.

Like XBT's may be made expendable and inexpensive.

Recommendations

1. Direct spectroscopic measurements (infrared, laser fluorometric, raman) on natural films in laboratory troughs coupled with concurrent proximate analyses of the amino acid, carbohydrate and lipid components should give more realistic insights into the true molecular nature of film constituents. Using this knowledge, it will thus be possible to relate molecular structure to remote sensing signatures, should such a relationship exist.
2. Turnover times (half-lives) of films at the surface should be determined by appropriate tracer techniques (dyes, artificial "natural" films) to establish a baseline in evaluating possible biological and photochemical film alterations which could occur with time, and hence whether the resulting surface activity changes as a result of residence time at the interface.
3. Require development of continuous, in-situ instrumental methods for surface tension or surface dilational modulus, and possibly for determination of capillary-wave attenuation.
4. Should use methods to measure surface-film concentration and film-forming potential in future coordinated remote sensing/surface film field programs.

Monolayer Dynamics

Y. Rabin (Chairman)

E. H. Lucassen-Reynders

J. A. Mann

J. C. Scott

The most important physico-chemical parameters having an effect on sea roughness, and hence on reflectivity, were felt to be:

1. The surface elasticity and viscosity (combined in a surface elastic module) arising from the presence of films.
2. The surface tension as affected by the films.

Surface elasticity/viscosity is the most important parameter determining the damping characteristics of the capillary waves that are held to be important both in determining surface roughness and in preventing the generation of larger waves. By far the greater part of both elasticity and viscosity consists of resistance against changes in area (compression/dilation) as distinguished from changes in shape (shear), at least in systems studied so far. Surface *shear* viscosity was thus felt to be of negligible importance, but it might have greater relevance for surface films consisting of e.g., polymers.

The surface tension, on the other hand, determines the wavelength of the capillary ripples, not their damping characteristics. Measuring the surface tension as a function of surface enrichment provides a means of (a) characterizing the films and (b) gaining knowledge of the maximum possible value of the surface elasticity.

Surface potential was not felt to be a parameter exerting any measurable direct influence on the relevant behavior of a surface.

Suggestions for Future Research:

It is felt that *in situ* state-of-the-art measurements on ocean systems are not practical with present day technology. Thus, such measurements will have to be performed *ex situ* (by transferring ocean water to the lab) or, alternatively on model surface-active materials. The latter include polymeric materials which have received insufficient attention in the past.

We propose:

1. Measurements of surface tension and dilational elastic modulus spectrum, combining driven waves with light scattering techniques—on *ex situ* ocean systems.
2. Study of hydrodynamic effects of monolayers and films formed by surface-active polymers (and polyelectrolytes). Various aspects of surface gelation/aggregate formation (occurring naturally in the ocean?) should be examined. The mechanical properties of such gels and, in particular, the possibility of large elastic effects at very low polymer concentrations, may play an important role in wave damping by natural films.

3. Study of the relation between microscopic structure and dynamics of films (by fluorescent "tagging") and their wave damping and spreading characteristics.
4. Determination of the structure of the interfacial region by the method of x-ray reflection variation with q_{\perp} — *ex situ* with sea water samples and calibration model systems, again including polymers and surfactants of models of sea slick.
5. Development of *in situ* methods for determining the surface tension and elastic moduli that will give the former to about 0.1-0.5 dyne/cm and the latter to 20 percent or better, at the same time.
6. Tank experiments for study of wind-driven film spreading, possibly in conjunction with fluorescent techniques that will allow one to perform direct observations on the film.
7. Investigation of the mechanism of wave damping by greasy ice films.
8. Development of nondestructive methods for *in situ* sampling of monolayers (without perturbing the bulk material), possibly by adsorption of the monolayer on strongly hydrophobic solid surfaces.

COMMENTARY OF THE REMOTE SENSING WORKING GROUP ON MICROLAYER-REMOTE SENSING RELATIONSHIPS

J. F. Vesecky (Editor), W. R. Alpers, W. D. Garrett, H. Huhnerfuss,
P. S. Liss, P. P. Lombardini, J. A. Mann, J. C. Scott, and J. Wu

INTRODUCTION

This commentary presents a consensus view (among working group members) of the relationship between ocean remote sensing and the marine microlayer. To begin, we think that remote sensing and the marine microlayer are, in fact, related and in two distinct ways: first, remote sensing techniques should prove useful in the study of surface films, e.g. spatial distribution and temporal history of surface films on the ocean; second, the marine microlayer has a significant impact on remote sensing of ocean properties in general, e.g. winds, waves and other surface properties. This state of affairs comes about because most remote sensing techniques respond to ocean surface roughness and the marine microlayer can profoundly affect ocean roughness as in the formation of slicks.

REMOTE SENSING TECHNIQUES RELEVANT TO THE MICROLAYER

Virtually all remote sensing techniques are relevant to the microlayer simply because the microlayer can have a significant impact on surface roughness. In terms of sensing the microlayer remote sensing high resolution techniques, such as visible, infrared, mm-wave and microwave imaging, are particularly important since they can observe the spatial and temporal properties of surface film slicks. Multiple wavelength (in a broad sense) remote sensing measurements combined with in-situ observations are likely to be productive in understanding both the aspects of microlayer-remote sensing relationships mentioned above. Here we have in mind combinations such as active and passive microwave together with visible and/or infrared.

RESEARCH STRATEGY

In terms of better understanding remote sensing-microlayer relationships it appears that initial research efforts should focus on laboratory and theoretical work while taking advantage of field experiment opportunities which arise from

other programs, i.e. piggyback experiments. For example, wind wave tank and other laboratory experiments are very relevant to the interpretation of remote sensing observations of ocean surface films. Likewise, a vigorous theoretical program, interacting with experimental work, is essential in directing and stimulating both experimental and theoretical efforts. Towards the end of the five-year period a comprehensive field experiment should be given serious consideration. Such an experiment would involve multiple wavelength remote sensing coupled with in-situ measurements.

Joint research between Americans and Europeans is good research strategy. Sharing of research facilities, such as off-shore platforms, ships, wind-wave tanks and computational facilities, is particularly encouraged. Funding for travel and visitor support is essential in stimulating such joint research.

RESEARCH PROGRAM

While this commentary makes no attempt to set up a research program, a number of useful comments arose in discussion. We have grouped these comments into three categories: laboratory research, in-situ measurements, theoretical research and field experiments.

Laboratory Research: Much very useful laboratory research on surface films is currently underway. The comments here do not review this work but focus on new items and applications. To help focus laboratory research, a set of standard surface films should be created. This set should include both artificial and quasi-natural surfactant materials and should be applicable both laboratory and field use.

Visible and infrared Raman spectroscopy using focused lasers may be useful in sensing and studying the marine microlayer. The focus can be narrowed to distances of a few to tens of microns.

The emissivity and reflectance of the ocean surface at microwave frequencies requires careful study to follow up on MARSEN results which indicate resonant effects in emissivity. Both slick and non-slick conditions should be considered. While field experiments are probably most important, laboratory experiments can complement the field work and provide more quantitative information.

In Situ Measurements: New methods of detecting microlayer and measuring microlayer properties are urgently needed for both laboratory and field experiment applications. Laser observations of thermal fluctuations of

microlayers and very high frequency (MHz to GHz) acoustic sounding (as in acoustic microscopy) are new techniques which should be explored.

For experiments relevant to remote sensing of the ocean microlayer a particularly pressing need is for a buoy type (unattended) instrument which will sense the existence and basic properties of the local marine microlayer. Both capillary-wave sounding and the new techniques mentioned above should be explored as means of local microlayer observations.

Theoretical Research: It is important that vigorous theoretical research accompany laboratory and field experiments. Theoretical work codifies experimental results and stimulates new lines of thought for experiments and instrumental techniques. A theoretical framework and better interpretation of experiment results allows new hypotheses to be formed for experimental test. For example, theoretical research on elastic properties of microlayers and wave propagation is directly related to the new laser and acoustic techniques mentioned above.

Field Experiments: Direct investigation of remote sensing-marine microlayer relationships requires field experiments. There are a wide variety of ocean features which could play a useful role in microlayer remote sensing field experiments, e.g. internal waves, ship wakes, eddies, etc. Hence there are no particular ocean features upon which field experiments should focus. 'Breeze' wind conditions (~ few m/s) would be desirable for microlayer remote sensing experiments for several reasons. First, high wind speeds destroy the microlayer and make observations difficult. Also, wind wave tank measurements are most accurately applicable to the real ocean under 'breeze' conditions.

Artificial surface films are very useful in natural settings for experiments on remote sensing and the marine microlayer. Remote sensing platforms are often available only for specific periods when natural surface films may or may not be at the desired state. Artificial films can be distributed as required. Artificial surface films could be tailored to simulate natural films. For example, it might be useful to collect natural surfactant material for redistribution at a later time, e.g. around an off-shore platform.

In a microlayer-remote sensing experiment the primary requirements for local measurement (sea truth) of the microlayer are summarized as follows:

1. Surface tension to an accuracy of ~ 0.2 to 0.5 dyne/cm
2. Surface elasticity to an accuracy of $\pm 20\%$
3. Surface wave spectrum measurements from very short (\sim mm) wavelengths to 100's of meters - in particular 1 to 16 Hz wave frequencies.

The most distinctive remote sensing observation of microlayers on the ocean occurred during the 1978-79 MARSEN field experiment. Microwave emissivity of the ocean was observed to be drastically altered by the presence of an artificial microlayer-brightness temperature reduced by ~ 100 K. Further this decrease in emissivity was observed to be frequency dependent - large decrease in brightness temperature at ~ 23 cm wavelength, but very small decrease at ~ 10 cm wavelength. An experiment to further explore this phenomenon is being planned in Germany for early 1987 using a scanning microwave radiometer built by German Aerospace.

MARINE MICROLAYER WORKSHOP
ONRL 9-11 APRIL 1986

ATTENDEES LIST

Professor Dr. Werner Alpers Fachbereich 1 (Physik/Electrotechnik) Universitat Bremen 2800 Bremen 33 FEDERAL REPUBLIC OF GERMANY	(49) (421) 218-3283 3216 Telex: 245811 Telemail: W. Alpers (Oceans)
Dr. Brian C. Barber Space Department Royal Aircraft Establishment Farnborough Hants GU14 6ID	(0252) 24461 Ext 3020
Mr. William D. Garrett Space Systems & Technology Div. Naval Research Laboratory Washington, DC 20375	(202) 767-3185
Dr. Heinrich Huhnerfuss Institute for Organische Chemie University Hamburg Martin-Luther-King-Platz 6 2000 Hamburg 13 FEDERAL REPUBLIC OF GERMANY	(40) 4-123-4240
Dr. Ola M. Johannessen Nansen Ocean and Remote Sensing Center University of Bergen Griegs Vei 3A, Bergen NORWAY	(47) 5-297288 298433 212603
Dr. Peter S. Liss School of Environmental Sciences University of East Anglia Norwich NR4 7TJ	(0603) 56161 Ext 2563
Dr. Pietro Paola Lombardini Consiglio Nazionale delle Ricerche Istituto Di Cosmo - Geofisca Corso Fiume 4 10133 Torino ITALY	(11) 350297

Attendees List (cont)

Dr. E.H. Lucassen - Reynders
Unilever Research
Postbus 114
3130 AC Vlaardingen
HOLLAND

Dr. J. Adin Mann
Department of Chemical
Engineering
Case Western Reserve University
Cleveland, OH 44106

(216) 368-4150

Dr. Yitzhak Rabin
Department of Chemical Physics
Weizmann Institute
Rehovot 76100
ISRAEL

(97-2) 8-482094

Dr. John C. Scott
Ocean Science Division
Admiralty Research Establishment
Portland Dorset DT5 2JS

(0305) 820381
Ext 3436

Dr. Ira Skurnick
DARDA/DSO
1400 Wilson Blvd.
Arlington, VA 22209

(202) 694-5800

Prof. John F. Vesecky
STAR Laboratory
Electrical Engineering Department
233 Durand Bldg.
Stanford, CA 94305

(415) 723-2669

Dr. Peter M. Williams
A-018 Scripps Institution of Oceanography
La Jolla, CA 92093

(619) 452-2929
2434

Dr. Jin Wu
Air-Sea Interaction Laboratory
University of Delaware
Lewes, DE 19958

(302) 645-4216

Attendees List (cont)

Dr. Frank Herr
Ocean Sciences Division
Office of Naval Research
Arlington, VA 22332

(202) 696-4590

Jerome Williams
Office of Naval Research, Branch Office
223 Old Marylebone Road
London NW1 5TH

(44) 1-409-4478

END

2-87

DTIC